University of Oxford

Department of Physiology, Anatomy and Genetics

Metabolic Control of Energetics in Human Heart and Skeletal Muscle

Thesis for the examination of Doctor of Philosophy

A W Johnson MBBS FRCA

Hilary term 2012

Supervisors: Professor Kieran Clarke

Dr Rhys Evans

Thesis Abstract

Myocardial and skeletal muscle high energy phosphate metabolism is abnormal in heart failure, but the pathophysiology is not understood. Plasma non-esterified fatty acids (NEFA) increase in heart failure due to increased sympathetic drive, and regulate the transcription of mitochondrial uncoupling protein-3 (UCP3), through peroxisome proliferator-activated receptor-α. The aim of the work in this thesis was to determine whether cardiac PCr/ATP ratios and skeletal muscle PCr kinetics during exercise were related to cardiac and skeletal muscle UCP3 levels respectively, thus providing a mechanism for the apparent mitochondrial dysfunction observed in heart failure. Patients having cardiac surgery underwent pre-operative testing, including cardiac and gastrocnemius ^{31}P magnetic resonance spectroscopy. Intra-operatively, ventricular, atrial and skeletal muscle biopsies were taken for measurement of mitochondrial protein levels by immunoblotting, along with mitochondrial function by tissue respiration rates. Fasting plasma NEFA concentrations increased in patients with ventricular dysfunction and with New York Heart Association (NYHA) class. Ventricular UCP3 levels increased and cardiac PCr/ATP decreased with NYHA class, however, demonstrated no relationship to each other. In skeletal muscle, maximal rates of oxidative ATP synthesis (Q_{max}) related to functional capacity. Skeletal muscle UCP3 levels increased with NYHA class but were unrelated to skeletal muscle Q_{max}. Tissue respiration experiments revealed no relationship between ventricular function and indices of mitochondrial coupling, furthermore, indices of mitochondrial coupling were unrelated to tissue UCP3 levels. No evidence was found to support mitochondrial uncoupling, mediated through UCP3, as a cause of the abnormalities in cardiac and skeletal muscle high energy phosphate metabolism.

Acknowledgements

There are many people who deserve thanks for enabling me to complete this research. Without the willing selflessness of the patients who gave up their time to take part I would have no data to present, and so to them I offer my heartfelt thanks and hope that I was able to make their stay in the John Radcliffe Cardiothoracic ward a little bit more tolerable.

I owe a large debt of gratitude to my supervisors Kieran Clarke and Rhys Evans who gave me this opportunity and then guided me through to its conclusion. Without their wisdom and support this research would not have been possible.

I would also like to thank the members of the Cardiac Metabolism Research Group who had to put up with having a medic in the lab! In particular Lowri Cochlin and Damian Tyler, without whose patient teaching and instruction with the magnetic resonance experiments, I would be lost. A big thank you also goes to Lisa Heather whose rigorous approach to laboratory based science will leave a lasting impression on any future research that I do and whose gentle encouragement was pitched at just the right level! Thanks also to Emma Carter who performed the metabolite analyses, ran ELISAs and generally looked after me.

I would like to thank my colleagues and friends at the Oxford Centre for Clinical Magnetic Resonance (OCMR). Thanks to Stefan Neubauer for allowing me the use of his fantastic facility and giving me space to work in his lab. Without the understanding and willingness of the other researchers at the OCMR to help, no-one could get any research done; so a big thank you goes to everyone who came in at the weekend to help me scan: Pete, Joe, Sairia, Vanessa and Banjo.

A particular debt of gratitude goes to Cameron Holloway and Lindsay Edwards in whose footsteps I was lucky enough to follow. Their work in establishing the MR protocols used,

ensured I was able to start without too much delay, and without whose help, not just with the MR, I couldn't have done this. I am also very grateful to Czezary Smigielski, for performing on many of the subjects, and teaching me, transthoracic echocardiography; and also to Dan Lunn, whose guidance on statistical matters was vital.

Finally a special thank you goes to my beautiful wife Olivia who has had to bring up Louis almost single-handedly whilst I've been writing this. Without her unfailing support I would not be where I am today.

Personal contribution

The concept and overall design of the work presented in this thesis was conceived by Professor Kieran Clarke. My personal contribution involved aspects of study design and methodology, application for, and achieving ethics committee and trust research and development approval. I performed all patient recruitment and carried out all pre-operative investigations (often initially under supervision) including clinical history taking, blood sampling and subsequent sample preparation and storage, cardiac MRI, cardiac ^{31}P MRS, skeletal muscle ^{31}P MRS, skeletal muscle NIRS and 6MWT. The MR based experiments were all conducted using protocols designed previously by specialist MR physicists, and used in prior experiments performed by other members of the group. Dr Czezary Smigielski (echocardiography fellow) performed approximately the first 60% of the transthoracic echocardiograms until he left the trust, afterwhich I carried out the remainder (again often supervised by Dr Cameron Holloway - consultant cardiologist).

I collected all operative blood samples and tissue biopsies including subsequent sample preparation and storage and conducted all tissue respiration experiments (initially supervised by Dr Lisa Heather - postdoctoral researcher). Emma Carter performed all plasma sample

assays, including the automated assays for NEFA and glucose, and also performed ELISA on plasma samples. I performed all aspects of immunoblotting including: sample preparation, protein assays, gell casting, electrophoresis, protein transfer, antibody probing and exposure (supervised by Dr Lisa Heather and Dr Lindsay Edwards - postdoctoral researchers). I performed the data analysis with statistical advice from Dr Dan Lunn of the Oxford University Department of Statistics consultancy service. Lastly, I wrote the thesis presented here. This work was externally reviewed and funded by the British Heart Foundation.

Presentations and publications arising from this work

Presentations arising from this work

Energetic and functional abnormalities in human heart failure are associated with increased ventricular and skeletal muscle mitochondrial uncoupling protein-3 levels. Poster presentation. AHA scientific sessions. Orlando, USA 2011.

Mitochondrial Uncoupling Proteins and Energetics in Human Heart and Skeletal Muscle. Oral presentation. GAT annual scientific meeting. Cardiff, UK 2010. President's medal and Registrars' prize - winner.

Metabolic Control of Energetics in Human Heart and Skeletal Muscle. Poster presentation. NIAA study day. London, UK 2010. President's award for outstanding achievement - runner-up.

Published abstracts arising from this work

Andrew W Johnson, Cameron Holloway, Lindsay Edwards, Chandi Ratnatunga, Ravi Pillai, Stefan Neubauer, Rhys Evans, Kieran Clarke. Energetic and Functional Abnormalities in Human Heart Failure are Associated with Increased Ventricular and Skeletal Muscle Mitochondrial Uncoupling Protein-3 Levels. *Circulation*. 2011; 124:A15021

A. Johnson, C. Holloway, L. Edwards, L. Heather, L. Cochlin, D. Taggart, C. Ratnatunga, R. Pillai, R. Evans and K. Clarke. Mitochondrial Uncoupling Proteins and Energetics in Human Heart and Skeletal Muscle. *Anaesthesia.* 2011;66(1):69

Contents

INDEX OF FIGURES

INDEX OF TABLES

ABBREVIATIONS

ADP	Adenosine diphosphate
AMP	Adenosine monophosphate
ANT	Adenine nucleotide transporter
AS	Aortic stenosis
ATP	Adenosine triphosphate
AVR	Aortic valve replacement
BAT	Brown adipose tissue
BME	β-mercaptoethanol
BMI	Body mass index
BNP	B-type natriuretic peptide
CAD	Coronary artery disease
CONSORT	Consolidated standards of reporting trials
CS	Citrate synthase
CSI	Chemical shift imaging
CK	Creatine kinase
CO	Cardiac output
DCM	Dilated cardiomyopathy
ECG	Electrocardiograph
ECL	Enhanced chemiluminescence
EGTA	Ethylene glycol tetra-acetic acid

ELISA	Enzyme-linked immunosorbent assay
ETC	Electron transport chain
$FADH_2$	Flavin adenine dinucleotide (reduced)
FCCP	carbonyl cyanide p-trifluoromethoxyphenylhydrazone
FID	Free induction decay
GDP	Guanosine diphosphate
GLUT4	Glucose transporter-4
Hb	Haemoglobin
HCM	Hypertrophic cardiomyopathy
HEP	High energy phosphate
HR	Heart rate
IQR	Interquartile range
JT	Jonkheere-Terpstra
αKGD	α-ketoglutarate dehydrogenase
LBM	Lean body mass
LV-EDV	Left ventricular end-diastolic volume
LVEF	Left ventricular ejection fraction
MCAD	Medium chain acyl-CoA dehydrogenase
MDMA	Methylene dioxymetamphetamine
MOPS	Morpholinepropanesulphate
MR	Mitral regurgitation
MRI	Magnetic resonance imaging

mRNA	Messenger ribonucleic acid
MRS	Magnetic resonance spectroscopy
MW	Mann-Witney U test
NADH	nicotine adenine dinucleotide (reduced)
NEFA	Non-esterified fatty acid
NIRS	Near-infrared spectroscopy
NOE	Nuclear Overhauser effect
NYHA	New York Heart Association
PCr	Phosphocreatine
Pi	Inorganic phosphate
PPARα	Peroxisome proliferator-activated receptor-α
Q_{max}	Theoretical maximal rate of ATP production
RCR	Respiratory control ratio
RF	Radio frequency
ROS	Reactive oxygen species
SD	Standard deviation
SEM	Standard error of the mean
SDS	Sodium dodecyl sulphate
SmO_2	Muscle oxygen saturation
SNR	Signal-to-noise ratio
SSFP	Steady-state free precession
SV	Stroke volume
T1DM	Type 1 diabetes mellitus

T2DM	Type 2 diabetes mellitus
Tris	2-amino-2-(hydroxymethyl)propane-1,3-diol
TTE	Transthoracic echocardiography
UCP3	Mitochondrial uncoupling protein-3
6MWT	Six minute walk test

CHAPTER 1

INTRODUCTION

1.1. Background

Despite optimal current therapy, heart failure is a progressive disease with a poor prognosis and an annual mortality of almost 40% from initial diagnosis (Cowie, Wood *et al* 2000). The implication of this observation is that the fundamental cellular and molecular mechanisms involved in the pathogenesis of the disease are not being addressed. With improving survival rates following acute myocardial infarction, the prevalence of heart failure is likely to increase (Gajarsa and Kloner 2011). The annual inpatient cost to the National Health Service was estimated to be in the region of £400 million in 2000/2001 (British Heart Foundation 2010) and so improvements in treatment are likely to have a significant economic impact. A greater understanding of the underlying pathophysiology of heart failure is required to enable future therapeutic advances.

For many years it has been demonstrated that in heart failure there are abnormalities in energy metabolism, not just in the heart, but also in skeletal muscle. Such abnormalities may underlie many of the symptoms associated with heart failure, but the underlying mechanisms are still elusive. There is also evidence that the metabolic changes which occur in heart failure may be amenable to therapeutic manipulation, with improvements in cardiac function (Lee, Campbell *et al* 2005). In particular, a great deal of interest is now directed at the mitochondrion, the source of most of the energy required for muscle contraction.

1.2. Heart Failure

Heart failure denotes an inability of the heart to maintain adequate tissue perfusion, and has been defined by the European Society of Cardiology as "a clinical syndrome in which patients have the following features: symptoms typical of heart failure – breathless at rest or on exercise, fatigue, tiredness, ankle swelling; and signs typical of heart failure – tachycardia, tachypnoea, pulmonary rales, pleural effusion, raised jugular venous pressure, peripheral oedema, hepatomegaly; and objective evidence of a structural or functional abnormality of the heart at rest" (Dickstein, Cohen-Solal *et al* 2008).

Epidemiology and aetiology of heart failure

There are ~15 million patients with heart failure in Europe alone. The prevalence of asymptomatic ventricular dysfunction is similar, resulting in ~4% of the population suffering from heart failure or asymptomatic ventricular dysfunction. The prevalence of heart failure rises sharply at 75 years and is estimated to be 10-20% above this age. In younger age groups, men are affected more commonly than women (secondary to coronary artery disease), in the elderly, men and women are affected approximately equally (Dickstein, Cohen-Solal *et al* 2008).

Heart failure can be congenital or acquired. A decrease in the ability of the heart to pump blood can arise from a variety of different mechanisms: damage or loss of heart muscle, acute or chronic ischaemia, increased vascular resistance, or the development of a tachydysrhythmia. By far the most common (~70%) underlying cause of heart failure is coronary artery disease, which can result in damage or loss of myocardium through infarction, or impairment of muscle function through acute or chronic ischaemia. Valve

disease and cardiomyopathies account for approximately 10% each of the remaining initiating diseases (Dickstein, Cohen-Solal *et al* 2008).

Diagnosis

Following clinical assessment of the presence or absence of the symptoms and signs of heart failure, the diagnosis of heart failure relies mainly on the objective evidence of cardiac dysfunction. This is most commonly provided by echocardiography which is able to assess systolic and diastolic function, together with cardiac morphology which may assist in diagnosing the underlying cause. Echocardiography can be used to measure the left ventricular ejection fraction – the proportion of blood in the ventricle at the end of diastole that is ejected from the ventricle during systole (stroke volume/end-diastolic volume). The ejection fraction is altered by changes in ventricular preload and afterload, and so is not a true reflection of contractility; however, it is the most common clinically used index of ventricular systolic function and has prognostic significance (Dickstein, Cohen-Solal *et al* 2008).

It is now well understood that some patients have the symptoms and signs of heart failure with preserved ejection fractions (HFpEF) – or diastolic heart failure, and this may account for 50% of all heart failure patients (Paulus, Tschope *et al* 2007). HFpEF is diagnosed when the following conditions are satisfied: signs or symptoms of heart failure, normal or mildly abnormal systolic function (ejection fraction (EF) >50 % and left ventricular end-diastolic volume index <97 $mL.m^{-2}$) and evidence of left ventricular diastolic dysfunction (LV end-diastolic pressure >16 mmHg, mean pulmonary capillary wedge pressure >12 mmHg or non-invasively using echocardiography - tissue Doppler E/E' >15) (Paulus, Tschope *et al* 2007).

Cardiac magnetic resonance imaging (CMR) is a highly accurate and reproducible method for assessing cardiac function (Longmore, Klipstein *et al* 1985). Cine CMR images can be acquired in slices of known thickness from the base of the ventricle to the apex (see Methods), allowing assessment of cardiac volumes, mass and wall motion for which it has become the gold standard (Pennell 2003). However, its use is limited by cost, availability and patient tolerance.

Radionuclide ventriculography can provide an accurate measure of LVEF and is commonly used to assess myocardial perfusion in order to ascertain myocardial viability or ischaemia. It is of limited value however in assessing cardiac volumes, and more subtle aspects of systolic and/or diastolic function.

Assessment and classification of severity

The symptoms of heart failure do not correlate with the degree of cardiac dysfunction. The severity of heart failure is most often classified using the New York Heart Association functional classification (Appendix 1), which has been shown to be clinically useful, and is employed in most randomised controlled trials (Dickstein, Cohen-Solal *et al* 2008).

Exercise testing provides an objective measure of exercise capacity and exercise-related symptoms. The six minute walk test (6MWT) is simple, reproducible and widely used (Crapo, Casaburi *et al* 2002). The distance walked during six minutes has been shown to correlate with peak oxygen consumption in patients with LV systolic dysfunction (Zugck, Kruger *et al* 2000; Ingle, Goode *et al* 2006). The gold standard measurement for the assessment of exercise capacity in heart failure is peak oxygen consumption during an incremental exercise test with respiratory gas analysis (Balady, Arena *et al* 2010), and this has been shown to provide prognostic information in heart failure (Cohn, Johnson *et al*

1993). To perform accurate and reproducible measurements of peak oxygen consumption requires expertise and specialist equipment. Its use is increasing however, and it may become a key investigation in the diagnosis and assessment of heart failure in the future.

Prognosis

Despite optimal current therapy, heart failure is a progressive disease with an annual mortality of 40% from initial diagnosis (Cowie, Wood *et al* 2000). The reasons underlying heart failure progression are currently unclear, but the suggestion is that the current pharmacological strategy of neurohumoral antagonism is either incomplete, or that disease progression and remodelling occurs independently.

Ventricular remodelling is a process whereby progressive eccentric hypertrophy of the heart occurs. The underlying processes have not been fully elucidated but can be, at least temporarily, interrupted by neurohumoral antagonism (Yusuf, Pitt *et al* 1992). The ventricular wall thickness increases in functional myocardium, as an adaptive response to increased work, and overall myocardial function can initially improve; however, fibrosis and collagen accumulation also occur, with decreases in capillary density. As the hypertrophy progresses, the ventricle changes to a more spherical shape with activation of matrix metalloproteinases (MMP) and breakdown of the extra-cellular matrix, resulting in wall thinning and further contractile dysfunction (Mann, Bogaev *et al* 2010). This final common pathway of wall thinning and dilatation has led to an appreciation that measuring ventricular volumes rather than the ejection fraction may have greater prognostic significance (Vasan, Larson *et al* 1997). As well as geometric remodelling the myocardium undergoes changes in calcium handling, perfusion and substrate metabolism (see later sections). All of these processes result in progression of heart failure.

1.3. Overview of muscle bioenergetics

Muscle contraction, together with protein synthesis and the maintenance of ionic gradients, requires a source of energy. This energy is provided by the breakdown of adenosine triphosphate (ATP) (Figure 1.1) to adenosine diphosphate (ADP) and inorganic phosphate (Pi, HPO_4^{2-}) as in the following reaction:

$$MgATP^{2-} + H_2O \leftrightharpoons MgADP^{-} + Pi^{2-} + H^{+}$$

This reaction is associated with a free energy change (ΔG) of -30.5 $KJ.mol^{-1}$ (under standard conditions) (Ingwall 1999), and the energy released can be coupled to other reactions, such as cross bridge cycling in muscle, allowing them to proceed, when otherwise they would be thermodynamically unfavourable.

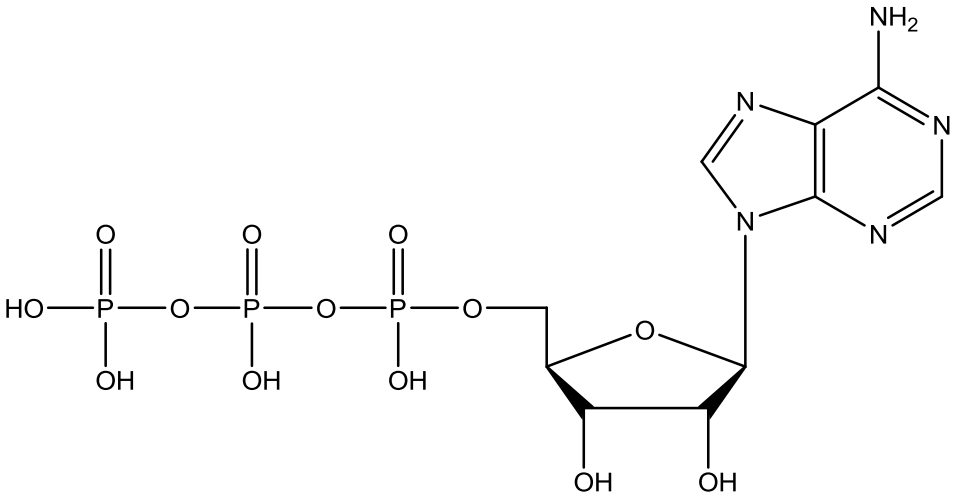

Figure 1.1. The chemical structure of adenosine triphosphate.

The *actual* amount of energy available from ATP hydrolysis can be calculated by correcting the ΔG° (ΔG under standard conditions of temperature and concentration) for the actual concentrations of ATP, ADP and Pi:

$$\Delta G = \Delta G^{\circ} - RT.\ln\left\{\frac{[ATP]}{[ADP].[Pi]}\right\}$$

where R is the universal gas constant and T is the absolute temperature (Ingwall 1999).

In the physiological situation where temperature varies very little, the energy released from the hydrolysis of ATP depends upon the concentrations of the reactants and products i.e. [ATP] / [ADP].[Pi], and this term is known as the "phosphorylation potential" (Kemp and Radda 1994).

The energy required for myosin ATPase to function normally (the energy consuming component of muscle contraction), is almost as great (in terms of magnitude) as the physiological ΔG for ATP breakdown (Wolcott and Boyer 1974). Consequently, decreases in [ATP] and increases in [ADP] and [Pi] will ultimately result in impaired myosin ATPase function and impaired force generation (Kammermeier, Schmidt *et al* 1982).

Oxidative phosphorylation and ATP synthesis

The mitochondrion is the organelle which synthesises the vast majority of ATP by oxidative phosphorylation. This is the process by which electrons from reduced nicotine adenine dinucleotide (NADH) and flavin adenine dinucleotide ($FADH_2$), substances produced from the metabolism of carbohydrates and fats, are transferred through the electron transport chain

in a series of coupled reduction and oxidation (redox) reactions. These reactions take place in the inner mitochondrial membrane and involve complexes 1-4 of the electron transport chain, with the electrons finally reducing oxygen to water. Associated with these redox reactions at complexes 1, 3 and 4 is the extrusion of protons from the inside of the mitochondrial matrix to the inter-membrane space, with the establishment of an electrochemical proton gradient (Δp) across the inner-mitochondrial membrane. The proton gradient is comprised of a membrane potential ($\Delta\psi$) and a pH gradient (ΔpH) (Brown 1992). Protons are able to return, down the electrochemical gradient, to the matrix via either facilitated proton leak through the membrane, or via ATP synthase. ATP synthase is the enzyme which couples the energy available from the proton translocation, to ATP synthesis within the matrix (Figure 1.2).

As ATP and ADP are negatively charged ions at physiological pH, they are unable to freely cross the inner-mitochondrial membrane, resulting in a fixed purine pool within the matrix. It is necessary however for ATP to leave the matrix and be delivered to ATPases within the cytosol and similarly for the resulting ADP to be returned to the matrix for rephosphorylation back to ATP. This exchange is accomplished by the adenine nucleotide transporter (ANT), the most abundant mitochondrial protein (Klingenberg 1979). ANT shuttles ATP out of the matrix and ADP into the matrix in a ratio of 1:1. The ANT operates in such a way that, within the matrix where ATP synthesis takes place, the ATP/ADP ratio is kept low (to promote ATP synthesis), and outside the matrix where ATP consumption takes place, the ATP/ADP ratio is high (to promote ATP breakdown).

ADP and ATP transport in and out of the matrix is controlled to match the requirements of oxidative phosphorylation by the same mechanism driving the synthesis of ATP: the proton

gradient across the inner mitochondrial membrane. This is able to control the ANT because of the charge difference between ATP^{4-} and ADP^{3-}. In order to maintain electroneutrality a proton is transferred across the inner-mitochondrial membrane with ATP. Therefore, when the proton gradient Δp is low (as occurs in high rates of ATP synthesis), export of ATP and import of ADP is facilitated (Pfaff and Klingenberg 1968).

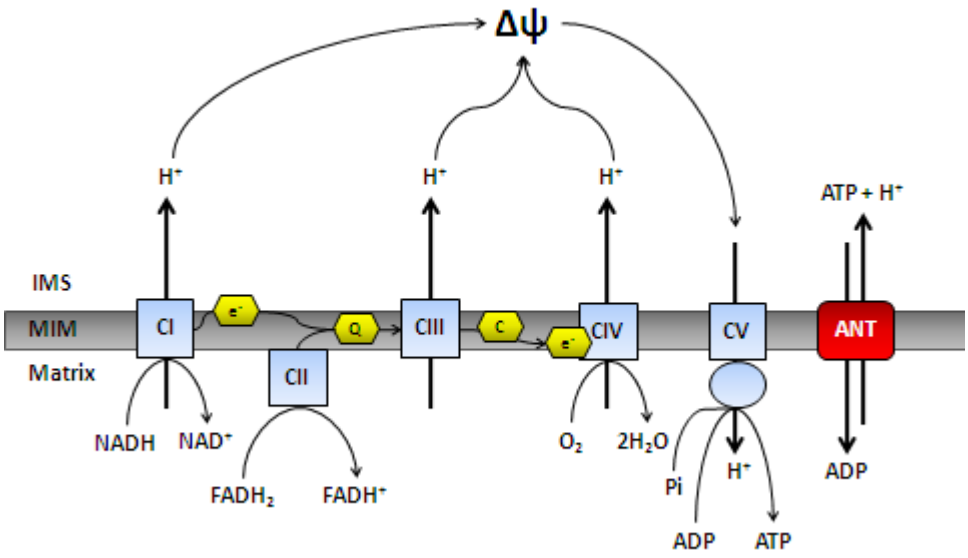

Figure 1.2. Schematic diagram of the mitochondrial inner membrane showing the electron transport chain and adenine nucleotide transporter.

IMS – inter-membrane space, MIM – mitochondrial inner membrane, $\Delta\psi$ – membrane potential, CI – CIV – complexes 1 – 4 of the electron transport chain, CV – complex 5 or ATP synthase, ANT – adenine nucleotide transporter, e^- - electrons, Q – coenzyme Q, C – cytochrome C, NADH – nicotine adenine dinucleotide (reduced), NAD^+ – nicotine adenine dinucleotide (oxidised), $FADH_2$ – flavin adenine dinucleotide (reduced), $FADH^+$ – flavin adenine dinucleotide (oxidised), Pi – inorganic phosphate, ADP – adenosine diphosphate, ATP – adenosine triphosphate.

Creatine and adenylate kinase

In muscle, the demand for ATP can vary suddenly and greatly, yet intracellular [ATP] remains remarkably constant. This is achieved principally by two enzymes: creatine kinase and adenylate kinase.

Creatine kinase catalyses the rapid and reversible transfer of a phosphate group from ATP to creatine (Cr) making phosphocreatine (PCr).

$$MgATP^{2-} + Cr \overset{CK}{\leftrightharpoons} PCr^{2-} + MgADP^{-} + H^{+}$$

CK – creatine kinase

Phosphocreatine (Figure 1.3) acts as a temporal and spatial energy buffer. At the onset of muscle contraction in skeletal muscle, or an acute increase in cardiac work, PCr is quickly broken down, resulting in a rapid source of ATP.

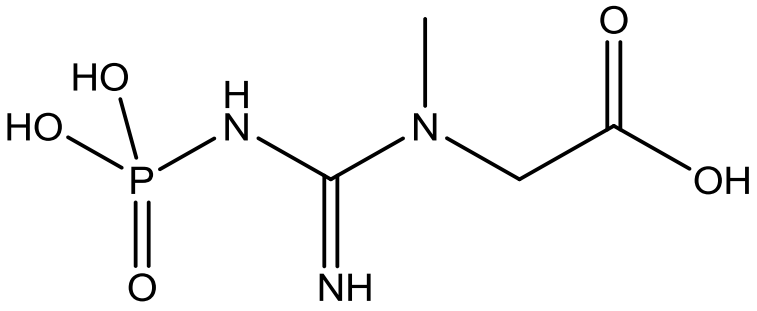

Figure 1.3. The chemical structure of phosphocreatine.

The creatine kinase system can only support ATP concentrations for a very short time and so to maintain increased ATP consumption, glycolysis and oxidative phosphorylation must be increased. Phosphocreatine also acts as a spatial energy shuttle, whereby sequences of CK catalysed reactions occur hand-in-hand to deliver ATP to sites of ATP consumption in the cytosol (Figure 1.4) (Neubauer 2007). By operating in this way, creatine kinase plays a major role in the control of compartmental ADP concentration. This is important in order to keep [ADP] high in the matrix to stimulate oxidative phosphorylation and to keep [ADP] low in the cytosol to preserve cytosolic ATPase function. Thirdly, by controlling [ADP], CK has a role in preventing detrimental purine loss from the cell (see below) (Wallimann, Wyss *et al* 1992).

Adenylate kinase also functions to support [ATP] by catalysing the transfer of a phosphate group, in this case from one ADP to another ADP, resulting in ATP and adenosine monophosphate (AMP):

$$2\mathrm{MgADP}^{-} \overset{\mathbf{AK}}{\leftrightharpoons} \mathrm{MgATP}^{2-} + \mathrm{AMP}^{2-} + \mathrm{Mg}^{2+}$$

AK – adenylate kinase.

Using this reaction to support [ATP] is, however, not without cost. AMP is further broken down to inositol monophosphate (IMP) which, along with AMP is dephosphorylated by 5'-nucleotidase to adenine and inosine which are free to leave the cell. In this way, use of the adenylate kinase system to support [ATP] leads to cellular purine loss (Wallimann, Wyss *et al* 1992).

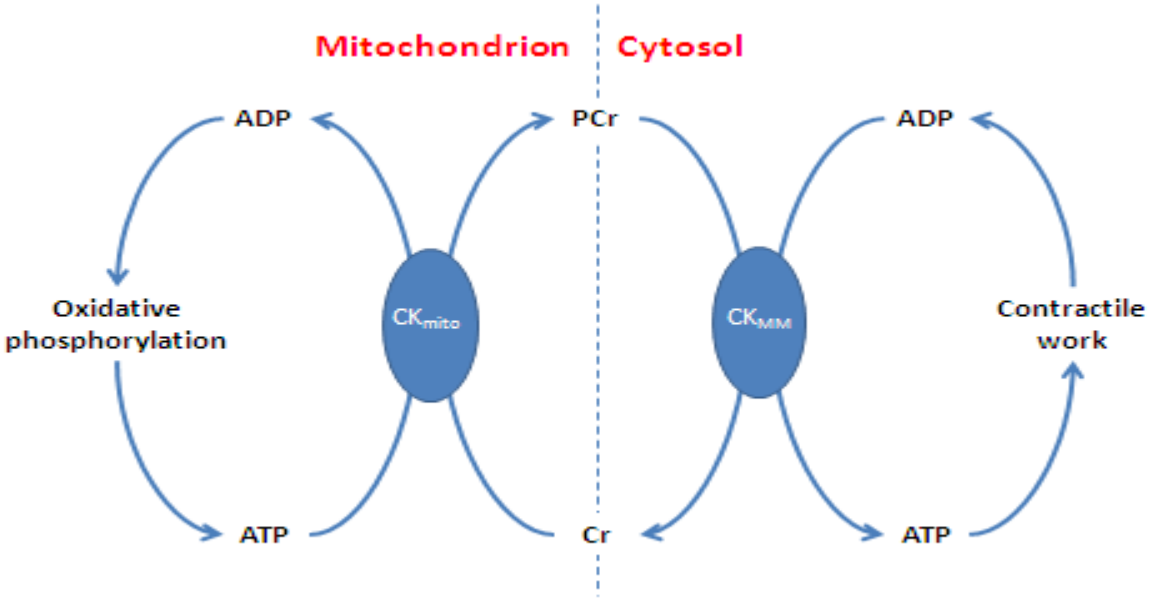

Figure 1.4. The Creatine Kinase Shuttle.

The enzyme creatine kinase acts as to deliver ATP to the cytosolic ATPases and ADP to the mitochondrial ATP synthase thereby maintaining optimal ΔG at both.

ADP – adenosine diphosphate, ATP – adenosine triphosphate, PCr – phosphocreatine, Cr – creatine, CK_{mito} – mitochondrial creatine kinase, CK_{MM} – cytosolic muscle sub-type creatine kinase.

1.4. ^{31}P Magnetic resonance spectroscopy

^{31}P Magnetic resonance spectroscopy (MRS) is a non-invasive method for measuring the concentrations of phosphorus-containing metabolites within a tissue of interest *in vivo*. Whilst not without its limitations, the non-invasive nature of the method makes it possible to perform repeated measurement of the same tissue, enabling the effect of an intervention on energetic processes to be investigated, therefore making it a powerful technique. ^{31}P MRS makes use of the odd number of protons within the phosphorus nucleus which give it a "non-zero" nuclear spin and a magnetic moment. Therefore, when exposed to an external magnetic field, the phosphorus nuclei will align within the field. Radiofrequency (RF) pulses of the appropriate frequency applied to the sample will be absorbed by the nuclei which, upon termination of the RF pulse, will return to their equilibrium state in the magnetic field, accompanied by the release of energy. The energy released can be represented graphically in the frequency domain as the free induction decay (FID). Fourier transformation of the FID renders a spectrum – essentially a frequency/intensity plot (Hudsmith and Neubauer 2008).

A number of different phosphorus-containing compounds can be resolved in tissue using ^{31}P MRS. This is possible because the electromagnetic effects of surrounding nuclei, and their orientation in space, results in PCr resonating at a slightly different frequency to that of γ-ATP (γ refers to the third phosphate group of ATP), a phenomenon termed chemical shift (Figure 1.5) (Beer 2004). The concentration of each metabolite within the tissue is proportional to the area under the respective peak. Absolute quantification of metabolite concentrations is possible, but requires the use of internal or external references of known volume and concentration, and the application of correction factors for differences in coil

sensitivity and magnetic field between the reference and the sample (Bottomley 2009). These difficulties are avoided by expressing the metabolites as ratios of each other e.g. PCr/ATP.

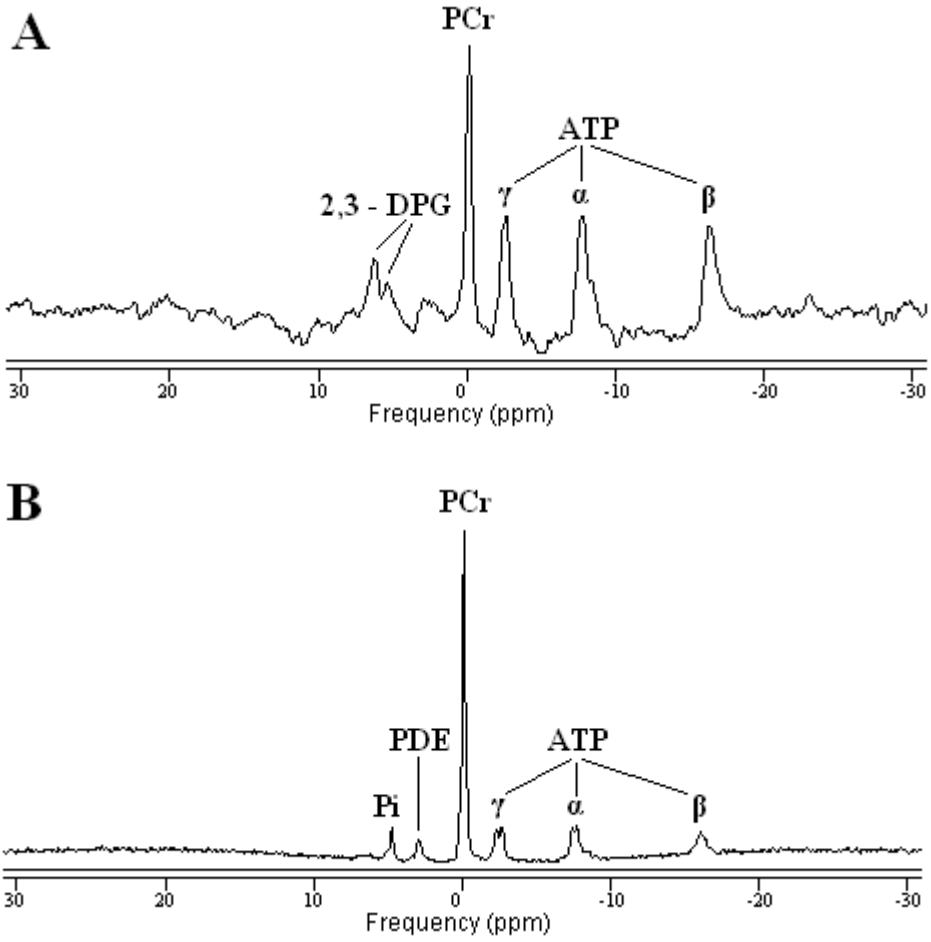

Figure 1.5. ^{31}P Nuclear magnetic resonance spectrum acquired at 3 Tesla.

A – Human myocardium. B – Human gastrocnemius muscle.

It is possible to resolve phosphocreatine (PCr) and three ATP peaks in both myocardium and skeletal muscle. The inorganic phosphate (Pi) peak is obscured by 2,3 – diphosphoglycerate (2,3 – DPG) in myocardium arising from ventricular blood.

PDE – phosphodiesters.

The main limitation of ^{31}P MRS is the low concentration of phosphorus-containing metabolites *in vivo,* resulting in low signal/noise ratios (SNR). The SNR for ^{31}P MRS is ~2,000,000 times less than that achieved by ^{1}H MRS of tissue water in the same volume at the same field strength (Bottomley 2009). This results in ^{31}P MRS having poorer spatial resolution and necessitates longer scan times. Spectra with the quality of Figure 1.4.A can, however, be obtained at 3 Tesla in approximately half an hour (making it clinically feasible), from a volume of ~50 cm^3 (i.e. without too much signal contamination from surrounding structures). In the case of skeletal muscle, the requirement for small regions of interest is less because of the large size and relative homogeneity of the tissue. Therefore the technique is generally not thought of as SNR-limited and it is possible to acquire spectra of reasonable quality in only 5 seconds, enabling accurate measurement of metabolites during exercise and recovery.

There are further differences in the spectra that are obtained from the myocardium or from skeletal muscle. Predominantly, this is due to contamination of the volume of interest (voxel) with blood within the heart, resulting in the Pi resonance being obscured by 2,3–diphosphoglycerate (2,3–DPG) arising from red blood cells. The blood contamination causes an artefactual lowering of the PCr/ATP ratio, as red blood cells contain ATP but not PCr. A correction factor can, however, be applied to allow for this, determined by the size of the 2,3–DPG peaks (Neubauer, Krahe *et al* 1992).

The ability to resolve Pi in skeletal muscle enables estimation of the intracellular pH, as the chemical shift (position in the spectrum) of Pi is pH-dependant (Taylor, Bore *et al* 1983). Knowledge of the pH allows derivation of the free [ADP] by rearranging the creatine kinase equilibrium:

$$[ADP] = \frac{[ATP][Cr]}{[PCr][H^+]K}$$

ADP – adenosine diphosphate, ATP – adenosine triphosphate, Cr – creatine (found by subtracting PCr concentration from an assumed total creatine concentration of 42.5 $mmol.L^{-1}$), PCr – phosphocreatine, K – creatine kinase equilibrium constant (1.7×10^6 $L.mmol^{-1}$) (Kemp and Radda 1994).

1.5. Cardiac ^{31}P MRS

Using ^{31}P MRS in humans with heart failure, it has been found that, regardless of the aetiology of the heart failure, the ratio of PCr/ATP is decreased (Shivu, Abozguia *et al* 2010; Conway, Allis *et al* 1991; de Roos, Doornbos *et al* 1992; Neubauer, Krahe *et al* 1992; Conway, Bottomley *et al* 1998; Beyerbacht, Lamb *et al* 2001). The PCr/ATP ratio has also been shown to predict mortality in heart failure better than the left ventricular ejection fraction (EF) and the NYHA classification (Neubauer, Horn *et al* 1997). The significance of a low PCr/ATP ratio is that, as [ATP] remains constant, [ADP] must increase, resulting in a decrease in the phosphorylation potential and ΔG. There has, however, been much controversy in the literature over the temporal sequence of events, specifically whether energetic dysfunction precedes contractile dysfunction, or *vice-versa* (Vogt and Kubler 1998).

Dilated Cardiomyopathy

Much of the human ^{31}P MRS work investigating heart failure has used dilated cardiomyopathy (DCM) as a disease model. DCM is a good choice for MRS studies as the myocardium is affected globally, which overcomes some of the problems with spatial localisation. It has been found that the myocardial PCr/ATP ratio is lower in patients with DCM compared with controls (Hardy, Weiss *et al* 1991; de Roos, Doornbos *et al* 1992; Neubauer, Krahe *et al* 1992; Neubauer, Horn *et al* 1997) and correlates with heart failure severity measured by the New York Heart Association (NYHA) functional classification (Appendix 1), but not with ejection fraction (EF) (Neubauer, Krahe *et al* 1992). One study did not show a decrease in PCr/ATP (de Roos, Doornbos *et al* 1992) but this may have been

as a result of large amounts of blood contamination in the voxel which is a potential problem with DCM patients as the ventricles are thin walled (Bottomley 2009).

In DCM, cardiac PCr/ATP ratio was found to be a better predictor of cardiovascular and all-cause 5-year mortality than EF or NYHA class (Neubauer, Horn *et al* 1997), demonstrating that it is perhaps a more fundamental measure of the underlying pathology than functional measures.

Hypertrophic cardiomyopathy and aortic stenosis

In a similar way to DCM, cardiac hypertrophy is associated with decreased myocardial PCr/ATP ratio compared with controls (Shivu, Abozguia *et al* 2010; de Roos, Doornbos *et al* 1992; Beyerbacht, Lamb *et al* 2001; Smith, Bottomley *et al* 2006). However, an association with the severity of cardiac failure is less clear. Again, an association with NYHA class was shown in one study (Neubauer, Horn *et al* 1997), and in another, PCr/ATP correlated with measures of diastolic function (early acceleration and early deceleration peaks corrected for cardiac output, measured by MRI) (Beyerbacht, Lamb *et al* 2001). Both of these studies were in patients with aortic stenosis (AS). Other investigators did not find a relationship between cardiac function and PCr/ATP (Smith, Bottomley *et al* 2006). The metabolic changes in hypertrophy are not the same as those in dilated cardiomyopathy, and myocardial ischaemia is also present, particularly in sub-endocardial regions, so perhaps it is not surprising to see differences in the way PCr/ATP relates to disease progression. PCr/ATP has been shown to recover to normal following aortic valve replacement in patients with AS, with corresponding improvement in diastolic function (Beyerbacht, Lamb *et al* 2001).

Coronary artery disease

A number of studies have used ^{31}P MRS to investigate phosphate metabolism in coronary artery disease (CAD) (Weiss, Bottomley *et al* 1990; Neubauer, Krahe *et al* 1992; Yabe, Mitsunami *et al* 1995; Beer, Sandstede *et al* 2000; Beer, Machann *et al* 2007). CAD is not ideally suited to investigation with MRS due to its heterogeneous nature, with regions of myocardium potentially infarcted, stunned, hibernating, failing or normal, each potentially having different metabolic profiles. Infarcted tissue is presumed to have a minimal PCr or ATP content. Multi-voxel type MRS protocols are more suited to studying CAD as they have the potential to study different myocardial regions simultaneously.

Two studies demonstrated normal cardiac PCr/ATP ratios at rest, which decreased in myocardium supplied by a stenotic vessel during hand-grip exercise (Weiss, Bottomley *et al* 1990; Yabe, Mitsunami *et al* 1994). In one study the defect resolved after revascularisation (Weiss, Bottomley *et al* 1990), in the other, it corresponded to reversible ischaemia demonstrated with ^{201}Tl scintigraphy (Yabe, Mitsunami *et al* 1994). A third study looked only at resting cardiac PCr/ATP in patients with coronary stenosis and found normal values (Neubauer, Krahe *et al* 1992), though the patients did not have clinical heart failure.

More recently, multi-voxel techniques have been used to study different regions of myocardium (infarcted and non-infarcted) simultaneously, showing that PCr/ATP ratios were decreased not only in the infarcted region, but also in remote muscle at 6 months following revascularisation in patients with non-salvageable infarcted muscle (Beer, Machann *et al* 2007). This implies that the "normal" or remote myocardium in patients who have either depressed ventricular function, or compensated remodelled function, has a low PCr/ATP ratio.

Other conditions

The cardiac PCr/ATP ratio has also been studied in other conditions: type 1 diabetes mellitus (T1DM) (Shivu, Phan *et al* 2010), type 2 diabetes mellitus (T2DM) (Scheuermann-Freestone, Madsen *et al* 2003), mitral regurgitation (Conway, Bottomley *et al* 1998) and heart failure with preserved ejection fraction (HFpEF) (Phan, Abozguia *et al* 2009). In all cases, PCr/ATP was lower in patients than in controls. In the mitral regurgitation study, the cardiac PCr/ATP was related to measures of disease severity and ventricular function (Conway, Bottomley *et al* 1998). In both diabetes studies, subjects were asymptomatic and had normal ventricular function. Moreover it was found that there was no relationship between PCr/ATP and the degree of coronary microvascular obstruction (Shivu, Phan *et al* 2010), implying a metabolic rather than a perfusion cause for the decreased ratios. Cardiac PCr/ATP also correlated negatively with plasma non-esterified fatty acids (NEFA) (Scheuermann-Freestone, Madsen *et al* 2003), perhaps suggesting a role for lipid metabolism in the generation of energetic impairment.

To summarise, decreased cardiac PCr/ATP ratios have been found in cardiac dilation and volume overload (DCM and mitral regurgitation) and would appear to be related to disease severity, with lower ratios found in more severe disease. Decreased cardiac PCr/ATP has also been demonstrated in hypertrophic and pressure overload conditions (HCM and AS), but its relationship to cardiac function in this setting is less clear, although it has been shown to relate to the NYHA functional classification. Very few studies have attempted to show a mechanism underlying the decrease in cardiac PCr/ATP, although in CAD a clear potential mechanism (ischaemia) exists. Patients with DM have decreased cardiac PCr/ATP which precedes impairment in LV function, suggesting that, at least in diabetic cardiomyopathy,

energetic failure may occur before, and therefore be part of, the pathogenesis of overt contractile failure. There is further evidence of energetic abnormalities preceding cardiac dysfunction from animal studies, where the CK system has been manipulated (Tian, Christe *et al* 1997; Tian 1998; Wallis, Lygate *et al* 2005) or in adriamycin-induced cardiomyopathy (Maslov, Chacko *et al* 2010).

1.6. Skeletal muscle ^{31}P MRS

^{31}P MRS has also been used to investigate skeletal muscle in patients with heart failure. It is well established that heart failure is associated with a decrease in exercise capacity, with early fatigue and skeletal muscle weakness (Middlekauff 2010; Poole-Wilson and Ferrari 1996). The original hypothesis for this phenomenon was that it was related to the inability of the heart to augment the cardiac output during exercise, resulting in skeletal muscle hypoperfusion, but this view has been challenged by evidence that skeletal muscle metabolic derangement does not relate to blood flow, and hence substrate and oxygen delivery, measured directly (Massie, Conway *et al* 1987), and more recently with a combination of ^{31}P MRS and near-infrared spectroscopy (NIRS) (Hanada, Okita *et al* 2000). These studies suggest that there is an intrinsic energetic dysfunction of skeletal muscle in heart failure, possibly mitochondrial in nature. In patients with heart failure, skeletal muscle MRS has shown increased PCr consumption and decreased pH during aerobic exercise (Massie, Conway *et al* 1987; Massie, Conway *et al* 1988; Kemp, Thompson *et al* 1996; Hanada, Okita *et al* 2000), a high resting [Pi] (Massie, Conway *et al* 1987) and prolonged PCr recovery times following exercise compared with controls (Kemps, Prompers *et al* 2010; Massie, Conway *et al* 1987; Massie, Conway *et al* 1988; Kemp, Thompson *et al* 1996;

Hanada, Okita *et al* 2000). These findings are all indicative of a failure of oxidative ATP synthesis, but shed no light on the underlying cause of the defect. To investigate this further, NIRS has been used in conjunction with MRS.

Near-infrared spectroscopy

NIRS makes use of the differential absorption of light in the near-infrared region, between oxy- and deoxyhaemoglobin. Using two wavelengths, one at ~800 nm (the isobestic point) to determine total haemoglobin (Hb), and one at another wavelength, e.g. ~760 nm, to determine Hb or HbO_2 (depending on the frequency), measurement of the oxygen saturation of a region of tissue underlying the sensor is possible (Madsen and Secher 1999). The depth of tissue penetration is determined by the distance between the emitting and sensing diodes, and in this way, contamination of the signal by skin and subcutaneous tissue can be avoided (Hamaoka, McCully *et al* 2007). Near-infrared light absorption is related to Hb concentration by Beer and Lambert's law (Owen-Reece, Smith *et al* 1999). As photon absorption is dependent on the "thickness" of the solution, NIRS absorption changes reflect the oxygenation in small vessels – arterioles, capillaries and venules, as photons are unable to traverse larger vessels (Mancini, Bolinger *et al* 1994). As the arteriolar oxygen saturation (Sa_{O2}) remains constant (assuming no change in inspired oxygen concentration and pulmonary diffusion capacity), a NIRS signal change is proportional to the change in S_{O2} in the venules. Regional S_{O2} therefore reflects the overall balance between oxygen supply and oxygen consumption and, following the termination of exercise in a muscle, the rate of change is related to oxygen delivery (and ongoing mitochondrial oxygen consumption).

Studies using a combination of ^{31}P MRS and NIRS to investigate PCr and SmO_2 (muscle oxygen saturation) kinetics in heart failure have shown that muscle PCr re-synthesis times

and re-oxygenation times are both prolonged in heart failure patients compared with controls (Kemps, Prompers *et al* 2010; Hanada, Okita *et al* 2000). Controversy exists, however, in how the two variables relate to each other. Hananda *et al* examined cardiac patients and demonstrated a much greater increase in PCr re-synthesis time than re-oxygenation time in the heart failure group, and concluded that O_2 delivery was therefore not limiting PCr re-synthesis (Hanada, Okita *et al* 2000), whereas Kemps *et al* showed that re-oxygenation was much slower than PCr re-synthesis, and consequently concluded that O_2 delivery was the limiting factor (Kemps, Prompers *et al* 2010). This difference is probably explained by the use of different exercise protocols resulting in different end-exercise conditions, such as intracellular pH, which is well known to affect PCr recovery times (Jubrias, Crowther *et al* 2003).

The problem with the interpretation of NIRS data is that a delay in re-oxygenation could theoretically be attributable to excessive oxygen consumption (e.g. due to mitochondrial inefficiency), and not necessarily to inadequate oxygen supply. Studies combining MRS and NIRS in heart failure are so far inconclusive in helping to determine whether skeletal muscle dysfunction is secondary to intrinsic mitochondrial dysfunction or a failure of O_2 delivery.

1.7. Metabolic substrate oxidation in heart failure

Mitochondrial ATP production is fundamentally influenced by substrate metabolism, which changes in heart failure. When the heart fails there are a number of neurohumoral responses that occur, including an increase in sympathetic drive, which results in increased adipose tissue lipolysis and increased plasma NEFA concentrations (Paolisso, Gambardella *et al* 1994; Lommi, Kupari *et al* 1998). Corresponding to this increase in plasma NEFA

concentration, an increase in myocardial lipid oxidation might be expected and has been found to occur in some studies (Paolisso, Gambardella *et al* 1994; Lommi, Kupari *et al* 1998; Taylor, Wallhaus *et al* 2001), but not in others (Davila-Roman, Vedala *et al* 2002). Discrepancies of this kind are likely explained by the dynamic nature of the disease progression, with subjects having heart failure at different stages and being treated with different therapeutic agents.

Studies in animal models have generally shown that gross changes in substrate metabolism occur relatively late in the disease process, at around the point of cardiac decompensation, and involve down-regulation of metabolic machinery for lipid oxidation and subsequently an increased reliance on glucose metabolism (Osorio, Stanley *et al* 2002; Chandler, Kerner *et al* 2004; Lei, Lionetti *et al* 2004). These changes have a theoretical benefit in the later stages of heart failure, as oxygen supply may become limited. Glucose is a more efficient substrate in terms of oxygen usage (3.17 ATP per oxygen atom) compared with fatty acid (palmitate – 2.80; oleate – 2.82 ATP per oxygen atom) (Ashrafian, Frenneaux *et al* 2007) and can generate ATP entirely anaerobically through substrate-level phosphorylation in glycolysis. Fatty acid oxidation may be associated with even greater oxygen cost due to uncoupling of oxidative phosphorylation (see later).

Studies of mitochondrial respiration in human heart failure are relatively rare due to difficulties in obtaining tissue biopsies of sufficient size to isolate the required mitochondria. The problem of biopsy size has been partly overcome by the technique of muscle fibre permeabilisation (Kuznetsov, Veksler *et al* 2008). Saponins are naturally occurring detergent-like substances that selectively "permeabilise" the cell membrane, leaving the organelles intact. This occurs because of the difference in cholesterol content between the

sarcolemma and the membranes surrounding the internal organelles. In this way, the mitochondria become accessible to compounds that would normally be unable to cross the cell membrane (e.g. ADP). The advantages of this technique are that the mitochondria remain in an intact intracellular environment where their interaction with other organelles remains and, perhaps more importantly, much smaller quantities of tissue are required (~500 mg of tissue necessary for mitochondrial isolation, but only ~5 mg required for the *in-situ* technique) (Kuznetsov, Veksler *et al* 2008). The main disadvantage is that because functional ATPases remain in the cytosol, estimation of the amount of ATP formed per oxygen atom (P/O ratio) from a given amount of ADP is impossible, because the ADP is continually recycled by the ATPases.

Sharov *et al* reported decreased oxygen consumption under ADP stimulation using the *in-situ* method on human left ventricular biopsies from patients with end-stage cardiac failure undergoing transplantation, compared with unused donor normal hearts (Sharov, Todor *et al* 2000). A study on skeletal muscle (vastus lateralis) biopsies, comparing heart failure patients with normal sedentary and normal active controls, found similar maximal oxygen consumption between heart failure patients and sedentary controls, with only the active controls having higher maximal oxygen consumption; they did report differences in mitochondrial protein levels, with heart failure patients having less citrate synthase and creatine kinase, along with decreased lactate dehydrogenase activity (Mettauer, Zoll *et al* 2001).

Animal studies have also shown a decrease in mitochondrial respiration in heart failure compared with controls (Hoppel, Tandler *et al* 1982; Sanbe, Tanonaka *et al* 1993; Sharov, Goussev *et al* 1998) indicating mitochondrial dysfunction, but the underlying mitochondrial

defects are not clear. Decreases in electron transport chain complex activity have been described but are not consistent. Rapid pacing-induced cardiac failure in dogs demonstrated decreased activity in complexes 3 and 5 (ATP synthase) (Marin-Garcia, Goldenthal *et al* 2001), whereas humans with dilated or ischaemic cardiomyopathy were shown to have decreased complex 1 activity (Scheubel, Tostlebe *et al* 2002) or, in dilated cardiomyopathy only, decreased complex 3 and 4 activity (Buchwald, Till *et al* 1990). What is clear is that in heart failure there is mitochondrial dysfunction, which is borne out as an inability to harness the full chemical energy available from metabolic substrates.

1.8. Mitochondrial uncoupling protein-3

Mitochondrial uncoupling proteins are members of the mitochondrial anion carrier protein family localised to the inner mitochondrial membrane. The first uncoupling protein to be discovered, UCP1 or thermogenin, is highly expressed in brown adipose tissue (BAT), and was found to be responsible for non-shivering thermogenesis – the process where mammals generate body heat through mitochondrial uncoupling of oxidative phosphorylation, rather than through repeated skeletal muscle contraction (shivering) (Nicholls, Bernson *et al* 1978). As metabolism is inherently inefficient, the increase in metabolic rate caused by widespread mitochondrial uncoupling generates more heat than usual and increases body temperature. Since then, a further 4 uncoupling proteins have been discovered which have a high sequence homology to UCP1. Mitochondrial uncoupling protein-3 (UCP3) is highly expressed in mitochondria in skeletal muscle and to a lesser extent in the heart (Bezaire, Seifert *et al* 2007). Based on its relationship to UCP1, it is assumed that UCP3 also uncouples oxidative phosphorylation (Figure 1.6), although to what extent this occurs *in vivo* remains a point of controversy.

Uncoupling proteins are thought to dissipate $\Delta\psi$ (mitochondrial membrane potential) by providing an alternative pathway for protons to re-enter the matrix, other than through ATP synthase. Lowering the membrane potential allows NADH and $FADH_2$ oxidation to proceed unchecked (with the generation of heat – as above in BAT). As ATP synthesis is $\Delta\psi$-dependent (Nicholls 2004), the consequences of uncoupling in muscle would be a decrease in the capacity of oxidative phosphorylation to synthesise ATP and a decrease in ΔG_{ATP}, potentially resulting in contractile dysfunction as previously described.

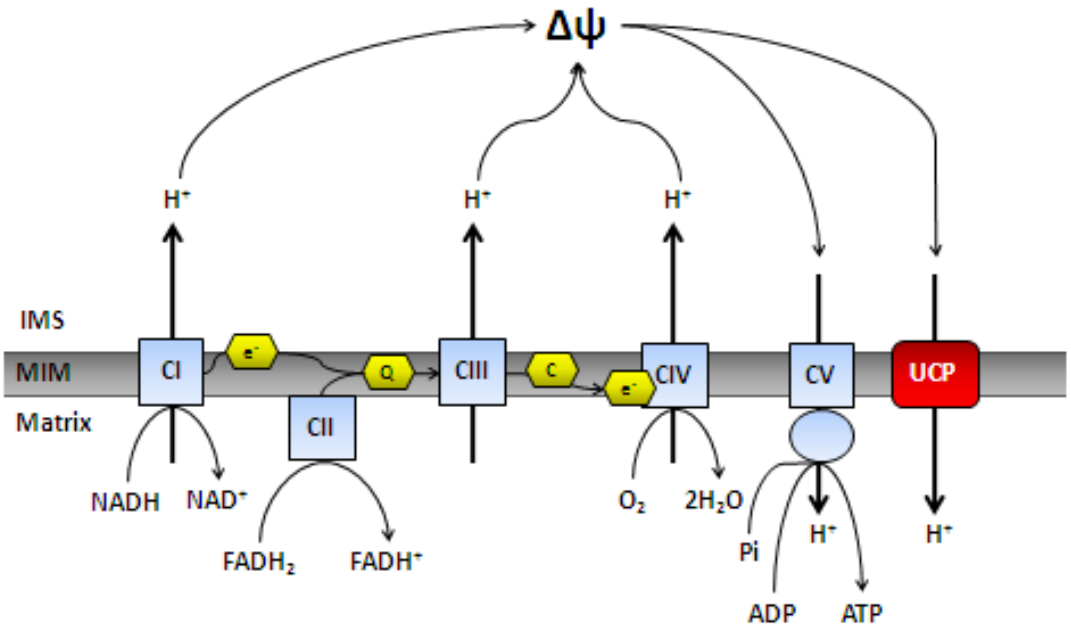

Figure 1.6. Schematic diagram of the basic mechanism through which uncoupling proteins dissipate the mitochondrial membrane potential.

IMS – inter-membrane space, MIM – mitochondrial inner membrane, Δψ – membrane potential, CI – CIV – complexes 1 – 4 of the electron transport chain, CV – complex 5 or ATP synthase, UCP – uncoupling protein, e^- - electrons, Q – coenzyme Q, C – cytochrome C, NADH – nicotine adenine dinucleotide (reduced), NAD^+ – nicotine adenine dinucleotide (oxidised), $FADH_2$ – flavin adenine dinucleotide (reduced), $FADH^+$ – flavin adenine dinucleotide (oxidised), Pi – inorganic phosphate, ADP – adenosine diphosphate, ATP – adenosine triphosphate.

Does UCP3 uncouple oxidative phosphorylation?

Genetic mutants provide a useful basis for investigating the function of a particular protein, and various experiments have been performed on mice with UCP3 "knocked-out" (KO, $UCP3^{-/-}$). It has been demonstrated that isolated mitochondria from these mice are better coupled (P/O ratio) than wild-type (WT) mice (Vidal-Puig, Grujic *et al* 2000) and the KO mice sustain a lesser temperature rise when given methylene dioxymetamphetamine (MDMA) compared with controls (Mills, Banks *et al* 2003). Mice over-expressing UCP3 have been shown to be hyperphagic and lean with increased resting oxygen consumption (Clapham, Arch *et al* 2000). Mitochondria from diabetic (db/db) mice, a model of obesity and severe type 2 DM, demonstrated increased proton leak, which was inhibited by guanosine diphosphate (GDP, a UCP inhibitor) (Boudina, Sena *et al* 2007).

Using the chronic infarction model of heart failure in rats, it has been demonstrated that cardiac UCP3 levels increase and are associated with less well coupled mitochondria (P/O ratio) and reduced cardiac efficiency (hydraulic power/O_2 consumption) (Murray, Cole *et al* 2008). Hyperthyroid rat heart mitochondria also showed decreased coupling and efficiency, with increased UCP3 levels (Boehm, Jones *et al* 2001). These findings all indicate that UCP3 is able to uncouple oxidative phosphorylation, at least *in vitro*.

Attempting to show an uncoupling effect in humans *in vivo*, however, has been less successful. Hesselink *et al* used a high fat diet to induce increased UCP3 expression (see later) and used serial skeletal muscle biopsies after ischaemic exercise to measure PCr recovery times; they found no evidence of uncoupling as PCr re-synthesis times between subjects and controls were not different, despite increases in tissue UCP3 levels (Hesselink, Greenhaff *et al* 2003). There are a number of possible reasons why the results from this

study were not consistent with mitochondrial uncoupling. There was no measurement of intracellular pH which was likely to be low following ischaemic exercise, and this can lead to unreliable PCr recovery rates (Jubrias, Crowther *et al* 2003), and secondly, at high rates of ATP synthesis (as immediately following exercise), the mitochondrial membrane potential or proton-motive force is low, and any effect of an uncoupler may be blunted. As such, the evidence from the literature is generally supportive of UCP3 being able to uncouple oxidative phosphorylation and consequently decrease ATP synthesis.

The regulation of UCP3 expression and function

Uncoupling protein-3 expression has been shown reproducibly to increase in situations where fatty acid supply is increased: high fat diet (Hesselink, Greenhaff *et al* 2003), starvation (Cadenas, Buckingham *et al* 1999), β3 adrenoceptor agonism (Nakamura, Nagase *et al* 2001), exercise (Jiang, Zhang *et al* 2009), and heart failure (Murray, Cole *et al* 2008), and it has been shown that there is a relationship between plasma NEFA concentration and UCP3 levels in human heart (Murray, Anderson *et al* 2004). These triggers for up-regulation of UCP3 are modulated through peroxisome proliferator-activated receptor alpha (PPARα), a nuclear hormone receptor, which, upon ligand binding, up-regulates the expression of a number of proteins involved in lipid metabolism (Kersten, Desvergne *et al* 2000). Endogenous ligands for PPARα include fatty acids and their derivatives (Desvergne and Wahli 1999). A synthetic specific PPARα agonist (WY-14,643) has been shown to increase UCP3 mRNA (Zungu, Young *et al* 2009) and protein levels (Murray, Panagia *et al* 2005). It has been demonstrated that a functional relationship exists between PPARα and the myogenic regulatory factor MyoD in the UCP3 promoter region which explains the specificity for muscle exhibited by UCP3 (Solanes, Pedraza *et al* 2003). Thyroid hormones

have also been shown to increase UCP3 protein levels (Boehm, Jones *et al* 2001) and a thyroid response element has been found in the proximal UCP3 promoter region (Solanes, Pedraza *et al* 2005).

Previous research has shown no relationship between UCP3 protein level and the degree of respiratory uncoupling, suggesting that specific activators are required (Boudina, Sena *et al* 2007), and it has also been shown that UCP3 is not responsible for the well recognised phenomenon termed "basal proton leak" of mitochondria (Brand, Pakay *et al* 2005). A variety of activators have been shown to induce UCP3-mediated uncoupling: superoxide (Echtay, Roussel *et al* 2002), lipid peroxidation products such as hydroxynonenol (Aguirre and Cadenas 2010) and fatty acids themselves (Echtay, Winkler *et al* 2001) have all been demonstrated to activate UCP3.

Mitochondrial uncoupling protein-3 has a rapid turnover. UCP3 messenger RNA expression was found to increase after 45 mins using exercise as the stimulus, with protein levels showing a more latent increase at 120 mins (Jiang, Zhang *et al* 2009). The half-life for the protein is thought to be between 1 – 4 hrs, which is much faster than other mitochondrial proteins, for example ANT (Azzu, Jastroch *et al* 2010). This rapid turnover is thought to enable the mitochondrion to respond quickly to changes in nutrient flux.

The physiological role of UCP3

Whilst the physiological role of UCP3 is still to be confirmed, two main hypotheses have currently emerged, with the central dogma being that UCP3 protects the mitochondrion from free-radical damage. The first of these hypotheses, postulated by Schrauwen and colleagues (Schrauwen, Saris *et al* 2001) has UCP3 acting as a fatty acid anion exporter from the mitochondrial matrix with the net effect of reducing the membrane potential ($\Delta\Psi$; Figure

1.7). In this way, excess fatty acids, in situations where supply exceeds the mitochondrial capacity to oxidise them, are exported from the matrix where they would otherwise be trapped by the proton gradient. If they were to remain in the matrix the fatty acids would be susceptible to lipid peroxidation by electrons "leaking" from the electron transport chain. Lipid peroxides are known to be detrimental to the mitochondrion (Schrauwen, Saris *et al* 2001). A link between lipid metabolism and UCP3 clearly exists, given the PPARα-mediated up-regulation of UCP3, and it has been demonstrated that physiological levels of UCP3 up-regulation in transgenic mice are associated with lower plasma NEFA concentrations and muscle triacylglycerol content, along with up-regulation of mitochondrial enzymes involved in lipid metabolism, all suggestive of an increased capacity for muscle to metabolise lipid (Bezaire, Spriet *et al* 2005). The finding that treatment with etomoxir, a carnitine palmitoyl transferase-1 inhibitor, which therefore blocks fatty acyl-CoA entry into the mitochondrion, resulted in an increase of UCP3 at the protein level in humans also suggests that UCP3 is up-regulated when supply to the mitochondrion of non-esterified, non-metabolisable fatty acids increases (Schrauwen, Hinderling *et al* 2002).

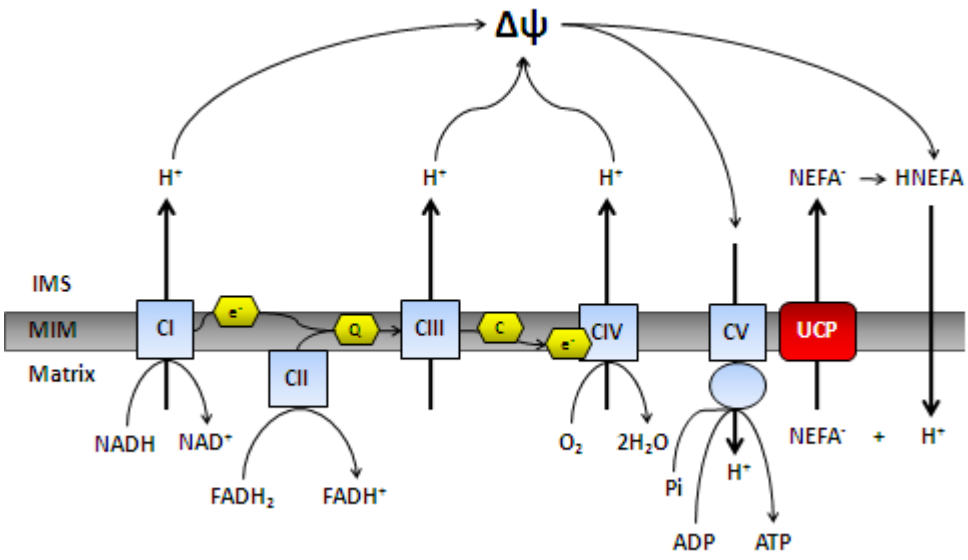

Figure 1.7. Schrauwen's fatty acid exporter hypothesis.

In situations where NEFA supply exceeds oxidative capacity NEFAs may become trapped as anions in the matrix by the proton gradient. UCP3 acts as a NEFA exporter leading to fatty acid anions being protonated in the inter-membrane space and then returning to the matrix in their unionised form with the effect of lowering the proton gradient and increasing oxidative capacity. This protects the mitochondrion from potentially damaging lipid peroxides (Schrauwen, Saris *et al* 2001).

IMS – inter-membrane space, MIM – mitochondrial inner-membrane, $\Delta\psi$ – membrane potential, CI – CIV – complexes 1 – 4 of the electron transport chain, CV – complex 5 or ATP synthase, UCP – uncoupling protein, e^- - electrons, Q – coenzyme Q, C – cytochrome C, NADH – nicotine adenine dinucleotide (reduced), NAD^+ – nicotine adenine dinucleotide (oxidised), $FADH_2$ – flavin adenine dinucleotide (reduced), $FADH^+$ – flavin adenine dinucleotide (oxidised), Pi – inorganic phosphate, ADP – adenosine diphosphate, ATP – adenosine triphosphate, $NEFA^-$ - non-esterified fatty acid anion, HNEFA – non-esterified fatty acid.

A different proposal put forward by Brand suggests that mild uncoupling by UCP3 acts to mitigate reactive oxygen species (ROS) generation. Complexes 1 and 3 of the electron transport chain are important sites of ROS generation (Brand 2010) and it has been shown that ROS generation is proportional to the membrane potential (Korshunov, Skulachev *et al* 1997). Mild uncoupling through UCP3, having the effect of lowering the membrane potential, would therefore decrease ROS generation at these sites. Supportive evidence comes from UCP3 KO and under-expressing mice, which have higher levels of ROS production and oxidative damage (Vidal-Puig, Grujic *et al* 2000; Brand, Pamplona *et al* 2002).

Whichever hypothesis turns out to be correct, the central tenet is that UCP3 serves to protect mitochondria from free-radical induced damage either from ROS or lipid peroxides, and does so by lowering the membrane potential. The downside of this mechanism is a decrease in the efficiency of ATP synthesis; however the magnitude of the uncoupling effect is greatest at high membrane potential in situations when ATP demand is low.

1.9. Statement of hypothesis and aims

The hypothesis of this thesis is that, in heart failure, the increased plasma NEFA concentration resulting from adipose tissue lipolysis, leads to an increase in UCP3 levels in the heart and skeletal muscle via activation of PPARα. The increase in UCP3 levels results in mitochondrial inefficiency, decreasing the capacity for ATP synthesis, and is manifested by abnormalities in cardiac and skeletal muscle high energy phosphate metabolism. This hypothesis provides a unifying mechanism for the mitochondrial dysfunction observed in cardiac and skeletal muscle in heart failure (Figure 1.8).

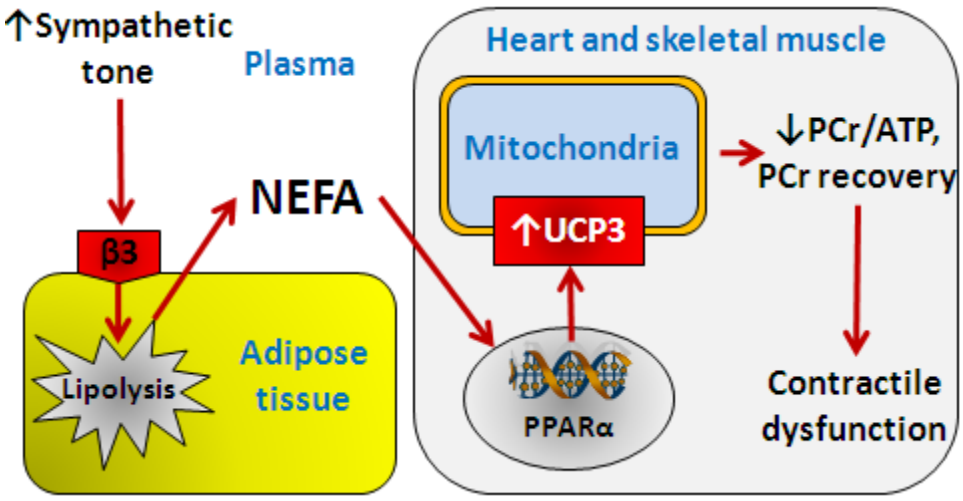

Figure 1.8. Schematic diagram of the hypothesis.

β3 – β3 adrenoceptor, NEFA – non-esterified fatty acid, UCP3 – mitochondrial uncoupling protein-3, PPARα – peroxisome proliferator-activated receptor alpha, PCr – phosphocreatine, ATP – adenosine triphosphate.

The principle aim of this work is:

1. To investigate whether increased ventricular UCP3 levels are associated with decreased cardiac PCr/ATP ratio in humans and, whether increased skeletal muscle UCP3 levels are associated with longer skeletal muscle PCr resynthesis times following exercise in humans.

Also, to add support to the hypothesis outlined:

2. To investigate whether plasma NEFA concentrations increase with increasing heart failure severity, and to determine how they relate to left ventricular volumes and ejection fraction in humans.
3. To investigate whether increased plasma NEFA concentration is associated with increased UCP3 levels in atrial, ventricular and skeletal muscle tissue in humans.
4. To investigate whether cardiac PCr/ATP ratio relates to heart failure severity, and to determine its relationship to left ventricular volumes and ejection fraction in humans.
5. To investigate whether increased skeletal muscle PCr resynthesis time after exercise is related to heart failure severity and to determine how it relates to left ventricular volumes and ejection fraction in humans.
6. To investigate whether increased UCP3 levels are associated with decreased mitochondrial coupling in atrial and skeletal muscle tissue from humans.
7. To investigate whether atrial and skeletal muscle tissue respiration rate and mitochondrial protein level relate to heart failure severity, and to determine how they relate to left ventricular volumes and ejection fraction in humans.

Heart failure severity was graded by the NYHA classification and the 6MWT distance. Left ventricular volumes and ejection fraction were measured by cardiac MRI at 3 Tesla. Cardiac PCr/ATP ratio and skeletal muscle PCr resynthesis time were measured using ^{31}P MRS at 3 Tesla. Tissue UCP3 levels were measured by immunoblotting from biopsies taken during cardiac surgery. Mitochondrial respiration was measured using saponin-permeabilised whole tissue taken during cardiac surgery. See Chapter 2 for full details of methods.

CHAPTER 2

GENERAL METHODS

2.1. Patient selection

After obtaining local ethics committee approval (Mid and South Buckinghamshire Research Ethics Committee), human subjects scheduled to undergo elective cardiac surgery were recruited. Cardiac surgical patients were recruited in order that atrial, ventricular and skeletal muscle biopsies could be taken at the time of surgery. Whilst endomyocardial biopsies can be obtained during cardiac catheterisation, it was felt that the biopsy size would be insufficient, as would patient numbers, preventing this from being a practicable approach to addressing the study aims.

The study population was not limited to a particular surgical pathology in order to maximise the number of subjects recruited, recognising that recruitment of human subjects, particularly to a study with a relatively arduous experimental protocol, involving procedures such as prolonged periods of MRI scanning and the donation of cardiac tissue, can be difficult. Whilst this meant a heterogenous study population, comprising both coronary artery and valve disease, this was felt to be scientifically valid, because the energetic abnormalities occurring in heart failure (described in Chapter 1) are the same regardless of the underlying disease (Neubauer 2007) - the hypothesis described is aetiology independent, relating only to the result of heart failure or to the degree of ventricular dysfunction, and not to a specific underlying cause.

No control group was included in the experimental design because obtaining control ventricular or atrial biopsies was not feasible. Whilst previous human studies have utilised unused normal human donor hearts as a source of control tissue, there are concerns regarding the validity of “normal” samples from excised hearts, unsuitable for transplantation, which have been preserved on ice for a number of hours (Stanley, Recchia *et al* 2005).

Instead of a control group, patients were recruited with a full range of cardiac function, including those with systolic failure, diastolic failure, normal function or any combination. Using this approach meant that there was no specific heart failure group, but instead, regression analysis was used to determine associations between the degree of ventricular dysfunction (systolic or diastolic) and other variables. Regression was considered to be more suitable than correlation in these data as clear "cause and effect" was present, for example, increased ventricular UCP3 was expected to result in decreased cardiac PCr/ATP ratio. Correlation is unsuitable in this example as an increase in cardiac PCr/ATP ratio would not be expected to result in decreased ventricular UCP3 levels.

Listed below are the exclusion criteria that were used together with the justification:

- Uncontrolled hypertension (BP >180/110) – unsafe to exercise clinically unstable patients awaiting cardiac surgery in a remote location such as within the bore of the MRI scanner.
- Age more than 85 or less than 18 – the effect of extremes of age on cardiac and skeletal muscle energetics is unknown.
- Previous cardiac surgery – presence of sternal wires has an unknown effect on cardiac ^{31}P MRS.
- Alcohol/drug abuse – concerns over consent, compliance and pharmacodynamics.
- Taking insulin, fibrates or thiazolidinediones – patients taking insulin were not included because of the potential for harm in managing the fasting period required in the protocol. Patients on fibrates and thiazolidinediones were not included as these drugs are PPAR agonists.

- Clinically significant respiratory disease – confounding the assessment of heart failure severity, 6MWT and NYHA.
- Peripheral vascular disease – known to have prolonged gastrocnemius PCr recovery times following exercise secondary to ischaemia.
- Possibility of pregnancy – unknown effects of magnetic field on teratogenicity.
- Contraindication to MRI – unable to complete the experimental protocol.
- Refusing consent

2.2. Sample size estimate

There are four constituents required for hypothesis testing: the significance level (or Type 1 error rate), the power (or Type 2 error rate; power = 1- Type 2 error rate), the critical region (the set of values of the test statistic for which the null hypothesis is rejected) and the sample size. Knowledge of at least two constituents enables calculation of the others (provided the distribution of the test statistic is known). The Type 1 and 2 error rates can be predefined, therefore allowing calculation of the minimum sample size required.

Previous studies have demonstrated statistically significant correlations between plasma non-esterified fatty acids and atrial UCP3 levels ($r = 0.46$, $p = <0.001$, $n=39$) (Murray, Anderson *et al* 2004), and between cardiac PCr/ATP ratio and plasma non-esterified fatty acids ($r = -0.59$, $p = <0.01$, $n=36$) (Scheuermann-Freestone, Madsen *et al* 2003). Based upon these studies, one might expect a correlation between UCP3 and PCr/ATP ratio of at least medium effect size, using Cohen's suggestions regarding the magnitude of effect sizes ($r > 0.1$ – small effect, $r > 0.3$ – medium effect, $r > 0.5$ – large effect) (Cohen 1992).

The program GPower 3.1 (Dusseldorf, Germany) was used to calculate the sample size necessary to adequately power a simple linear regression model with a medium effect size of 0.35, and setting α (the Type 1 error rate) at 0.05, 34 patients would be required to achieve a power of 0.8 (Figure 2.1). The aim was therefore to study as close to 50 patients as possible within the available time period, to allow for subjects not being able to complete all tests, or for data acquisition failure.

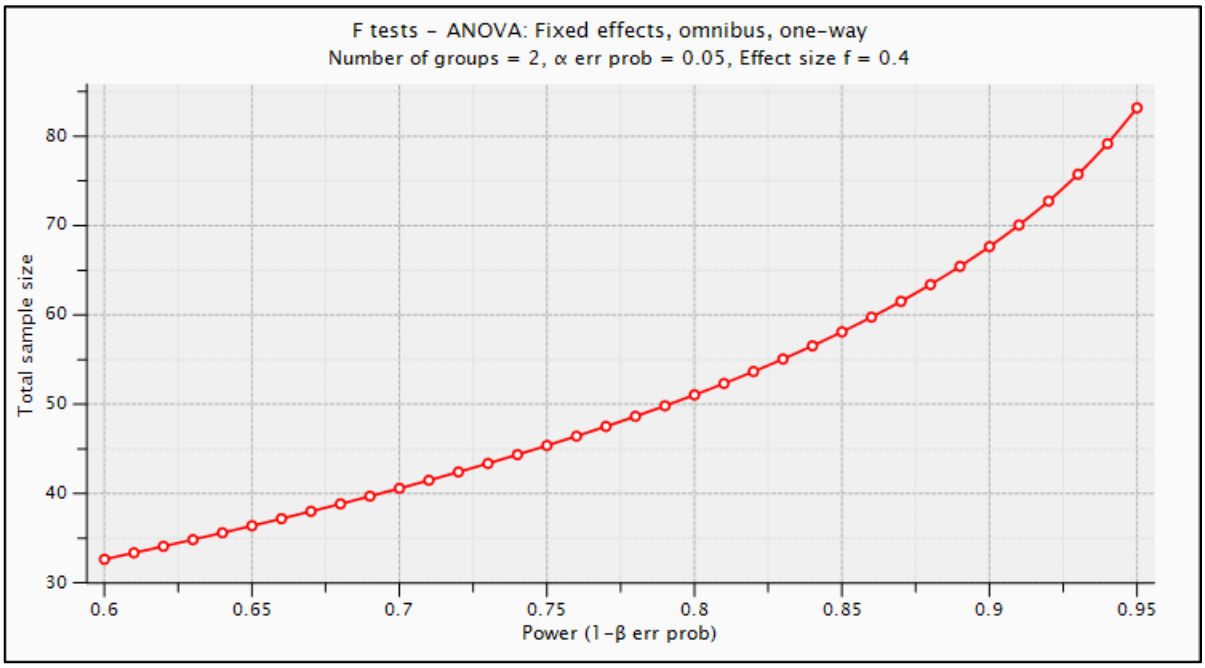

Figure 2.1. The relationship between sample size and power given the Type 1 error rate and effect size.

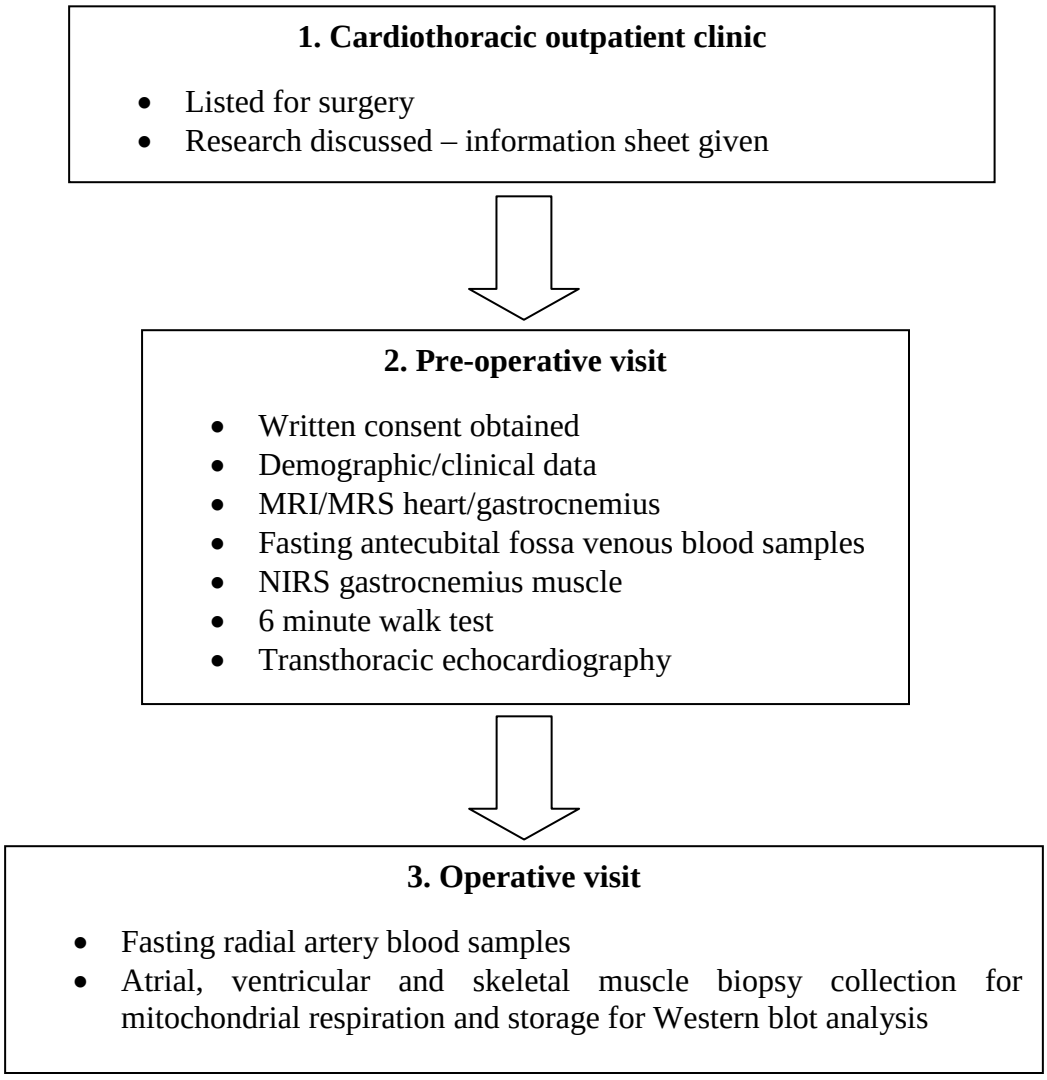

Figure 2.2. Temporal sequence of study phases and experimental content.

Visit 2 occured at a convenient time pre-operatively, determined by patient and MRI scanner availability. Visit 3 occured at the time of scheduled surgery.

2.3. Experimental protocols

Figure 2.2 demonstrates the general outline of the experiments. Peri-operative investigations were carried out at the Oxford Centre for Clinical Magnetic Resonance Research (OCMR), John Radcliffe Hospital, Oxford, UK. Patients' attendance for the pre-operative visit was dictated by their, and the 3T MRI scanner, availability. This resulted in some patients being tested well in advance of surgery (40 days) and others the day before. All pre-operative investigations were carried out at one visit.

2.3.1. Anthropometrics, hormones and metabolites

Body weight and composition

After a fast of at least six hours (typically overnight), patients attended the OCMR where their weight and height were measured together with waist and hip circumferences. Body composition analysis was performed using a bio-impedance method (Bodystat, Douglas, Isle of Man). Variables estimated included lean body mass, body fat percentage and water content.

Fasting blood samples

Venous blood was taken from an antecubital fossa vein whilst fasted and immediately centrifuged at 4˚C. The plasma was then frozen at -80˚C until batch analysis for glucose, insulin and glycerol. Plasma for the measurement of non-esterified fatty acids was frozen after the addition of a lipoprotein lipase inhibitor (tetrahydrolipstatin, Xenical, Roche, Welwyn Garden City, UK) at a final concentration of 30μg/ml. Plasma metabolites were measured using an ABX Pentra Clinical Chemistry bench-top analyser (Horiba ABX, Montpellier, France). Enzyme-Linked ImmunoSorbent Assays (ELISA) were performed

with commercially available kits: insulin (Mercodia AB, Uppsala, Sweden) and glycerol (Cayman Chemical Company, Ann Arbor, MI, USA).

Fasting arterial blood was taken at the operative visit prior to the induction of anaesthesia for measurement of NEFAs. This was done so that biopsy and respiration data could be related to plasma NEFA concentration acquired at the same visit, rather than the NEFA concentration obtained at the pre-operative visit.

2.3.2 ^{31}P magnetic resonance spectroscopy

Cardiac ^{31}P magnetic resonance spectroscopy

Myocardial phosphorus metabolites were measured using a Siemens 3T Trio MR system (Erlangen, Germany). The method used was as described previously by our group with an intra-subject variability of 20%, an inter-subject variability of 18% and an intra-observer variability of 5% (Tyler, Emmanuel *et al* 2009). Subjects were positioned prone on a ^{31}P heart/liver coil with the heart positioned over the centre of the coil. A pilot scan was then run to ensure central location of the heart. Cod liver oil capsules, located within the coil casing at fixed positions, were used to orientate the coil and map the excitation flip angle onto the cardiac images. A sequence of spectroscopic inversion recovery acquisitions were acquired with various inversion times (T_I) centred on a phenylphosphonic acid reference phantom located in the coil housing. These data were fit to provide an estimate of the flip angle of the inversion pulse, which was compared with data acquired from a phantom so that the calculated excitation flip angle maps could be corrected for the effects of variable coil loading. A series of images were then taken through the heart's short axis which were ECG gated with a trigger delay of 400ms. The 3D-chemical shift imaging (CSI) acquisition

protocol was set up so the highest resolution acquisition plane was parallel with the cardiac short axis, and three voxels were centred over the septum in a mid-ventricular slice (figure 2.3). See Appendix 2 for the details of the 3D-CSI sequence.

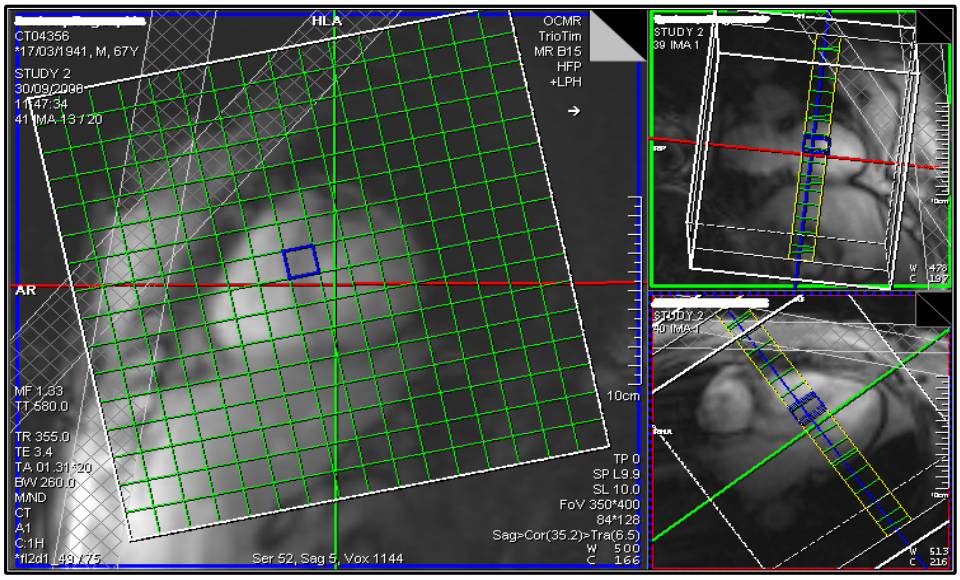

Figure 2.3. The MR console screen demonstrating the positioning of the CSI grid.

Two saturation bands can be seen positioned over the anterior chest to remove potential skeletal muscle contamination of the myocardial voxels.

Quantification of the spectral peaks

Acquired data were loaded into home-written software in Matlab (version R2007b, The MathWorks, Natick, MA, USA) to allow co-registration of spectral data and the excitation flip angle with the short axis image data. Spectra from 3 mid-ventricular septal voxels, selected on anatomical criteria, were then pre-processed and fitted using AMARES (Advanced Method of Accurate, Robust and Efficient Spectroscopic fitting) (Naressi,

Couturier *et al* 2001) within jMRUI (java Magnetic Resonance User Interface) software (Version 2.2). The spectra from the 3 voxels were also summed, then fitted in the same way, improving the signal/noise ratio and the accuracy of the peak fitting. Spectral peak integrals were corrected for the effects of radiofrequency saturation, actual flip angle and nuclear Overhauser effect (NOE) enhancement. The ATP concentration was taken as being proportional to the average of its 3 spectral peaks and was corrected for blood contamination within the voxels by subtracting 11% of the 2,3-diphosphoglycerate (DPG) peak area (Neubauer, Krahe *et al* 1992).

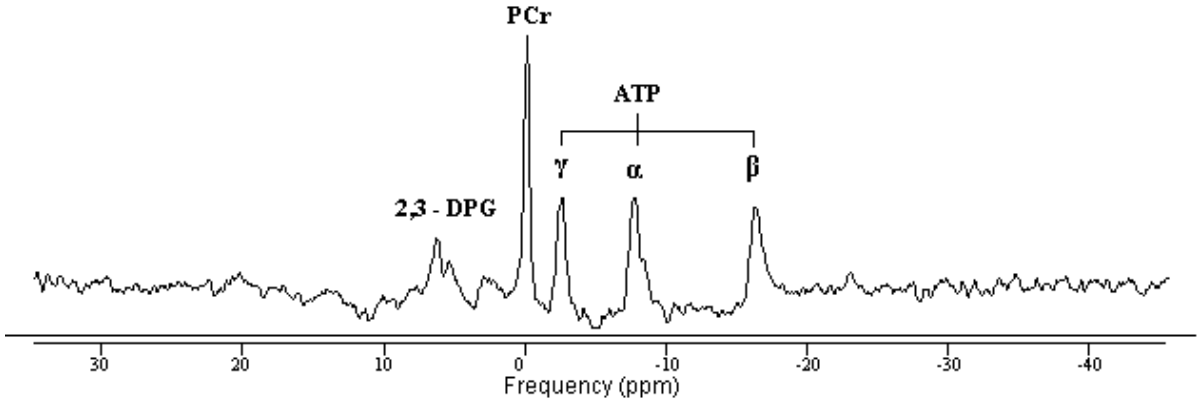

Figure 2.4. An example of a myocardial ^{31}P spectrum summed from 3 mid-ventricular septal voxels.

DPG – diphosphoglycerate, PCr – phosphocreatine, ATP – adenosine triphosphate.

Skeletal muscle ^{31}P magnetic resonance spectroscopy

Subjects were positioned supine in a 3T MRI scanner (Siemens Trio, Erlangen, Germany) with their right gastrocnemius muscle overlying a surface coil (Figure 2.5). Strapping was applied above and below the right knee and across both shoulders in order to minimise movement during exercise.

Exercise spectra were acquired by asking the patient to plantar flex the right foot against a foot pedal, which provided an adjustable resistance to flexion, at a frequency of 1Hz. The frequency was dictated by use of a metronome (Boss DB-66, China). Patients exercised until they were unable to continue or the PCr peak of the ^{31}P spectrum decreased by approximately 50% (Figure 2.6). Recovery spectra were obtained for at least 5 minutes after exercise. Details of the MRS acquisition can be found in Appendix 3.

Resistance to plantar flexion was standardised to patient lean body mass (LBM). Based on previous studies (Scheuermann-Freestone, Madsen *et al* 2003), an initial work of 0.035 W/kg (LBM) was performed. This was then augmented by a stepped increase at rate +0.007 W/kg (LBM) at the appropriate times during exercise (Figure 2.7).

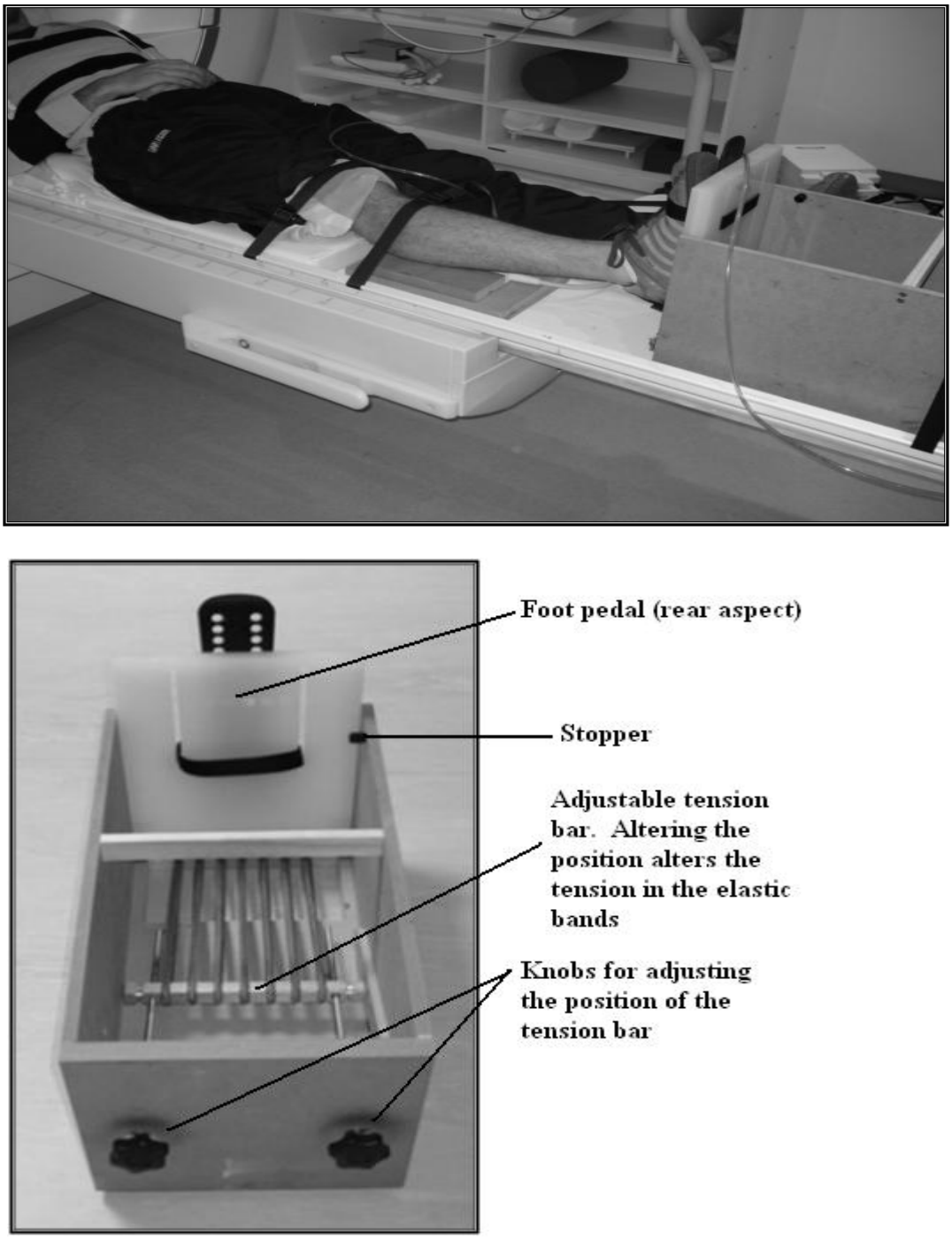

Figure 2.5. Photographs to show the set up for skeletal muscle ^{31}P MRS.

The upper image demonstrates the application of strapping to minimise movement. The lower image is a more detailed view of the plantar-flexion ergometer.

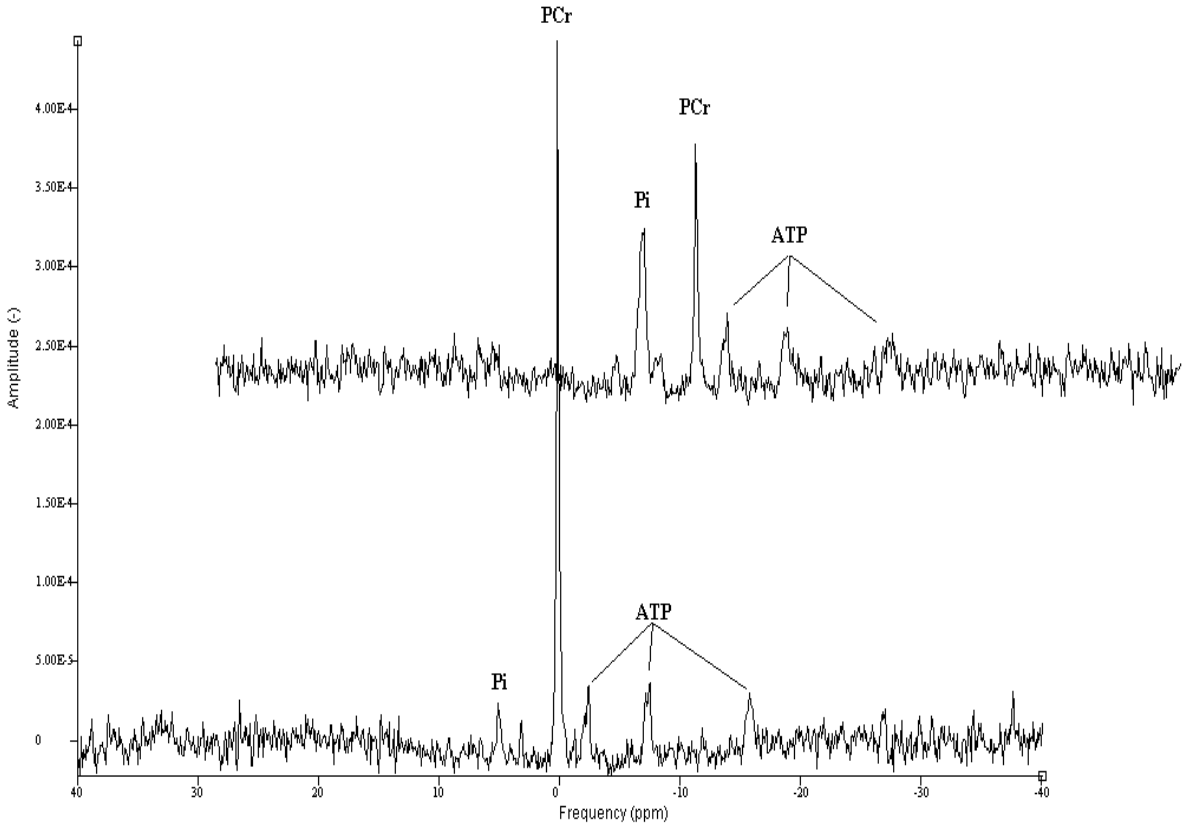

Figure 2.6. Skeletal muscle spectra at rest (lower spectrum) and at the end of exercise (upper spectrum).

Note the decrease in PCr and the increase in Pi at the end of exercise.

Pi – inorganic phosphate, PCr – phosphocreatine, ATP – adenosine triphosphate, ppm – parts per million.

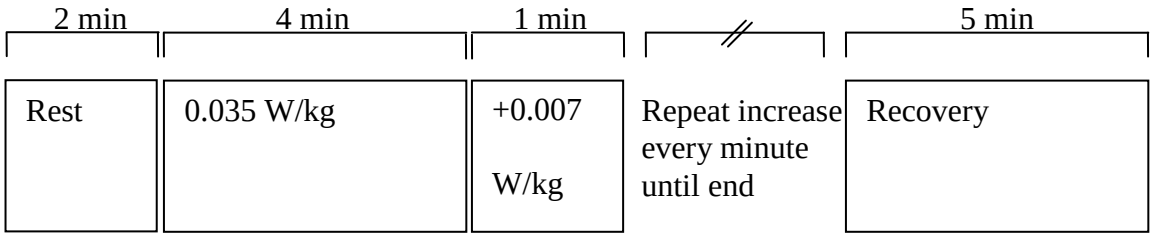

Figure 2.7. Outline of the exercise protocol used for gastrocnemius ^{31}P MRS.

Quantification of the spectral peaks

Spectra were processed with jMRUI software (Version 2.2) and quantified using AMARES. The values obtained for the metabolites during the acquisition were corrected for NOE and saturation effects (Appendix 3).

Resting ^{31}P metabolite concentrations were obtained by summing the resting spectra to optimise the signal/noise ratio and thereby improve accuracy of fitting. Intracellular pH was calculated from the chemical shift of the Pi peak (σ, ppm) using a modified form of the Henderson Hasselbalch equation:

$$pH = 6.75 + \log\{(\sigma - 3.27) \div (5.63 - \sigma)\}$$

Analysis of PCr kinetics

The rate of PCr hydrolysis at the onset of exercise is a measure of the cost in ATP of contraction and was calculated using a linear best fit. The total PCr change divided by the exercise time (ΔPCr/t) was calculated as an overall measure of the failure of oxidative ATP synthesis to supply ATP for muscular contraction (the glycolytic contribution to ATP synthesis is small in this type of exercise protocol and was discounted). Finally the recovery of PCr following cessation of exercise was fitted with an exponential function ($1 - e^{-kt}$) in order to calculate time constants for the recovery of PCr (Figure 2.8). To simplify the exponential curve fitting, PCr concentration was divided by the PCr concentration at the end of recovery, i.e. the final "end recovery" PCr concentration becomes 1, referred to as

"normalised PCr". The theoretical maximum rate of oxidative ATP synthesis (Q_{max}) was calculated from the end-exercise [ADP] and the initial rate of PCr resynthesis:

$$Q_{\max} = V\left\{1 + \left({K_M}/{[ADP]}\right)^n\right\}$$

V is the initial post-exercise rate of PCr resynthesis, K_M is the [ADP] at which oxidative ATP synthesis is half maximal (25 μmol.L^{-1}) and n is a Hill coefficient describing the relationship between V and [ADP] (2.2) (Trenell, Sue *et al* 2006).

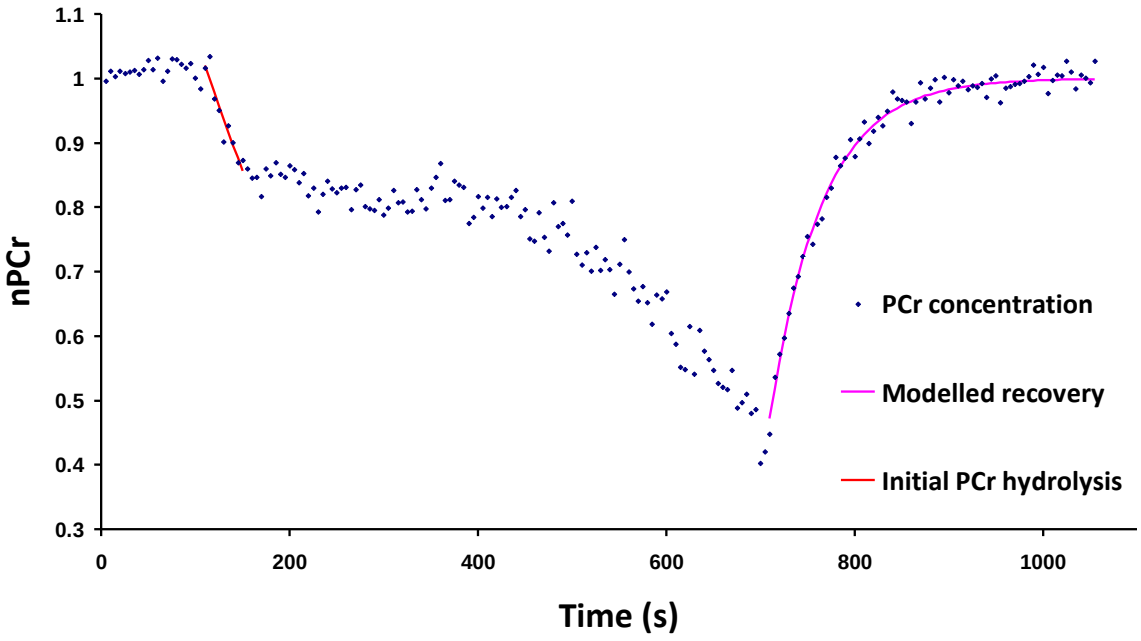

Figure 2.8. A graph of normalised PCr concentration against time, outlining the kinetic analysis.

nPCr – normalised phosphocreatine.

2.3.3 Skeletal muscle near-infrared spectroscopy (NIRS)

Patients repeated the exercise protocol as above for exactly the same length of time, except that on this occasion the exercise was performed outside the scan room as the NIRS equipment was not MRI compatible. An INVOS 4100 oximeter (Somanetics, Troy, MI, USA) was used to acquire regional muscle oxygen saturations ($rSmO_2$) at rest and during exercise. The oximeter probe was placed medially around the belly of gastrocnemius. The oximeter signal originates mostly from venular blood (Mancini, Bolinger *et al* 1994) and therefore provides a dynamic estimation of the mismatch between oxygen supply and demand. Data recordings were made via a computer and saved as a text file for later analysis with Excel (Microsoft Corporation, Redmond, WA, USA).

In a similar way to the above PCr kinetic analysis, the maximum rate of de-oxygenation was calculated, as was the mean overall de-oxygenation indexed to exercise time. Re-oxygenation following exercise cessation was fitted with a bi-exponential sigmoid function of the form:

$$f(t) = Ae^{-Be^{-t/C}} + D.$$

The constants A, B, C and D reflect the amount of change, the delay preceding the start of the second exponential phase, the general slope of the function and the initial starting point respectively (figure 2.9).

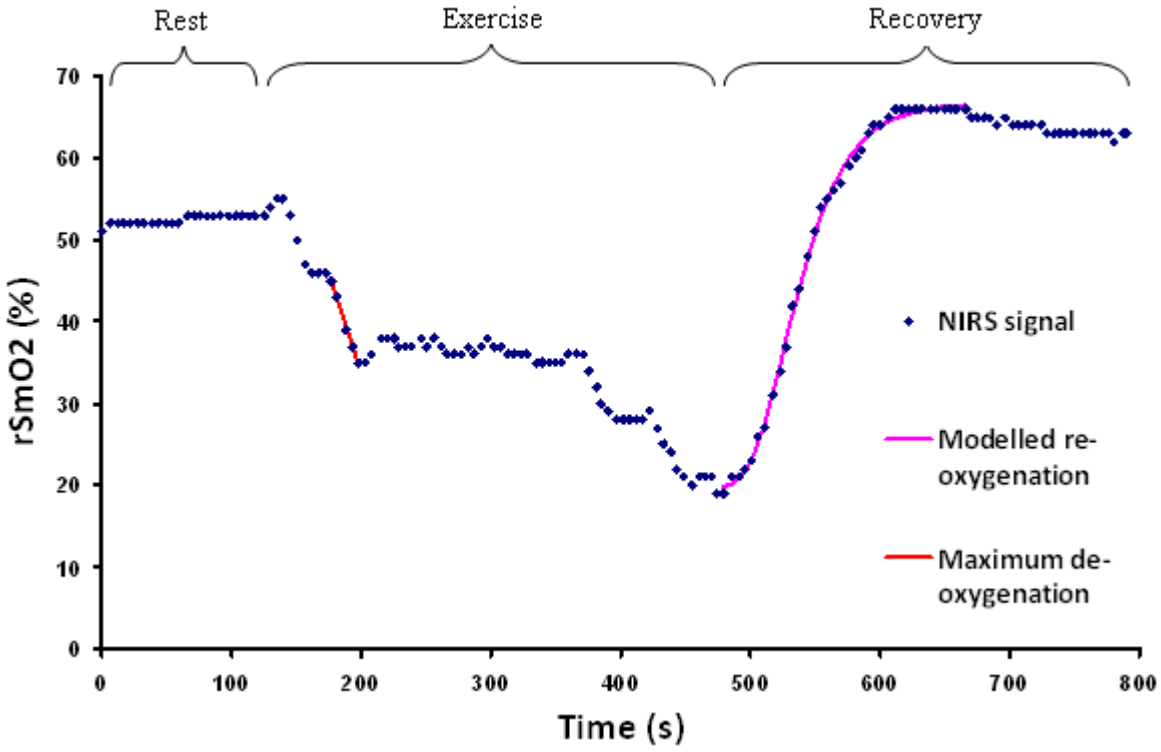

Figure 2.9. A graph of gastrocnemius tissue oxygenation plotted against time, outlining the kinetic analysis.

rSmO2 – regional muscle oxygen saturation.

2.3.4. Cardiac function

Cardiac volumes and mass

Cardiac volumes were acquired using a Siemens 3T Trio MR system (Erlangen, Germany). Patients lay supine in the scanner, and from a series of pilot images, horizontal and vertical long axis Steady-State Free Precession (SSFP) cine images were acquired. From these a stack of short axis SSFP cine slices were piloted from the base of the ventricles through to the apex. Each slice was 7 mm thick and retro-gated to ensure capture of the whole cardiac cycle. The slices were obtained during a breath-hold at the end of normal expiration to minimise the effects of ventilatory motion.

The epicardial and endocardial borders of the left ventricle (LV) in the short axis images were then contoured manually at end-diastole, and the endocardial border at end-systole, within a post-processing software package (Argus - Siemens Medical Solutions, Erlangen, Germany) (figure 2.10). Quantification of the LV cavity areas, and a known slice thickness enabled estimation of the LV end-systolic (ESV) and end-diastolic (EDV) volumes from which the stroke volume (SV) was calculated (SV = EDV-ESV). Ejection fraction (EF) and cardiac output (CO) were also calculated (EF = SV/EDV, CO = SV x HR). Myocardial mass was calculated by subtracting the endocardial volume from the epicardial volume giving the volume of myocardium. Myocardial mass was calculated from the volume by assuming the specific gravity of the myocardium ($1.05 g/cm^3$).

Prior to acquiring and analysing study subject data, an intensive two month training period was undertaken, described previously at the OCMR, to ensure acceptable inter-observer variation in volume and mass measurement (Karamitsos, Hudsmith *et al* 2007). Briefly, the left ventricular volumes and masses of 10 normal volunteers were acquired and analysed by

two experienced operators and also by the trainee, initially, and after 2 months of training. Trainees were allowed to analyse scans independently if their measurements were within 10% of the gold-standard measurements.

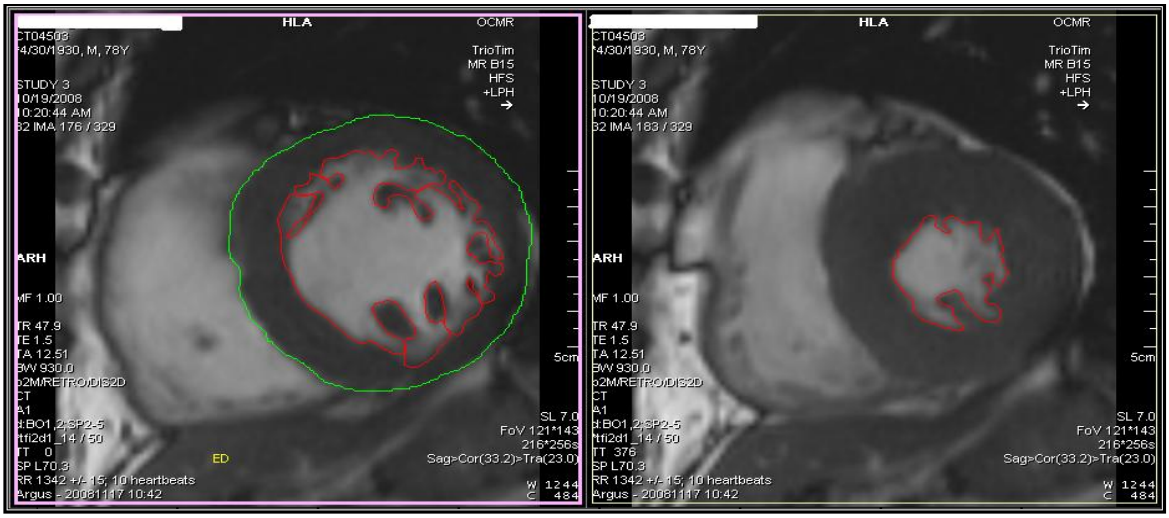

Figure 2.10. Screen shot from the Argus post-processing software.

The image on the left shows contouring of the epicardial (green) and endocardial (red) borders at end-diastole. The right hand image shows the same slice at end-systole with the endocardial border contoured (red).

Diastolic function

Diastolic parameters were measured using transthoracic echocardiography (iE33 Philips Healthcare, Best, Netherlands). Ventricular filling as trans-mitral peak velocity was measured along with septal and lateral mitral annulus motion using pulsed Doppler. E/A ratios (the ratio of early to atrial transmitral peak velocity) were calculated, along with the E/E' ratio (the ratio of early transmitral peak velocity to the corresponding peak mitral

annulus velocity (average of septal and lateral values)), with diastolic dysfunction defined as follows:

(i) E/E' > 15

(ii) E/E' 8 – 15 with E/A < 0.5 or LV mass index >122 g/m^2 (women), >149 g/m^2 (men) or atrial fibrillation (Paulus, Tschope *et al* 2007)

2.3.5. Functional capacity

Six minute walk test

The six minute walk test was performed on patients, as described by the American Thoracic Society (Crapo, Casaburi *et al* 2002). Patients were advised beforehand to wear comfortable walking shoes, and they walked backwards and forwards along a 30 metre length of corridor for 6 minutes, attempting to achieve as much distance as they could. Total distance covered was recorded along with Borg scores (Appendix 6) for dyspnoea and fatigue before and after walking. Distance covered in the test provided an objective assessment of functional capacity (Crapo, Casaburi *et al* 2002). This did not necessarily equate with heart failure severity as a proportion of patients had coronary artery (including left main stem) disease and/or severe aortic stenosis, and angina may have limited the distance covered or was itself manifested as breathlessness.

New York Heart Association Functional Class

A full symptomatic history was taken from the patients. On the basis of reported symptoms, patients were grouped according to the NYHA functional classification (The Criteria Committee of the New York Heart Association 1928.) As described in Chapter 1, many

clinical trials use this classification to categorise the severity of heart failure (Dickstein, Cohen-Solal *et al* 2008), and it has been shown previously to relate to cardiac PCr/ATP ratio in dilated cardiomyopathy, coronary artery disease (Neubauer, Krahe *et al* 1992) and aortic stenosis (Neubauer, Horn *et al* 1997), where left ventricular ejection fraction has not. Again the NYHA grouping may not necessarily reflect heart failure severity in this cohort as the presence of angina may have resulted in functional limitation, however, whilst it is accepted that NYHA class is not specific to heart failure, it will be used in this thesis as one method of categorising the severity of heart failure.

2.3.6. Biopsy collection

During the planned operative procedure, the operating surgeon took tissue biopsies from the right atrium and skeletal muscle from pectoralis major. Patients were anaesthetised according to local practice and the anaesthetic technique was not formally standardised but was similar in all patients. Patients were induced with 10 $\mu g.kg^{-1}$ fentanyl citrate and sodium thiopental titrated to loss of consciousness. Muscle relaxation was achieved with 0.05 $mg.kg^{-1}$ pancuronium bromide. Anaesthesia was maintained with isoflurane (1-2% v/v) off cardiopulmonary bypass, and with intravenous propofol 7 $mg.kg^{-1}.hr^{-1}$ during cardiopulmonary bypass. Heparin (300 $IU.kg^{-1}$) was given as an intravenous bolus prior to cardiopulmonary bypass or the commencement of off-pump coronary grafting.

The biopsies were obtained by the operating surgeon. Pectoralis major was obtained following sternotomy and immediately washed in physiological (0.9% w/v) saline to remove excess blood and then snap-frozen in liquid nitrogen and stored at -80˚C until Western blot analysis was carried out. Right atrial appendage tissue was obtained at venous cannulation if

on pump, or after exposure of the heart, prior to the commencement of grafting, if off-pump. Again the tissue was immediately washed in physiological (0.9% w/v) saline and snap-frozen in liquid nitrogen. A sub-section of the atrial and skeletal muscle biopsies were divided into two parts; one was snap-frozen as above, the other was placed into ice-cold sodium lactate (Hartmann's) solution and taken immediately for analysis of mitochondrial respiration (see below). In most cases the surgeons also provided left ventricular myocardial biopsies. The ventricular biopsies were taken from myocardium distant from evident scar within 5 minutes of the commencement of cardiopulmonary bypass in those patients undergoing surgery on-pump, and prior to the commencement of coronary grafting in the off-pump patients. The biopsies were from the epicardium, taken using a scalpel, and consequently did not include the endomyocardium. These, due to the small biopsy size, were not divided, only snap-frozen in liquid nitrogen for subsequent Western blotting analysis.

2.3.7. Molecular biology

Mitochondrial respiration experiments

Mitochondrial respiration was measured using the saponin-permeabilisation technique described by Kuznetsov and colleagues (Kuznetsov, Veksler *et al* 2008). Using a dissecting microscope and whilst submerged in ice-cold relaxing solution (10 mM EGTA, 3 mM $MgSO_4$, 20 mM taurine, 0.5 mM dithiothreitol, 20 mM imidazole, 0.16 M morpholinepropanesulphate (MOPS) and 5 mM ATP), connective tissue and fat were carefully dissected away from the atrial and skeletal muscle biopsies. The biopsies were then minced and bundles of muscle fibres were separated out (Figure 2.11). The fibres were

skinned for 20 minutes in iced relaxing solution containing 100 μg/ml saponin. Fibres were then transferred into iced KME solution (100 mM KCl, 50 mM MOPS and 0.5 mM EGTA) and washed for 20 minutes, changing the solution every 5 minutes in order to remove saponin and ATP.

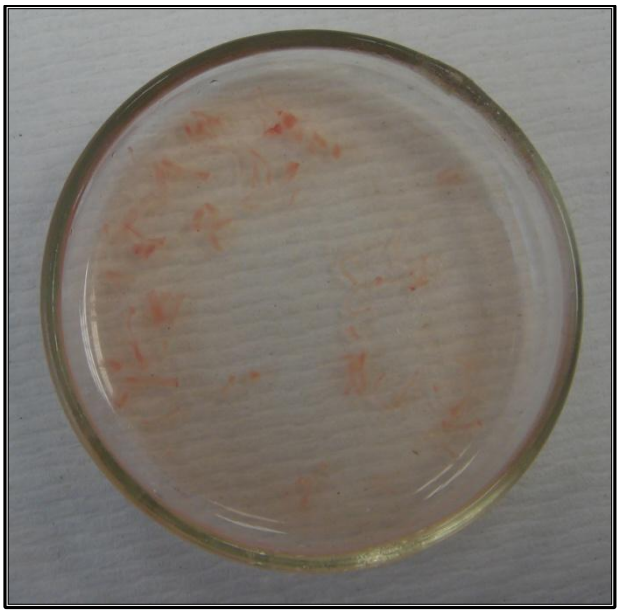

Figure 2.11. Photograph of the dissected skeletal muscle fibres, prior to saponin permeabilisation.

Respiration measurements were obtained using a Clarke electrode (Strathkelvin, North Lanarkshire, Scotland) at 30˚C in respiration medium (100 mM KCl, 50 mM MOPS, 1 mM EGTA, 5 mM KH_2PO_4, and 1 mg/mL bovine serum albumin). Substrates were selected to enter the metabolic pathway at different locations, namely: glutamate 20 mM; pyruvate 5 mM with malate 5 mM; and palmitoyl-CoA 40 μM with malate 5 mM and carnitine 5 mM. Measurements were taken with substrate alone, with the addition of ADP 100 nM, with oligomycin 2 μM (an ATP synthase inhibitor), and with the chemical uncoupler carbonyl cyanide p-trifluoromethoxyphenylhydrazone (FCCP) 20 μM. Fibres were weighed prior to

being placed into the electrode and respiration rates were indexed to wet weight (Figure 2.12).

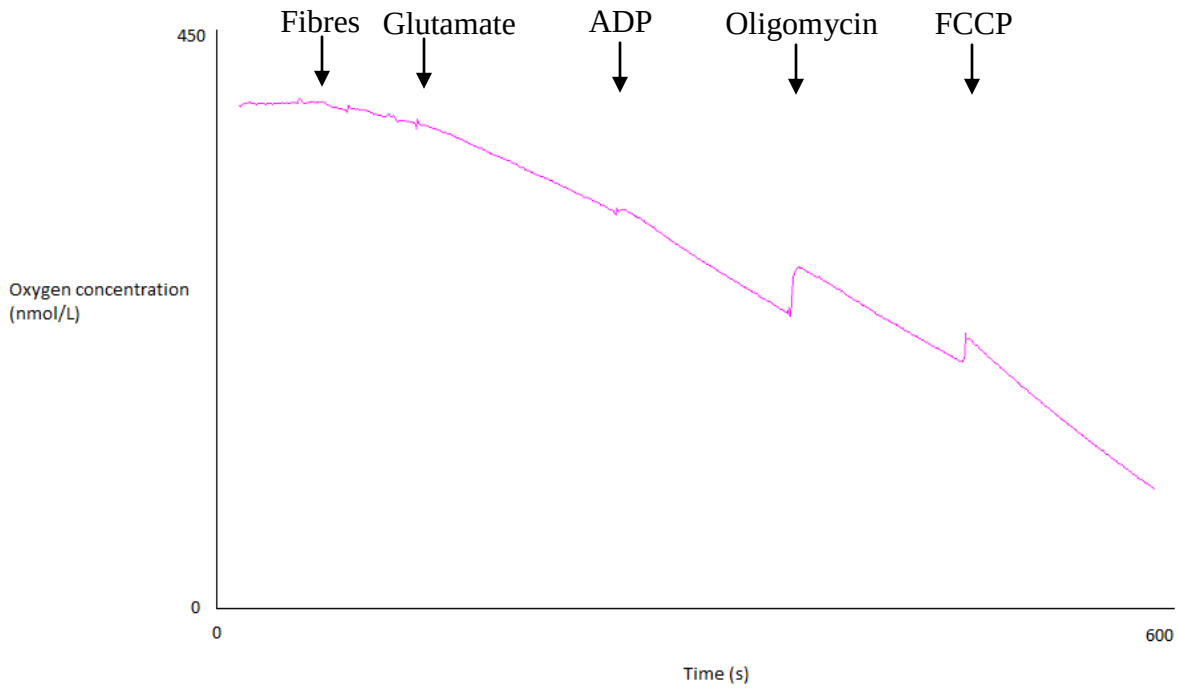

Figure 2.12. Experimental tracing from a mitochondrial respiration experiment.

Once a stable baseline was achieved, minced muscle fibres were added to respiration media in the electrode. In this example glutamate 20 mM was added followed by ADP 100 nM, oligomycin 2 µM and FCCP 20 µM at the time points indicated. Mitochondrial oxygen consumption was calculated from the gradients of the graph and indexed to fibre wet weight. ADP - adenosine diphosphate, FCCP - carbonyl cyanide p-trifluoromethoxyphenylhydrazone

Western blotting

Samples were crushed under liquid nitrogen and then homogenised in lysis buffer (see Appendix 4 for details of buffers used). Lysates were then boiled for 5 minutes and centrifuged at 7558 x g. Lysate (10 μL) was decanted for spectrophotometric determination of protein concentration.

Lysates were diluted with further lysis buffer to a final protein concentration of 75 μg in 50 μL. To 50 μL of this protein solution a further 25 μL of sample buffer was added. The sample buffer included 10% (w/v) β-mercaptoethanol (BME) leaving a final BME concentration of 3.3% (w/v) and a protein concentration of 1 μg/μL in the solution ready for loading.

Polyacrylamide gels were cast the night before to allow adequate time for setting. Resolving gel consisted of: 30% acrylamide-bisacrylamide (w/v) (Sigma-Aldrich, Dorset, England) 3.75 ml per gel, resolving gel buffer 3.13 ml per gel, ddH_2O 2.5 ml per gel, 10% ammonium persulphate (w/v) 93.75 μL per gel and tetramethylethylenediamine 10 μL per gel. Stacking gel consisted of: 30% acrylamide-bisacrylamide (w/v) (Sigma-Aldrich, Dorset, England) 0.85 ml per gel, stacking gel buffer 1.25 ml per gel, ddH_2O 1.9 ml per gel, 10% ammonium persulphate (w/v) 20 μL per gel and tetramethylethylenediamine 10 μL per gel. Gels were 1.5 mm thick and consisted of 15 wells.

Protein (30 μg) was loaded into 13 lanes of the 12% (w/v) polyacrylamide gels. The other two lanes were loaded with molecular weight marker (Santa Cruz Biotechnology, Santa Cruz, CA, USA) and molecular weight (rainbow) marker (Amersham – GE Healthcare, Bucks, UK). The gels then underwent sodium dodecyl sulphate (SDS) electrophoresis at 120 V until good separation of the protein was judged to have occurred by visualising the

separation of molecular weight (rainbow) marker. The separated proteins were then transferred onto Immobilon-P membranes (Millipore, Watford, UK) using a semi-dry transfer apparatus (BioRad, Hemel Hempstead, UK) at a current of 0.07 A per gel for 1 hour. Ponceau staining was carried out to ensure even protein loading and transfer. The membranes were blocked for 1 hour in Tris-buffered saline (pH 7.4) with 0.05% (v/v) Tween 20 (TBS-T) + 5% (w/v) fat-free powdered milk, then incubated overnight at 4˚C with the primary antibody (see Appendix 5 for details of primary antibody concentrations).

The following morning the membranes were washed in TBS-T for 2 hours, changing the solution every 15 minutes. The secondary antibody (Appendix 5) was then added and the membranes were incubated at room temperature for at least 1 hour, before washing with TBS-T for 1 hour, changing the solution every 10 minutes. Finally, the membranes were treated with enhanced chemiluminescence (ECL) detection solution (Amersham, GE Healthcare, Bucks, UK) and exposed to X-ray film. Bands were quantified using commercially-available densitometry software (UN-SCAN-IT, Silk Scientific, Orem, UT, USA) (Figure 2.13). Western blots were performed in duplicate on two separate occasions to corroborate results.

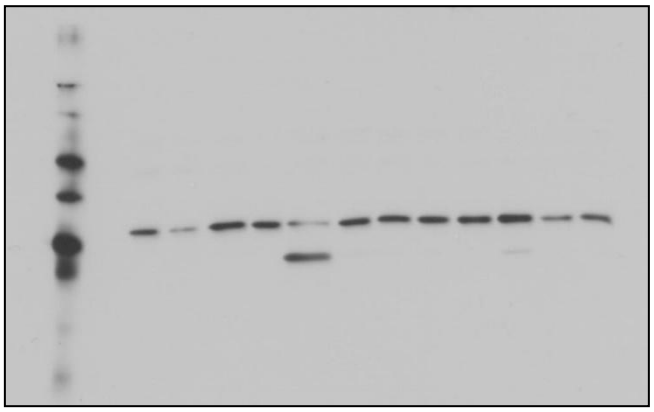

Figure 2.13. An exposed Western blot for UCP3

Whole tissue was snap frozen in liquid nitrogen then crushed and homogenised in lysis buffer to make a solution with final protein concentration of 1.5 $\mu g.\mu L^{-1}$. 30 μg protein from each sample was loaded into polyacrylamide gels for electrophoresis. Seperated proteins were transfered onto Immobilon-P membranes before probing with primary and secondary antibodies. Finally membranes were exposed to X-ray film before band quantification was performed using densitometry software to quantify pixel density and area. The left hand lane contains molecular weight marker.

UCP3 - uncoupling protein-3

2.4. Statistical Analysis

Variables or sub-groups of variables were assessed for normality using the Shapiro-Wilk test along with visual inspection of quantile-quantile plots. Levene's test was employed to confirm homogeneity of variance. If necessary, variables were transformed to normality using appropriate transformations. In the majority of cases the data were found to be positively skewed; in such cases log transformations produced acceptable normality and stability of variance. If the variable could not be transformed to normality adequately, or

violated other assumptions required for parametric tests, appropriate non-parametric tests were employed. Data are presented as means ± standard deviation for normally distributed, continuous variables; or medians and interquartile ranges for non-parametric data unless stated otherwise.

Correlations between continuous, normally distributed variables were presented as Pearson's correlation co-efficient (r), and associated p value (p). Regression analysis is presented as the standardised beta (β) and associated p value (p). Standardised beta refers to the amount of change of the outcome variable for a unit change in the predictor variable with the units being the standard deviation of the variable (Field 2009).

Comparisons between two means of parametric data were performed using t-tests (paired as appropriate) and presented as t (degrees of freedom) and associated p value (p). Multiple groups (in the case of NYHA class) were assessed using Jonkheere – Terpstra's test as explained in the relevant chapters and are presented as JT with associated p value (p). Due to the directional nature of the hypotheses, one-tailed significance testing was used and $p < 0.05$ was taken as being statistically significant. Missing data were excluded from analyses on a case-by-case basis and were not imputed using any method. Statistical calculations were carried out in SPSS version 16.0 (SPSS Inc, IBM, Chicago, Il, USA).

CHAPTER 3

PATIENT DEMOGRAPHICS AND ANTHROPOMETRICS

Sample statistics

In total 47 patients were recruited into the study as a whole, 44 men and 3 women. Figure 3.1 summarises the recruitment pattern, data acquisition and analysis of the subjects.

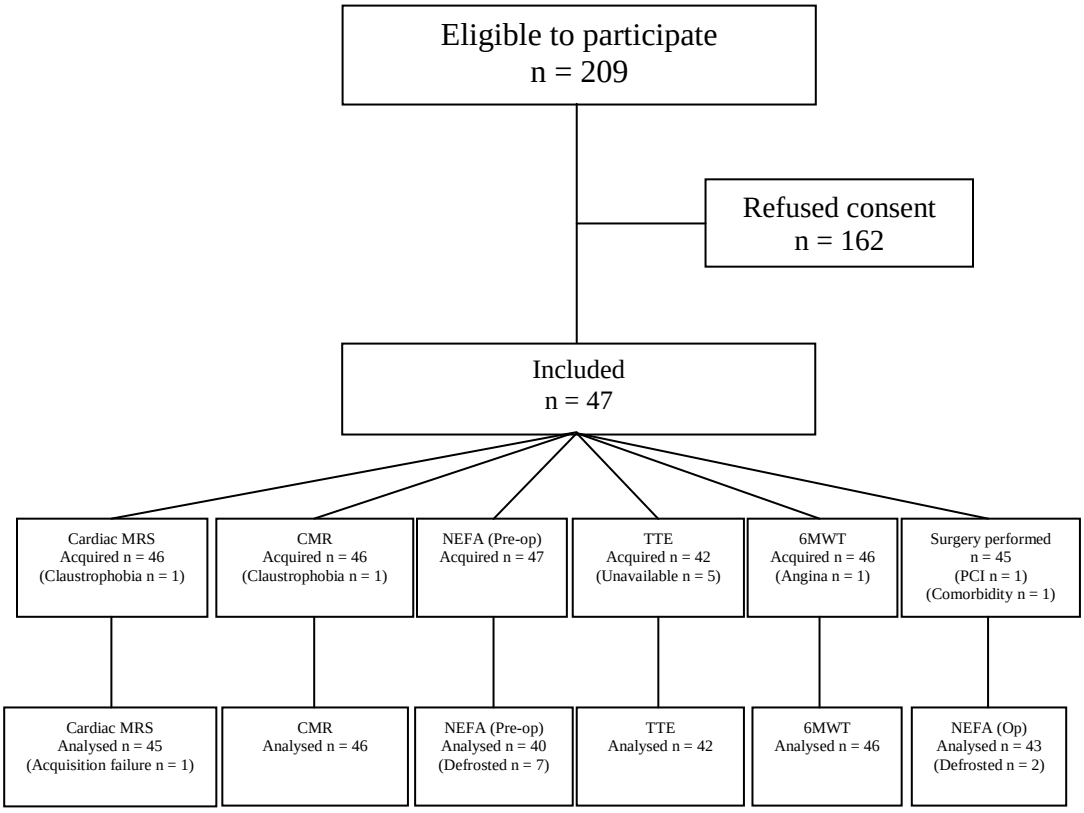

Figure 3.1. CONSORT-type flow diagram to describe the recruitment pattern and data acquisition of enrolled subjects.

MRS – magnetic resonance spectroscopy, CMR – cardiac magnetic resonance imaging, NEFA – non-esterified fatty acid, TTE – trans-thoracic echocardiography, 6MWT – six-minute walk test, PCI – percutaneous coronary intervention.

Table 3.1. Anthropometric data for the cohort.

Variable	Pre-operative (n = 47)
Age (y)	65.8 ± 10.0
Height (m)	1.71 ± 0.06
Weight (kg)	82.6 ± 12.5
BMI (kg.m^{-2})	28.1 ± 3.8
Waist:Hip	0.99 ± 0.06
Body fat content (%)	27.7 ± 5.8
Lean body mass (kg)	59.6 ± 8.5
Body water content (%)	55.9 ± 5.3

Data are expressed as means ± SD. BMI – body mass index.

Cardiac pathology and medication

Patients had four different surgical pathologies: coronary artery disease, aortic stenosis, aortic stenosis with coronary artery disease and mitral regurgitation (Figure 3.2). The cardiovascular medication that the patients were taking is shown in Table 3.2. Five patients were in rate-controlled atrial fibrillation (HR < 90/min), the remainder in sinus rhythm.

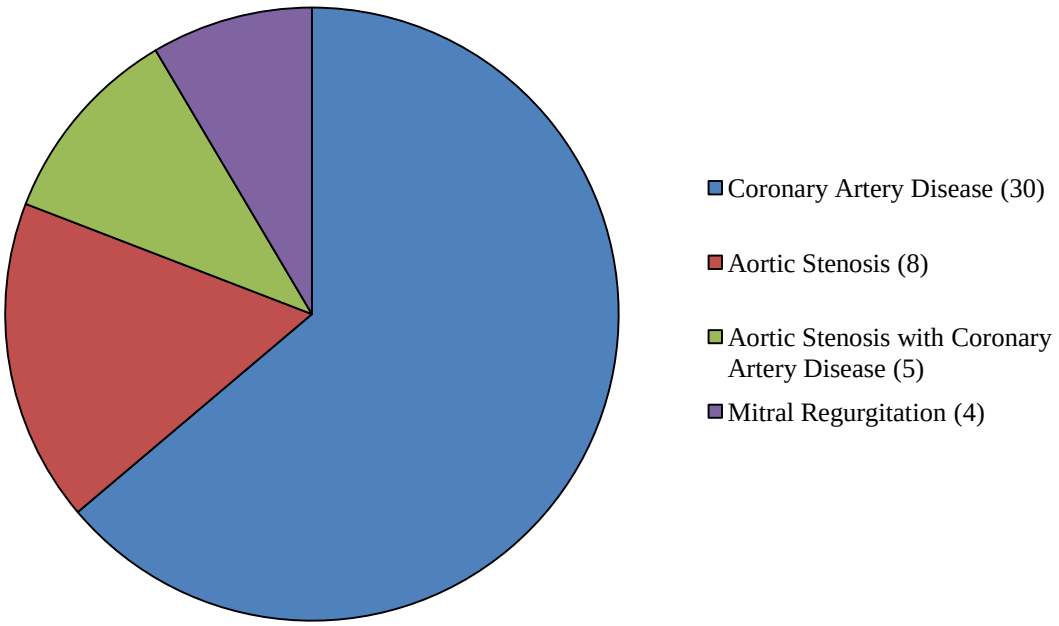

Figure 3.2. Analysis of surgical pathology in the recruited patients.

Table 3.2. Table showing the numbers of patients taking each class of cardiac medication.

Drug class	n
β-blockers	32
ACEI/A2RB	27
Thiazide diuretics	6
Nitrates (oral)	8
Loop diuretics	8
Calcium channel blockers	5
Digoxin	1

ACEI – angiotensin converting enzyme inhibitors, A2RB – angiotensin 2 receptor blockers.

Cardiac function

The patient cohort represented a mixture of systolic and diastolic cardiac dysfunction (Figure 3.3 and Table 3.3).

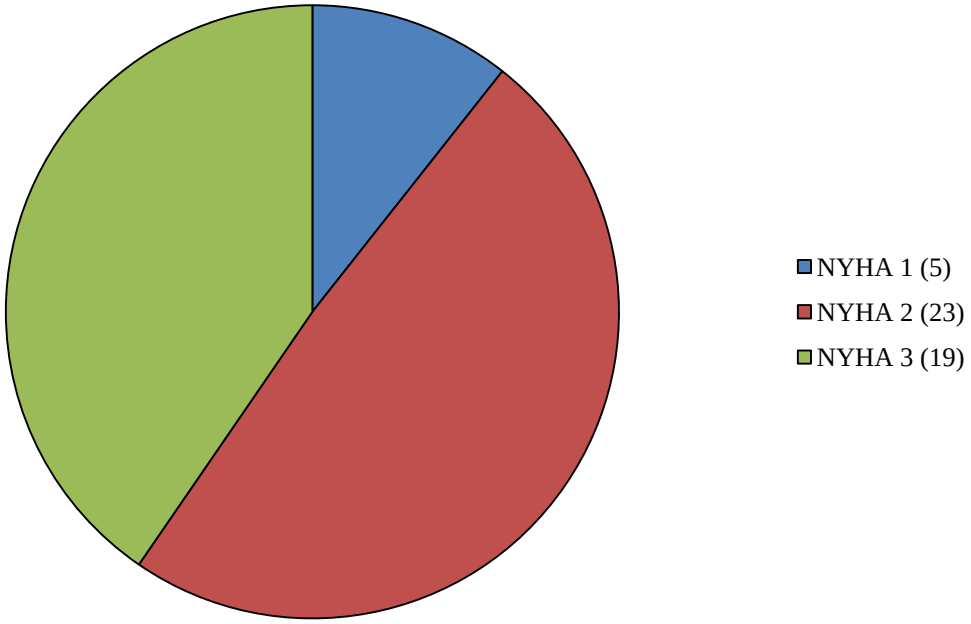

Figure 3.3. Pie-chart to show the patient frequencies grouped according to NYHA functional class.

NYHA – New York Heart Association functional classification.

NYHA classification and 6MWT distance did not demonstrate a significant ordered relationship with each other (JT, p = 0.29) (Figure 3.4).

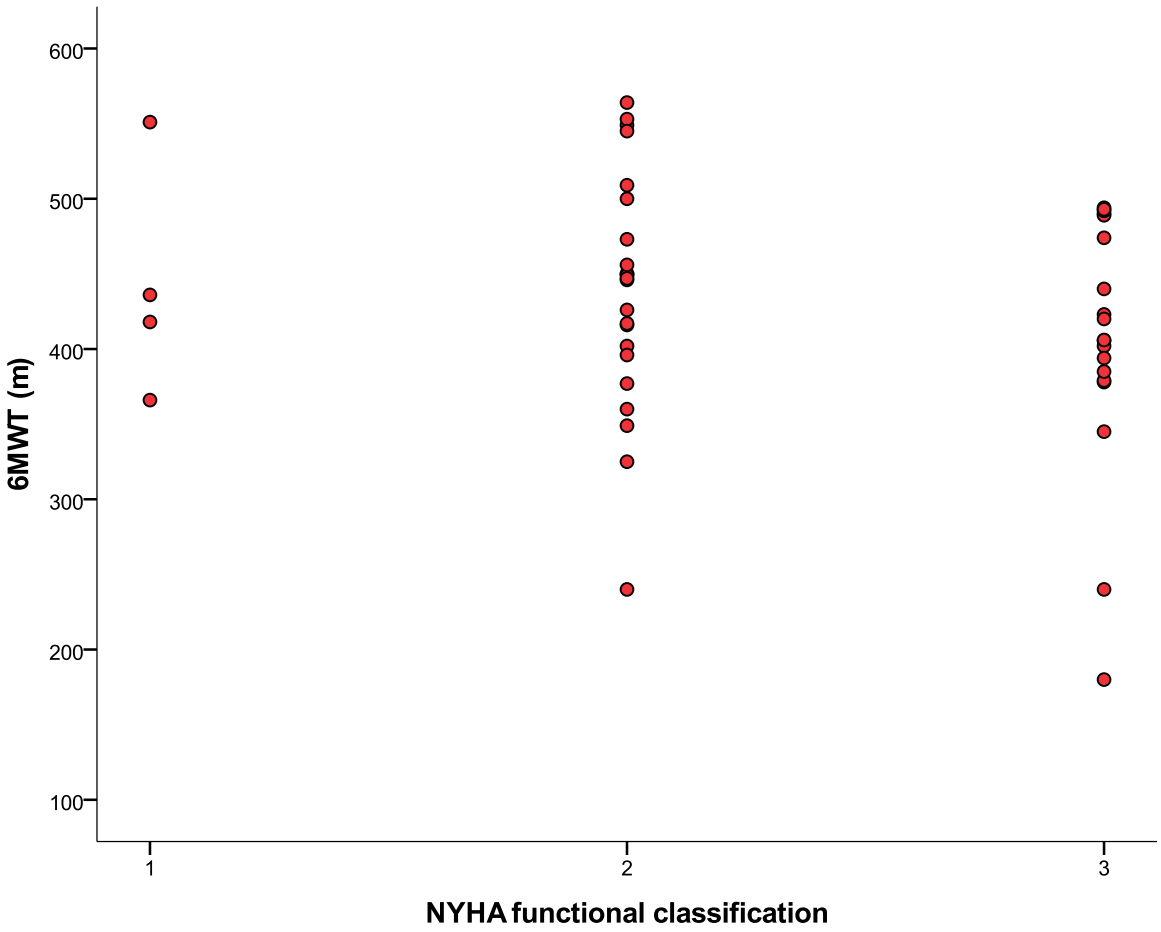

Figure 3.4. Scatter plot of six-minute walk test distance grouped according to NYHA class.

The Jonckheere-Terpstra test was used for analysis, as NYHA groups are ordered and, as such, trends were expected in the medians of the groups.

JT, p = 0.29

Table 3.3. Table showing baseline measures of cardiac function and haemodynamics.

Variable	Pre-operative	n
Heart Rate (min^{-1})	60 ± 14	47
Systolic Blood Pressure (mmHg)	131 ± 22	47
Diastolic Blood Pressure (mmHg)	74 ± 12	47
Left Ventricular Ejection Fraction (%)	63 ± 13	46
Left Ventricular End-Diastolic Volume (ml)	172 ± 65	46
Left Ventricular Myocardial Mass (g)	204 ± 62	46
Mitral inflow (E/A)	1.1 ± 0.4	42
Mitral annulus motion (E/E')	9.8 ± 4.1	42
New York Heart Association Functional Class	2 (1-3)	47
PCr/ATP	1.55 ± 0.28	45
6MWT (m)	426.1 ± 81.0	46

Data are presented as means ± SD except NYHA class which is presented as median (IQR). E – early phase of ventricular filling, A – atrial component of ventricular filling, E' – tissue velocity during early phase of ventricular filling, PCr – phosphocreatine, ATP – adenosine triphosphate, 6MWT – six minute walk test.

Plasma metabolites

Baseline fasting venous blood samples were taken pre-operatively to measure plasma metabolites and hormones; results are shown in Table 3.4. There were five patients with type 2 diabetes; two were diet-controlled and three were taking metformin.

Table 3.4. Table showing baseline pre-operative fasting plasma metabolite and hormone profiles.

Metabolite/hormone	**Pre-operative**	**n**
Non-esterified fatty acids (mmol.L^{-1})	0.42 ± 0.19	40
Operative non-esterified fatty acids (mmol.L^{-1})	0.68 ± 0.29*	43
Glycerol (mg.dL^{-1})	11.6 ± 5.6	40
Glucose (mmol.L^{-1})	5.1 ± 1.6	40
Insulin (mU.L^{-1})	7.8 ± 6.8	40
Lactate (mmol.L^{-1})	0.9 ± 0.5	40

Data are presented as means ± SD. * $p < 0.001$ compared with pre-operative NEFA sample.

CHAPTER 4

THE RELATIONSHIPS BETWEEN CARDIAC FUNCTION, PLASMA NON-ESTERIFIED FATTY ACIDS, CARDIAC ENERGETICS AND VENTRICULAR UNCOUPLING PROTEIN-3 LEVELS

4.1. Introduction

Despite optimal current therapy, heart failure is associated with a high mortality and morbidity (Cowie, Wood *et al* 2000). The implication is that the fundamental molecular and cellular mechanisms are not being addressed. Over recent years there has been interest in pursuing metabolic interventions for heart failure, due to mounting evidence of changes in substrate metabolism and mitochondrial dysfunction, and some promise has been shown (Lee, Campbell *et al* 2005). ^{31}Phosphorus magnetic resonance spectroscopy (^{31}P MRS) is a useful non-invasive method for studying energetic abnormalities within the myocardium *in vivo*, and has been used to study heart failure in a variety of patient groups. Regardless of the aetiology, it has repeatedly been shown that in heart failure there is a decrease in the ratio of myocardial PCr/ATP (Shivu, Abozguia *et al* 2010; Conway, Allis *et al* 1991; de Roos, Doornbos *et al* 1992; Neubauer, Krahe *et al* 1992; Conway, Bottomley *et al* 1998; Beyerbacht, Lamb *et al* 2001). The cause and temporal sequence of this apparent abnormality in ATP synthesis or utilisation has been debated (Vogt and Kubler 1998), but is very likely multifactorial.

However, it has been shown that plasma non-esterified fatty acid (NEFA) concentrations correlate negatively with myocardial PCr/ATP ratio in type 2 diabetic patients (Scheuermann-Freestone, Madsen *et al* 2003) and myocardial PCr/ATP is unrelated to the degree of microvascular obstruction in Type 1 diabetics (Shivu, Phan *et al* 2010) providing evidence for a metabolic cause for the decreased PCr/ATP ratio. Plasma NEFA concentrations are elevated in heart failure secondary to an increased sympathetic drive and subsequent adipose tissue lipolysis. As fatty acids are more reduced than glucose, the stoichiometry of lipid catabolism demands greater oxygen consumption for a given ATP

yield than carbohydrates (Ashrafian, Frenneaux *et al* 2007). Increased plasma NEFA concentrations are also associated with an increase in the expression of mitochondrial uncoupling protein-3 (UCP3) (Murray, Anderson *et al* 2004), a member of the mitochondrial anion carrier protein superfamily. Controversy remains as to what extent UCP3 truly uncouples oxidative metabolism *in vivo*, but even a mild uncoupling effect could provide a potential mechanism for the decrease in myocardial PCr/ATP ratio in heart failure.

4.2. Aims

The aim of this chapter was to investigate the hypothesis that myocardial PCr/ATP ratio would be negatively predicted by ventricular UCP3 levels, and that fasting plasma NEFA concentration and hence ventricular UCP3 levels would be related to the degree of ventricular dysfunction. This hypothesis provides a potential process to decribe the well recognised, but mechanistically undetermined, decrease in myocardial PCr/ATP ratio in heart failure.

4.3 Methods

Having been recruited from the cardiothoracic surgery outpatient clinics, and following an overnight fast, the patients described in Chapter 3 attended the Oxford Centre for Clinical Magnetic Resonance Research (OCMR) at a convenient time before their scheduled surgery. A clinical history was taken and demographic and anthropometric data recorded as described in Chapter 2. Patients then underwent cardiac ^{31}P MRS and cardiac MRI cine imaging as described in Chapter 2. Venous blood samples were acquired from an anticubital fossa vein, and the blood immediately cooled and centrifuged at 4ºC. Plasma for the measurement of

NEFA concentration was frozen after the addition of a lipoprotein lipase inhibitor (tetrahydrolipstatin, Xenical, Roche, Welwyn Garden City, UK) at a final concentration of 30 $\mu g.ml^{-1}$ as described in Chapter 2. Patients were then provided with a mixed meal. Once refreshed, patients performed the six-minute walk test (6MWT) and underwent transthoracic echocardiography as described in Chapter 2, after which they were discharged home.

On the day of surgery, and again following an overnight fast, immediately prior to anaesthetic induction, blood was taken from an arterial cannula for further measurement of plasma NEFA concentration, in order that a contemporaneous measure was available to relate to Western blot results. During the operation, right atrial appendage tissue was obtained at venous cannulation if patients were having surgery under cardiopulmonary bypass (on-pump), or after exposure of the heart, prior to the commencement of grafting, if operated on without cardiopulmonary bypass (off-pump). The tissue was immediately washed in physiological (0.9 % w/v) saline and snap-frozen in liquid nitrogen. In most cases the surgeons also provided left ventricular biopsies. The ventricular biopsies were taken from myocardium distant from evident scar, within 5 minutes of the commencement of cardiopulmonary bypass in those patients receiving their surgery on-pump, and prior to the commencement of coronary grafting in the off-pump patients. The ventricular tissue was also snap-frozen in liquid nitrogen for later Western blot analysis to measure UCP3 levels.

Ventricular dysfunction was said to be present if patients had systolic and/or diastolic ventricular impairment, defined previously in Chapter 2.

Statistical analysis

Variables and sub-groups of variables were assessed for normality by Shapiro-Wilk tests and visual inspection of quantile-quantile plots and homogeneity of variance using Levene's test (Field 2009). Variables were transformed if necessary to render them normally distributed. In the majority of cases the data were found to be positively skewed; in such cases log transformations produced acceptable normality and stability of variance. One-tailed statistical tests were used because of the directional nature of the hypotheses being tested. Regression analyses were performed to assess the degree to which one variable could be predicted from another, with standardised beta (β) and associated p value (p) reported. Standardised beta refers to the degree of change of the outcome variable for a unit change of the predictor, with units being standard deviations (Field 2009). Standardised betas were categorised as small, medium and large effects as described by Cohen (small >0.1, medium >0.3, large >0.5) (Cohen 1992).

NYHA groups were compared using the non-parametric Jonckheere-Terpstra test. As group sizes were uneven, and there were only 5 patients in NYHA class one, the assumptions for analysis of variance were therefore not met and non-parametric methods were used. The Jonckheere-Terpstra test was used as NYHA groups are ordered and, as such, trends were expected in the medians of the groups. This was reported as JT and the p value.

If a variable was divided into two groups, for example normal or abnormal ventricular function, and each group met parametric assumptions, independent t-tests were used to compare means, and were reported mean1 ± SEM1 *vs* mean2 ± SEM2, the value of the test statistic t (degrees of freedom) and the associated p value. Missing data were excluded from analyses on a case-by-case basis and were not imputed using any method.

4.4. Results

The patient cohort studied in this chapter is the one described in Chapter 3 (Figure 4.1). One patient was unable to tolerate MRI cine imaging due to claustrophobia, so cardiac volumes and ^{31}P MRS were not obtained. The MRS data acquired from one patient was not quantifiable due to poor spectral quality (very low signal/noise ratio). Two patients did not undergo surgery despite being initially listed for surgical management, therefore biopsies were not taken for myocardial UCP3 measurement, or pre-anaesthetic induction blood for plasma NEFA concentration. The pre-operative plasma samples from 7 patients were accidently defrosted, along with 2 from the operative visit, and so were not analysed because of uncertainty over the veracity of results from those samples. The operating surgeon declined to provide ventricular biopsies on 9 occasions and on 2 occasions the ventricular biopsies were too small to enable Western blotting analysis.

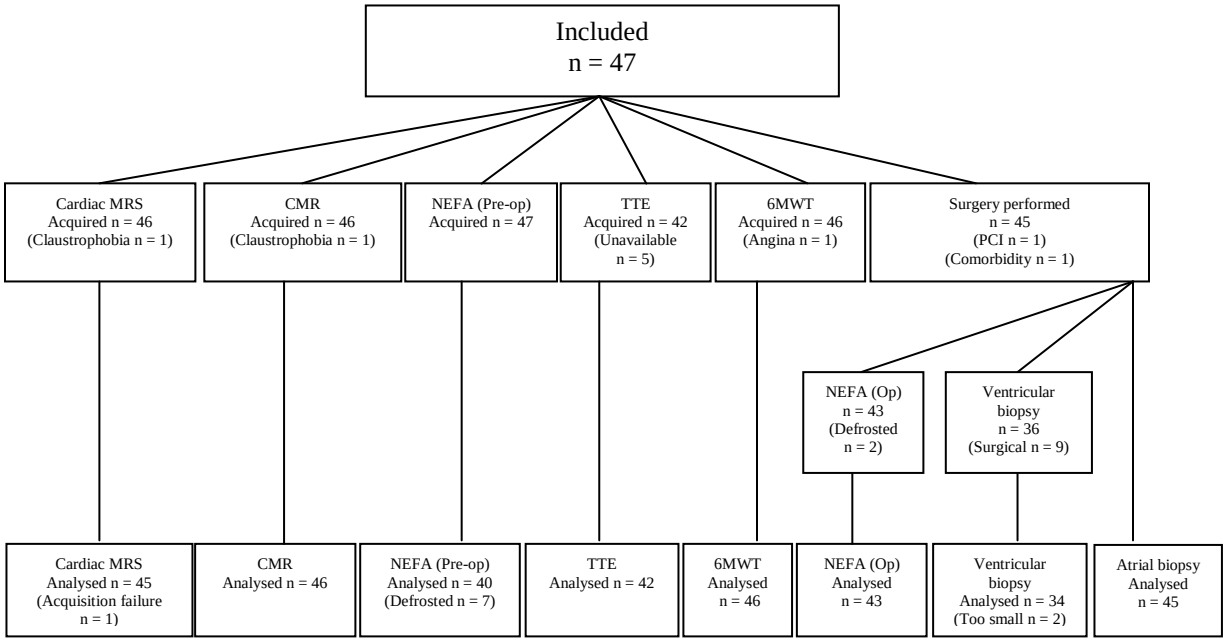

Figure 4.1. CONSORT-type flow diagram to describe the inclusion of subjects from the recruited cohort presented in Chapter 3.

MRS – magnetic resonance spectroscopy, CMR – cardiac magnetic resonance imaging, NEFA – non-esterified fatty acid, TTE – trans-thoracic echocardiography, 6MWT – six-minute walk test, PCI – percutaneous coronary intervention.

Plasma non-esterified fatty acids

Fasting plasma NEFA concentrations were measured at the pre-operative visit and at the operative visit pre-anaesthetic induction. The operative measurement was to relate biopsies taken at operation to a contemporaneous measurement of fasting plasma NEFA concentration. The samples differed (paired samples, 2-tailed t test) from each other (0.42 ± 0.19 *vs* 0.68 ± 0.29, $t(35) = -5.73$, $p < 0.001$) but correlated ($r = 0.30$, $p < 0.05$) (Figure 4.2). Pre-medication was recorded to assess whether this had any effect on operative plasma

NEFA concentration, as this was not controlled in the experimental protocol. No difference (unpaired samples, 2-tailed t test) was found in NEFA concentration change between patients premedicated with oral temazepam and with intra-muscular papaveretum and hyoscine (0.11 ± 0.05 *vs* 0.22 ± 0.05, t (33) = -1.56, p = 0.13).

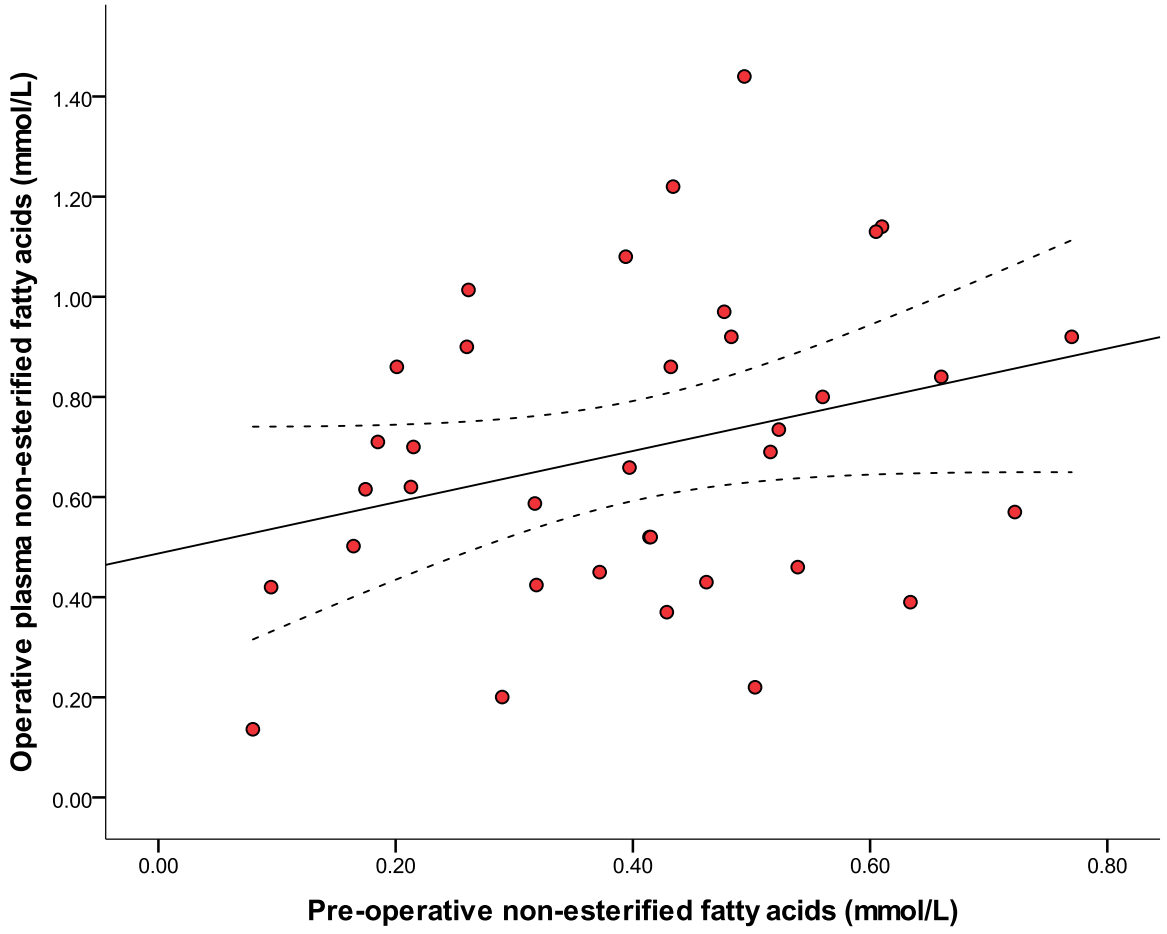

Figure 4.2. Scatter-plot of operative plasma non-esterified fatty acid concentration plotted against pre-operative plasma non-esterified fatty acid concentration.

The solid line is the regression line and the dashed lines are the 95% confidence intervals of the regression line.

r = 0.30, p < 0.05

Cardiac function and non-esterified fatty acids

Left ventricular ejection fraction (LVEF) was a significant predictor of plasma non-esterified fatty acid concentration ($\beta = -0.33$, $p < 0.05$) (Figure 4.3) but diastolic function (E/E' mitral annulus tissue Doppler) was not ($\beta = -0.05$, $p = 0.79$) (data not shown). There was no significant trend in NEFA concentrations grouped according to NYHA class (JT, $p = 0.07$) (Figure 4.4), however if patients were divided into two groups, one with ventricular dysfunction (systolic or diastolic – defined earlier), and one without, there was a significant difference in NEFA concentration between the two groups (0.35 ± 0.04 *vs* 0.48 ± 0.04 $mmol.L^{-1}$, $t(37) = -2.3$, $p < 0.05$) (Figure 4.5).

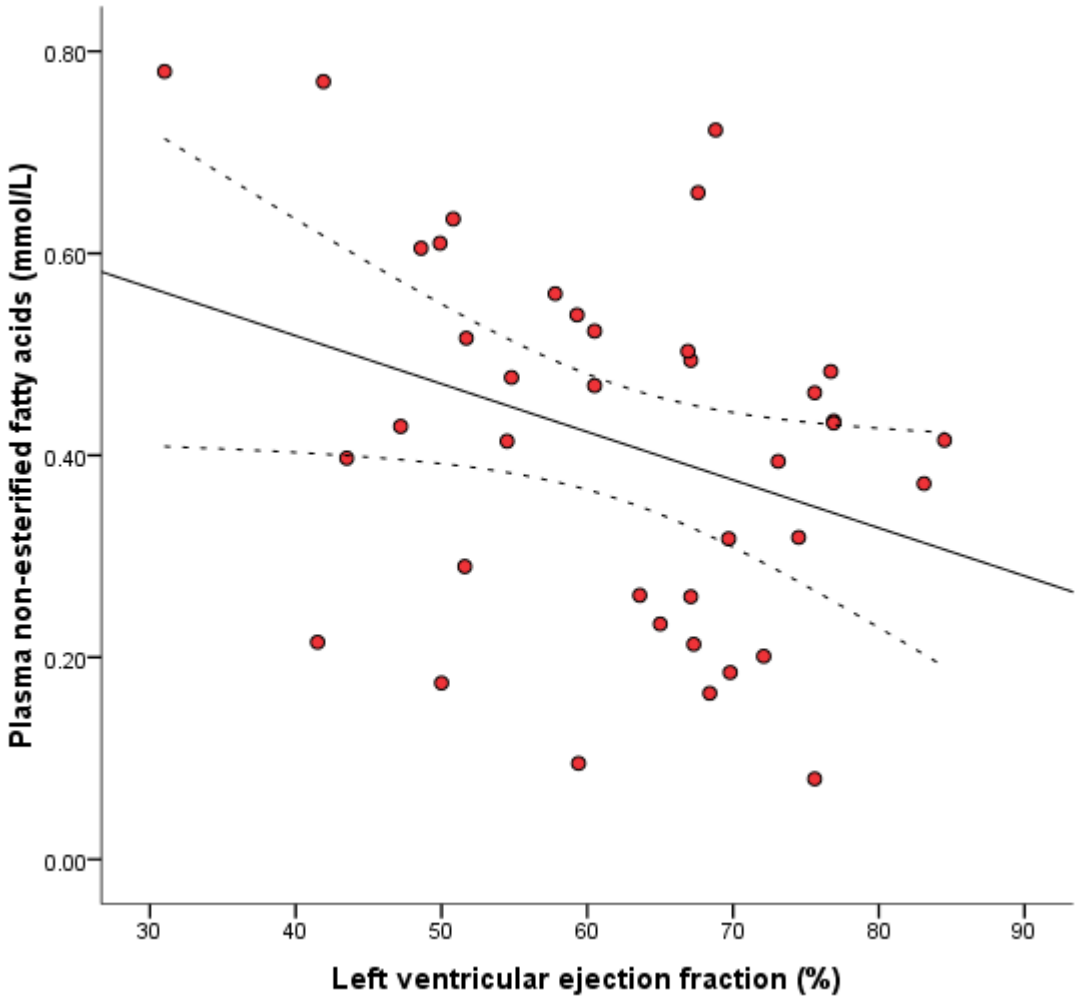

Figure 4.3. Scatter-plot of plasma non-esterified fatty acid concentration plotted against left ventricular ejection fraction.

The solid line is the regression line and the dashed lines are the 95% confidence intervals of the regression line.

$\beta = -0.33$, $p < 0.05$

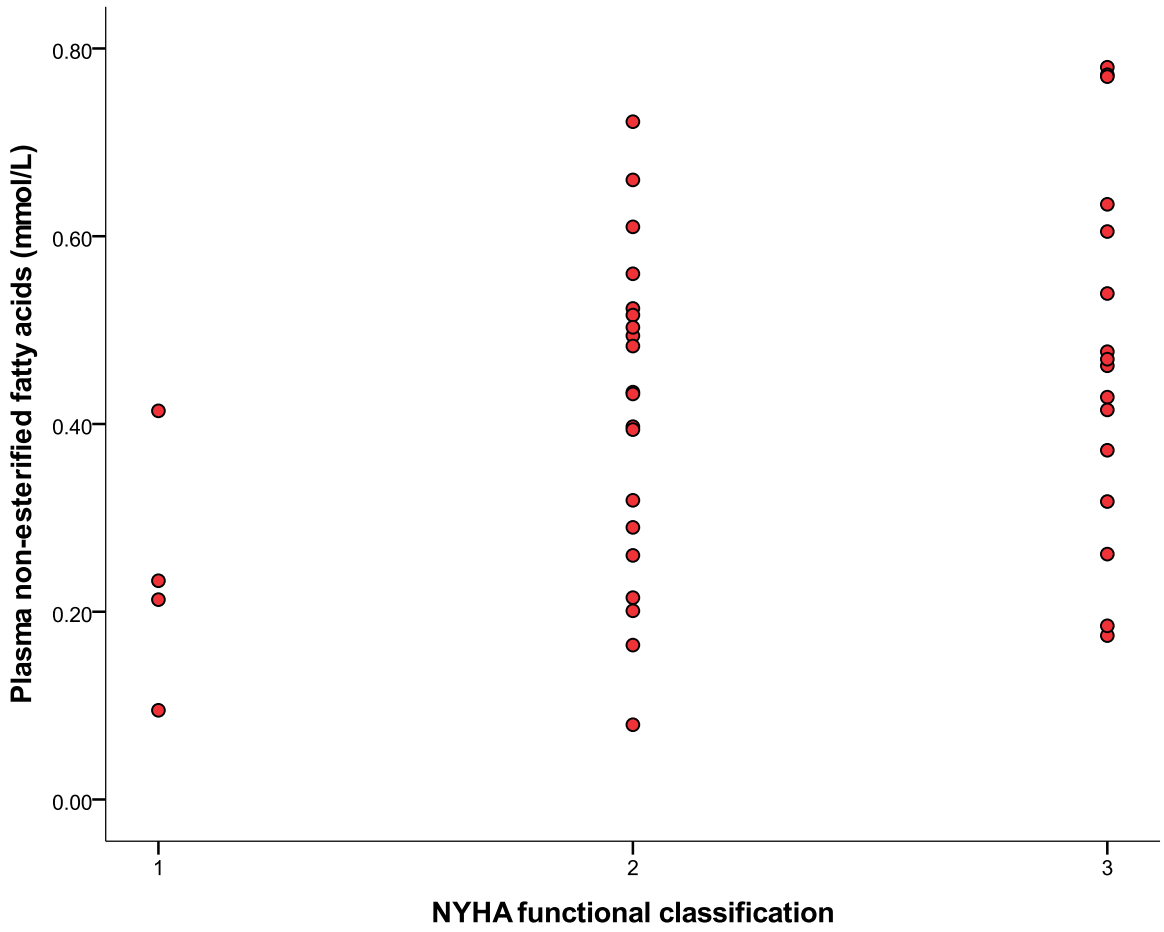

Figure 4.4. Plasma non-esterified fatty acids grouped according to NYHA class.

Jonckheere-Terpstra, p = 0.07.

NYHA – New York Heart Association.

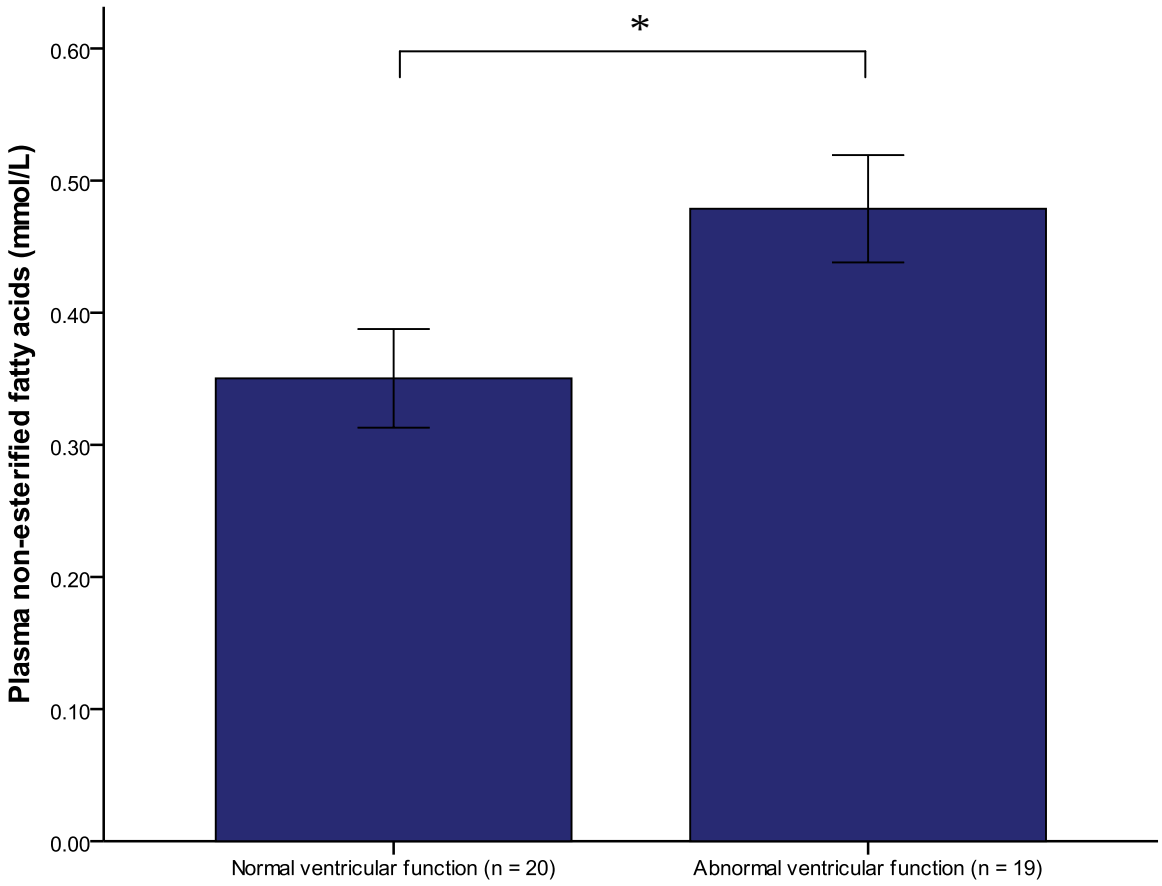

Figure 4.5. Plasma non-esterified fatty acids grouped according to the absence or presence of ventricular dysfunction.

Bars denote mean values, error bars SEM.

* p = < 0.05

Plasma non-esterified fatty acid concentrations were significantly increased in patients reporting dyspnoea at rest (0.65 ± 0.06 *vs* 0.39 ± 0.03 mmol.L^{-1}, t (37) = 3.7, p < 0.001) (Figure 4.6), but were not predicted by 6MWT distance (β = 0.09, p = 0.61) (Figure 4.7).

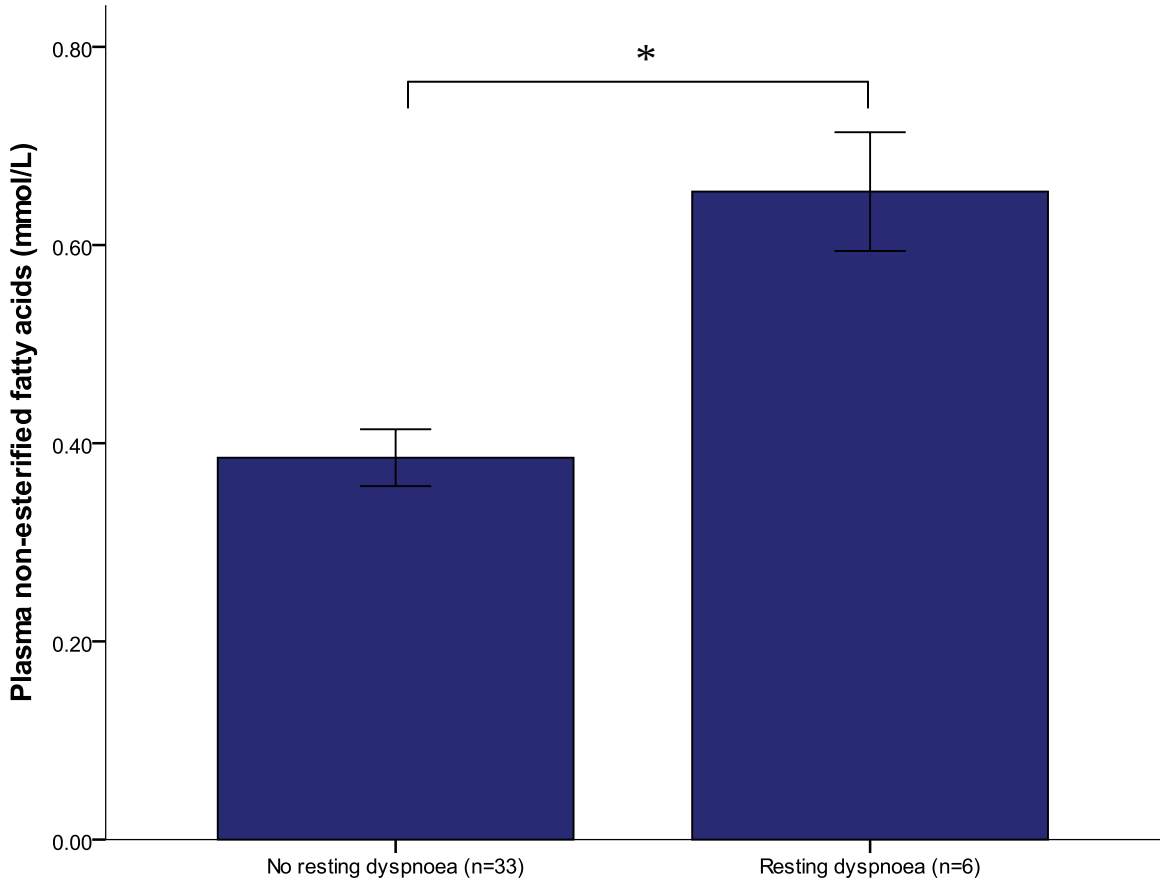

Figure 4.6. Plasma non-esterified fatty acid concentration grouped according to the absence or presence of dyspnoea at rest.

Bars denote mean values, error bars SEM.

* p < 0.001

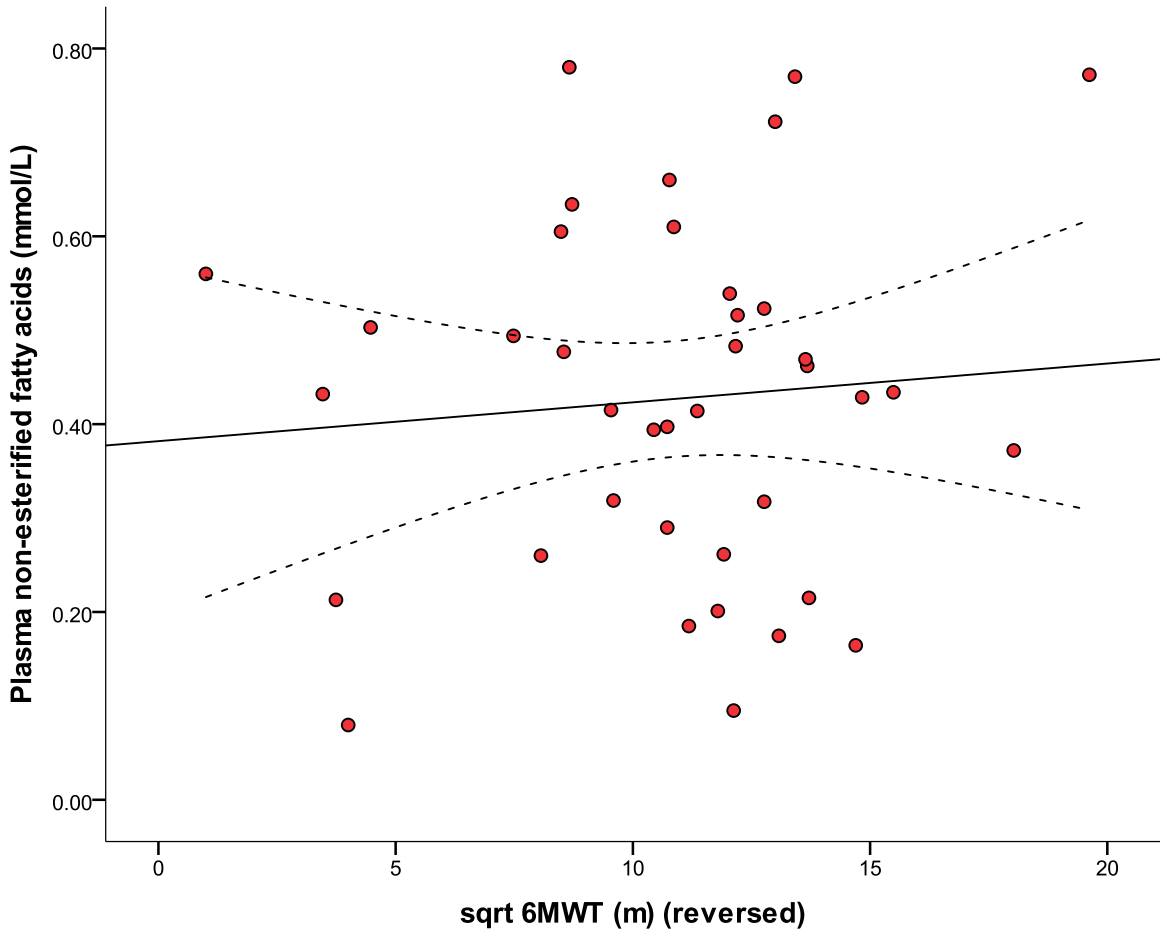

Figure 4.7. Scatter-plot of plasma non-esterified fatty acid concentration plotted against six-minute walk test distance.

The solid line is the regression line and the dashed lines are the 95% confidence intervals of the regression line. The 6MWT values were reversed and square-rooted to correct for negative skew in the data.

$\beta = 0.09$, $p = 0.61$

6MWT - six-minute walk test

Cardiac function and cardiac energetics

Cardiac PCr/ATP ratio was not predicted by LVEF ($\beta = 0.20$, $p = 0.11$), diastolic function (E/E' – $\beta = 0.01$, $p = 0.49$), left ventricular end-diastolic volume (LVEDV) ($\beta = -0.04$, $p = 0.41$), left ventricular mass (LVM) ($\beta = -0.12$, $p = 0.22$), cardiac output (CO) ($\beta = -0.13$, $p = 0.20$) or rate pressure product (RPP) ($\beta = -0.10$, $p = 0.27$) (data not shown).

In terms of heart failure symptoms, cardiac PCr/ATP ratio grouped according to NYHA class demonstrated a significant linear trend (JT, $p < 0.01$) (Figure 4.8). By contrast however, cardiac PCr/ATP was not predicted by 6MWT distance ($\beta = 0.05$, $p = 0.38$) (Figure 4.9). If grouped according to the presence or absence of ventricular dysfunction (defined earlier), cardiac PCr/ATP ratio differed significantly (1.61 ± 0.05 vs 1.48 ± 0.06, $t(43) = 1.7$, $p < 0.05$) (Figure 4.10).

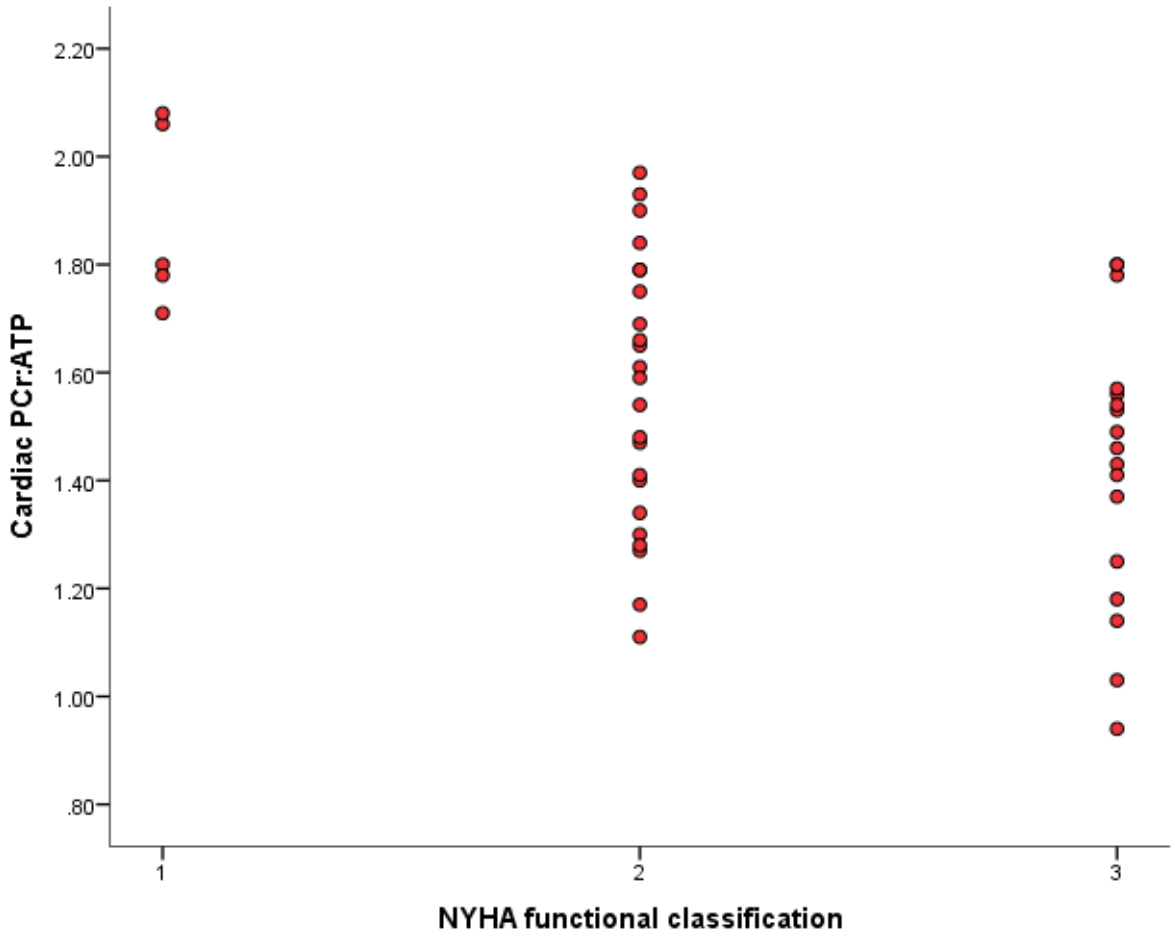

Figure 4.8. Cardiac PCr/ATP ratio grouped according to NYHA class.

Jonckheere-Terpstra, $p < 0.01$.

NYHA – New York Heart Association, PCr – phosphocreatine, ATP – adenosine triphosphate.

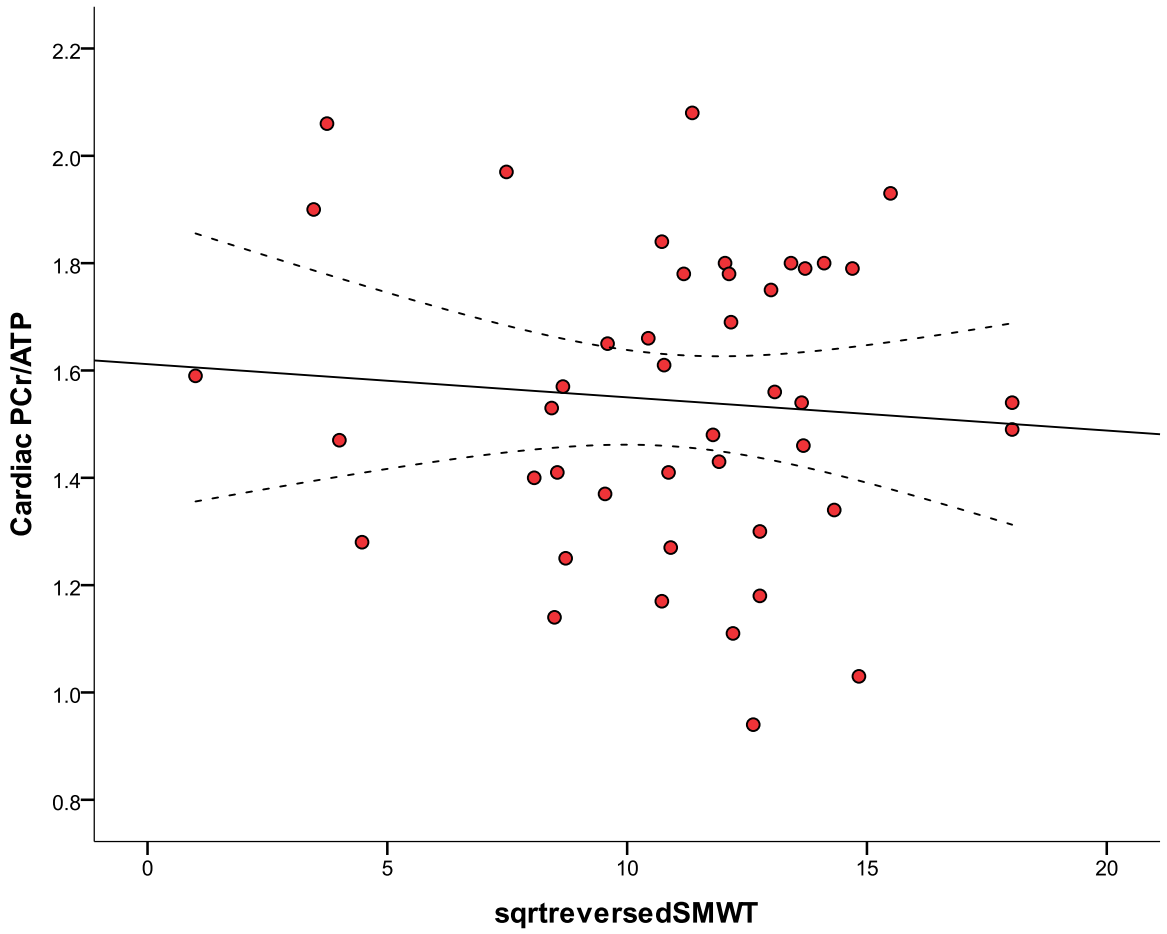

Figure 4.9. Scatter-plot of cardiac PCr/ATP ratio plotted against six-minute walk test distance.

The solid line is the regression line and the dashed lines are the 95% confidence intervals of the regression line. The 6MWT values were reversed and square-rooted to correct for negative skew in the data.

$\beta = 0.05$, $p = 0.38$

6MWT - six-minute walk test

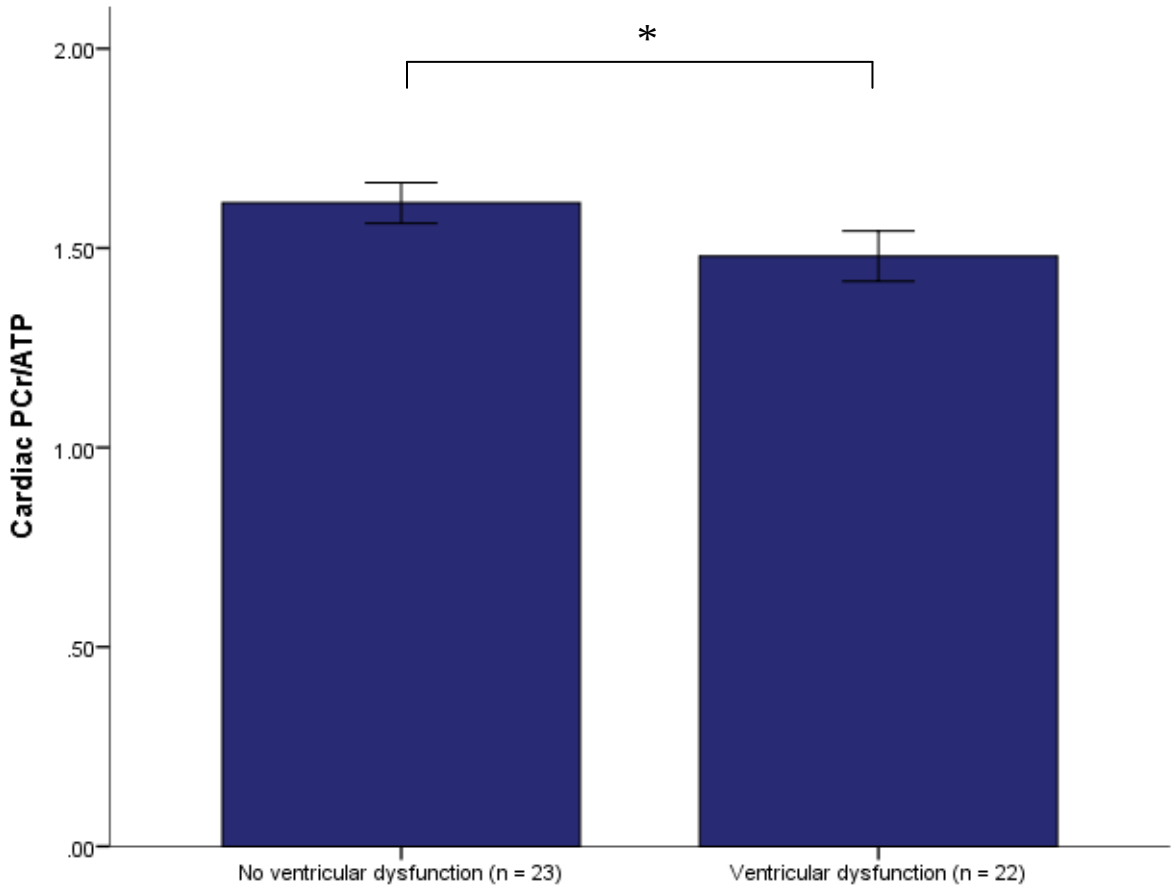

Figure 4.10. Cardiac PCr/ATP ratio grouped according to the absence or presence of ventricular dysfunction.

Ventricular dysfunction was defined as a left ventricular ejection fraction of less than 55% and/or diastolic dysfunction (defined as (i) E/E' > 15 or (ii) E/E' 8 – 15 with E/A < 0.5 or LV mass index >122 g/m^2 (women), >149 g/m^2 (men) or atrial fibrillation (Paulus, Tschope *et al* 2007).

Bars denote mean values, error bars SEM.

* $p < 0.05$

PCr – phosphocreatine, ATP – adenosine triphosphate

Plasma metabolites and cardiac energetics

Neither fasting plasma NEFA concentrations (β = -0.13, p = 0.22), nor fasting plasma glucose concentrations, (β = 0.21, p = 0.14) were predictive of cardiac PCr/ATP ratio (data not shown).

Cardiac UCP3 protein levels and cardiac function

Ventricular UCP3 levels, as measured by Western blotting, were not predicted by LVEF (β = -0.04, p = 0.42), LVEDV (β = 0.05, p = 0.38), LVM (β = -0.21, p = 0.12), CO (β = -0.10, p = 0.29) or E/E' (β = 0.13, p = 0.26) (data not shown). Ventricular UCP3 levels grouped according to NYHA class demonstrated a significant tend (JT, $p < 0.05$) (Figure 4.11), but there was no difference in ventricular UCP3 levels between the groups with and without ventricular dysfunction (0.72 ± 1.2 *vs* 0.73 ± 1.2, t (32) = -0.08, p = 0.47).

Atrial UCP3 levels were not predicted by LVEF (β = -0.06, p = 0.33), LVEDV (β = -0.04, p = 0.39), LVM (β = -0.12, p = 0.22), CO (β = -0.21, p = 0.09) or E/E' (β = 0.19, p = 0.12) (data not shown). There was no trend in atrial UCP3 grouped according to NYHA class (JT, p = 0.56), and no difference in atrial UCP3 levels if grouped according to normal or abnormal ventricular function (0.9 ± 0.07 *vs* 1.1 ± 0.08 a.u., t(41) = -1.4, p = 0.09).

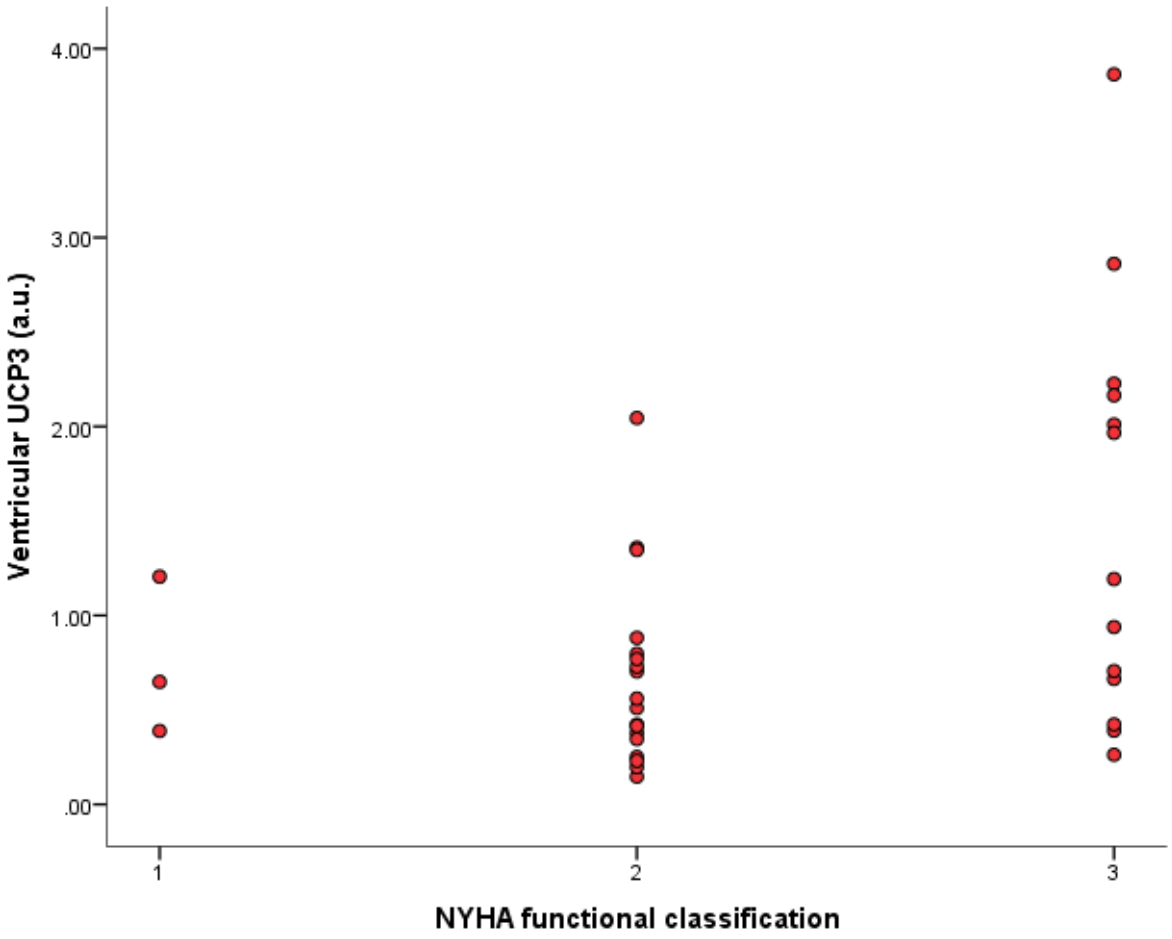

Figure 4.11. Ventricular UCP3 grouped according to NYHA class.

Jonckheere-Terpstra, $p < 0.05$

UCP3 – uncoupling protein-3, NYHA – New York Heart Association, a.u. - arbitrary units

Cardiac UCP3 level, fasting plasma NEFA concentrations and cardiac energetics

Ventricular UCP3 levels were not predicted by plasma NEFA concentration ($r = -0.09$, $p = 0.32$) and did not predict cardiac PCr/ATP ratio ($r = -0.18$, $p = 0.15$) (Figure 4.12). Plasma NEFA concentration predicted atrial UCP3 levels significantly ($\beta = 0.35$, $p < 0.05$) (Figure 4.13). Atrial UCP3 levels were not predictive of cardiac PCr/ATP ratio ($\beta = -0.12$, $p = 0.23$)

(data not shown). Atrial and ventricular UCP3 levels correlated with each other ($r = 0.30$, $p < 0.05$) (Figure 4.14).

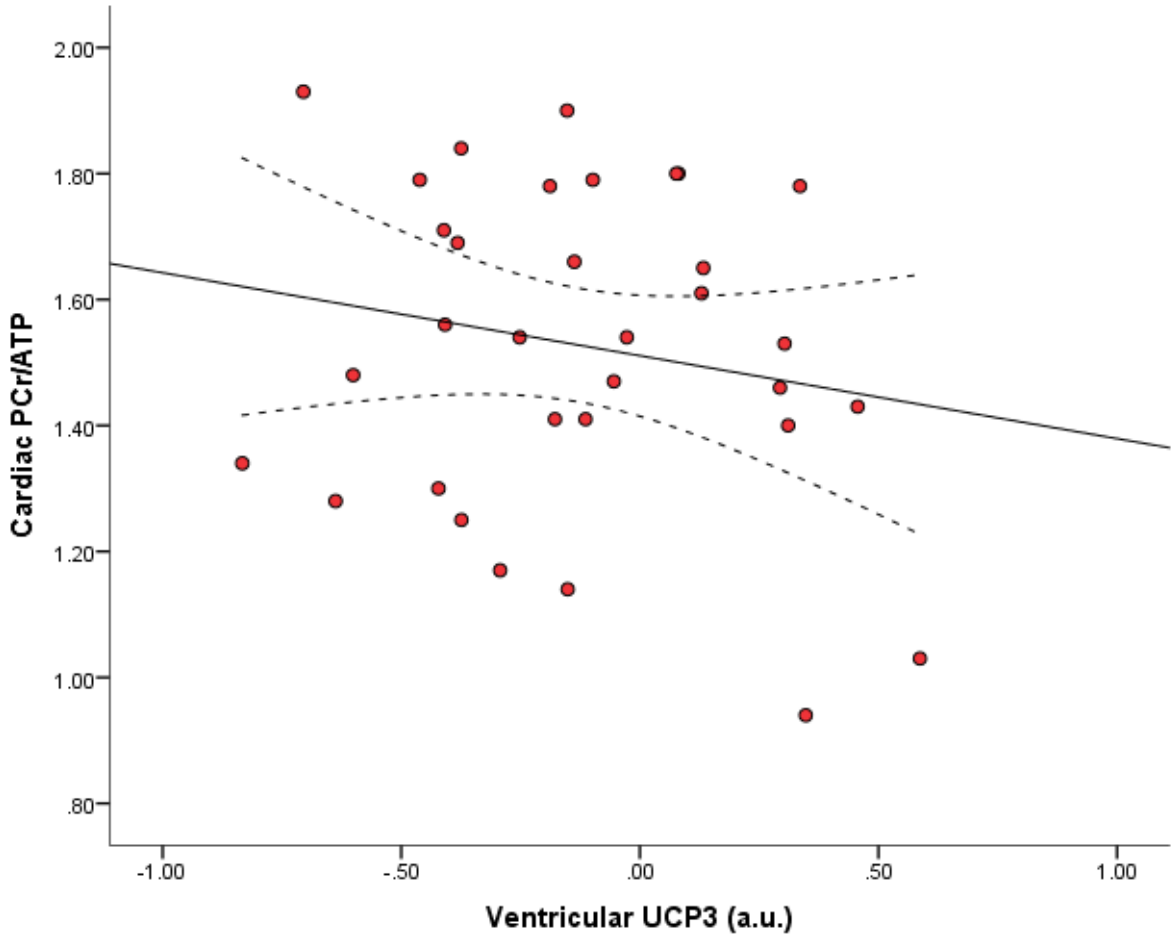

Figure 4.12. Scatter-plot of cardiac PCr/ATP ratio plotted against ventricular UCP3 level.

The solid line is the regression line and the dashed lines are the 95% confidence intervals of the regression line.

$\beta = -0.18$, $p = 0.15$

UCP3 – mitochondrial uncoupling protein-3, PCr – phosphocreatine, ATP – adenosine triphosphate, a.u. - arbitrary units

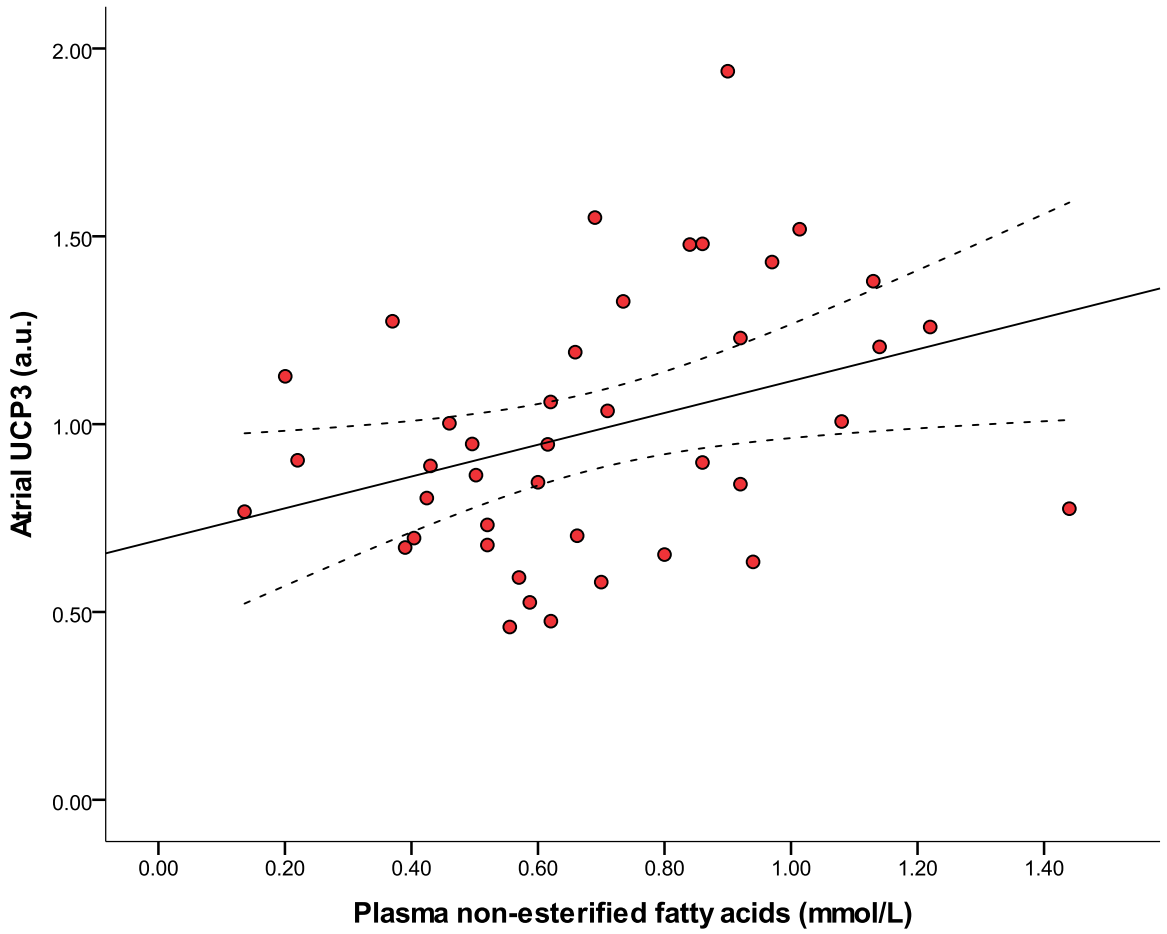

Figure 4.13. Scatter-plot of atrial UCP3 level plotted against plasma non-esterified fatty acid concentration.

The solid line is the regression line and the dashed lines are the 95% confidence intervals of the regression line.

$\beta = 0.35$, $p < 0.05$

UCP3 – mitochondrial uncoupling protein-3, a.u. - arbitrary units

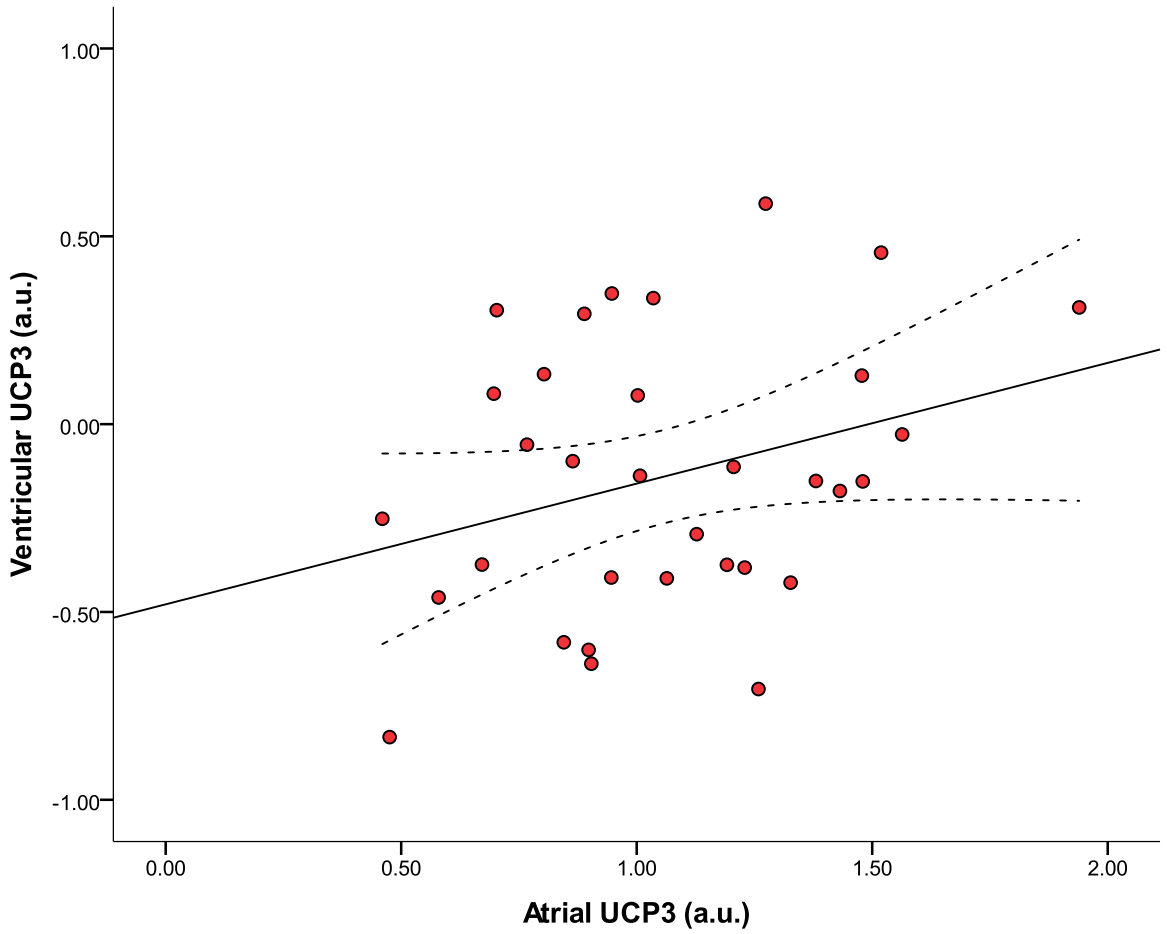

Figure 4.14. Scatter-plot of ventricular UCP3 level plotted against atrial UCP3 level.

The solid line is the regression line and the dashed lines are the 95% confidence intervals of the regression line.

$\beta = 0.30$, $p < 0.05$

UCP3 – mitochondrial uncoupling protein-3

4.4. Discussion

The principal finding of this study was that ventricular UCP3 levels were not predictive of cardiac PCr/ATP ratio (Figure 4.12). Cardiac PCr/ATP ratio was found to be lower in patients with ventricular dysfunction compared to patients without ventricular dysfunction (Figure 4.10) and correlated with heart failure severity grouped according to NYHA class (Figure 4.8) consistent with previous research (Neubauer, Krahe *et al* 1992).

There are a number of possible reasons why this study failed to show an association between ventricular UCP3 levels and cardiac PCr/ATP ratio. Firstly, it may be that the uncoupling effect of UCP3 in human myocardium is not great enough to affect the PCr/ATP ratio. Lowering the proton gradient by uncoupling oxidative phosphorylation makes ATP synthesis less efficient, but not necessarily inadequate for the prevailing workload, unless substrate (including oxygen) supply is limited. This may be the case in very severe heart failure, but may not have been the case in the cohort studied here. The reasons for studying cardiac surgical patients were explained in Chapter 2, but a consequence is that there were no patients with severe heart failure recruited into the study, as one of the aims of valvular surgery is to prevent the onset of heart failure, and patients with severe ischaemic cardiomyopathy are often not suitable for coronary artery bypass grafting due to lack of viable myocardium.

Secondly, it has been shown previously, that absolute UCP3 protein levels are not related to the magnitude of the uncoupling effect, which is instead related to the presence or absence of UCP3 activators (Boudina, Sena *et al* 2007). Known activators of UCP3 (superoxide, hydroxynonenol and intracellular fatty acids) were not measured in this study. The plasma

concentration of non-esterified fatty acids was measured, but it is the concentration of fatty acids within the mitochondria which would be of relevance in this context.

Thirdly, it may be that the effect of ventricular UCP3 on PCr/ATP ratio was smaller than the study was powered to detect – a type 2 statistical error. Figure 4.12 demonstrates no emerging relationship between ventricular UCP3 and PCr/ATP ratio, suggesting therefore that this was not the case.

The evidence that UCP3 levels increase in heart failure from this study is not convincing, despite some evidence that plasma NEFA concentrations were increased in patients with heart failure. Neither ventricular nor atrial UCP3 levels were increased in those patients with ventricular dysfunction compared to those without. Ventricular UCP3 levels increased with NYHA class but atrial UCP3 levels did not; the two correlating moderately with each other. Plasma NEFA are ligands for peroxisome proliferator-activated receptor alpha (PPARα), a nuclear hormone receptor which controls the expression of, amongst other proteins, UCP3 (Desvergne and Wahli 1999). If plasma NEFA concentrations increase in heart failure, then UCP3 levels should also increase if PPARα was the only controlling influence. As increases in UCP3 levels did not occur, this suggests that control of UCP3 levels does not rest solely with PPARα, and indeed, thyroid hormones have been shown to exert control over UCP3 levels, with a thyroid response element having been found in the proximal UCP3 gene promoter region (Solanes, Pedraza *et al* 2005). Plasma NEFA concentration was a significant predictor of atrial UCP3 levels albeit with only a moderate effect (Figure 4.13) and was not predictive of ventricular UCP3 levels. It is perhaps surprising to have found a relationship between fasting plasma NEFA concentration and UCP3 levels. Plasma NEFA concentration is known to fluctuate rapidly in response to the

prevailing neurohumoral milieu (Frayn 1998), with changes in protein levels occurring much more slowly (Jiang, Zhang *et al* 2009). It is therefore the underlying mean level of NEFA concentration, rather than a concentration taken at one particular time point, that is likely to relate to UCP3 protein level. The finding that atrial UCP3 levels correlated with plasma NEFA concentration, however, is similar to Murray's previous findings in human heart (Murray, Anderson *et al* 2004). Cardiac UCP3 levels have been shown to be increased in chronically infarcted and failing rat heart compared with normal controls (Murray, Cole *et al* 2008), but to date no other human studies have been performed to compare with the results of this study.

Plasma NEFA concentration was shown to be increased in patients with ventricular dysfunction, and was predicted by LVEF, though not by the diastolic parameter E/E'. This was despite most patients taking medication to antagonise the neurohumoral activation of heart failure. These data are supportive of the hypothesis that the increased sympathetic tone associated with heart failure results in net adipose tissue lipolysis and increased plasma NEFA concentration (Paolisso, Gambardella *et al* 1994; Lommi, Kupari *et al* 1998).

No association was found between plasma NEFA concentration and cardiac PCr/ATP ratio which differs from previous work in patients with type 2 diabetes mellitus (Scheuermann-Freestone, Madsen *et al* 2003). This may be because the plasma NEFA concentrations in this study were not as high, perhaps making it more difficult to reveal the underlying relationship between the variables.

Cardiac PCr/ATP ratio was related to heart failure symptoms (NYHA class), but not to LV volumes, mass, ejection fraction or cardiac output. This is consistent with previous work in dilated cardiomyopathy patients which also found a negative relationship between NYHA

class and PCr/ATP, but no relationship to LVEF (Neubauer, Krahe *et al* 1992). It was also found in this study that cardiac PCr/ATP ratio was lower in those patients defined as having ventricular dysfunction (see methods) compared with those without. Interestingly however, there was no relationship between 6MWT distance and cardiac PCr/ATP ratio. The reason why PCr/ATP is related to NYHA class but not to 6MWT distance is not clear. It could be that 6MWT distance was confounded by symptoms of angina, or by patients' volitional effort.

Associations between PCr/ATP and diastolic function have previously been demonstrated (Beyerbacht, Lamb *et al* 2001) which is contrary to the findings here. Beyerbacht *et al* measured a number of diastolic parameters, with only one (early wave mean acceleration corrected for cardiac output) correlating to cardiac PCr/ATP ratio. The diastolic parameter measured here was different (E/E') which might explain the discrepant findings.

It appears that resting cardiac PCr/ATP ratio is related to cardiac function, as suggested by this and other studies, but does not relate closely to other clinically used measures of ventricular performance. Indeed, it has been shown previously that cardiac PCr/ATP ratio is a better predictor of mortality than LVEF or the NYHA classification, and may represent a more fundamental measure of myocardial health (Neubauer, Horn *et al* 1997). The mechanisms underlying the decrease in cardiac PCr/ATP ratio in heart failure are not fully understood. It is interesting that there were no obvious relationships between cardiac PCr/ATP and estimations of cardiac work (cardiac output and rate pressure product). This implies that ATP consumption (ignoring changes in efficiency of ATP utilisation) is not a major factor in determining the overall cardiac PCr/ATP ratio and that oxygen delivery to the mitochondrion, or mitochondrial function itself, are of greater significance. The finding

that the PCr/ATP ratio is not related to cardiac volume or mass implies also that changes in ATP utilisation, secondary to changes in chamber geometry and wall stress, do not have a significant effect on the cardiac PCr/ATP ratio. Previous work has shown PCr/ATP ratio to be unrelated to myocardial microvascular perfusion (Shivu, Phan *et al* 2010), and to be normal at rest in coronary artery stenosis (Weiss, Bottomley *et al* 1990). Therefore, it is perhaps most reflective of mitochondrial function, with a decreased ratio suggesting impairment of oxidative phosphorylation. Such an impairment could occur at a multitude of sites within the metabolic pathways constituting oxidative phosphorylation, but it appears from this work that uncoupling of oxidative phosphorylation through an increase in UCP3 levels within the heart, does not play a major role, at least in mild-to-moderate heart failure. It may be in severe heart failure, as oxygen delivery to myocardial mitochondria becomes limited, that uncoupled oxidative phosphorylation then exerts a significant influence on ATP synthesis, and the cardiac PCr/ATP ratio may then relate to UCP3 levels or activity.

Limitations

This study has a number of limitations. Firstly, the study was designed as an observational study with no control group. This was because it was considered not possible to obtain reliable control tissue. The only option for obtaining normal control myocardial biopsies comes from unused normal donor hearts. These are kept on ice for a number of hours whilst delivered to the transplant centre before the decision not to transplant is made. The effect of the cold ischaemic time on UCP3 protein levels is unknown, but the half life of UCP3 is known to be relatively short for a mitochondrial protein (Azzu, Jastroch *et al* 2010). The control hearts are also very unlikely to be age matched – the majority coming from young trauma victims as opposed to the older patients presenting for cardiac surgery. However,

within the cohort studied it was possible to divide patients into those with ventricular dysfunction and those without ventricular dysfunction, based upon LVEF and E/E'.

Secondly, in order to obtain myocardial tissue biopsies, the cohort studied was comprised of patients undergoing cardiac surgery. Particularly in the case of valvular pathology, one of the aims of surgery is to prevent heart failure from occurring, so there were relatively few patients with severely impaired systolic function, as could have been the case if patients with dilated cardiomyopathy, for example, were studied. On the other hand, the advantage of not selecting a group only comprising of patients with impaired ventricular function, was that there was a wide range of ventricular function in the cohort, making regression analyses more likely to be successful.

One way in which this study classified heart failure severity was with the NYHA classification of functional capacity. This is a subjective method of classifying the severity of heart failure, relying on patients' reporting of symptoms. The use of the NYHA classification, however, is a widely clinically accepted means to classify the severity of heart failure (Dickstein, Cohen-Solal *et al* 2008), and is consistent with much of the previous reported work examining the relationship between heart failure severity and cardiac PCr/ATP ratio (Neubauer, Krahe *et al* 1992; Neubauer, Horn *et al* 1997). The 6MWT was used as a more objective method to assess functional capacity, albeit in the context of subjects with angina, but the most objective method of assessing heart failure, cardiopulmonary exercise testing, was not performed, partly because of concerns over exercising patients with left main coronary artery disease or critical aortic stenosis, and also because of the lack of local expertise in performing this test. It was further felt that the

protocol was onerous enough on patients, and the addition of further arduous testing may have limited the number of patients willing to take part.

It was decided to define systolic dysfunction as a left ventricular ejection fraction of less than 55%, and this is somewhat arbitrary. This value was chosen because the normal range for ejection fraction, measured by MRI, used locally (OCMR, John Radcliffe Hospital, Oxford), is 57-81%. It can be argued that ejection fraction is not a completely representative measure of systolic function, and is not reflective of subtle systolic dysfunction which might involve changes in torsion, longitudinal shortening and strain rates, for example, but it is widely clinically used and has been shown to be prognosticlly important (Dickstein, Cohen-Solal *et al* 2008).

The patients studied in the cohort also had different diseases. There is general consensus that the cardiac energetic abnormalities in heart failure appear to be similar regardless of the aetiology of the failure (Shivu, Abozguia *et al* 2010; Conway, Allis *et al* 1991; de Roos, Doornbos *et al* 1992; Neubauer, Krahe *et al* 1992; Conway, Bottomley *et al* 1998; Beyerbacht, Lamb *et al* 2001), therefore a study such as this, testing a unifying hypothesis, would need to include different aetiologies. It may have been preferable to enrol equal numbers of patients into different groups comprising aortic stenosis, coronary artery disease and mitral regurgitation, each with sufficient numbers to be powered to detect effect sizes of moderate magnitude. The paucity of local patients undergoing valve surgery meant that this approach was not feasible, and it was decided that, in order to enrol sufficient numbers within a reasonable time frame, all surgical pathology would be recruited and treated as a single group.

The ventricular biopsies taken were from the epicardial layer which may have a different metabolic profile to the endocardium. It would have been preferable for full thickness biopsies to be taken from the ventricle, but the provision of ventricular biopsies was left to the judgement of the operating surgeon and the techniques with which they were familiar, in order to avoid exposing patients to undue risk.

It was only possible to measure relative concentrations of phosphorus metabolites using ^{31}P MRS. A "normal" ratio of PCr/ATP therefore may be misleading if ATP concentration is decreased as well as PCr. This does occur in heart failure, but is thought to be a relatively late phenomenon (Shen, Asai *et al* 1999; Beer, Seyfarth *et al* 2002) occurring at around the time of clinical decompensation, and therefore the patients in this cohort were assumed to have normal ATP concentrations.

The hypothesised sequence of events, following the onset of ventricular dysfunction and tissue hypoperfusion, begins with an increase in sympathetic tone, but this was not directly measured in this study. There is a well established relationship between ventricular function and plasma noradrenaline concentration (Thomas and Marks 1978; Francis, Goldsmith *et al* 1982; Levine, Francis *et al* 1983), so it was felt unnecessary to repeat this.

The measurement of plasma NEFA concentration is known to vary considerably, depending on the dietary state and prevailing sympathetic tone (Frayn 1998). Plasma NEFA concentrations were always measured in fasted patients, and at the same point within the protocol, therefore trying to minimise diurnal or contextual variations. Plasma NEFA concentrations measured on the day of surgery were again taken in the fasted state, although from arterial blood on this occasion. These were only related to Western blot results from the biopsies taken on the same day and not to the pre-operative investigations carried out

previously, which were compared with the venous plasma NEFA concentration taken contemporaneously.

The pre-operative investigations were necessarily carried out on a separate day to the biopsy collection. This resulted in cardiac PCr/ATP being related to ventricular UCP3 levels, for example, measured at a different time. This was unavoidable due to the time required to collect all necessary pre-operative data, and it was felt that disease progression would be minimal in the time between the pre-operative tests and the biopsies being taken. It is possible, however, that on the day of surgery, patients' anxiety levels were different, resulting in different degrees of sympathetic stimulation and hence UCP3 expression. All patients received sedative premedication in order to limit pre-operative anxiety; however, plasma NEFA concentrations were higher in those samples taken immediately pre-anaesthetic induction, compared with those samples taken at the pre-operative tests. This finding does suggest increased sympathetic tone was present, as the samples were again taken in the fasting state. The effect this may have had on changes in cardiac UCP3 levels is not known.

Further research

Future work is required to clarify a number of issues arising from this work. Firstly, it is not clear from this work whether UCP3 levels increase in human myocardium in heart failure. This could be tested by comparing ventricular UCP3 levels from patients with normal ventricular function presenting for CABG surgery, in a similar way to this study, with ventricular UCP3 levels from patients with end-stage heart failure having cardiac transplantation surgery.

Secondly, the relationship between UCP3 levels and PCr/ATP ratio requires further exploration. It would be interesting to upregulate UCP3 levels, which may be possible using a high fat diet (Hesselink, Greenhaff *et al* 2003), and measure the cardiac PCr/ATP ratio before and after the diet. This would be difficult to do in humans because of the need to take repeated myocardial biopsies, to confirm increased UCP3 levels, but could be performed in animals. The relationship to oxygen availability could be explored by rendering some animals hypoxic whilst measuring the PCr/ATP ratio, in order to ascertain whether UCP3 levels influence PCr/ATP only under conditions of limited oxygen supply.

It may be impossible to confirm a direct relationship between PCr/ATP ratio and UCP3 because of the requirement to measure the activity of, instead of the amount of, UCP3 at the time of acquiring measurements of PCr and ATP concentration. The effect that UCP3 has on mitochondrial respiration rates could be measured *in vitro*, however, and extrapolated to the *in vivo* situation.

4.5. Conclusions

No relationship was found between absolute ventricular UCP3 protein levels and cardiac PCr/ATP ratio in this cohort of mild-moderate human heart failure. The concentrations of local UCP3 activators were not measured, however, so a decrease in PCr/ATP ratio in heart failure occurring through mitochondrial uncoupling via UCP3 cannot be entirely ruled out. Further work is required to ascertain the extent to which UCP3 uncouples oxidative phosphorylation *in vivo*, whether uncoupled oxidative phosphorylation decreases the cardiac PCr/ATP ratio, and whether cardiac UCP3 levels increase in human heart failure.

CHAPTER 5

THE RELATIONSHIPS BETWEEN CARDIAC FUNCTION, SKELETAL MUSCLE ENERGETICS AND UNCOUPLING PROTEIN-3 LEVELS

5.1. Introduction

Heart failure is associated with a decrease in exercise capacity characterised by early fatigue and skeletal muscle weakness (Middlekauff 2010; Poole-Wilson and Ferrari 1996). Originally it was thought that this related to the inability of the heart to augment cardiac output during exercise, resulting in skeletal muscle hypo-perfusion, but this view has been challenged by evidence that skeletal muscle metabolic abnormalities are not related to blood flow, measured directly (Massie, Conway *et al* 1987), and more recently with a combination of ^{31}P MRS and near-infrared spectroscopy (NIRS) (Hanada, Okita *et al* 2000). These studies suggest that there is an intrinsic mitochondrial dysfunction in skeletal muscle in heart failure. Compared with controls, heart failure patients have increased muscle PCr consumption and decreased pH during aerobic exercise (Massie, Conway *et al* 1987; Massie, Conway *et al* 1988; Kemp, Thompson *et al* 1996; Hanada, Okita *et al* 2000), a high resting [Pi] (Massie, Conway *et al* 1987) and prolonged PCr recovery times following exercise (Kemps, Prompers *et al* 2010; Massie, Conway *et al* 1987; Massie, Conway *et al* 1988; Kemp, Thompson *et al* 1996; Hanada, Okita *et al* 2000). These findings are indicative of a failure of oxidative ATP synthesis, but shed no light on the mechanism of the failure.

Studies using a combination of ^{31}P MRS and NIRS to investigate PCr and skeletal muscle oxygen saturation (Sm_{O2}) kinetics in heart failure have shown that muscle PCr re-synthesis times and reoxygenation times are both prolonged in heart failure patients compared with controls (Kemps, Prompers *et al* 2010; Hanada, Okita *et al* 2000). One of the problems with the interpretation of NIRS data is that prolonged reoxygenation times could theoretically be attributable to excessive O_2 consumption and mitochondrial inefficiency, not necessarily to inadequate O_2 supply.

5.2. Aims

The aim of this chapter was to investigate the hypothesis that gastrocnemius mitochondrial oxidative capacity would be negatively predicted by skeletal muscle UCP3 levels, and that skeletal muscle UCP3 levels would be related to the degree of ventricular dysfunction secondary to increased plasma NEFA concentration. This hypothesis provides a potential process to describe the well recognised, but mechanistically undetermined, skeletal muscle mitochondrial dysfunction in heart failure. Using ^{31}P MRS in combination with NIRS, this chapter also aims to investigate whether any observed mitochondrial dysfunction originates from abnormalities in blood flow, and hence substrate supply, to gastrocnemius, or whether intrinsic mitochondrial dysfunction is more likely.

5.3. Methods

Having been recruited from the cardiothoracic surgery outpatient clinic, and following an overnight fast, the patients described in Chapter 3 attended the Oxford Centre for Clinical Magnetic Resonance Research (OCMR) at a convenient time before their scheduled surgery. A clinical history was taken and demographic and anthropometric data recorded as described in Chapter 2. Patients then underwent skeletal muscle ^{31}P MRS and cardiac MRI cine imaging as described in Chapter 2. The order of tests was always skeletal muscle ^{31}P MRS first, followed by cardiac MRI, in order that patients were rested before repeating the exercise protocol outside the MRI suite to measure Sm_{O2} kinetics using near-infrared spectroscopy as described in Chapter 2.

Venous blood samples were acquired from an anticubital fossa vein, and the blood immediately cooled and centrifuged at 4ºC. Plasma for the measurement of NEFA

concentration was frozen after the addition of a lipoprotein lipase inhibitor (tetrahydrolipstatin, Xenical, Roche, Welwyn Garden City, UK) at a final concentration of $30\mu g.ml^{-1}$ as described in Chapter 2. Patients were then provided with a mixed meal. Once refreshed, patients performed the six-minute walk test (6MWT) and underwent transthoracic echocardiography as described in Chapter 2, afterwhich they were discharged home.

On the day of surgery, following an overnight fast, immediately prior to anaesthetic induction, blood was taken from an arterial cannula for further measurement of NEFA concentration, so that a contemporaneous measure was available to relate to Western blot results. During the operation, a pectoralis major muscle biopsy was obtained following sternotomy, and immediately washed in physiological (0.9 % w/v) saline to remove excess blood, then snap-frozen in liquid nitrogen and stored at -80 ˚C until Western blot analysis was performed.

Ventricular dysfunction was said to be present if patients had systolic and/or diastolic ventricular impairment which was defined previously in Chapter 2.

Statistical analysis

Variables and sub-groups of variables were assessed for normality by Shapiro-Wilk tests and visual inspection of quantile-quantile plots. Homogeneity of variance was assessed using Levene's tests (Field 2009). Variables were transformed if necessary to render them normally distributed. In the majority of cases, data were found to be positively skewed; in such cases log transformations produced acceptable normality and stability of variance. One-tailed statistical tests were used because of the directional nature of the hypothesis. Regression analyses were performed to assess the degree to which one variable could be predicted from another, with standardised beta (β) and associated p value (p) reported. The

standardised beta is the amount of change of the outcome variable for a unit change in the predictor, in standard deviation units (Field 2009). Standardised betas were categorised as small, medium and large effects as described by Cohen (small >0.1, medium >0.3, large >0.5) (Cohen 1992). NYHA groups were compared using the non-parametric Jonckheere-Terpstra test. As group sizes were uneven, and there were only 5 patients in NYHA class one, the assumptions for analysis of variance were therefore not met and non-parametric methods were used. The Jonckheere-Terpstra test was used as NYHA groups are ordered and, as such, trends were expected in the medians of the groups. This was reported as JT and the p value.

If a variable was divided into two groups, for example ventricular dysfunction and no dysfunction, and each group met parametric assumptions, independent t-tests were used to compare means and were reported mean1 ± SEM1 *vs* mean2 ± SEM2, the value of the test statistic t (degrees of freedom) and the associated p value. If parametric assumptions were not met after transformations, then groups were compared using the Mann-Whitney U test. Missing data were excluded from analyses on a case-by-case basis and were not imputed using any method.

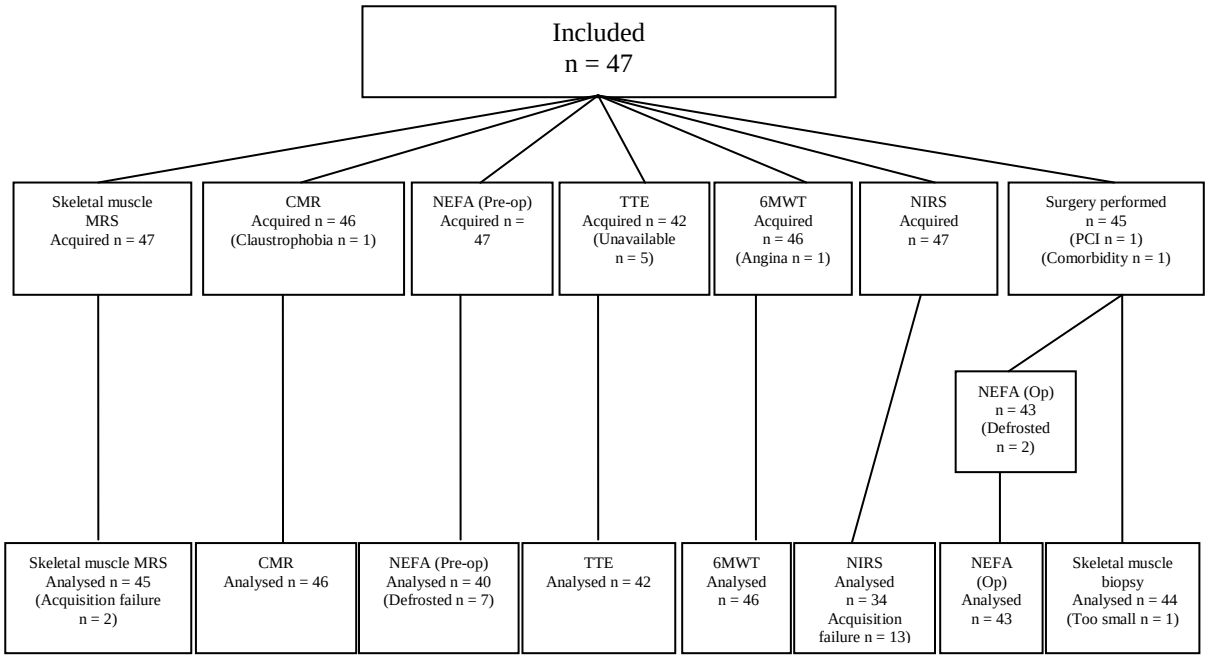

Figure 5.1. CONSORT-type flow diagram to describe the inclusion of subjects from the recruited cohort presented in Chapter 3.

MRS – magnetic resonance spectroscopy, CMR – cardiac magnetic resonance imaging, NEFA – non-esterified fatty acid, TTE – trans-thoracic echocardiography, 6MWT – six-minute walk test, NIRS – near-infrared spectroscopy, PCI – percutaneous coronary intervention.

5.4. Results

The patient cohort was identical to that described in Chapter 3. One patient was unable to tolerate MRI cine imaging due to claustrophobia, so cardiac volumes were not obtained. The MRS data acquired from two patients were unanalysable due to poor spectral quality (very low signal/noise ratio). NIRS data was not acquired on 13 patients. This was because the NIRS system was fully automated with no manual adjustment possible; and on these patients, signal quality was reported as too poor, presumably due to depth of subcutaneous tissue. Two patients did not undergo surgery despite being initially listed for surgical management, therefore biopsies were not taken for skeletal muscle UCP3 measurement, or pre-anaesthetic induction blood for plasma NEFA concentration. The pre-operative plasma samples from 7 patients were accidently defrosted, along with 2 from the operative visit, and so were not analysed because of uncertainty over the veracity of results from those samples. On one occasion the skeletal muscle biopsy was too small to enable Western blotting analysis. Table 5.1 presents the resting and end-exercise ^{31}P MRS data.

Table 5.1. Table of baseline and end-exercise muscle high energy phosphorus metabolites and pH.

	Rest	End-exercise
PCr/ATP	3.87 ± 0.06	1.82 ± 0.10*
Pi (mmol.L^{-1})	3.5 ± 0.2	13.4 ± 0.7*
ADP (μmol.L^{-1})	20 ± 1	95 ± 6*
PP (L.mmol^{-1})	142.1 ± 10.7	9.4 ± 1.3*
pH	7.07 ± 0.004	6.98 ± 0.01*
Exercise time (s)		475 ± 28

Data are presented as mean ± SEM *$p < 0.001$ compared with resting value

PCr – phosphocreatine, ATP – adenosine triphosphate, Pi – inorganic phosphate, ADP – adenosine diphosphate, PP – phosphorylation potential

Skeletal muscle high energy phosphorus metabolites and cardiac function

Resting gastrocnemius PCr/ATP ratio, [ADP] and [Pi] were not predicted by left ventricular ejection fraction (LVEF) or NYHA classification (data not shown). Exercise duration was predicted by LVEF ($\beta = 0.40$, $p < 0.01$) (Figure 5.2) as was mean PCr consumption during exercise ($\beta = -0.47$, $p < 0.001$) (Figure 5.3), together with the initial rate of PCr consumption at the onset of exercise ($\beta = -0.39$, $p < 0.01$) (Figure 5.4).

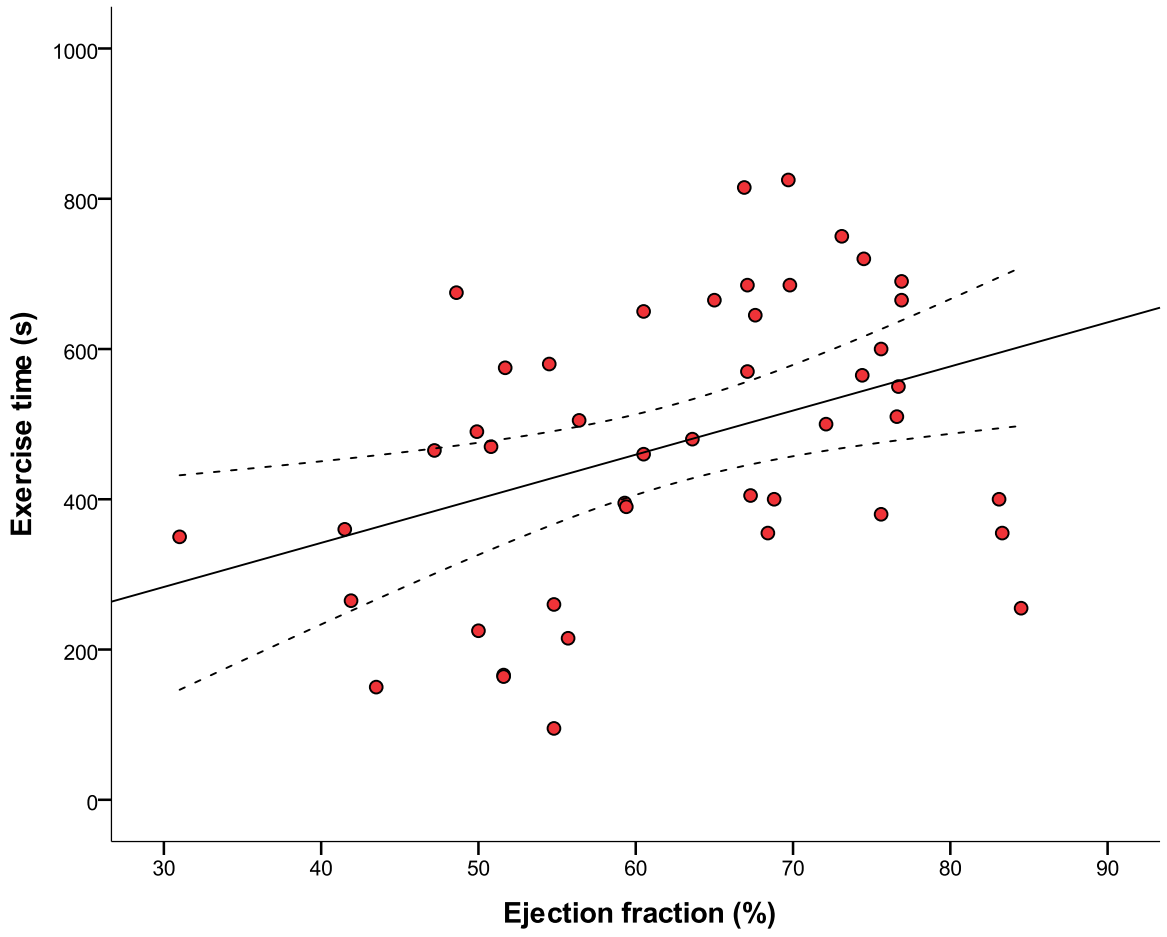

Figure 5.2. Scatter-plot showing total exercise time plotted against left ventricular ejection fraction at rest.

The solid line is the regression line and the dashed lines are the 95% confidence intervals of the regression line.

$\beta = 0.40$, $p < 0.01$

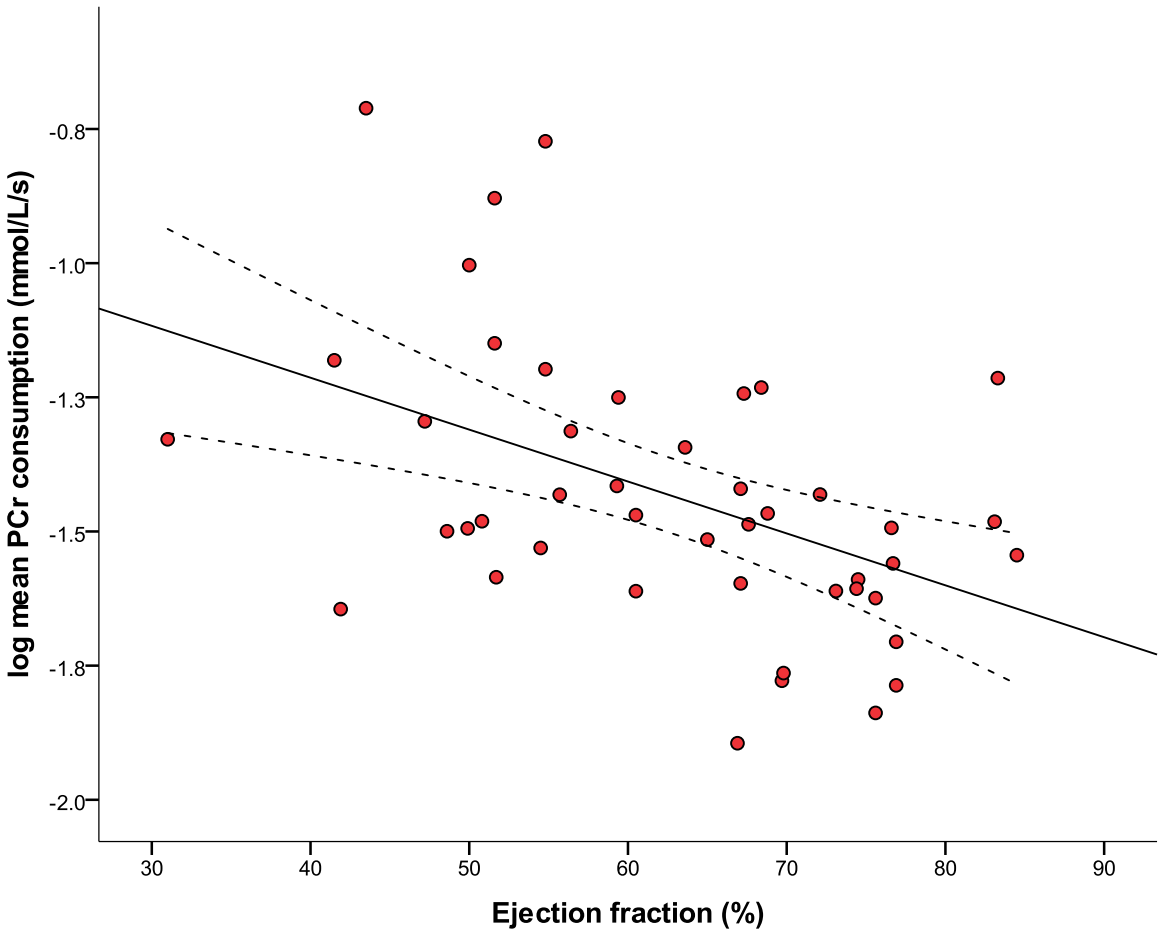

Figure 5.3. Scatter-plot showing mean skeletal muscle PCr consumption during exercise plotted against left ventricular ejection fraction.

The solid line is the regression line and the dashed lines are the 95% confidence intervals of the regression line. To transform the distribution of mean PCr consumption values to normal, logarithms (base 10) were taken.

$\beta = -0.47$, $p < 0.001$

PCr - phosphocreatine

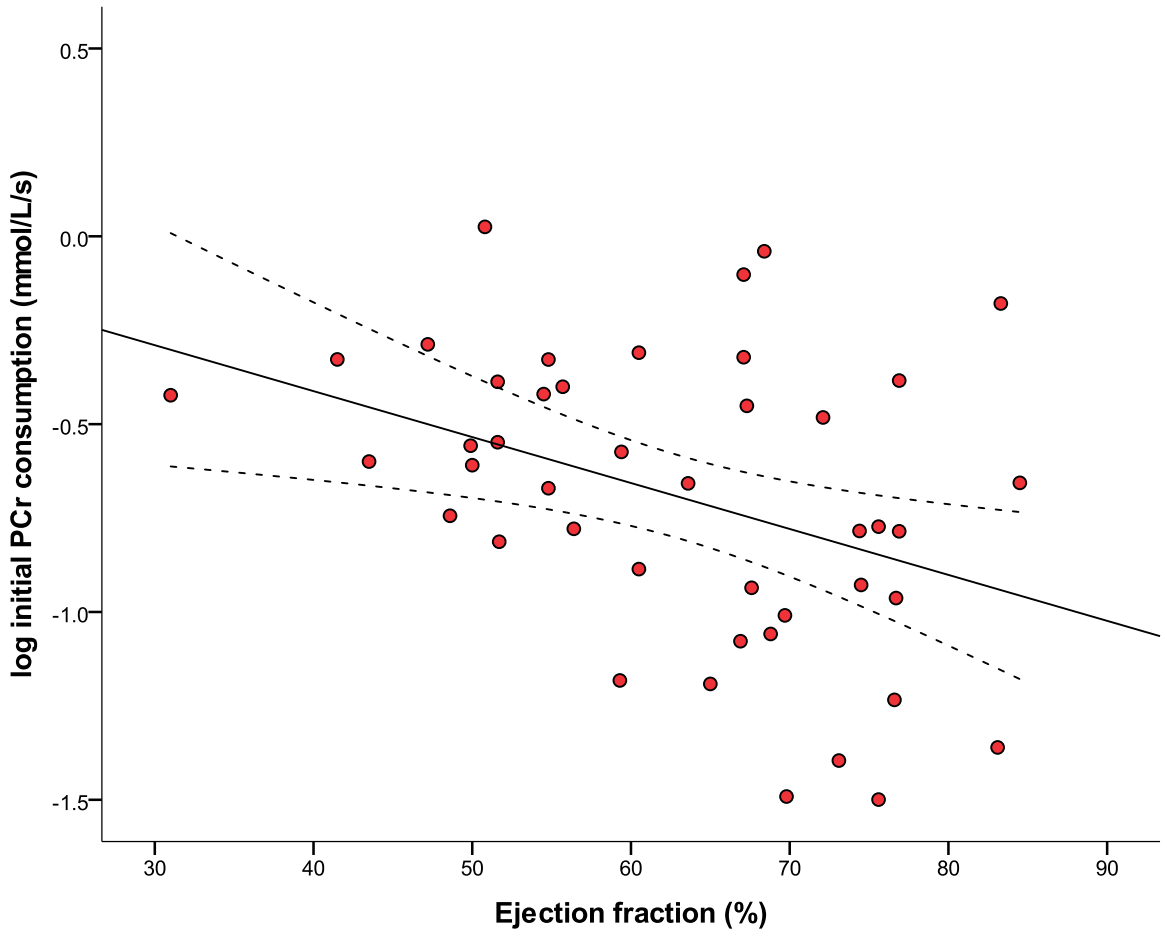

Figure 5.4. Scatter-plot showing the initial rate of PCr consumption by skeletal muscle at the onset of exercise plotted against left ventricular ejection fraction.

The solid line is the regression line and the dashed lines are the 95% confidence intervals of the regression line. To transform the distribution of initial PCr consumption values to normal, logarithms (base 10) were taken.

$\beta = -0.39$, $p < 0.01$

Phosphocreatine recovery time was unrelated to LVEF ($\beta = -0.24$, $p = 0.06$) (data not shown) and did not increase with increasing heart failure symptoms (JT, $p = 0.07$) (data not shown).

The theoretical maximum rate of ATP synthesis (Q_{max} – derived from the end-exercise [ADP] and the PCr recovery rate) decreased with increasing heart failure symptoms (JT, $p < 0.05$) (Figure 5.5).

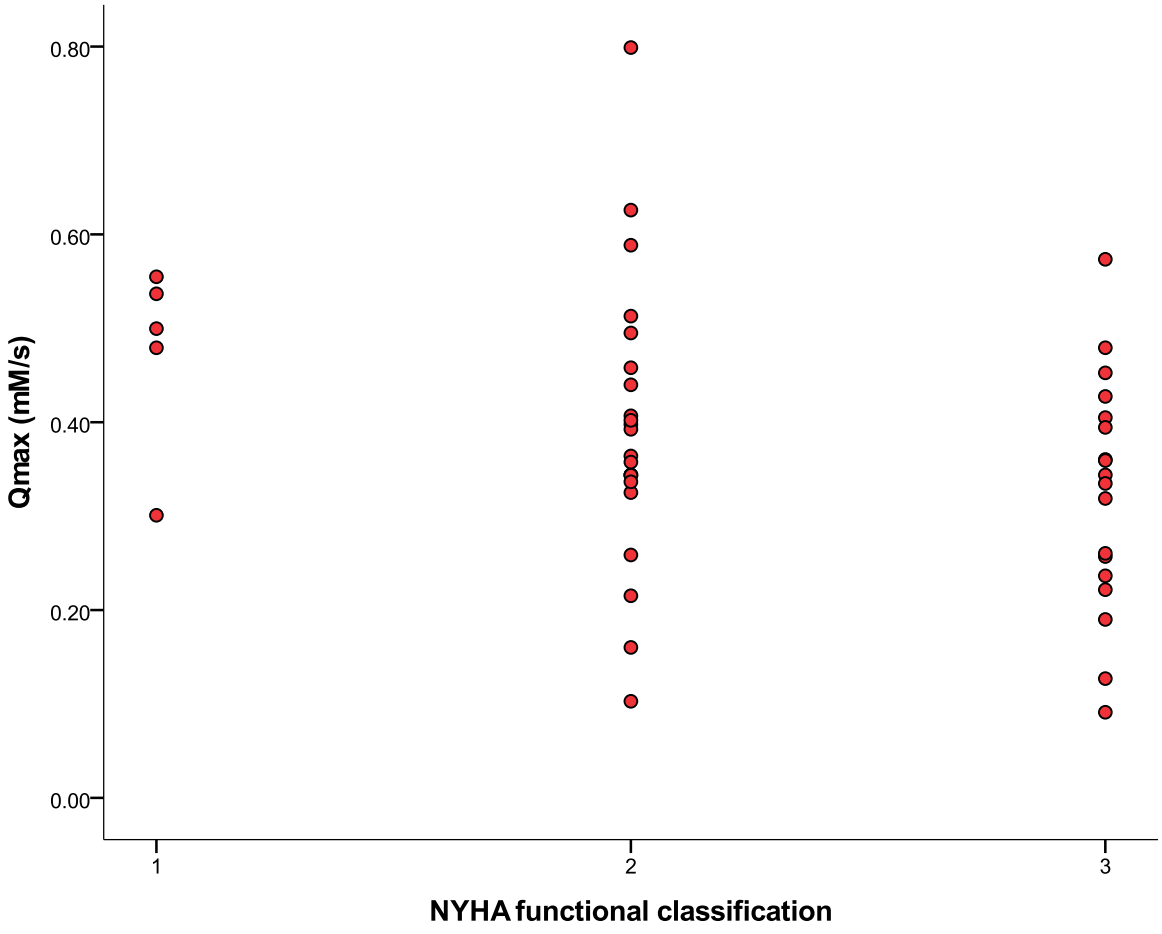

Figure 5.5. Skeletal muscle Q_{max} grouped according to NYHA class.

Jonkheere-Terpstra, $p < 0.05$

NYHA – New York Heart Association

Q_{max} – the theoretical maximum rate of oxidative ATP synthesis

Resting skeletal muscle high energy phosphorus metabolite concentrations were not predicted by the E/E' ratio (data not shown), neither were initial, nor mean PCr consumption during exercise, nor PCr recovery rate or Q_{max} (data not shown). If patients were divided into groups according to the presence or absence of ventricular dysfunction, there was no difference between groups for resting high energy phosphorus metabolite concentrations, but exercise time was significantly less in those with ventricular dysfunction (533 ± 37 *vs* 414 ± 39 s, t (43) = 2.2, $p < 0.05$), and initial (0.16 ± 0.03 *vs* 0.27 ± 0.03 $mmol.L^{-1}.s^{-1}$, t (43) = -2.1, $p < 0.05$) and mean PCr consumption (0.03 ± 0.002 *vs* 0.05 ± 0.004 $mmol.L^{-1}.s^{-1}$, t (43) = -2.8, $p < 0.05$) were significantly greater in those with ventricular dysfunction (Table 5.2).

The six-minute walk test (6MWT) distance was not predictive of resting high energy phosphorus metabolites, initial PCr consumption, mean PCr consumption and PCr recovery rate (data not shown), but was predictive of exercise time ($\beta = 0.31$, $p < 0.05$) (Figure 5.6) and Q_{max} ($\beta = 0.39$, $p < 0.01$) (Figure 5.7).

Table 5.2. Table of high energy phosphorus metabolites and pH, grouped by presence/absence of ventricular dysfunction.

	Normal ventricular function (n = 23)	**Ventricular dysfunction (n = 22)**
Resting PCr/ATP	3.88 ± 0.10	3.85 ± 0.07
Resting [ADP] ($\mu mol.L^{-1}$)	20.3 ± 2.2	20.3 ± 1.6
Resting [Pi] ($mmol.L^{-1}$)	3.6 ± 0.2	3.6 ± 0.2
Resting pH	7.07 ± 0.01	7.08 ± 0.01
Exercise time (s)	533 ± 37	414 ± 39*
Initial PCr consumption ($mmol.L^{-1}.s^{-1}$)	0.16 ± 0.03	0.27 ± 0.03*
Mean PCr consumption ($mmol.L^{-1}.s^{-1}$)	0.03 ± 0.002	0.05 ± 0.004*
τ PCr recovery (s)	43.9 ± 2.5	46.9 ± 3.3
Q_{max} ($mmol.L^{-1}.s^{-1}$)	0.40 ± 0.03	0.35 ± 0.03

Data are presented as mean ± SEM *$p < 0.05$ compared with resting value

PCr – phosphocreatine, ATP – adenosine triphosphate, Pi – inorganic phosphate, ADP – adenosine diphosphate, τ – time constant, Q_{max} – theoretical maximum rate of ATP synthesis

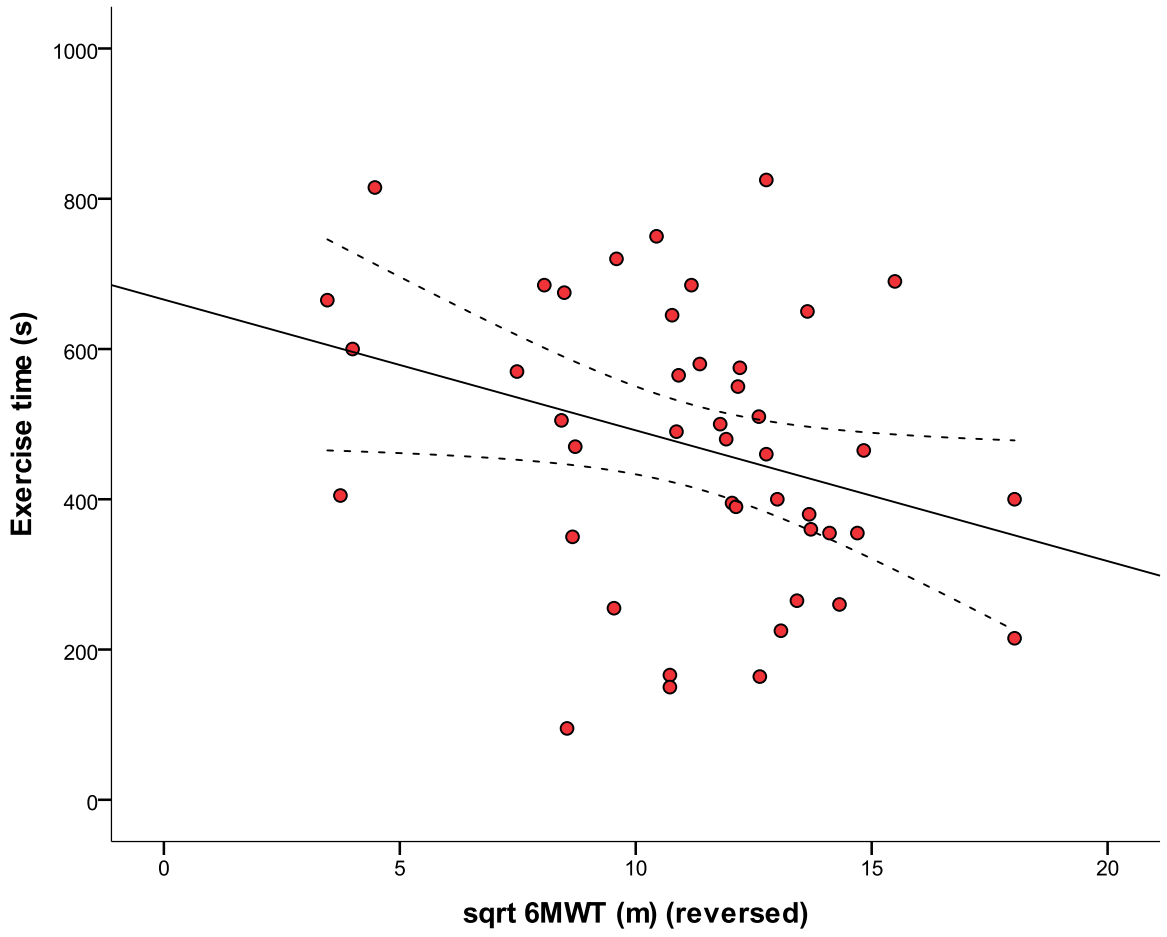

Figure 5.6. Scatter-plot showing exercise time plotted against six-minute walk test distance.

The solid line is the regression line and the dashed lines are the 95% confidence intervals of the regression line. The 6MWT values were reversed and square-rooted (sqrt) to correct for negative skew in the data, hence there is a positive relationship between exercise time and 6MWT distance.

$\beta = -0.31$, $p < 0.05$

6MWT – six-minute walk test

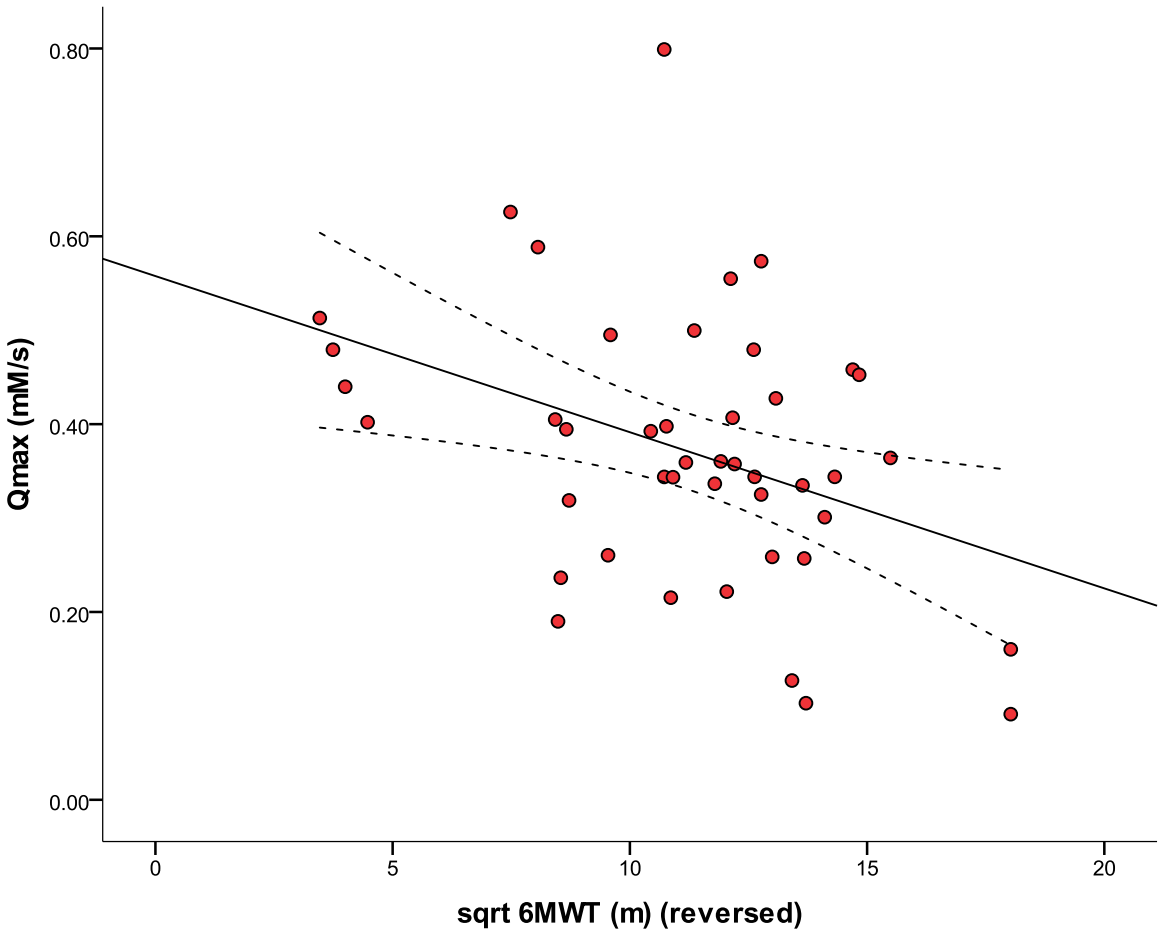

Figure 5.7. Scatter-plot showing Q_{max} plotted against six-minute walk test distance.

The solid line is the regression line and the dashed lines are the 95% confidence intervals of the regression line. The 6MWT values were reversed and square-rooted (sqrt) to correct for negative skew in the data, hence there is a positive relationship between Q_{max} and 6MWT distance.

$\beta = -0.31$, $p < 0.05$

Q_{max} – theorectical maximum rate of ATP synthesis, 6MWT – six-minute walk test

Skeletal muscle high energy phosphorus metabolites and fasting plasma NEFA concentrations

Resting skeletal muscle PCr/ATP ratio (β = -0.37, $p < 0.05$) (Figure 5.8) and [ADP] (β = 0.34, $p < 0.05$) (Figure 5.9) were predicted by fasting plasma NEFA concentration. Fasting plasma NEFA concentrations predicted Q_{max} (β = -0.35, $p < 0.05$) (Figure 5.10), but not PCr resynthesis time (β = 0.15, $p = 0.19$), mean PCr consumption (β = -0.12, $p = 0.24$) or initial rate of PCr consumption (β = 0.08, $p = 0.32$) (data not shown).

Skeletal muscle high energy phosphorus metabolites and uncoupling protein-3 levels

Skeletal muscle UCP3 levels increased with worsening heart failure symptoms (JT, $p < 0.05$) (Figure 5.11) and were predicted by LVEF (β = -0.27, $p < 0.05$) (Figure 5.12), but not diastolic function (data not shown). However, if grouped according to the presence or absence of ventricular dysfunction, there was no statistically significant difference in UCP3 levels between those without, and those with, dysfunction (0.87 ± 0.14 *vs* 1.13 ± 0.16 (a.u.), $t(42) = -1.2$, $p = 0.11$). Skeletal muscle UCP3 levels were not predicted by 6MWT distance (β = 0.03, $p = 0.43$) (data not shown).

Skeletal muscle UCP3 levels were not predicted by fasting plasma NEFA concentration (r = 0.11, $p = 0.26$) (data not shown). Skeletal muscle UCP3 levels did not predict resting high energy phosphorus metabolites, initial rate of PCr hydrolysis (β = 0.04, $p = 0.38$), mean PCr consumption (β = 0.13, $p = 0.18$) (Figure 5.13), PCr recovery rate (β = 0.15, $p = 0.17$) (Figure 5.14) or Q_{max} (β = -0.06, $p = 0.34$) (Figure 5.15).

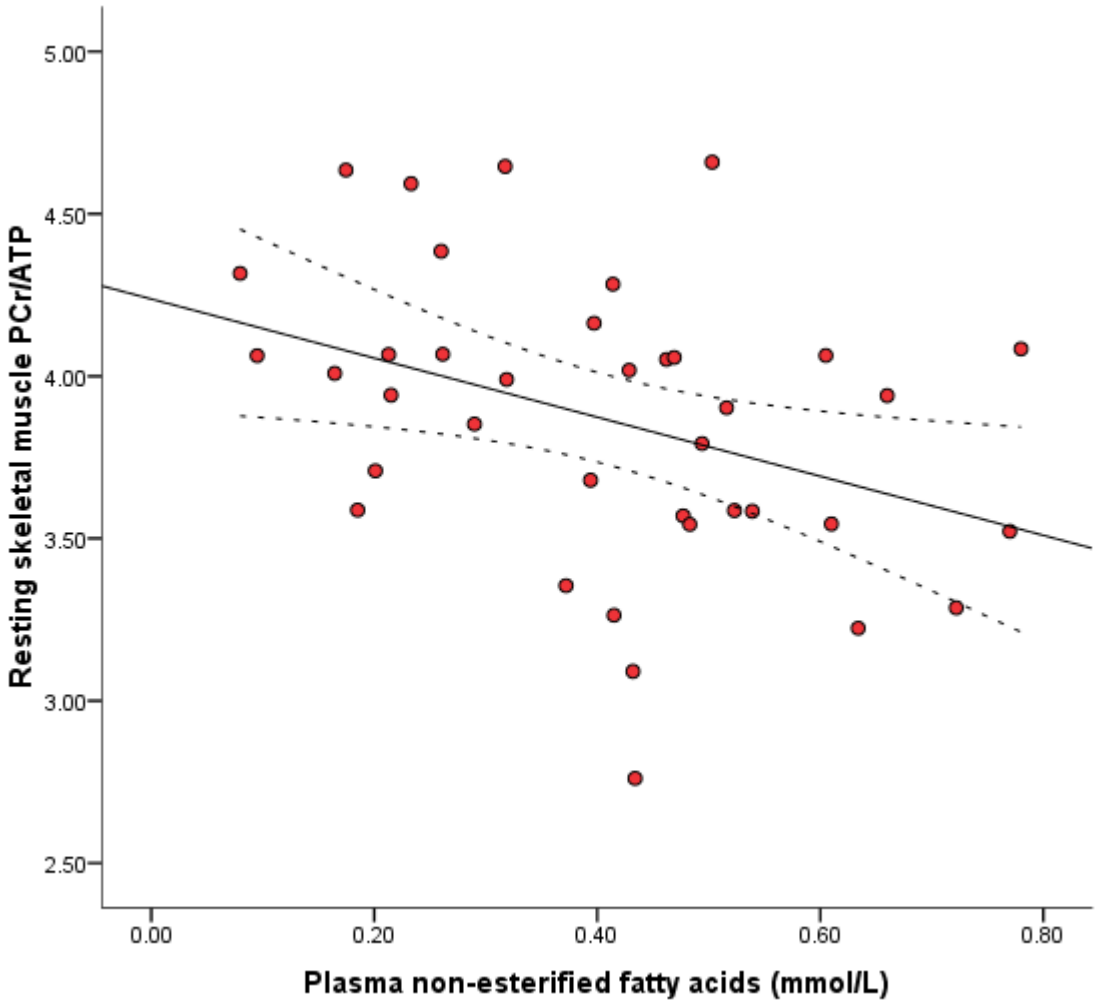

Figure 5.8. Scatter-plot showing resting skeletal muscle PCr/ATP ratio plotted against fasting plasma non-esterified fatty acid concentration.

The solid line is the regression line and the dashed lines are the 95% confidence intervals of the regression line.

$\beta = -0.37$, $p < 0.05$

PCr – phosphocreatine, ATP – adenosine triphosphate

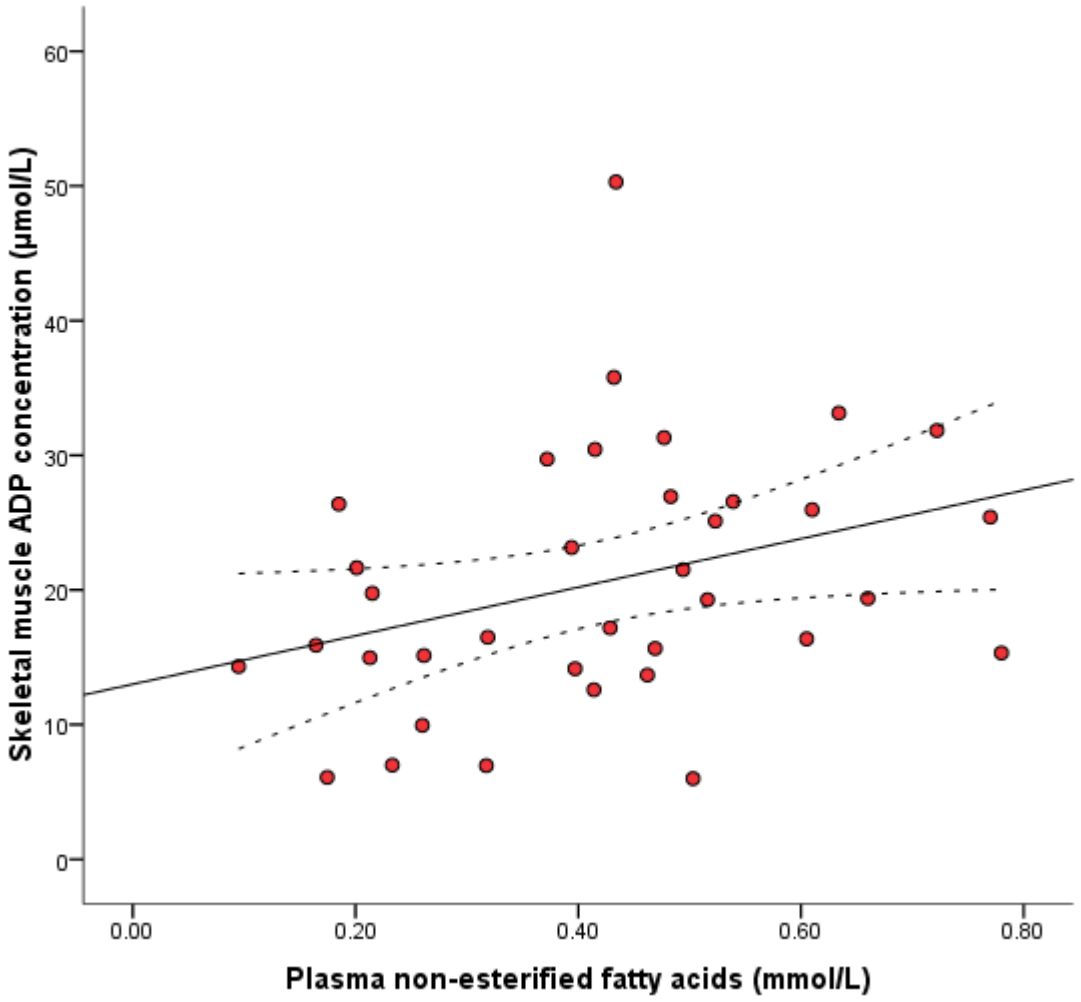

Figure 5.9. Scatter-plot showing resting skeletal muscle ADP concentration plotted against fasting plasma non-esterified fatty acid concentration.

The solid line is the regression line and the dashed lines are the 95% confidence intervals of the regression line.

$\beta = 0.34$, $p < 0.05$

ADP – adenosine diphosphate

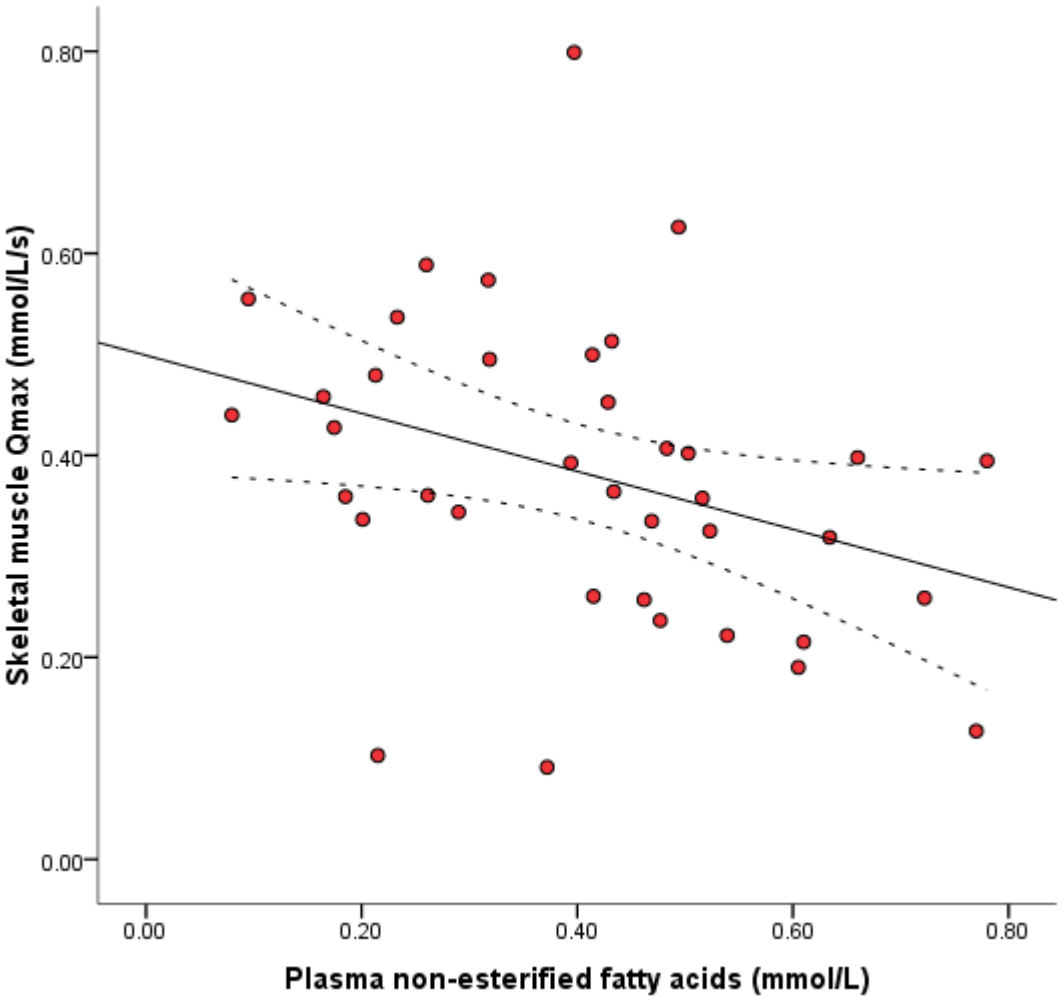

Figure 5.10. Scatter-plot showing skeletal muscle Q_{max} plotted against fasting plasma non-esterified fatty acid concentration.

The solid line is the regression line and the dashed lines are the 95% confidence intervals of the regression line.

$\beta = -0.35$, $p < 0.05$

Q_{max} – the theoretical maximum rate of oxidative ATP synthesis (see Chapter 2).

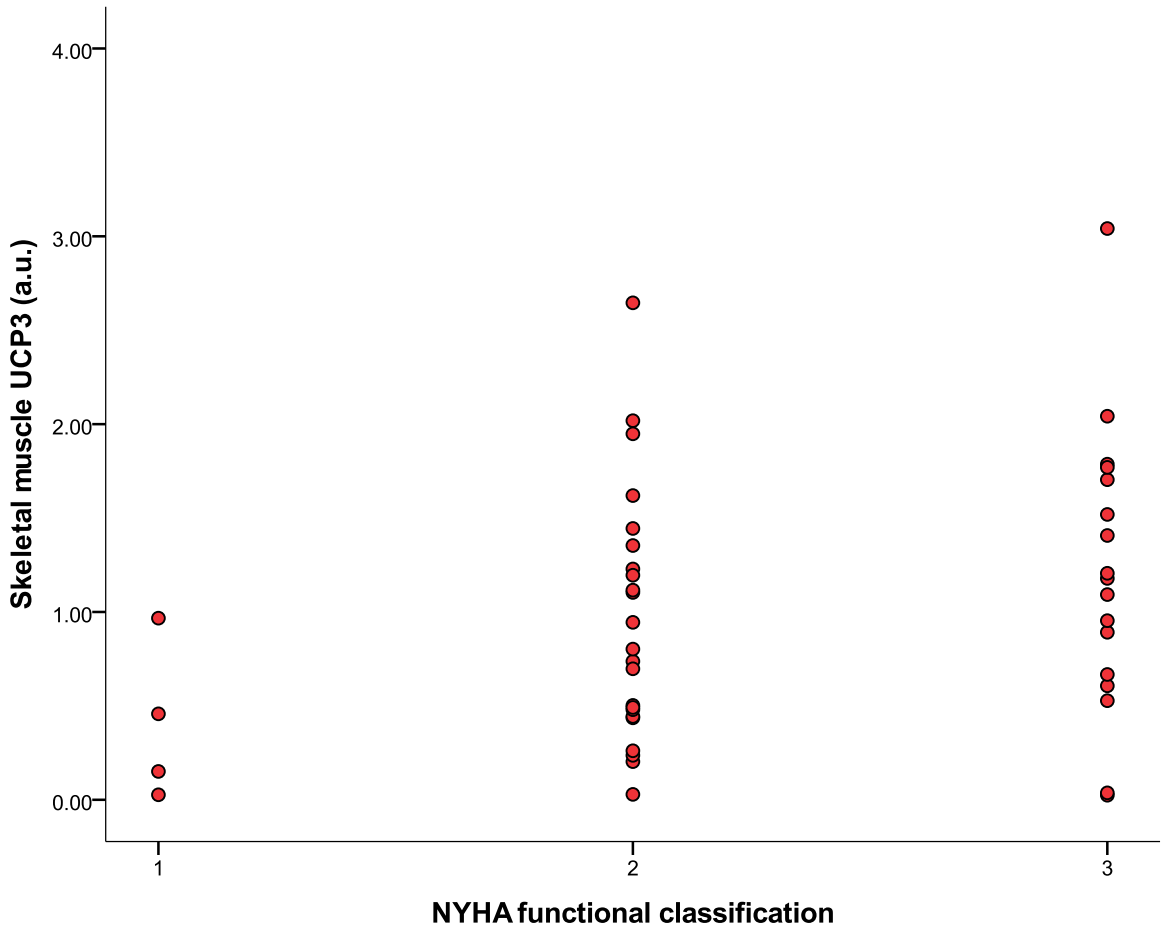

Figure 5.11. Skeletal muscle UCP3 grouped according to NYHA class.

Jonckheere-Terpstra, $p < 0.05$

NYHA – New York Heart Association

UCP3 – uncoupling protein-3

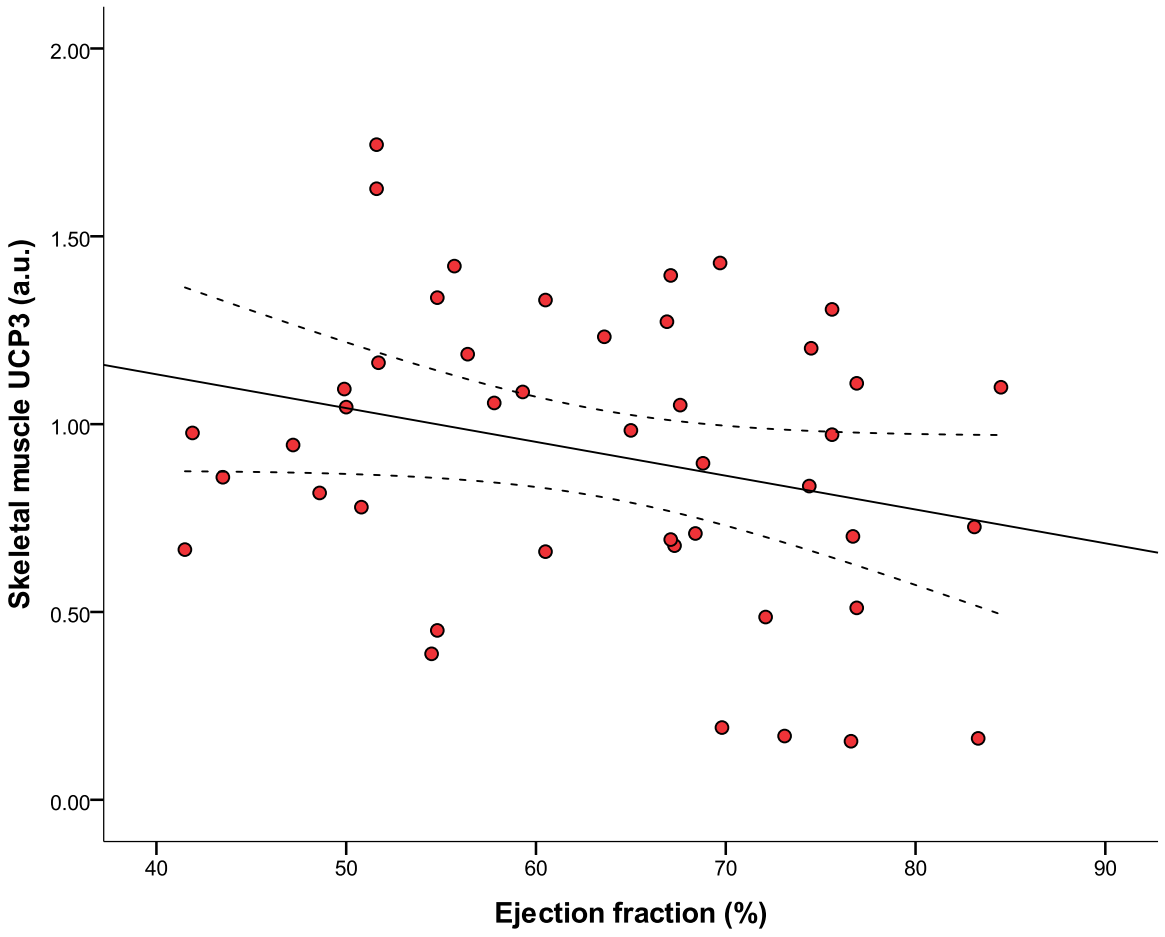

Figure 5.12. Scatter-plot showing skeletal muscle UCP3 level plotted against left ventricular ejection fraction.

The solid line is the regression line and the dashed lines are the 95% confidence intervals of the regression line.

$\beta = -0.27$, $p < 0.05$

UCP3 – uncoupling protein-3

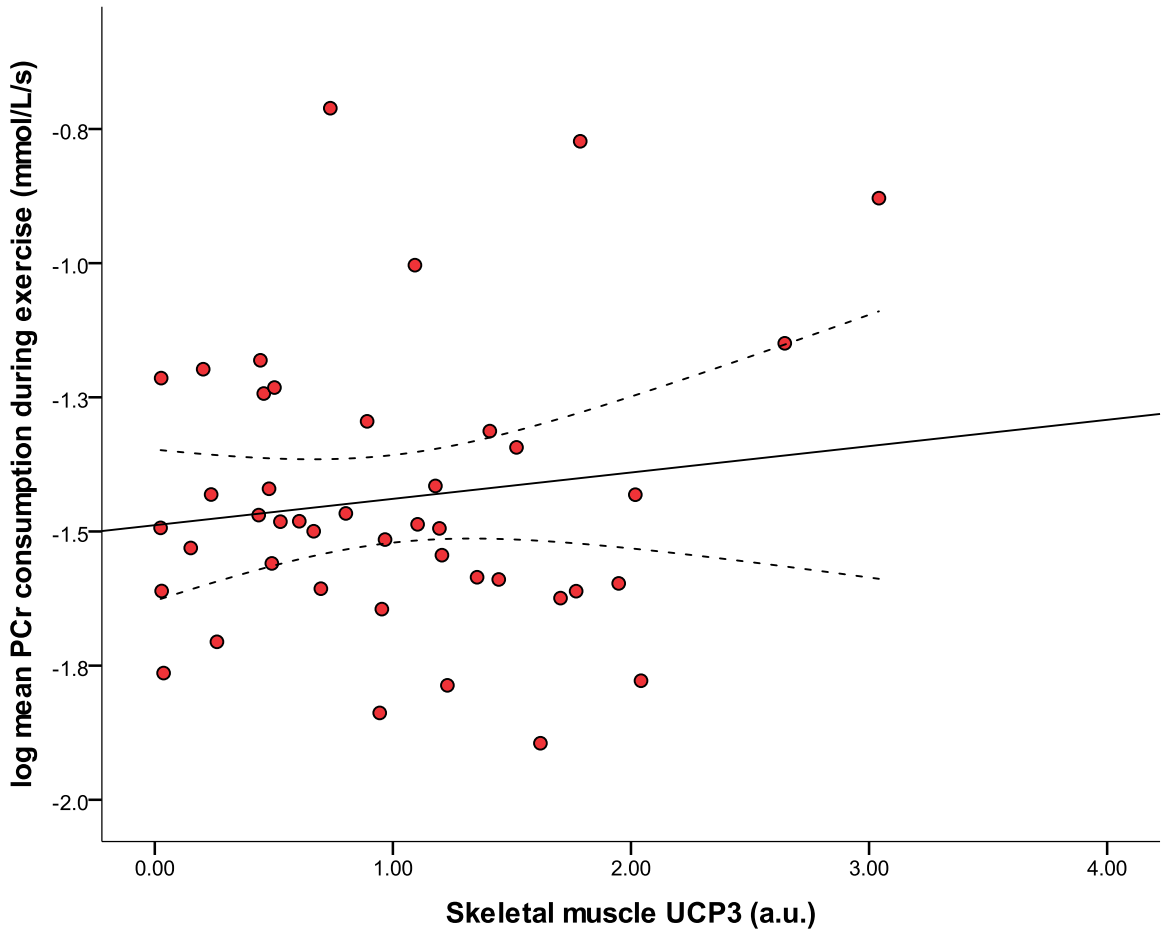

Figure 5.13. Scatter-plot showing mean PCr consumption during exercise plotted against skeletal muscle UCP3 levels.

The solid line is the regression line and the dashed lines are the 95% confidence intervals of the regression line. To transform the distribution of mean PCr consumption values to normal, logarithms (base 10) were taken.

$\beta = 0.13$, $p = 0.18$

PCr – phosphocreatine, UCP3 – mitochondrial uncoupling protein-3

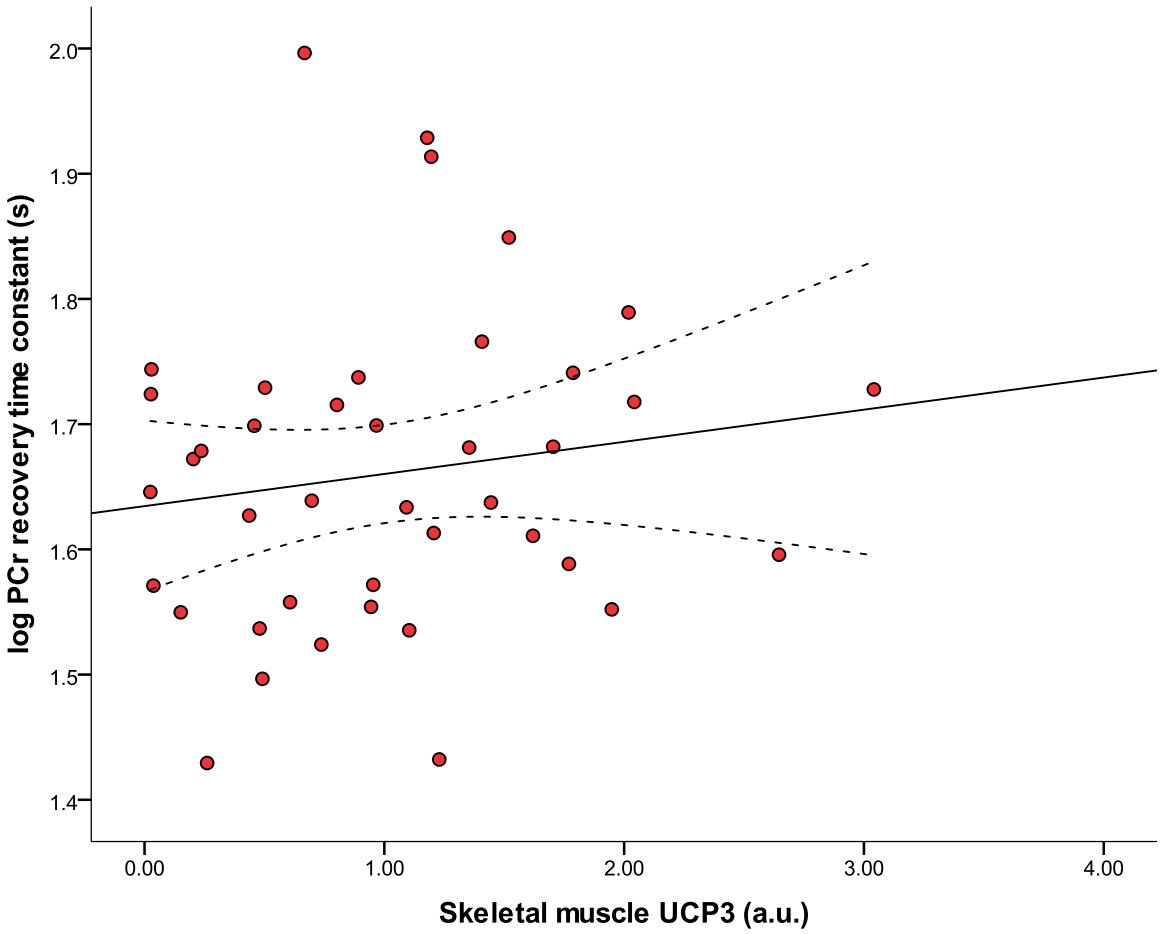

Figure 5.14. Scatter-plot showing skeletal muscle PCr recovery rate plotted against skeletal muscle UCP3 levels.

The solid line is the regression line and the dashed lines are the 95% confidence intervals of the regression line. To transform the distribution of PCr recovery time constants to normal, logarithms (base 10) were taken.

$\beta = 0.15$, $p = 0.17$

PCr – phosphocreatine, UCP3 – mitochondrial uncoupling protein-3

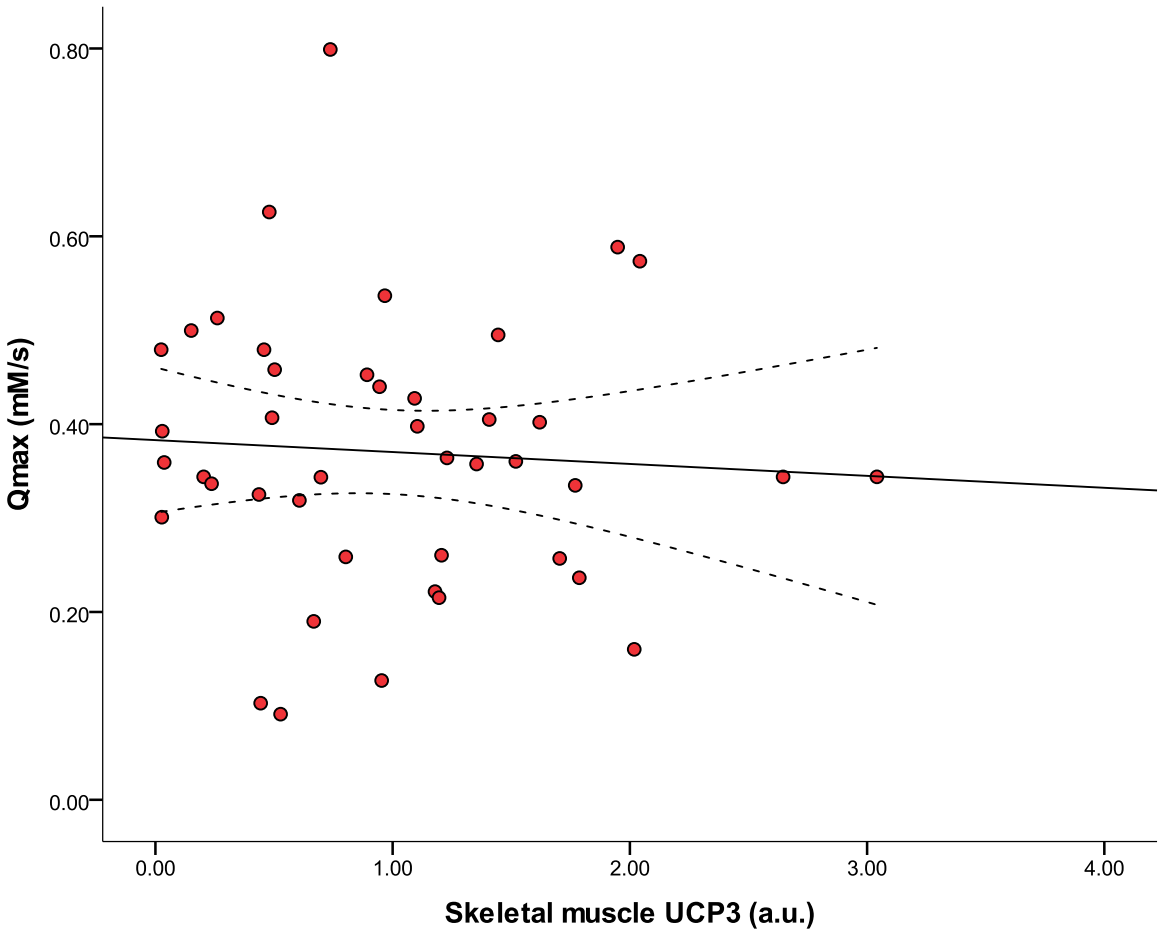

Figure 5.15. Scatter-plot showing skeletal muscle Q_{max} plotted against skeletal muscle UCP3 levels.

The solid line is the regression line and the dashed lines are the 95% confidence intervals of the regression line.

$\beta = -0.06$, $p = 0.34$

Q_{max} – the theoretical maximum rate of oxidative ATP synthesis (see Chapter 2), UCP3 - mitochondrial uncoupling protein-3.

Skeletal muscle oxygenation and cardiac function

Mean muscle oxygen consumption ($\Delta SmO_2/\Delta t$), the maximal rate of muscle deoxygenation and muscle reoxygenation rate following exercise, were not predicted by LVEF, end-diastolic volume or E/E' ratio (data not shown). There was no relationship between mean muscle oxygen consumption, maximal rate of muscle deoxygenation, muscle reoxygenation rate and NYHA class (data not shown). There was no difference in mean muscle oxygen consumption (0.04 ± 0.01 *vs* 0.05 ± 0.01 $\%.s^{-1}$, $t(32) = -0.58$, $p = 0.28$), maximal rate of muscle deoxygenation (0.66 ± 0.06 *vs* 0.81 ± 0.11 $\%.s^{-1}$, $t(33) = -1.12$, $p = 0.13$) and muscle reoxygenation rate (statistical significance assessed using Mann-Whitney U test, as unable to transform both groups to statistical normality) (M-W, $p = 0.35$) if the patients were divided into those without, or with, ventricular dysfunction. The 6MWT distance was predictive of mean oxygen consumption during exercise ($\beta = -0.41$, $p < 0.01$) (Figure 5.16) and the rate of reoxygenation following exercise ($\beta = -0.33$, $p < 0.05$) (Figure 5.17), but not maximal rate of deoxygenation ($\beta = -0.12$, $p = 0.25$) (data not shown).

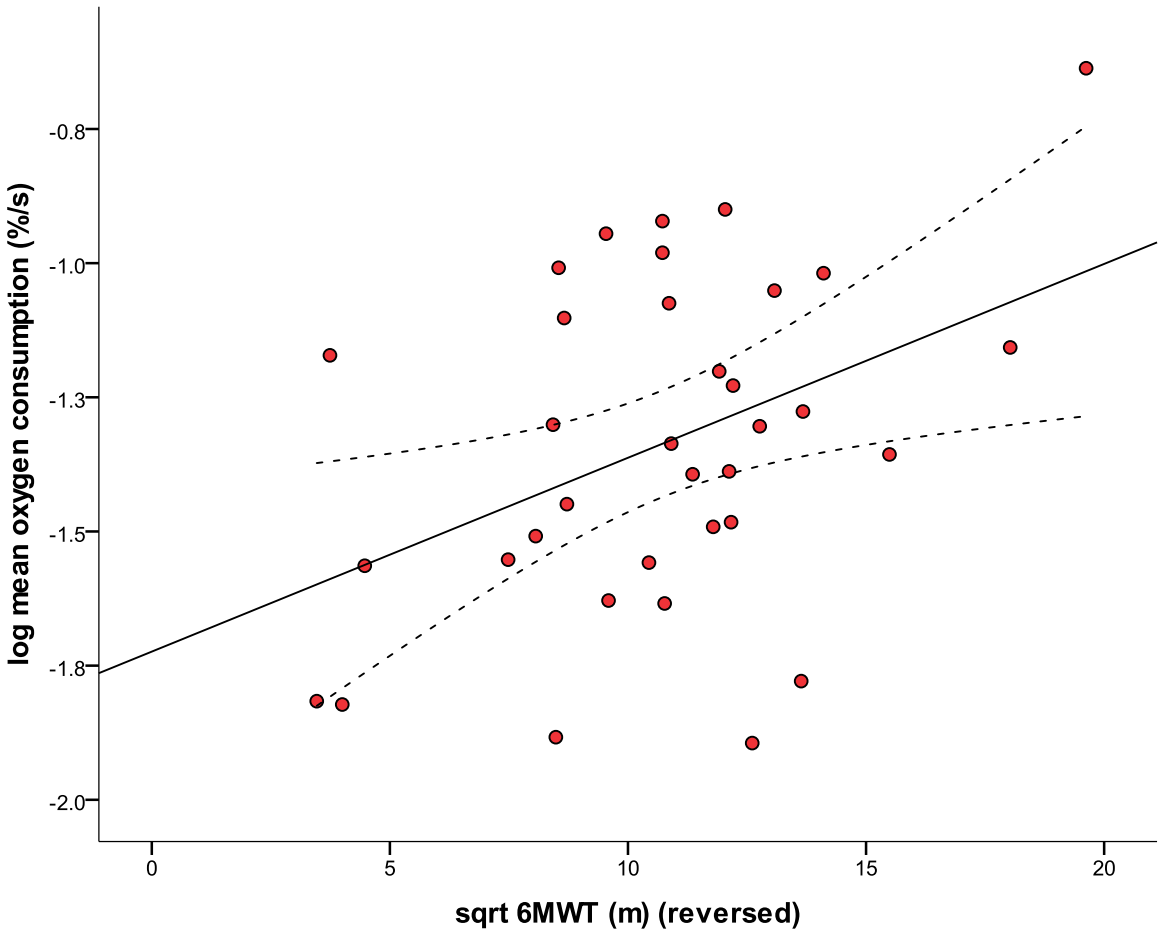

Figure 5.16. Scatter-plot showing skeletal muscle mean oxygen consumption plotted against six-minute walk test distance.

The solid line is the regression line and the dashed lines are the 95% confidence intervals of the regression line. To transform the distribution of mean oxygen consumption to normal, logarithms (base 10) were taken. The 6MWT values were reversed and square-rooted (sqrt) to correct for negative skew in the data, hence there is a negative relationship between mean muscle oxygen consumption and 6MWT distance.

$\beta = 0.41$, $p < 0.01$

6MWT – six-minute walk test

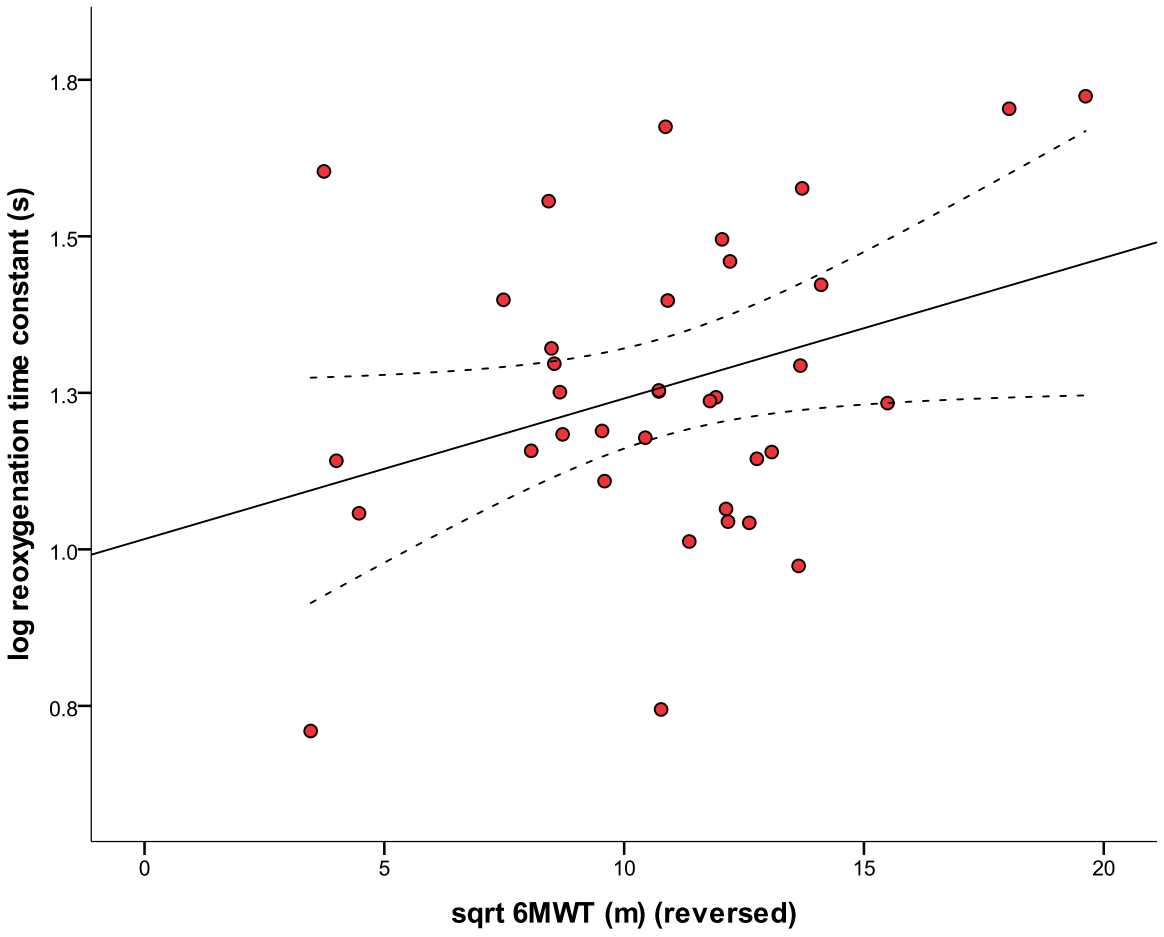

Figure 5.17. Scatter-plot showing skeletal muscle reoxygenation rate following exercise plotted against six-minute walk test distance.

The solid line is the regression line and the dashed lines are the 95% confidence intervals of the regression line. To transform the distribution of reoxygenation time constants to normal, logarithms (base 10) were taken. The 6MWT values were reversed and square-rooted (sqrt) to correct for negative skew in the data, hence there is a negative relationship between muscle reoxygenation rate and 6MWT distance.

$\beta = 0.33$, $p < 0.05$

6MWT – six-minute walk test

Skeletal muscle oxygenation and phosphorus metabolites during exercise

Skeletal muscle oxygenation was a strong predictor of [PCr] kinetics: mean oxygen and PCr consumption ($\beta = 0.60$, $p < 0.001$) (Figure 5.18), maximal oxygen consumption and initial rate of PCr hydrolysis ($\beta = 0.35$, $p < 0.05$) (Figure 5.19) and time constants of reoxygenation and PCr resynthesis ($\beta = 0.62$, $p < 0.001$) (Figure 5.20). The differences between the time constants of reoxygenation and PCr resynthesis demonstrated heteroscedasticity, that is as the magnitude of the time constants increased so did the difference between them (Figure 5.21). The differences between the time constants of skeletal muscle reoxygenation and PCr resynthesis were related to heart failure symptoms (JT, $p < 0.01$) (Figure 5.22) and 6MWT distance ($\beta = 0.33$, $p < 0.05$) (Figure 5.23) but not to LVEF ($\beta = -0.15$, $p = 0.19$), EDV ($\beta = 0.05$, $p = 0.38$) or E/E' ($\beta = 0.17$, $p = 0.18$) (data not shown).

Skeletal muscle oxygenation during exercise and UCP3 levels

Skeletal muscle UCP3 levels were not predictive of the maximal rate of muscle deoxygenation ($\beta = -0.11$, $p = 0.28$), mean skeletal muscle oxygen consumption during exercise ($\beta = 0.27$, $p = 0.07$), or the reoxygenation time constant ($\beta = 0.17$, $p = 0.17$) (data not shown).

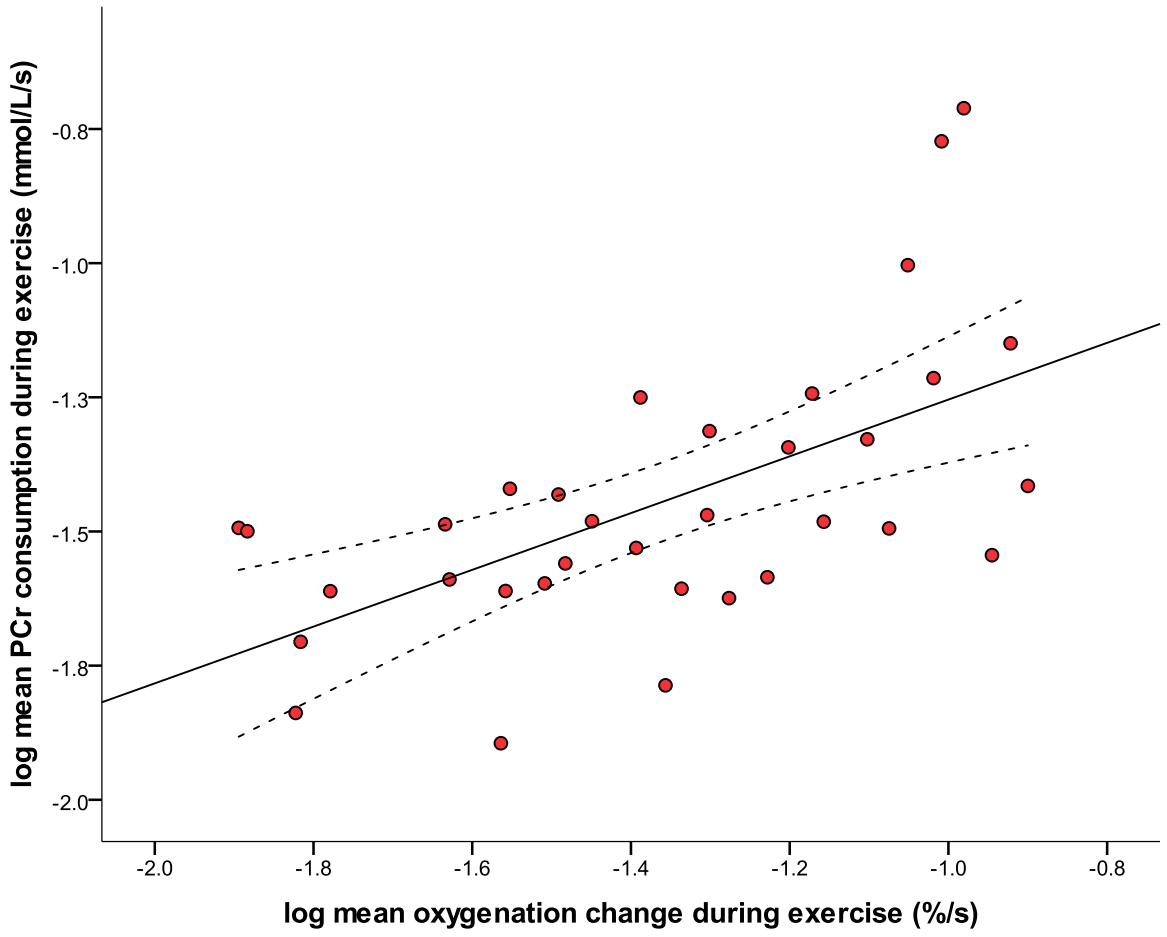

Figure 5.18. Scatter-plot showing mean PCr consumption and mean oxygenation change during exercise plotted against each other.

The solid line is the regression line and the dashed lines are the 95% confidence intervals of the regression line. To transform the distributions of mean PCr consumption and mean oxygenation change to normal, logarithms (base 10) were taken.

$\beta = 0.60$, $p < 0.001$

PCr – phosphocreatine

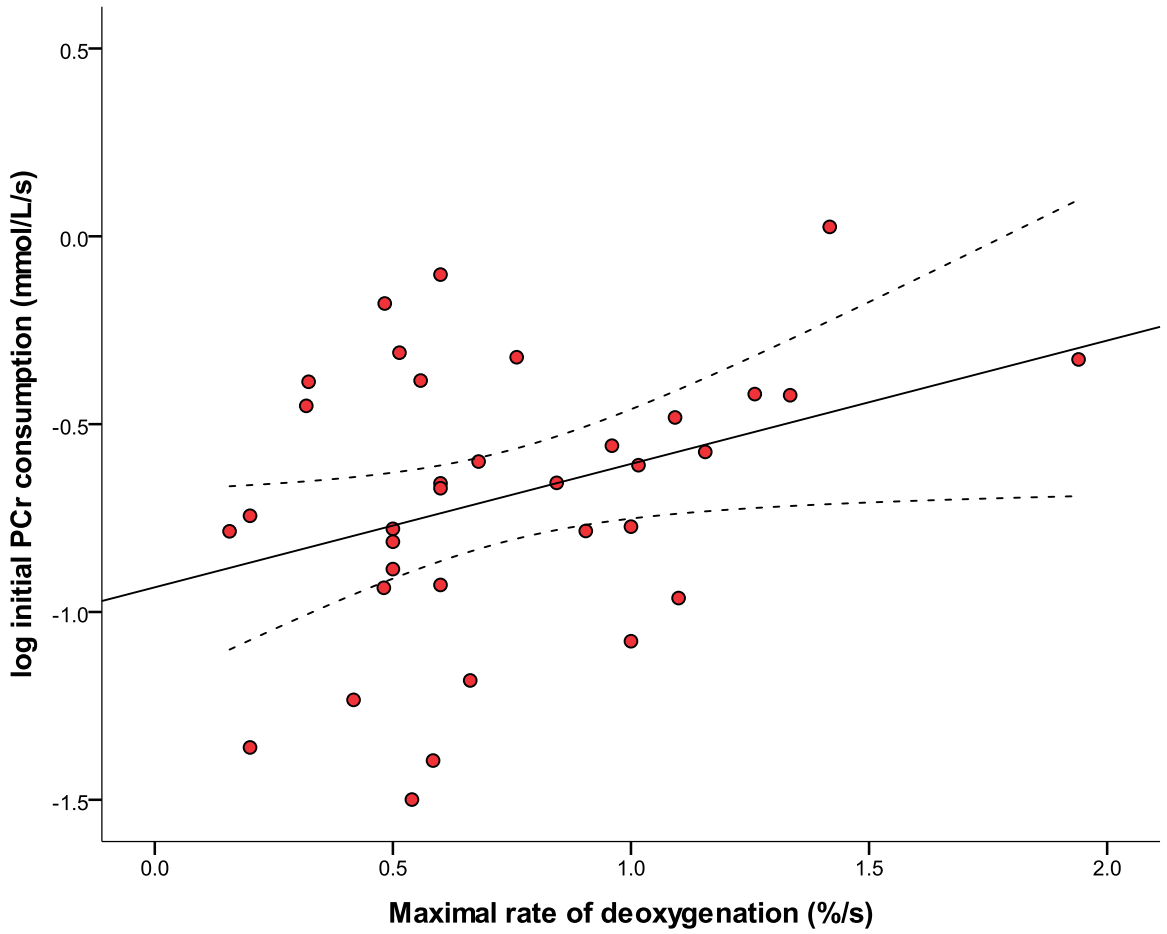

Figure 5.19. Scatter-plot showing initial PCr consumption and the maximal deoxygenation rate during exercise plotted against each other.

The solid line is the regression line and the dashed lines are the 95% confidence intervals of the regression line. To transform the distribution of initial PCr consumption to normal, logarithms (base 10) were taken.

$\beta = 0.35$, $p < 0.05$

PCr – phosphocreatine

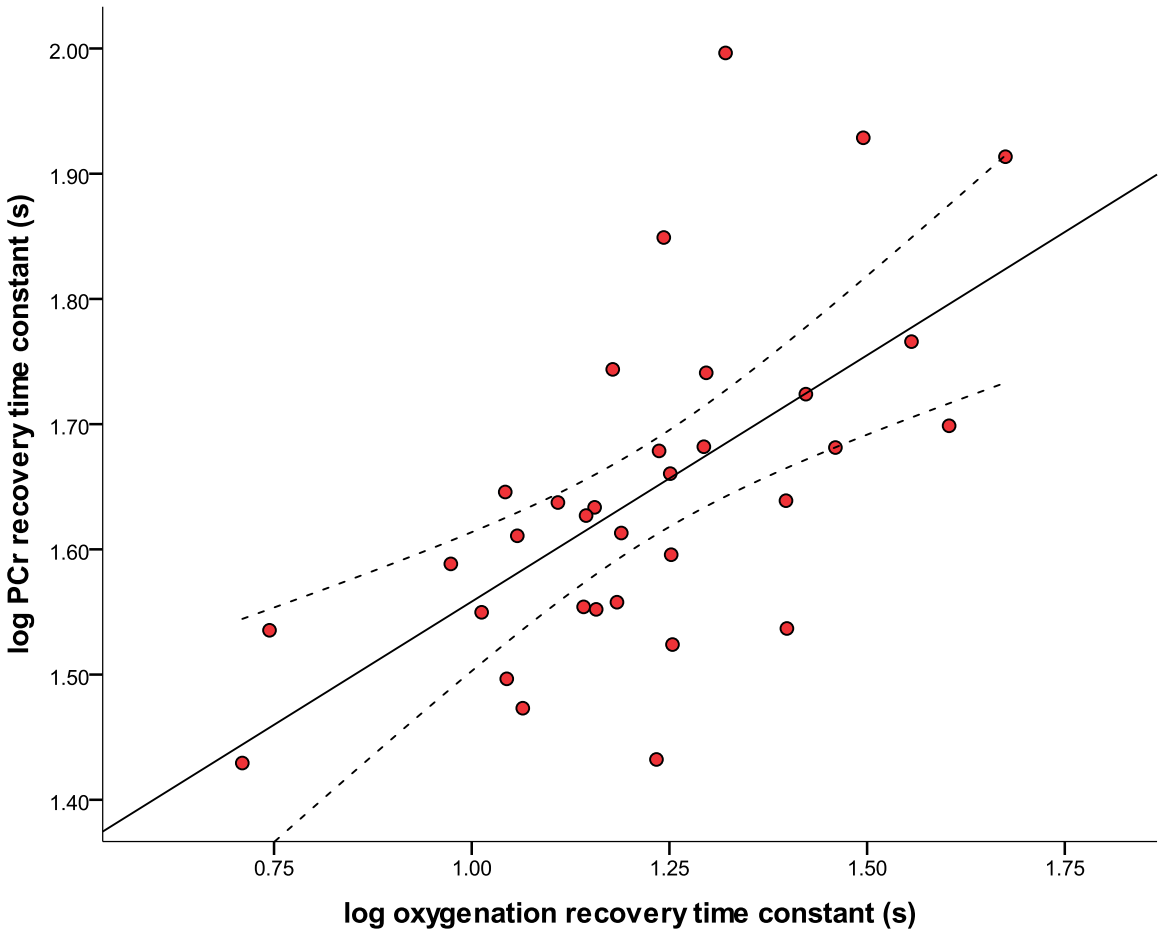

Figure 5.20. Scatter-plot showing time constants of skeletal muscle reoxygenation and PCr resynthesis following exercise plotted against each other.

The solid line is the regression line and the dashed lines are the 95% confidence intervals of the regression line. To transform the distributions of PCr and oxygenation recovery time constants to normal, logarithms (base 10) were taken.

$\beta = 0.62$, $p < 0.001$

PCr – phosphocreatine

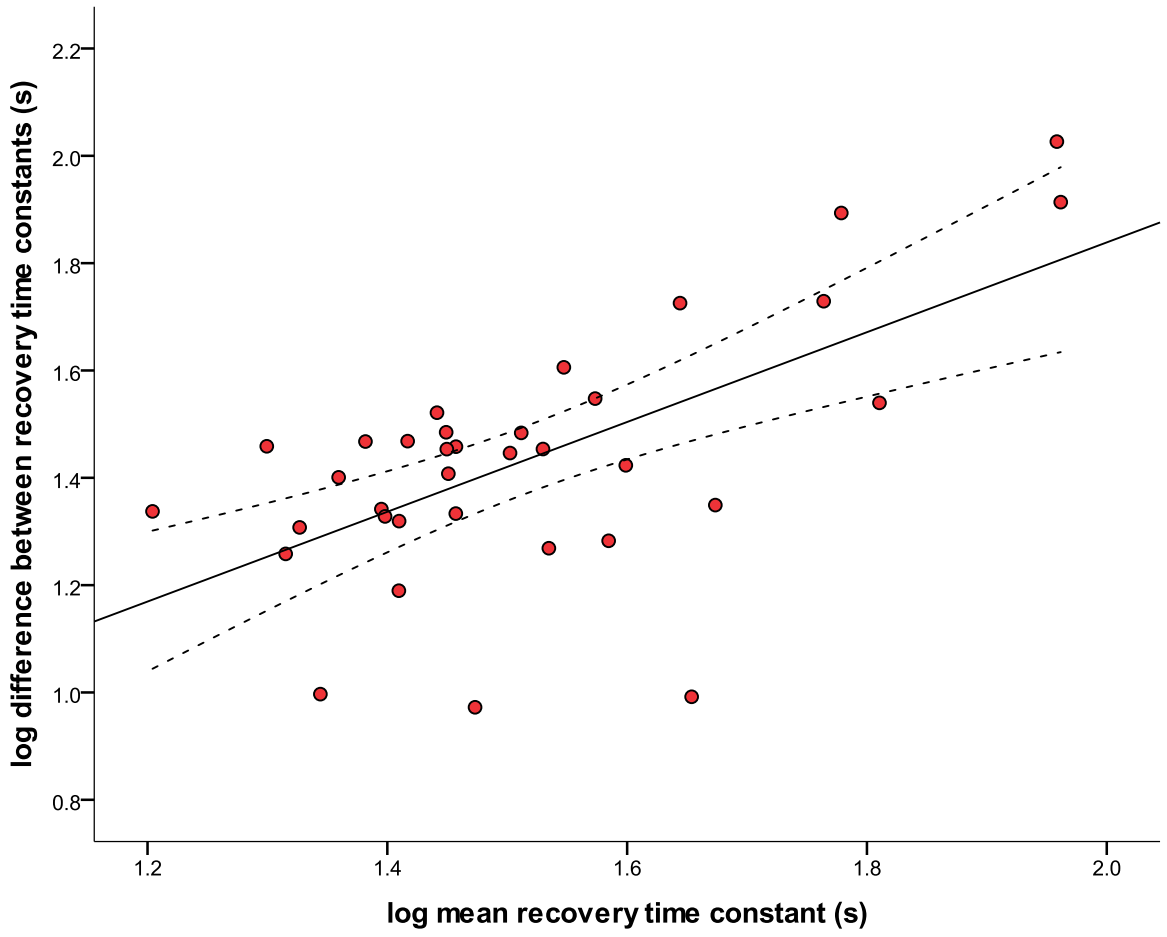

Figure 5.21. Scatter-plot showing the difference between the time constants of PCr resynthesis and skeletal muscle reoxygenation plotted against mean recovery time constant.

The solid line is the regression line and the dashed lines are the 95% confidence intervals of the regression line. To transform the distribution of difference between recovery time constants and mean recovery time constant to normal, logarithms (base 10) were taken.

$\beta = 0.64$, $p < 0.001$

PCr – phosphcreatine

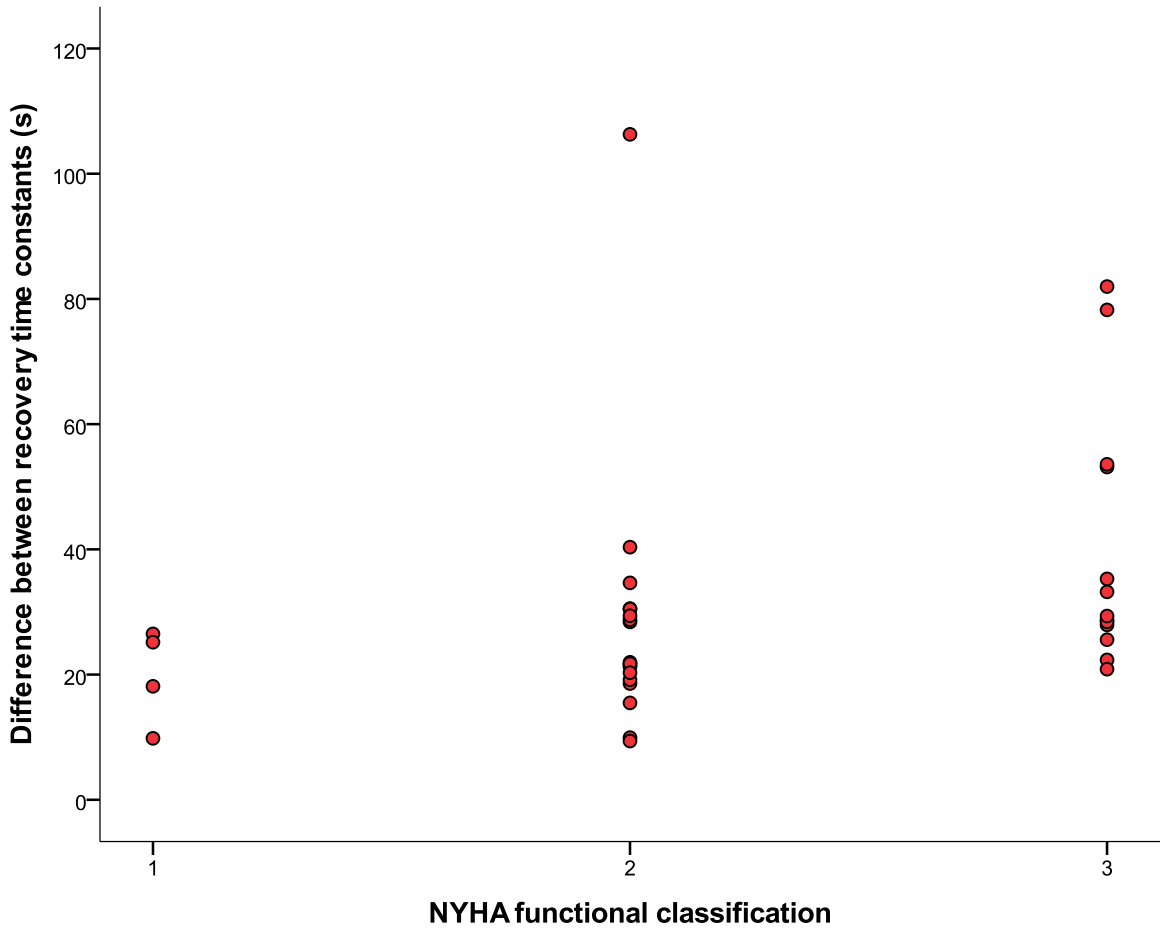

Figure 5.22. Scatter-plot of the differences between the skeletal muscle reoxygenation and PCr resynthesis time constants, grouped according to NYHA class.

JT, $p < 0.01$

NYHA – New York Heart Association

PCr – phosphcreatine

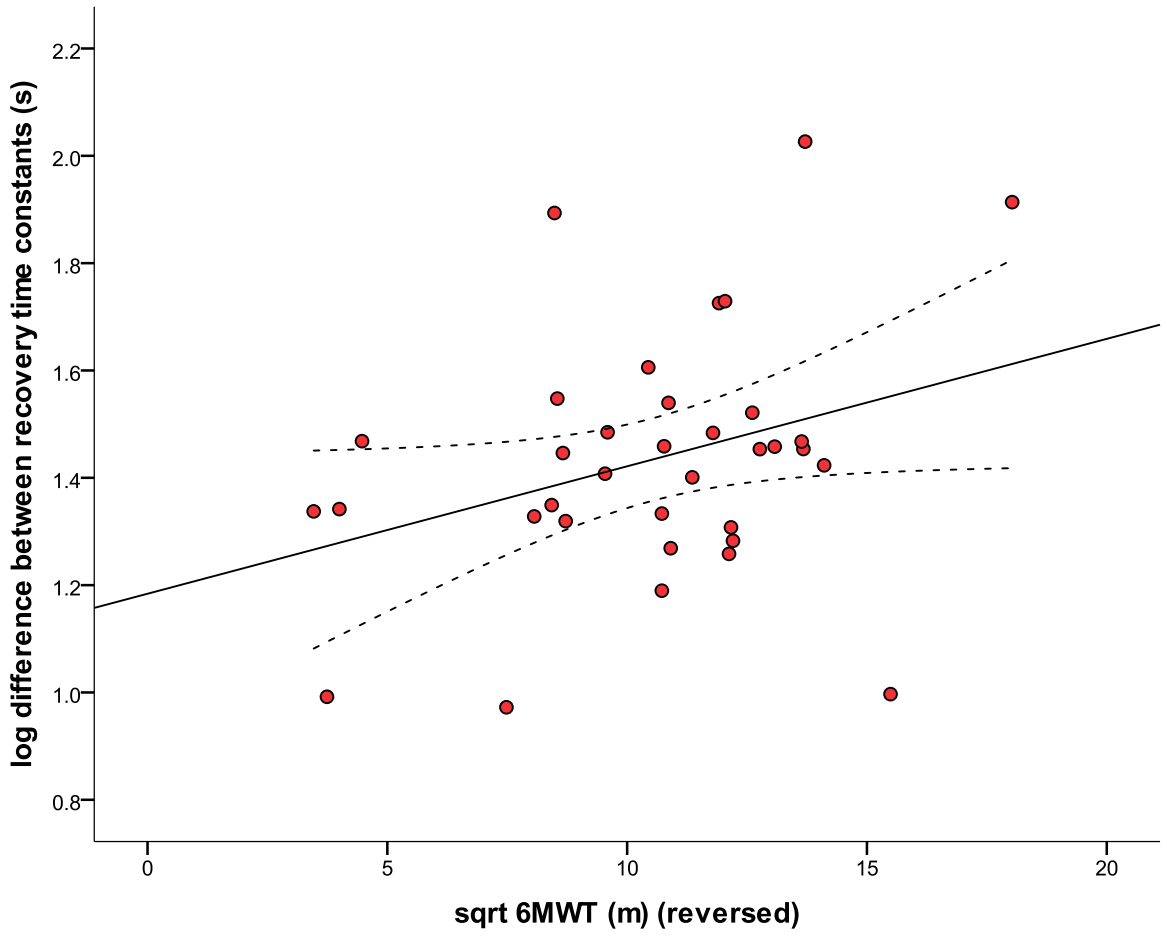

Figure 5.23. Scatter-plot of the differences between the time-constants of skeletal muscle PCr resynthesis and re-oxygenation following exercise, plotted against six-minute walk test distance.

The solid line is the regression line and the dashed lines are the 95% confidence intervals of the regression line. To transform the distribution of difference between recovery time constants to normal, logarithms (base 10) were taken. The 6MWT values were reversed and square-rooted (sqrt) to correct for negative skew in the data, hence there is a negative relationship between the time-constant differences and 6MWT distance.

$\beta = 0.33$, $p < 0.05$

PCr – phosphcreatine, 6MWT – six-minute walk test

5.5. Discussion

The aim of this study was to investigate relationships between heart failure severity and impaired skeletal muscle energy metabolism and skeletal muscle oxygenation, and their relationship with skeletal muscle UCP3 levels. It was found that patients with ventricular dysfunction were able to perform the exercise protocol for less time and had greater skeletal muscle PCr consumption during exercise. Functional capacity was found to be related to Q_{max}, and left ventricular ejection fraction (LVEF) was negatively predictive of skeletal muscle UCP3 levels, which also related to the NYHA class of the patients. However, skeletal muscle UCP3 levels were not found to be predictive of high energy phosphorus metabolite concentrations or ^{31}P MRS measures of mitochondrial function.

Left ventricular ejection fraction negatively predicted initial skeletal muscle PCr consumption at the onset of exercise, which was also greater in those with ventricular dysfunction compared with those without ventricular dysfunction. The consumption of PCr by muscle at the onset of exercise reflects the ATP requirement for the work done, as the initial ATP requirement is met by PCr hydrolysis (Kemp, Thompson *et al* 1994). The exercise protocol is standardized to lean body mass (LBM), consequently the work done is related to the patient's muscle mass. Therefore, these results demonstrate that lower LVEF is associated with decreased efficiency of ATP utilization in skeletal muscle. This could be explained by changes in muscle fibre-type (Crow and Kushmerick 1982), known to occur in heart failure (Mancini, Coyle *et al* 1989), or by decreases in mitochondrial number within the same fibre-type, or alternatively, by any mechanism whereby a given change in muscle fibre length requires greater cross bridge cycling to occur. Kemp and colleagues demonstrated increased PCr hydrolysis at the onset of exercise in heart failure patients

compared with controls (Kemp, Thompson *et al* 1996), but concluded that this was due to a decrease in muscle mass, as the experimenters used an exercise protocol that was the same for all subjects, and not indexed to LBM. The results from this study suggest that the observed increase in PCr hydrolysis is due to an impairment of ATP utilization.

Mean PCr consumption during exercise, which can be interpreted as the overall shortfall of oxidative ATP synthesis (ignoring the small glycolytic component), was also related to LVEF and the presence/absence of ventricular dysfunction. This is consistent with previous findings that patients with heart failure have greater PCr consumption during exercise (Massie, Conway *et al* 1987; Massie, Conway *et al* 1988; Kemp, Thompson *et al* 1996; Hanada, Okita *et al* 2000).

Previous studies have suggested a decrease in the mitochondrial capacity to synthesise ATP in heart failure, by demonstrating increased PCr recovery times and/or decreased Q_{max} (Kemps, Prompers *et al* 2010; Massie, Conway *et al* 1987; Massie, Conway *et al* 1988; Kemp, Thompson *et al* 1996; Hanada, Okita *et al* 2000). In this study, measures of functional capacity were found to relate to Q_{max}, with 6MWT distance being moderately predictive, and a relationship demonstrated with the NYHA functional classification. In these results however, it may be the case that it is the oxidative capacity of skeletal muscle that is determining the 6MWT performance and reported functional limitation, rather than being viewed as increased heart failure severity resulting in decreased skeletal muscle oxidative capacity. The proposal that heart failure symptoms may at least in part originate from skeletal muscle myopathy is not novel (Poole-Wilson and Buller 1988), and the present results support this concept.

The combination of NIRS and ^{31}P MRS was used in this study to assess skeletal muscle oxygenation changes along with ATP synthesis and utilisation, as has been employed previously in heart failure patients with conflicting results (Kemps, Prompers *et al* 2010; Hanada, Okita *et al* 2000). In the present study it was found that skeletal muscle PCr recovery and muscle reoxygenation were related to each other, but there was a dissociation between reoxygenation and PCr resynthesis kinetics as recovery following exercise became more impaired, and this dissociation was associated with NYHA classification i.e. subjects with worse heart failure symptoms had a greater difference between their reoxygenation and PCr resynthesis kinetics, and with 6MWT distance. The implication of this observation is that blood flow and hence oxygen delivery may have been relatively preserved in these patients, and the impairment in oxidative ATP synthesis is secondary to intrinsic mitochondrial dysfunction rather than a failure of oxygen delivery. This again highlights the haemodynamic paradox of heart failure, that measures of central haemodynamics and blood flow are unrelated to the symptoms of the condition (Franciosa, Park *et al* 1981; Massie, Conway *et al* 1988). However, NIRS is not a direct measurement of blood flow and relies on a number of assumptions which make such a conclusion tentative. In this study it was not possible to acquire NIRS data simultaneously with ^{31}P MRS data, necessitating the exercise to be repeated. This was always done at least two hours apart to ensure no residual fatigue and always in the same order and under the same conditions for each patient. Any error introduced by not collecting the data simultaneously was therefore minimised.

Having shown that the plasma NEFA concentration is related to ventricular function (Chapter 4) it was also shown in this study that it is associated with decreased resting skeletal muscle PCr/ATP ratio, higher resting [ADP] and decreased skeletal muscle Q_{max}. It

is not possible to assert that increased NEFA concentrations have caused these abnormalities in high energy metabolism, as they may both be independently related to heart failure severity, for example; however, these findings are consistent with the stated hypothesis that increased NEFA concentrations bring about mitochondrial dysfunction through an increased expression of UCP3 in skeletal muscle. However, no association was found between fasting plasma NEFA concentration and skeletal muscle UCP3 levels and, indeed, there were no relationships between skeletal muscle UCP3 levels and any of the MRS measures of high energy phosphate metabolism at rest, during or recovering from exercise. As discussed in Chapter 4, it is perhaps not surprising that plasma NEFA concentration was unrelated to UCP3 levels, because plasma NEFA concentration is known to fluctuate rapidly in response to the prevailing neurohumoral milieu (Frayn 1998), with changes in protein levels occurring more slowly (Jiang, Zhang *et al* 2009). It is therefore the underlying mean level of NEFA concentration, rather than a concentration taken at one particular time point, that is more likely to relate to UCP3 protein level.

The skeletal muscle biopsies were, however, taken from a different muscle than the muscle on which NIRS and ^{31}P MRS were performed, and this may explain the negative findings. The skeletal muscle expression of UCP3 is fibre-type dependant (Hesselink, Keizer *et al* 2001) and the fibre-type composition of the two muscles could perhaps have been different. The patient population, however, is that of relatively elderly, sedentary people with cardiac disease, who are not athletically trained. Therefore the fibre-type expression between gastrocnemius/soleus (NIRS/MRS) and pectoralis major (UCP3 levels) is not likely to be dissimilar secondary to a specific training effect impacting fibre-type expression. The human skeletal muscle fibre-type composition of gastrocnemius and parasternal intercostal

muscle has also been shown to be similar (Gollnick, Sjödin *et al* 1974; Mizuno and Secher 1989). It would though have been preferable to have acquired gastrocnemius biopsies with which to compare with MRS/NIRS data. This may have been possible from the patients having saphenous vein harvested as a coronary artery bypass graft, but more difficult from those not having coronary artery bypass grafting. It was felt that, as the proposed mechanism was not specific to a particular muscle group, and would be expected to occur throughout all skeletal muscle, it was preferable to avoid the inclusion of a separate invasive muscle biopsy, and instead, use the readily accessible pectoralis major muscle as a metabolic surrogate for gastrocnemius.

The finding that UCP3 levels were not related to PCr recovery rate following exercise is consistent with the previous findings of Hesselink and colleagues (Hesselink, Greenhaff *et al* 2003). It has also been shown that the proton leak mediated through UCP3 is not a basal, but an inducible leak, and the resulting effect is related to the degree of activation, rather than the absolute protein level (Boudina, Sena *et al* 2007). Known activators of UCP3 (superoxide, hydroxynonenol and fatty acids) were not measured in this study. The plasma concentration of non-esterified fatty acids was measured, but it is the concentration of fatty acids within the mitochondria which would be of relevance in this context. Furthermore, the effect that proton leak has on ATP synthesis may be dependant on the membrane potential ($\Delta\Psi$). At times when the membrane potential is low, i.e. at high rates of ATP synthesis during, or immediately after, exercise, the effects of proton leak may be limited (Nicholls 2004). No relationship was demonstrable, however, between resting skeletal muscle PCr/ATP ratio (high $\Delta\Psi$) and skeletal muscle UCP3 levels.

It was found that skeletal muscle UCP3 levels were related to LVEF, increasing with poorer systolic function, although the effect size was small, and it is far from certain that this would result in a clinically important effect.

Limitations

The main limitation to this study is that, as discussed above, a different muscle was biopsied for UCP3 immunoblotting to the one from which MRS/NIRS measurements were taken. The reasons underlying this methodological decision were discussed above.

Secondly, it was not possible to acquire NIRS data simultaneously with ^{31}P MRS data, due to the incompatibility of the NIRS equipment with the high magnetic field in the MRI scanner. This necessitated the exercise experiment to be repeated. The two bouts were always done at least two hours apart to ensure no residual fatigue, and always in the same order and under the same conditions for each patient. Any error introduced by not collecting the data simultaneously was therefore minimised.

This study used, amongst other methods, the NYHA classification of functional capacity to classify the severity of heart failure. As discussed previously in Chpater 4 this is a subjective method of classifying the severity of heart failure. The use of the NYHA classification, however, is a widely, clinically accepted, means to classify the severity of heart failure (Dickstein, Cohen-Solal *et al* 2008). The 6MWT was used as a more objective method to assess functional capacity, albeit in the context of subjects with angina. Cardiopulmonary exercise testing, the most objective measure of functional capacity, was not performed, partly because of concerns over exercising patients with left main coronary artery disease or critical aortic stenosis. It was also felt that the protocol was onerous on

patients as it was, and the addition of further arduous testing may have limited the number of willing paticipants.

Systolic dysfunction was defined as a left ventricular ejection fraction of less than 55%, and this is somewhat arbitrary. This value was chosen because the normal range for ejection fraction, measured by MRI, used locally (OCMR, John Radcliffe Hospital, Oxford), is 57-81%. Ejection fraction is not a completely representative measure of systolic function, and is not reflective of subtle systolic dysfunction possibly involving changes in torsion, longitudinal shortening and/or strain rates, but it is widely clinically used, and has been shown to be prognostically important (Dickstein, Cohen-Solal *et al* 2008).

The patients studied in the cohort had different diseases. It is not known whether the skeletal muscle energetic abnormalities are similar regardless of the underlying cause of cardiac failure. The reason behind including all patients presenting for cardiac surgery rather than limiting recruitment to a particular surgical pathology was to maximise the number of subjects enrolled, furthermore the hypothesis being tested was not specific to a particular aetiology, therefore it was felt valid to include patients with different aetiologies.

The hypothesised sequence of events, following ventricular dysfunction, begins with an increase in sympathetic tone, but this was not directly measured in this study. There is a well established relationship between ventricular function and plasma noradrenaline concentration (Thomas and Marks 1978; Francis, Goldsmith *et al* 1982; Levine, Francis *et al* 1983), so it was felt unnecessary to repeat this.

Plasma NEFA concentration is known to fluctuate depending on the dietary state and prevailing sympathetic tone (Frayn 1998) as discussed previously. In this study plasma NEFA concentration was always measured in the fasting state and at the same point within

the protocol, thereby minimising diurnal or contextual variation. Plasma NEFA concentrations measured on the day of surgery were again taken in the fasted state, although from arterial blood on this occasion. These were only related to Western blot results from the biopsies taken on the same day and not to the pre-operative investigations carried out previously, which were compared with the venous NEFA concentration taken contemporaneously.

The pre-operative investigations were carried out separately from the biopsy collection. The result of this was that skeletal muscle high energy phosphates and oxygenation were related to skeletal muscle UCP3 levels measured at a different time. This was unavoidable due to the time required to collect all necessary pre-operative data, and it was felt that disease progression would be minimal in the time between the pre-operative tests and the biopsies being taken. As discussed in the previous chapter, it is possible that the patients' anxiety levels concerning impending major surgery were different, resulting in differing degrees of sympathetic stimulation and hence UCP3 expression. All patients received sedative premedication in order to limit pre-operative anxiety; however, as demonstrated in Chapter 4, plasma NEFA concentrations were higher in those samples taken immediately pre-anaesthetic induction, compared with those samples taken at the pre-operative tests. This finding does suggest increased sympathetic tone was present, as the samples were again taken in the fasting state. Similarly, any effect this may have had on changes in skeletal muscle UCP3 levels is not known.

Further research

Further work is required to clarify a number of issues resulting from this work. It is not known whether the changes in skeletal muscle energy metabolism are the same in patients

with heart failure arising from different aetiologies. The metabolic changes taking place in the periphery may be different in heart failure with preserved ejection fraction (diastolic heart failure) compared with heart failure with reduced ejection fraction (systolic heart failure). This could be investigated by studying three groups: one with normal age matched controls, one with dilated cardiomyopathy patients who have predominantly systolic heart failure with low ejection fractions, and a third group comprising patients with predominantly diastolic heart failure - aortic stenotics or hypertensives for example. Muscle biopsies could be taken for direct assessment of mitochondrial function and immunoblotting for protein measurements, although needle biopsies may be too small to perform all desired experiments.

Further work is required to clarify the *in vivo* uncoupling effect of UCP3. Are protein copy numbers important or is the effect related to the concentrations of specific activators? The relationship of the mitochondrial inner-membrane potential to the uncoupling effect also needs to be confirmed. These experiments are difficult to perform *in vivo*, but further *in vitro* work may be able to address these issues.

5.6. Conclusions

No relationship was found between skeletal muscle UCP3 levels and skeletal muscle high energy phosphate concentrations, or their kinetics during exercise. UCP3 levels increased modestly with decreasing ejection fraction and were related to NYHA class. Patients with ventricular dysfunction had increased PCr consumption during exercise and were able to exercise for less time than those with normal ventricular function. Skeletal muscle Q_{max} was related to functional capacity, suggesting that exercise limitation in heart failure may

originate from the periphery. Indirect measurements of blood flow, using NIRS, were relatively preserved in patients, compared with PCr recovery rates, suggesting an intrinsic skeletal muscle mitochondrial myopathy in heart failure. Evidence for an impairment of skeletal muscle ATP utilisation in cardiac dysfunction has also been found, suggesting that mitochondrial dysfunction is not the only energetic abnormality in skeletal muscle in heart failure.

CHAPTER 6

ATRIAL AND SKELETAL MUSCLE MITOCHONDRIAL RESPIRATION AND PROTEIN EXPRESSION: RELATIONSHIPS TO VENTRICULAR FUNCTION AND ^{31}P MRS FINDINGS

6.1. Introduction

The work described in Chapters 4 and 5 investigated relationships between the degree of cardiac dysfunction and ^{31}P MRS measurements of mitochondrial function (i.e. cardiac PCr/ATP ratio (Chapter 3), and skeletal muscle PCr recovery times and Q_{max} (Chapter 4)). However, PCr/ATP ratios are only indirect measures of mitochondrial function. In order to explore the concept of mitochondrial dysfunction more precisely, and to quantify mitochondrial coupling, it is necessary to measure mitochondrial respiration directly.

Uncoupling of mitochondria in heart failure has been suggested by a number of studies. For example, human left ventricular biopsies from patients with end-stage cardiac failure undergoing transplantation, compared with unused normal donor hearts, had decreased oxygen consumption under ADP stimulation and decreased respiratory control ratios (RCR – the ratio of state 3 respiration, the respiratory rate in the presence of substrate and ADP, to state 4 respiration, the respiratory rate following the conversion of all added ADP to ATP), indicating uncoupling (Sharov, Todor *et al* 2000). However, a study on skeletal muscle (vastus lateralis) biopsies comparing heart failure patients with normal sedentary and normal active controls found similar maximal oxygen consumption in heart failure patients and sedentary controls, with only the active controls having higher maximal oxygen consumption (Mettauer, Zoll *et al* 2001). Using an acute myocardial infarction model in dogs, P/O ratios (the ratio of the amount of ATP synthesised from a known amount of ADP to the amount of oxygen consumed) were decreased, indicating mitochondrial uncoupling, and UCP3 protein levels were increased in mitochondria isolated from the non-infarcted ventricular wall (Almsherqi, McLachlan *et al* 2006). Similarly, the infarcted failing rat heart

has increased UCP3 levels and decreased P/O ratios, again indicating mitochondrial uncoupling, possibly mediated by UCP3 (Murray, Cole *et al* 2008).

6.2. Aims

The aims of the present study were to explore the relationship between heart failure severity and atrial and skeletal muscle mitochondrial respiration rates and, in particular, to look for direct evidence of mitochondrial uncoupling. It was hypothesised that mitochondrial coupling would be related to UCP3 levels, and that these variables would both relate to the severity of ventricular dysfunction. Because it is not possible to measure P/O ratios in permeabilised muscle biopsies (see Chapter 1), uncoupling was implied by either increased respiration rates in the presence of substrate alone, increased oligomycin-inhibited respiration rates, or decreased RCR. The manner in which mitochondrial respiration rates were related to cardiac and skeletal muscle ^{31}P MRS results was also studied, particularly as the decreased cardiac PCr/ATP ratio in heart failure is thought to be reflective of mitochondrial dysfunction.

6.3. Methods

Having been recruited from the cardiothoracic surgery outpatient clinic, and following an overnight fast, patients (n = 18) attended the Oxford Centre for Clinical Magnetic Resonance Research (OCMR) at a convenient time before their scheduled surgery. A clinical history was taken and demographic and anthropometric data recorded as described in Chapter 2.

Patients then underwent skeletal muscle and cardiac ^{31}P MRS and cardiac MRI cine imaging as described in Chapter 2. The order of tests was always skeletal muscle ^{31}P MRS first,

followed by cardiac MRI, in order that patients were rested before repeating the exercise protocol outside the MRI suite to measure skeletal muscle oxygen saturation Sm_{O2} using near-infrared spectroscopy, as described in Chapter 2. Patients were then provided with a light lunch. Once refreshed, patients performed the six-minute walk test (6MWT) and underwent transthoracic echocardiography as described in Chapter 2, afterwhich they were discharged.

During the scheduled operation, pectoralis major muscle was biopsied following sternotomy and right atrial appendage tissue was obtained at venous cannulation if surgery was performed using cardio-pulmonary bypass, or after exposure of the heart, prior to the commencement of grafting, if surgery was performed without cardio-pulmonary bypass. The tissue was immediately washed in physiological (0.9 % w/v) saline and divided into two parts; one was snap-frozen in liquid nitrogen, then stored at -80˚C for future Western blot analysis, the other was placed into ice cold sodium lactate (Hartmann's) solution and taken immediately for analysis of mitochondrial respiration as described in Chapter 2.

Ventricular dysfunction was said to be present if patients had systolic and/or diastolic ventricular impairment as defined in Chapter 2.

Statistical analysis

Variables and sub-groups of variables were assessed for normality by Shapiro-Wilk tests and visual inspection of quantile-quantile plots. Homogeneity of variance was assessed using Levene's tests (Field 2009). Variables were transformed if necessary to render them normally distributed. In the majority of cases the data were found to be positively skewed; in such cases log transformations produced acceptable normality and stability of variance.

Regression analyses were performed to assess the degree to which one variable could be predicted from another, with standardised beta (β) and associated p value (p) reported. Standardised beta is the degree of change of the outcome variable for unit change of the predictor in standard deviation units (Field 2009). One-tailed statistical tests were used, unless indicated, because of the directional nature of the hypothesis. Because of the low number of subjects in this study, NYHA groups were compared by combining classes 1 and 2 (class 1 comprised only one subject); and comparing the combination with class 3 patients. Groups were then compared using the non-parametric Mann-Whitney U test. When subjects were divided according to the presence or absence of ventricular dysfunction, parametric assumptions were not met, so the non-parametric Mann-Whitney U test was used and reported as MW and the p value. Missing data were excluded from analyses on a case-by-case basis and were not imputed using any method.

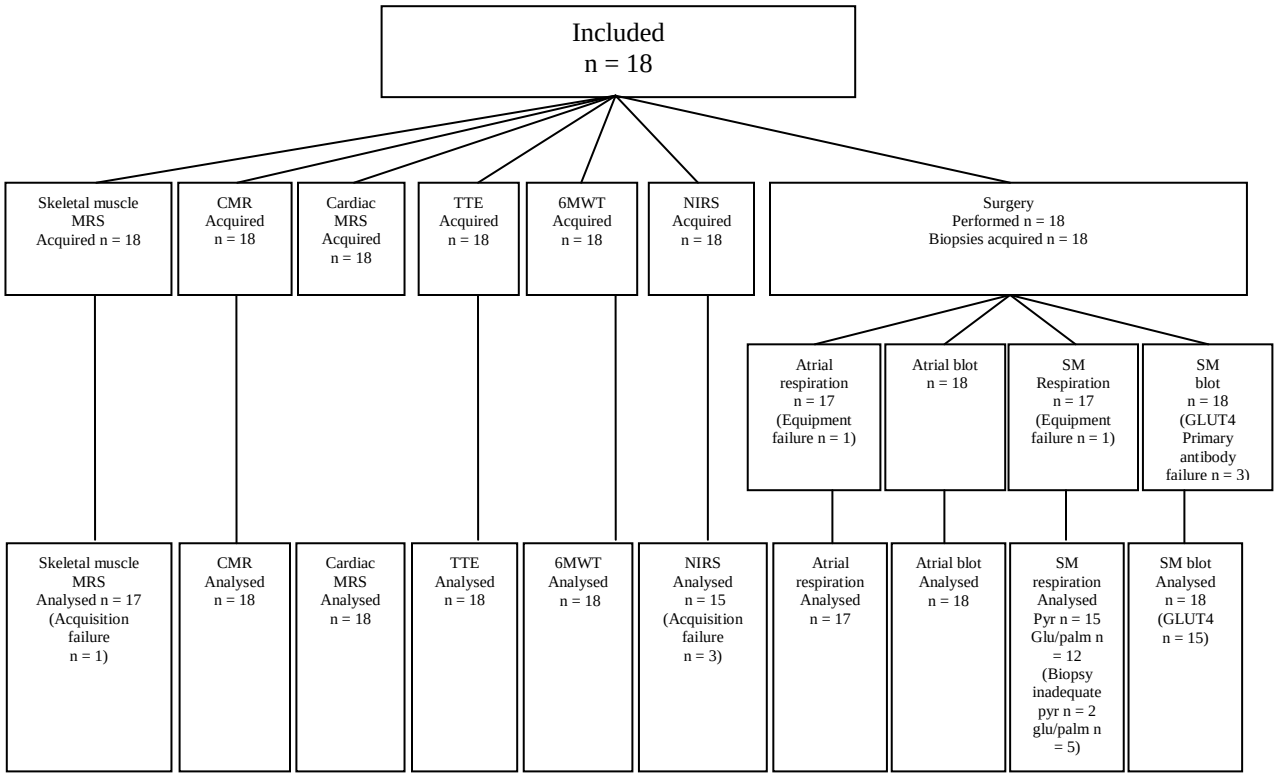

Figure 6.1. CONSORT-type flow diagram to describe the inclusion of subjects from the recruited cohort presented in Chapter 3.

MRS – magnetic resonance spectroscopy, CMR – cardiac magnetic resonance imaging, TTE – trans-thoracic echocardiography, 6MWT – six-minute walk test, NIRS – near-infrared spectroscopy, SM – skeletal muscle, blot – immunoblotting, GLUT4 – glucose transporter-4, pyr – pyruvate, glu – glutamate, palm – palmitate.

6.4. Results

Seventeen patients had successful mitochondrial respiration measurements performed on atrial biopsies; electrode failure prevented the experiments from being performed on one set of atrial and skeletal muscle biopsies. The number of successful skeletal muscle experiments varied because occasionally the skeletal muscle biopsy consisted of a large proportion of fat and connective tissue and consequently too few muscle fibres on which to perform complete respiration experiments. The final skeletal muscle numbers were therefore: 15 subjects for skeletal muscle pyruvate oxidation, and 12 subjects for skeletal muscle glutamate and palmitate oxidation.

The patient cohort for this study was a subsection of the one described in Chapter 3. There were 15 men and 2 women. Respiration rates for various substrates are shown in Table 6.1 for atrial biopsies and Table 6.2 for skeletal muscle biopsies.

Table 6.1. Atrial oxidation rates for the substrates tested

O_2 consumption (nmol/min/mg (ww))	**Substrate**	**+ ADP**	**+ Oligomycin**	**+ FCCP**	**RCR**
Glutamate (n = 17)	0.29 ± 0.09	0.41 ± 0.16	0.37 ± 0.18	0.57 ± 0.30	1.4 ± 0.5
Pyruvate (n = 17)	0.47 ± 0.21	0.56 ± 0.20	0.50 ± 0.18	0.82 ± 0.28	1.2 ± 0.1
Palmitate (n = 17)	0.43 ± 0.20	0.57 ± 0.19	0.52 ± 0.13	0.73 ± 0.19	1.3 ± 0.2

Data are expressed as means ± SD.

ww – wet weight, ADP – adenosine diphosphate, FCCP - carbonyl cyanide p-(trifluoromethoxy)phenylhydrazone, RCR – respiratory control ratio.

Table 6.2. Skeletal muscle oxidation rates for the substrates tested

O_2 consumption (nmol/min/mg (ww))	Substrate	+ ADP	+ Oligomycin	+ FCCP	RCR
Glutamate (n = 12)	0.21 ± 0.11	0.28 ± 0.16	0.27 ± 0.14	0.40 ± 0.24	1.4 ± 0.4
Pyruvate (n = 15)	0.31 ± 0.15	0.42 ± 0.20	0.40 ± 0.15	0.76 ± 0.34	1.6 ± 0.4
Palmitate (n = 12)	0.33 ± 0.14	0.38 ± 0.12	0.34 ± 0.10	0.45 ± 0.15	1.2 ± 0.2

Data are expressed as means ± SD

ww – wet weight, ADP – adenosine diphosphate, FCCP - carbonyl cyanide p-(trifluoromethoxy)phenylhydrazone, RCR - respiratory control ratio.

Mitochondrial respiration and cardiac function

Mitochondrial respiration rates with any substrate, from either atria or skeletal muscle, were not predicted by left ventricular ejection fraction (LVEF), left-ventricular end-diastolic volume (LV-EDV), E/E' ratio or six-minute walk test (6MWT) distance (data not shown). Comparisons between patients in NYHA class 1 and 2, and NYHA class 3, revealed no significant differences in respiration rates with any substrate or intervention (Table 6.3 and Table 6.4). There were no differences in respiration rate between those with ventricular dysfunction and those with normal ventricular function (defined earlier) (Table 6.5 and Table 6.6).

Table 6.3. Atrial mitochondrial respiration grouped according to NYHA class.

O_2 consumption	NYHA 1 + 2 (n = 11) (nmol/min/mg (ww))	NYHA 3 (n = 6) (nmol/min/mg (ww))	p value (2 – tailed)
Glu	0.31 (0.24 - 0.33)	0.26 (0.24 - 0.31)	0.46
Glu + ADP	0.41 (0.29 - 0.63)	0.34 (0.29 - 0.48)	0.69
Glu + ADP + Oligo	0.33 (0.26 - 0.54)	0.31 (0.24 - 0.41)	0.53
Glu + ADP + Oligo + FCCP	0.62 (0.38 - 0.70)	0.41 (0.35 - 0.71)	0.46
Pyr	0.44 (0.30 - 0.70)	0.45 (0.27 - 0.65)	0.69
Pyr + ADP	0.50 (0.40 - 0.78)	0.56 (0.36 - 0.78)	0.69
Pyr + ADP + Oligo	0.42 (0.40 - 0.72)	0.52 (0.32 - 0.67)	0.84
Pyr + ADP + Oligo + FCCP	0.81 (0.74 - 0.94)	0.84 (0.55 - 1.00)	0.76
Palm	0.50 (0.30 - 0.63)	0.38 (0.31 - 0.69)	0.84
Palm + ADP	0.50 (0.39 - 0.69)	0.53 (0.38 - 0.76)	0.99
Palm + ADP + Oligo	0.57 (0.46 - 0.55)	0.49 (0.36 - 0.64)	0.92
Palm + ADP + Oligo + FCCP	0.73 (0.56 - 0.94)	0.72 (0.52 - 0.92)	0.88

Data are presented as medians (IQR).

NYHA – New York Heart Association, Glu – glutamate, ADP – adenosine diphosphate, Oligo – oligomycin, FCCP - carbonyl cyanide p-(trifluoromethoxy)phenylhydrazone, Pyr – pyruvate, Palm – palmitate, ww – wet weight.

Table 6.4. Skeletal muscle mitochondrial respiration grouped according to NYHA class.

O_2 consumption	NYHA 1 + 2 (nmol/min/mg (ww)) (n)	NYHA 3 (nmol/min/mg (ww)) (n)	p value (2 – tailed)
Glu	0.18 (0.16 - 0.29) (8)	0.16 (0.07 - 0.28) (4)	0.40
Glu + ADP	0.27 (0.18 - 0.37) (8)	0.23 (0.08 - 0.44) (4)	0.61
Glu + ADP + Oligo	0.25 (0.19 - 0.40) (8)	0.21 (0.07 - 0.45) (4)	0.73
Glu + ADP + Oligo + FCCP	0.42 (0.19 - 0.58) (8)	0.35 (0.13 - 0.72) (4)	0.99
Pyr	0.28 (0.22 - 0.39) (10)	0.29 (0.17 - 0.40) (5)	0.91
Pyr + ADP	0.42 (0.33 - 0.58) (10)	0.40 (0.31 - 0.50) (5)	0.75
Pyr + ADP + Oligo	0.37 (0.29 - 0.48) (10)	0.36 (0.30 - 0.48) (5)	0.75
Pyr + ADP + Oligo + FCCP	0.75 (0.50 - 1.00) (10)	0.67 (0.51 - 1.09) (5)	0.91
Palm	0.31 (0.18 - 0.46) (8)	0.35 (0.23 - 0.42) (4)	0.88
Palm + ADP	0.43 (0.23 - 0.51) (8)	0.38 (0.30 - 0.40) (4)	0.54
Palm + ADP + Oligo	0.36 (0.23 - 0.46) (8)	0.34 (0.28 - 0.37) (4)	0.76
Palm + ADP + Oligo + FCCP	0.46 (0.34 - 0.64) (8)	0.39 (0.34 - 0.48) (4)	0.54

Data are presented as medians (IQR).

Medians compared using Mann-Witney U test.

NYHA – New York Heart Association, Glu – glutamate, ADP – adenosine diphosphate, Oligo – oligomycin, FCCP - carbonyl cyanide p-(trifluoromethoxy)phenylhydrazone, Pyr – pyruvate, Palm – palmitate, ww – wet weight.

Table 6.5. Atrial mitochondrial respiration grouped according to the presence or absence of ventricular dysfunction.

O_2 consumption	Normal ventricular function (n = 10) (nmol/min/mg (ww))	Ventricular dysfunction (n = 7) (nmol/min/mg (ww))	p value (2 – tailed)
Glu	0.28 (0.23 - 0.36)	0.31 (0.26 - 0.32)	0.63
Glu + ADP	0.33 (0.28 - 0.54)	0.43 (0.33 - 0.51)	0.52
Glu + ADP + Oligo	0.29 (0.24 - 0.48)	0.35 (0.29 - 0.45)	0.52
Glu + ADP + Oligo + FCCP	0.42 (0.30 - 0.68)	0.63 (0.41 - 0.98)	0.13
Pyr	0.52 (0.30 - 0.72)	0.31 (0.28 - 0.52)	0.21
Pyr + ADP	0.63 (0.41 - 0.81)	0.43 (0.40 - 0.58)	0.14
Pyr + ADP + Oligo	0.55 (0.37 - 0.73)	0.40 (0.34 - 0.49)	0.24
Pyr + ADP + Oligo + FCCP	0.92 (0.80 - 1.04)	0.70 (0.58 - 0.78)	0.02*
Palm	0.44 (0.31 - 0.64)	0.38 (0.29 - 0.51)	0.50
Palm + ADP	0.60 (0.36 - 0.70)	0.55 (0.39 - 0.66)	0.85
Palm + ADP + Oligo	0.51 (0.44 - 0.61)	0.49 (0.38 - 0.55)	0.63
Palm + ADP + Oligo + FCCP	0.68 (0.53 - 0.92)	0.80 (0.56 - 0.96)	0.70

Data are presented as medians (IQR). Medians compared using Mann-Witney U test.

* $p < 0.05$

Glu – glutamate, ADP – adenosine diphosphate, Oligo – oligomycin, FCCP - carbonyl cyanide p-(trifluoromethoxy)phenylhydrazone, Pyr – pyruvate, Palm – palmitate, ww – wet weight.

Table 6.6. Skeletal muscle mitochondrial respiration grouped according to the presence or absence of ventricular dysfunction.

O_2 consumption	Normal ventricular function (nmol/min/mg (ww)) (n)	Ventricular dysfunction (nmol/min/mg (ww)) (n)	p value (2 – tailed)
Glu	0.17 (0.13 - 0.22) (7)	0.24 (0.12 - 0.38) (5)	0.29
Glu + ADP	0.24 (0.17 - 0.38) (7)	0.34 (0.13 - 0.49) (5)	0.57
Glu + ADP + Oligo	0.22 (0.13 - 0.33) (7)	0.29 (0.15 - 0.46) (5)	0.47
Glu + ADP + Oligo + FCCP	0.33 (0.12 - 0.55) (7)	0.50 (0.19 - 0.65) (5)	0.57
Pyr	0.27 (0.17 - 0.39) (9)	0.32 (0.25 - 0.37) (6)	0.71
Pyr + ADP	0.40 (0.33 - 0.54) (9)	0.45 (0.33 - 0.47) (6)	0.79
Pyr + ADP + Oligo	0.36 (0.28 - 0.54) (9)	0.39 (0.31 - 0.44) (6)	0.87
Pyr + ADP + Oligo + FCCP	0.69 (0.52 - 0.99) (9)	0.71 (0.50 - 1.00) (6)	0.79
Palm	0.27 (0.19 - 0.42) (7)	0.43 (0.24 - 0.46) (5)	0.46
Palm + ADP	0.37 (0.27 - 0.47) (7)	0.39 (0.28 - 0.51) (5)	0.77
Palm + ADP + Oligo	0.33 (0.27 - 0.38) (7)	0.35 (0.25 - 0.46) (5)	0.66
Palm + ADP + Oligo + FCCP	0.42 (0.32 - 0.64) (7)	0.41 (0.38 - 0.54) (5)	0.77

Data are presented as medians (IQR).

Medians compared using Mann-Witney U test.

Glu – glutamate, ADP – adenosine diphosphate, Oligo – oligomycin, FCCP - carbonyl cyanide p-(trifluoromethoxy)phenylhydrazone, Pyr – pyruvate, Palm – palmitate, ww – wet weight.

Mitochondrial respiration and ^{31}P magnetic resonance spectroscopy data

Cardiac PCr/ATP ratio was not predicted by atrial mitochondrial respiration rates using any substrate or inhibitor (data not shown). Skeletal muscle mitochondrial respiration rates did not predict resting high energy phosphorus metabolites or phosphocreatine kinetic data (data not shown).

Mitochondrial proteins and cardiac function

Left ventricular ejection fraction did not predict atrial or skeletal muscle levels of citrate synthase (CS), adenine nucleotide transporter (ANT), α-ketoglutarate dehydrogenase (αKGD), medium chain acyl-CoA dehydrogenase (MCAD), glucose transporter-4 (GLUT4), or electron transport chain (ETC) complexes 1-5 (data not shown). Left-ventricular end-diastolic volume was found to predict atrial αKGD levels ($\beta = 0.56$, $p < 0.01$) (Figure 6.2), atrial ANT levels ($\beta = 0.69$, $p < 0.001$) (Figure 6.3), atrial ETC complex 1 ($\beta = 0.55$, $p < 0.01$) (Figure 6.4), complex 2 ($\beta = 0.60$, $p < 0.01$) (Figure 6.5) and complex 3 ($\beta = 0.63$, $p < 0.01$) (Figure 6.6) and atrial CS levels ($\beta = 0.50$, $p < 0.05$) (Figure 6.6). Left-ventricular end-diastolic volume did not predict GLUT4 ($\beta = 0.28$, $p = 0.14$), MCAD ($\beta = 0.39$, $p = 0.05$) or ETC complex 4 ($\beta = 0.17$, $p = 0.25$) and complex 5 ($\beta = 0.32$, $p = 0.10$). The diastolic parameter E/E' was not predictive of atrial or skeletal muscle levels of αKGD, ANT, GLUT4, MCAD, CS or ETC complexes, nor was 6MWT distance (data not shown). There were no differences in atrial levels of αKGD, ANT, GLUT4, MCAD, CS or ETC complexes, if patients were divided into groups according to NYHA class (Table 6.7), or according to the presence or absence of ventricular dysfunction (Table 6.8). Patients with ventricular dysfunction had decreased levels of skeletal muscle αKGD, ANT and MCAD levels, compared with patients without ventricular dysfunction (Table 6.9), however there

were no differences in skeletal muscle mitochondrial protein levels if patients were divided in NYHA groups (Table 6.10).

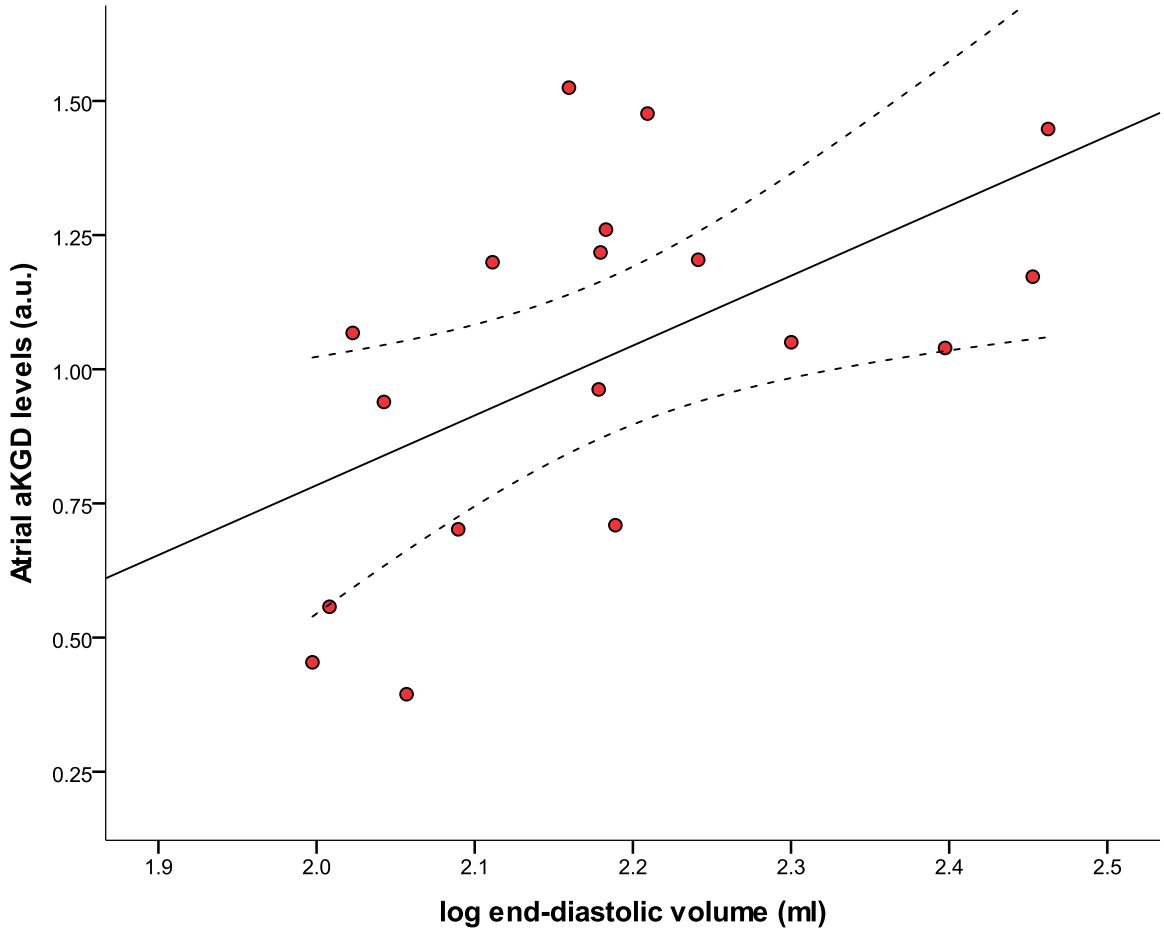

Figure 6.2. Scatter-plot showing atrial α-ketoglutarate dehydrogenase level plotted against left ventricular end-diastolic volume.

The solid line is the regression line and the dashed lines are the 95% confidence intervals of the regression line. Values of left ventricular end-diastolic volume had a positively skewed distribution. These were successfully transformed to statistical normality by taking logarithms (base 10).

$\beta = 0.56$, $p < 0.01$ aKGD – α-ketoglutarate dehydrogenase

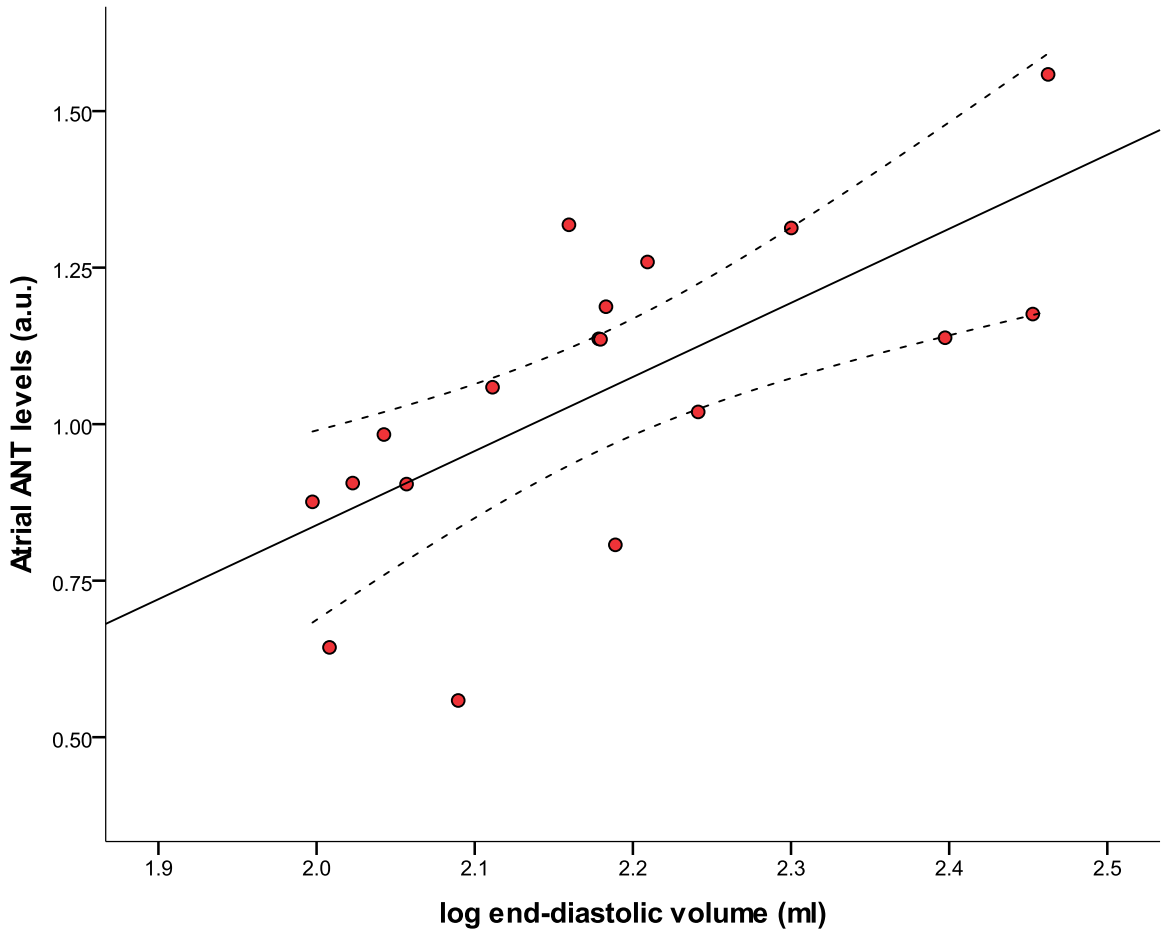

Figure 6.3. Scatter-plot showing the atrial adenine nucleotide transporter level plotted against left ventricular end-diastolic volume.

The solid line is the regression line and the dashed lines are the 95% confidence intervals of the regression line. Values of left ventricular end-diastolic volume had a positively skewed distribution. These were successfully transformed to statistical normality by taking logarithms (base 10).

$\beta = 0.69$, $p < 0.001$

ANT – adenine nucleotide transporter

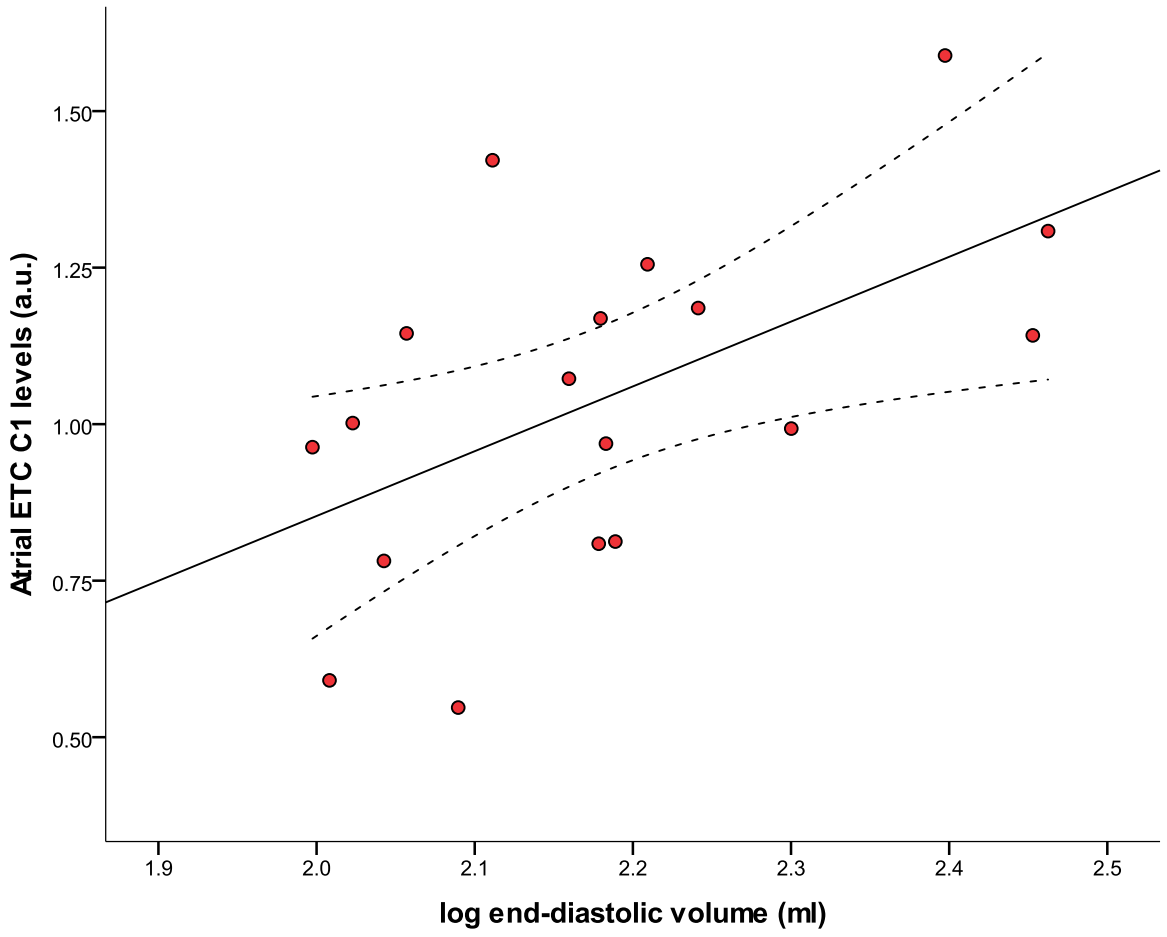

Figure 6.4. Scatter-plot showing atrial electron transport chain complex 1 level plotted against left ventricular end-diastolic volume.

The solid line is the regression line and the dashed lines are the 95% confidence intervals of the regression line. Values of left ventricular end-diastolic volume had a positively skewed distribution. These were successfully transformed to statistical normality by taking logarithms (base 10).

$\beta = 0.55$, $p < 0.01$

ETC C1 – electron transport chain complex-1

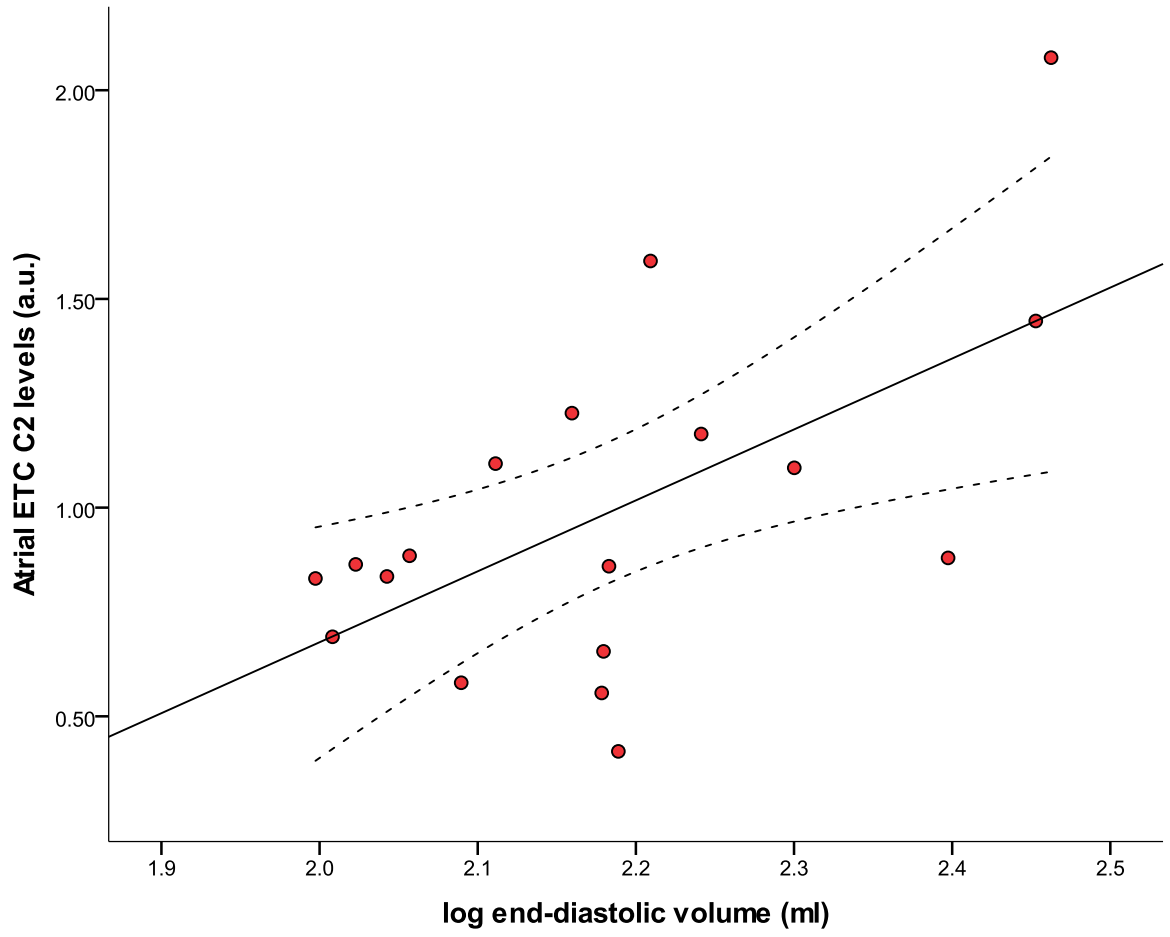

Figure 6.5. Scatter-plot showing atrial electron transport chain complex 2 level plotted against left ventricular end-diastolic volume.

The solid line is the regression line and the dashed lines are the 95% confidence intervals of the regression line. Values of left ventricular end-diastolic volume had a positively skewed distribution. These were successfully transformed to statistical normality by taking logarithms (base 10).

$\beta = 0.60$, $p < 0.01$

ETC C2 – electron transport chain complex-2

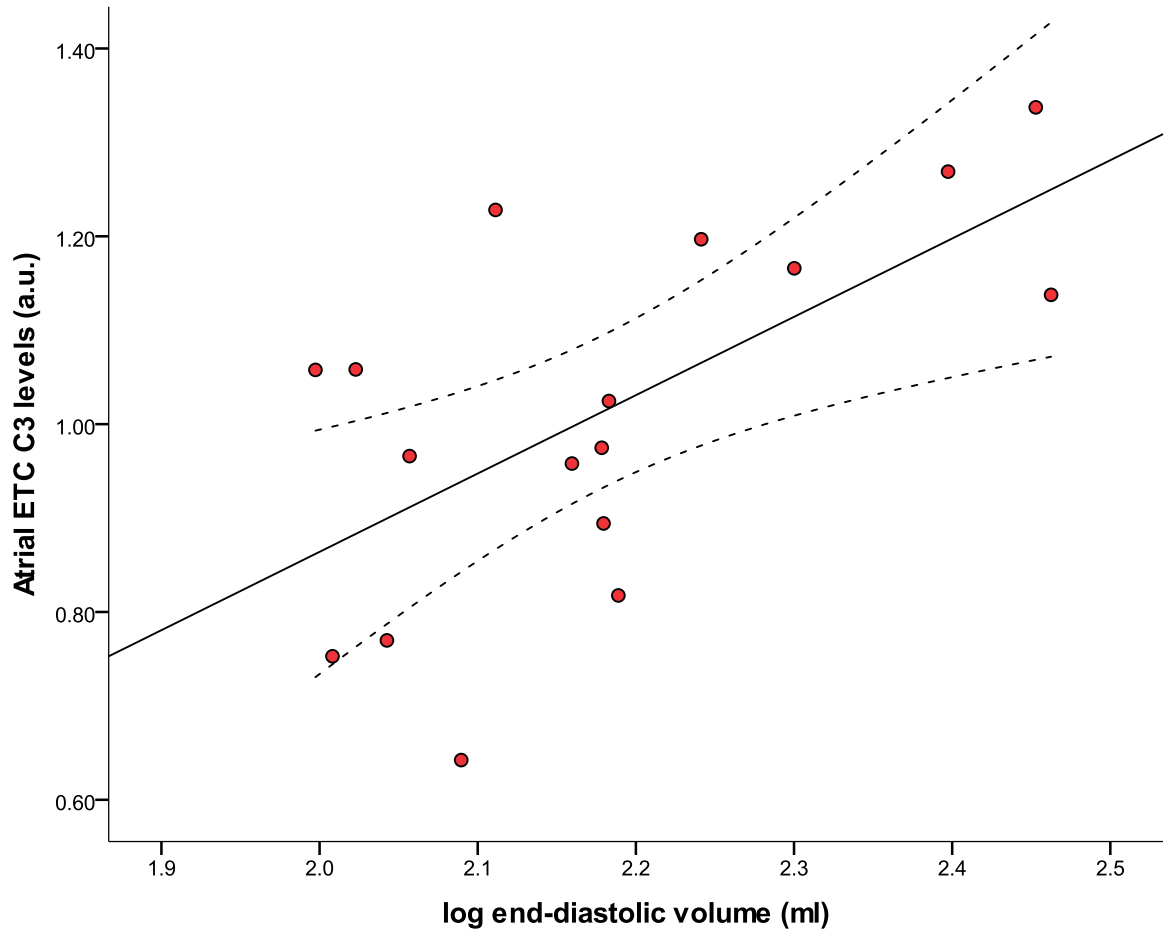

Figure 6.6. Scatter-plot showing atrial electron transport chain complex 3 level plotted against left ventricular end-diastolic volume.

The solid line is the regression line and the dashed lines are the 95% confidence intervals of the regression line. Values of left ventricular end-diastolic volume had a positively skewed distribution. These were successfully transformed to statistical normality by taking logarithms (base 10).

$\beta = 0.63$, $p < 0.01$

ETC C3 – electron transport chain complex-3

Table 6.7. Atrial mitochondrial proteins grouped according to NYHA class.

	NYHA 1 + 2 (n = 12) (a.u.)	NYHA 3 (n = 6) (a.u.)	p value (2 – tailed)
Citrate synthase	1.20 (0.68 - 1.49)	0.82 (0.73 - 1.17)	0.26
αKGD	1.05 (0.70 - 1.20)	1.13 (0.86 - 1.31)	0.51
ANT	1.00 (0.88 - 1.17)	1.16 (1.01 - 1.37)	0.19
GLUT4	1.00 (0.77 - 1.31)	0.93 (0.78 - 1.11)	0.84
MCAD	1.03 (0.88 - 1.21)	1.03 (0.82 - 1.34)	1.00
ETC C1	1.11 (0.85 - 1.24)	0.98 (0.75 - 1.20)	0.59
ETC C2	0.88 (0.83 - 1.21)	0.78 (0.63 - 1.34)	0.45
ETC C3	1.06 (0.82 - 1.23)	1.00 (0.86 - 1.14)	0.62
ETC C4	1.03 (0.93 - 1.25)	0.89 (0.73 - 1.05)	0.11
ETC C5	1.01 (0.68 - 1.27)	1.00 (0.89 - 1.31)	0.64

Data are presented as medians (IQR). Medians compared using Mann-Witney U test.

NYHA – New York Heart Association, αKGD – alpha-ketoglutarate dehydrogenase, ANT – adenine nucleotide translocase, GLUT4 – glucose transporter-4, MCAD – medium chain acyl-CoA dehydrogenase, ETC C – electron transport chain complex.

Table 6.8. Atrial mitochondrial proteins grouped according to the presence or absence of ventricular dysfunction.

	Normal ventricular function (n = 10) (a.u.)	Ventricular dysfunction (n = 8) (a.u.)	p value (2 – tailed)
Citrate synthase	0.89 (0.60 - 1.32)	1.15 (0.79 - 2.04)	0.29
αKGD	0.84 (0.53 - 1.26)	1.19 (1.04 - 1.25)	0.13
ANT	0.91 (0.77 - 1.18)	1.16 (1.05 - 1.24)	0.09
GLUT4	0.92 (0.61 - 1.15)	1.00 (0.83 - 1.31)	0.38
MCAD	1.07 (0.86 - 1.33)	1.00 (0.87 - 1.20)	0.72
ETC C1	0.98 (0.75 - 1.19)	1.16 (0.97 - 1.24)	0.25
ETC C2	0.85 (0.57 - 1.14)	0.99 (0.84 - 1.38)	0.29
ETC C3	0.97 (0.80 - 1.08)	1.17 (0.89 - 1.27)	0.17
ETC C4	0.97 (0.81 - 1.14)	1.03 (0.92 - 1.20)	0.59
ETC C5	1.00 (0.77 - 1.25)	1.06 (0.72 - 1.28)	0.99

Data are presented as medians (IQR). Medians compared using Mann-Witney U test.

αKGD – alpha-ketoglutarate dehydrogenase, ANT – adenine nucleotide translocase, GLUT4 – glucose transporter-4, MCAD – medium chain acyl-CoA dehydrogenase, ETC C – electron transport chain complex.

Table 6.9. Skeletal muscle mitochondrial proteins grouped according to the presence or absence of ventricular dysfunction.

	Normal ventricular function (n = 10) (a.u.)	Ventricular dysfunction (n = 8) (a.u.)	p value (2 – tailed)
Citrate synthase	1.16 (0.47 - 1.76)	0.72 (0.57 - 0.82)	0.12
αKGD	1.14 (0.93 - 1.87)	0.51 (0.39 - 1.00)	0.02*
ANT	1.13 (0.90 - 1.24)	0.62 (0.36 - 0.73)	0.02*
GLUT4	1.24 (0.82 - 1.59)	0.94 (0.55 - 1.19)	0.41
MCAD	0.82 (0.46 - 1.31)	0.35 (0.22 - 0.76)	0.03*
ETC C1	0.72 (0.51 - 1.03)	0.80 (0.31 - 1.22)	0.99
ETC C2	1.16 (0.76 - 1.59)	0.80 (0.60 - 0.91)	0.10
ETC C3	1.01 (0.65 - 1.43)	0.87 (0.42 - 1.20)	0.47
ETC C4	1.10 (0.76 - 1.51)	0.70 (0.29 - 0.99)	0.06
ETC C5	0.79 (0.55 - 1.18)	1.16 (0.93 - 1.31)	0.07

Data are presented as medians (IQR). Medians compared using Mann-Witney U test.

For GLUT4 analysis: normal ventricular function n = 8, ventricular dysfunction n = 7.

* $p < 0.05$.

αKGD – alpha-ketoglutarate dehydrogenase, ANT – adenine nucleotide translocase, GLUT4 – glucose transporter-4, MCAD – medium chain acyl-CoA dehydrogenase, ETC C – electron transport chain complex.

Table 6.10. Skeletal muscle mitochondrial proteins grouped according to NYHA class.

	NYHA 1 + 2 (n = 12) (a.u.)	NYHA 3 (n = 6) (a.u.)	p value (2 – tailed)
Citrate synthase	0.81 (0.63 - 1.24)	1.00 (0.38 - 1.50)	0.96
αKGD	0.92 (0.65 - 1.33)	1.27 (0.33 - 1.69)	0.95
ANT	0.87 (0.50 - 1.14)	0.87 (0.47 - 1.38)	0.80
GLUT4	1.05 (0.69 - 1.44)	0.90 (0.80 - 1.52)	0.95
MCAD	0.53 (0.29 - 0.82)	0.70 (0.35 - 1.54)	0.42
ETC C1	0.72 (0.55 - 0.95)	0.75 (0.28 - 1.46)	0.83
ETC C2	0.87 (0.60 - 1.10)	1.24 (0.78 - 1.48)	0.34
ETC C3	1.01 (0.74 - 1.09)	0.47 (0.37 - 0.47)	0.43
ETC C4	0.81 (0.46 - 1.21)	0.99 (0.72 - 1.92)	0.53
ETC C5	1.07 (0.55 - 1.21)	0.96 (0.77 - 1.52)	0.84

Data are presented as medians (IQR). Medians compared using Mann-Witney U test.

For GLUT4 analysis: NYHA 1+ 2 n = 9, NYHA 3 n = 6.

NYHA – New York Heart Association, αKGD – alpha-ketoglutarate dehydrogenase, ANT – adenine nucleotide translocase, GLUT4 – glucose transporter-4, MCAD – medium chain acyl-CoA dehydrogenase, ETC C – electron transport chain complex.

Mitochondrial proteins and energetics

Atrial mitochondrial CS, ANT, MCAD, GLUT4, αKGD and ETC complex protein levels were not predictive of cardiac PCr/ATP ratio (data not shown). Resting skeletal muscle high energy phosphorus metabolite concentrations were not predicted by skeletal muscle levels of CS, ANT, MCAD, GLUT4, αKGD and ETC complexes (data not shown). Maximum rate of gastrocnemius PCr consumption during exercise, mean PCr consumption during exercise and PCr recovery rate following exercise were not predicted by skeletal muscle levels of CS, ANT, MCAD, GLUT4, αKGD and ETC complexes (data not shown). Skeletal muscle GLUT4 levels predicted mean gastrocnemius oxygen consumption during exercise ($\beta = -0.58$, $p < 0.05$) (Figure 6.7).

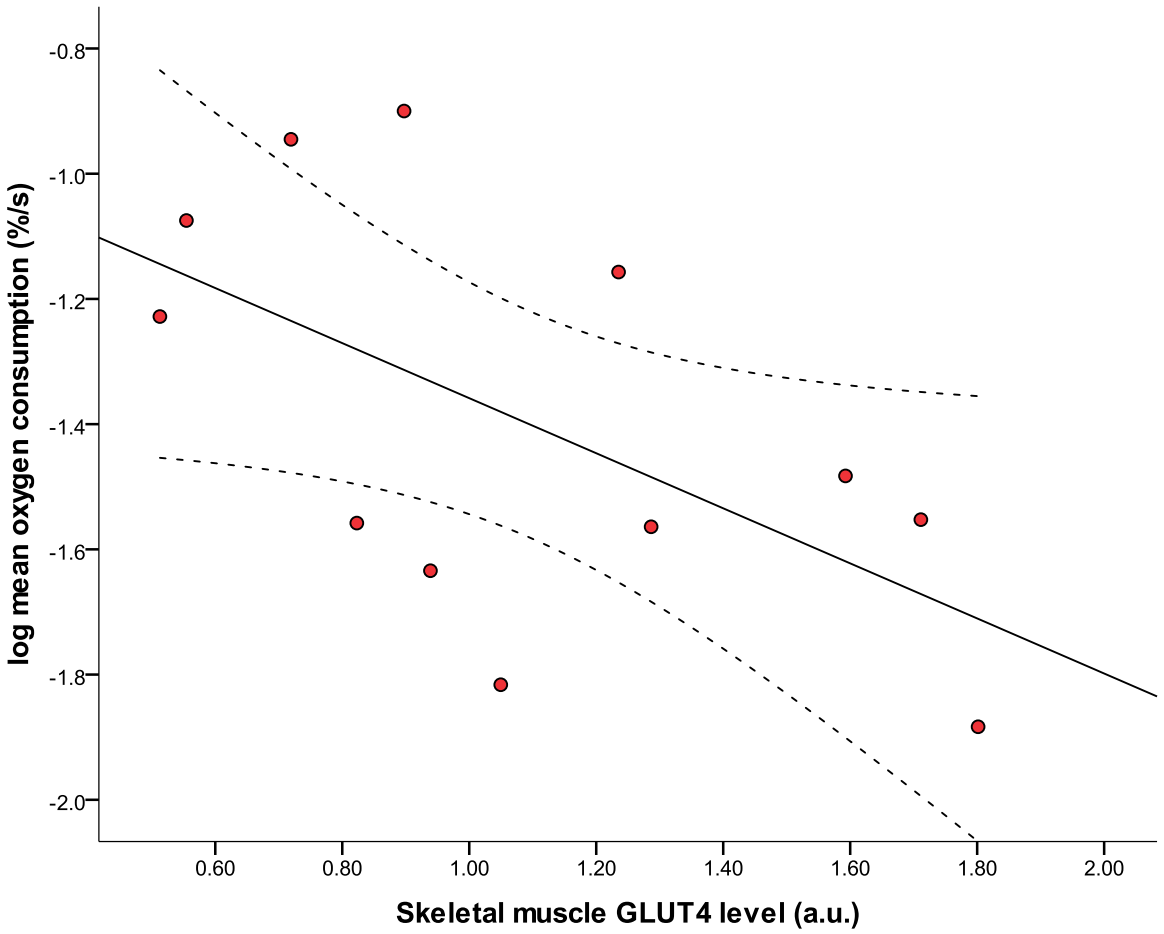

Figure 6.7. Scatter-plot showing mean gastrocnemius oxygen consumption during exercise plotted against skeletal muscle GLUT4 levels.

The solid line is the regression line and the dashed lines are the 95% confidence intervals of the regression line. Values of gastrocnemius mean oxygen consumption had a positively skewed distribution. These were successfully transformed to statistical normality by taking logarithms (base 10).

$\beta = -0.58$, $p < 0.05$

GLUT4 - glucose transporter-4

Mitochondrial proteins and tissue respiration rates

Atrial ANT levels were predictive of atrial tissue pyruvate respiration under conditions of: substrate alone ($\beta = 0.49$, $p < 0.05$) (data not shown), ADP-stimulation ($\beta = 0.53$, $p < 0.05$) (Figure 6.8) and oligomycin-inhibition ($\beta = 0.52$, $p < 0.05$) (data not shown). There was no relationship to uncoupled maximal respiration rates with the addition of the chemical uncoupler FCCP (data not shown). Atrial ANT levels were also predictive of atrial tissue palmitate oxidation rates under conditions of: substrate alone ($\beta = 0.41$, $p < 0.05$), ADP stimulation ($\beta = 0.47$, $p < 0.05$) (Figure 6.9), and oligomycin inhibition ($\beta = 0.47$, $p < 0.05$) (data not shown). There was no relationship to maximal FCCP-stimulated respiration rates (data not shown). Atrial ANT levels were not predictive of atrial glutamate respiration rates (data not shown). Skeletal muscle ANT levels did not predict skeletal muscle tissue respiration with any combination of substrates or inhibitors (data not shown).

Atrial ETC complexes did not predict atrial tissue respiration rates with any combination of substrate or inhibitor (data not shown). Skeletal muscle ETC complex levels were not predictive of skeletal muscle tissue pyruvate, glutamate or palmitate respiration rates (data not shown).

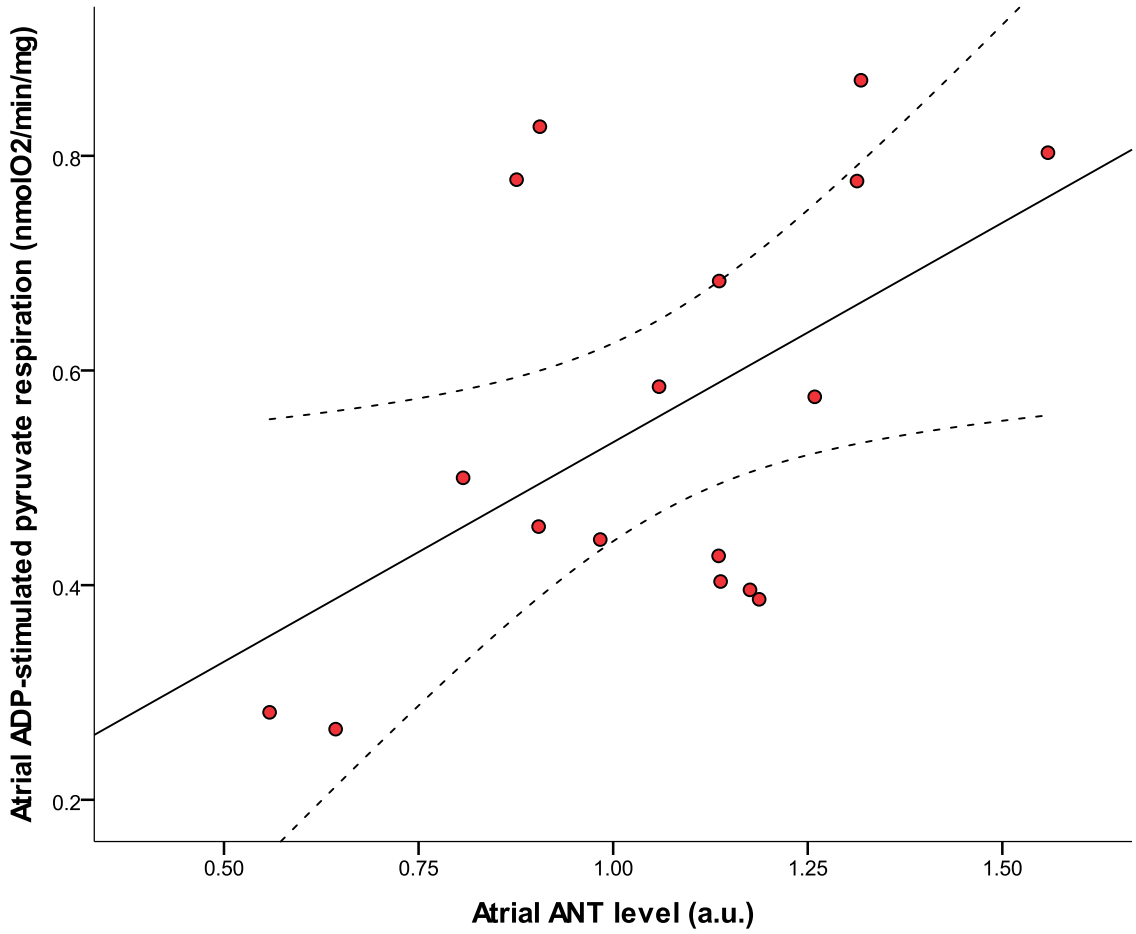

Figure 6.8. Scatter-plot showing atrial ADP-stimulated pyruvate respiration plotted against atrial ANT levels.

The solid line is the regression line and the dashed lines are the 95% confidence intervals of the regression line. Permeabilised tissue was incubated with pyruvate as substrate and respiration was stimulated by the addition of ADP. Respiration was measured as oxygen consumption and indexed to tissue wet weight.

$\beta = 0.53$, $p < 0.05$

ADP – adenosine diphosphate, ANT – adenine nucleotide transporter

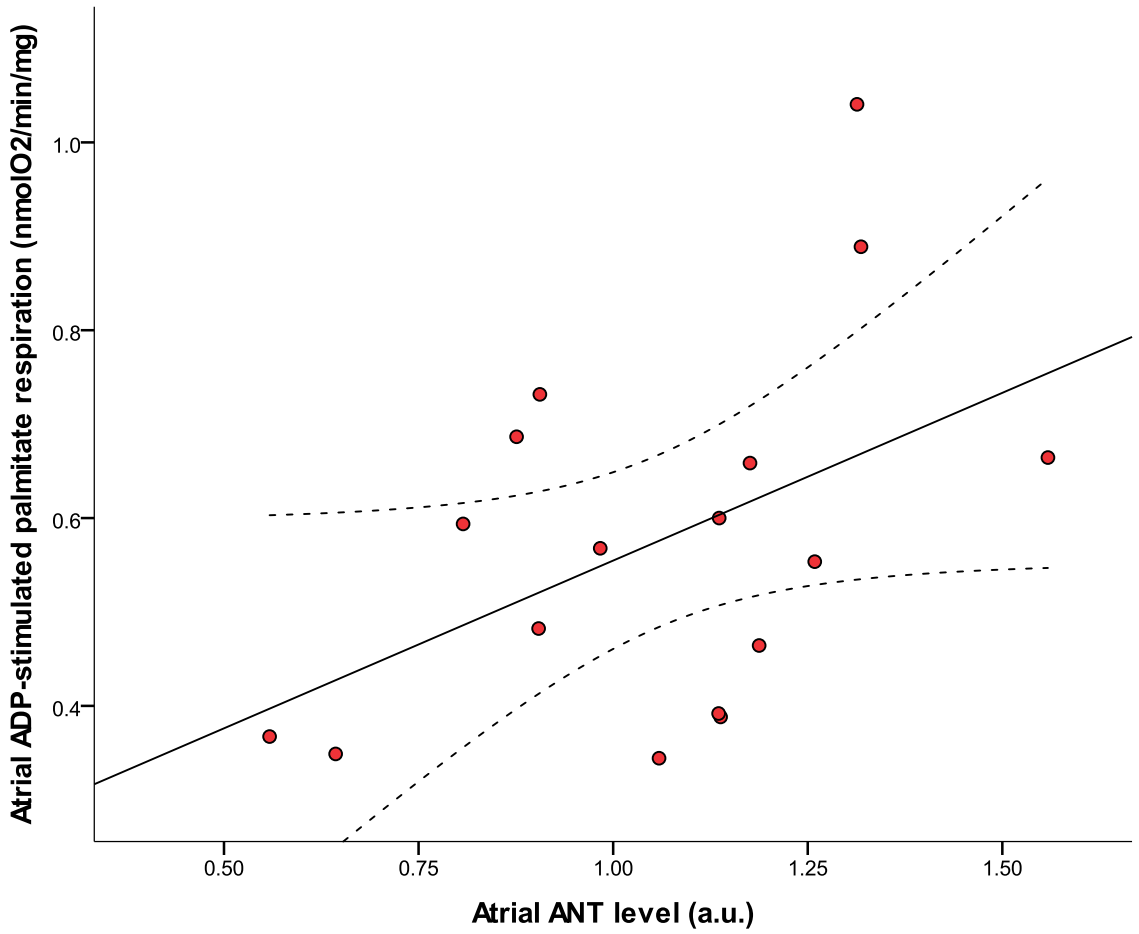

Figure 6.9. Scatter-plot showing atrial ADP-stimulated palmitate respiration plotted against atrial ANT levels.

The solid line is the regression line and the dashed lines are the 95% confidence intervals of the regression line. Permeabilised tissue was incubated with palmitate as substrate and respiration was stimulated by the addition of ADP. Respiration was measured as oxygen consumption and indexed to tissue wet weight.

$\beta = 0.47$, $p < 0.05$

ADP – adenosine diphosphate, ANT – adenine nucleotide transporter

Atrial citrate synthase levels were not predictive of atrial tissue pyruvate, palmitate or glutamate respiration rates (data not shown). Skeletal muscle citrate synthase levels were predictive of skeletal muscle tissue pyruvate respiration rates under conditions of substrate only ($\beta = 0.75$, $p < 0.001$) (data not shown), ADP stimulation ($\beta = 0.63$, $p < 0.01$) (Figure 6.10) and oligomycin inhibition ($\beta = 0.84$, $p = < 0.001$) (data not shown). Skeletal muscle citrate synthase levels did not predict FCCP-uncoupled pyruvate respiration rates (data not shown), nor palmitate or glutamate respiration rates with any combination of substrate or inhibitor (data not shown).

Atrial MCAD levels predicted the following atrial tissue palmitate respiration rates: substrate alone ($\beta = 0.63$, $p < 0.01$) (data not shown), ADP-stimulation ($\beta = 0.57$, $p < 0.05$) (Figure 6.11) and oligomycin-inhibition ($\beta = 0.55$, $p < 0.05$) (data not shown). Atrial MCAD levels were also predictive of the following atrial tissue pyruvate respiration rates: substrate alone ($\beta = 0.67$, $p < 0.01$), ADP-stimulation ($\beta = 0.66$, $p < 0.01$) (Figure 6.12) and oligomycin-inhibition ($\beta = 0.66$, $p < 0.01$) (data not shown), but were unrelated to glutamate respiration rates (data not shown).

Skeletal muscle MCAD levels negatively predicted skeletal muscle tissue palmitate oxidation rates: substrate alone ($\beta = -0.77$, $p = < 0.01$) (data not shown), ADP-stimulation ($\beta = -0.73$, $p < 0.01$) (Figure 6.13) and oligomycin-inhibition ($\beta = -0.68$, $p < 0.01$) (data not shown), but were not related to FCCP-uncoupled rates (data not shown). Skeletal muscle MCAD levels were unrelated to skeletal muscle tissue pyruvate or glutatmate respiration rates (data not shown).

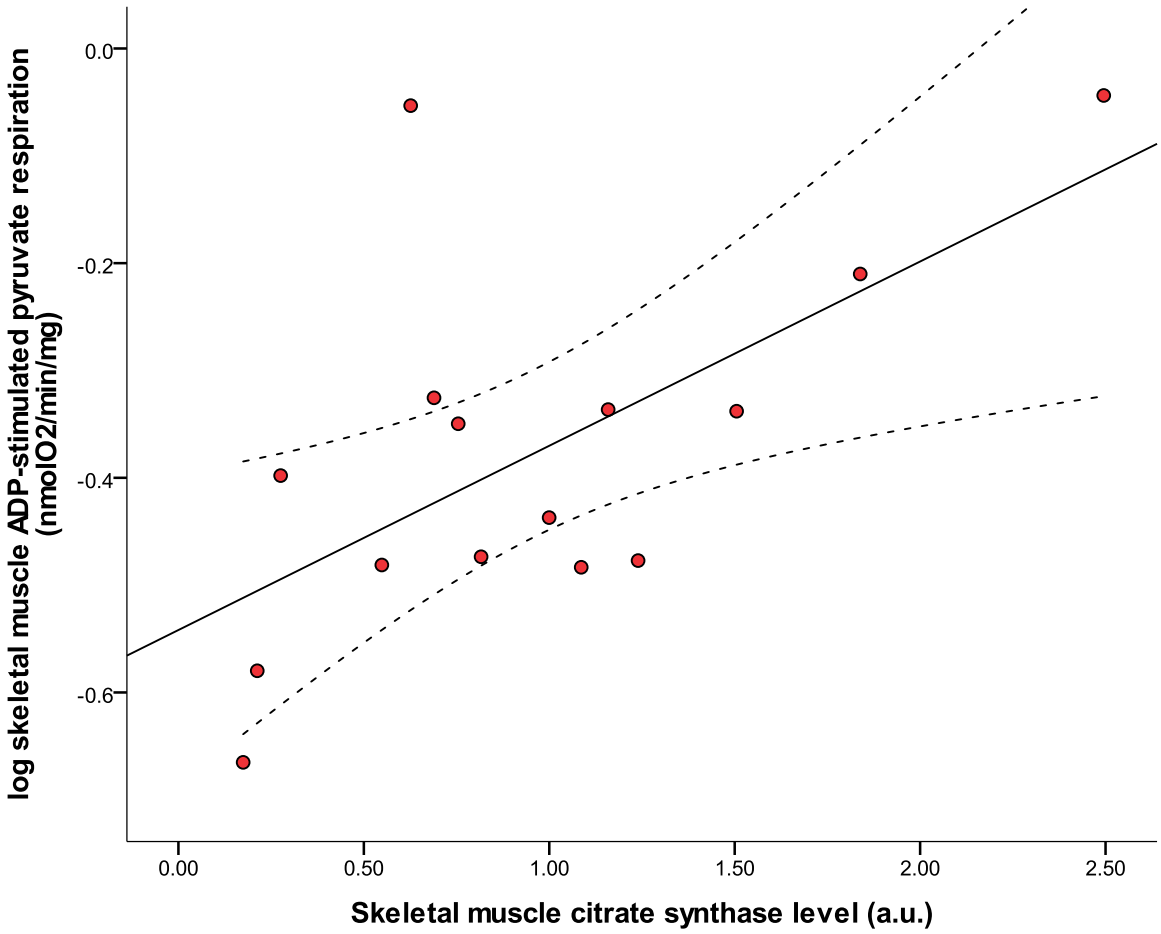

Figure 6.10. Scatter-plot showing skeletal muscle ADP-stimulated pyruvate respiration plotted against skeletal muscle citrate synthase levels.

The solid line is the regression line and the dashed lines are the 95% confidence intervals of the regression line. Values of skeletal muscle ADP-stimulated pyruvate respiration had a positively skewed distribution. These were successfully transformed to statistical normality by taking logarithms (base 10). Permeabilised tissue was incubated with pyruvate as substrate and respiration was stimulated by the addition of ADP. Respiration was measured as oxygen consumption and indexed to tissue wet weight.

$\beta = 0.63$, $p < 0.01$

ADP – adenosine diphosphate

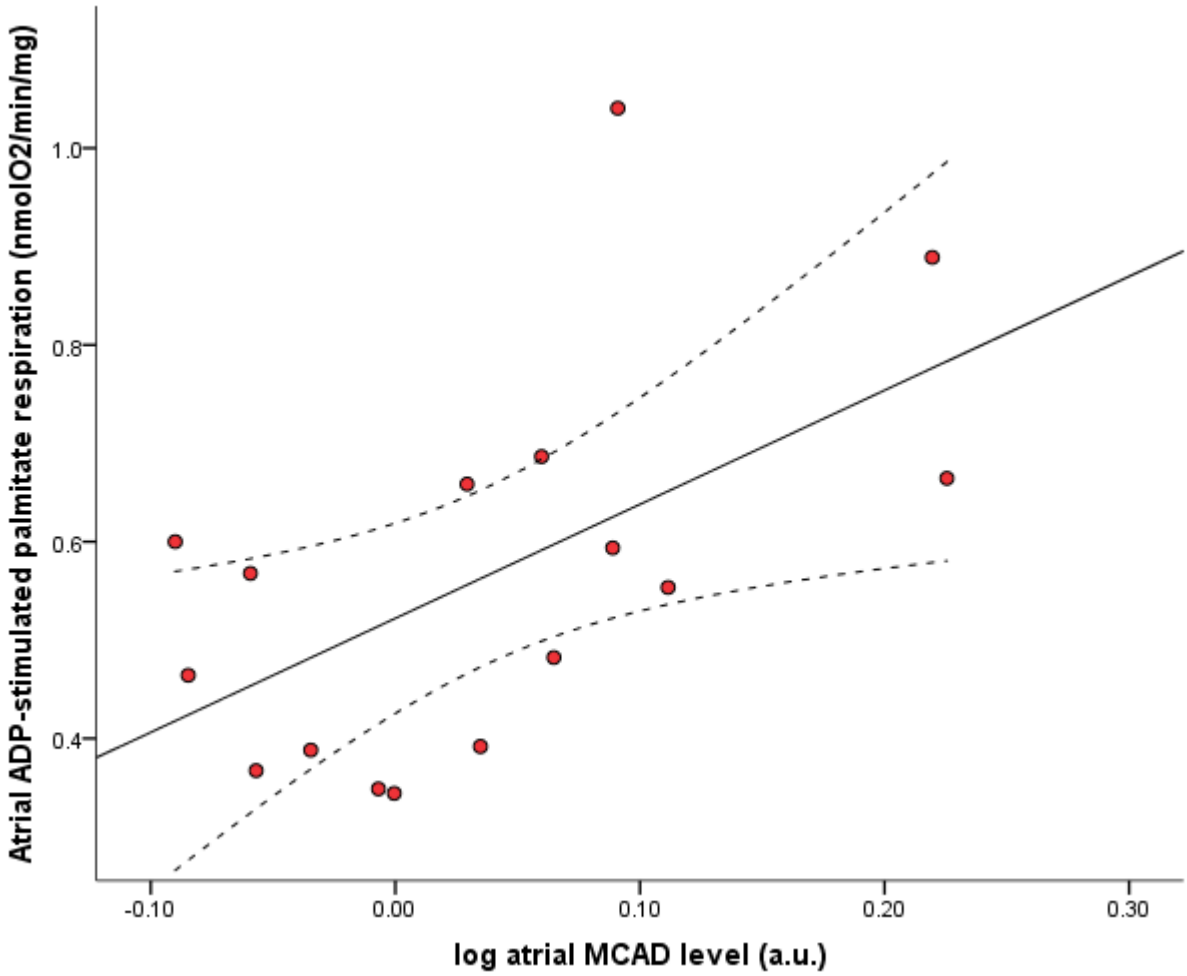

Figure 6.11. Scatter-plot showing atrial ADP-stimulated palmitate respiration plotted against atrial MCAD levels.

The solid line is the regression line and the dashed lines are the 95% confidence intervals of the regression line. Values of atrial MCAD level had a positively skewed distribution. These were successfully transformed to statistical normality by taking logarithms (base 10). Permeabilised tissue was incubated with palmitate as substrate and respiration was stimulated by the addition of ADP. Respiration was measured as oxygen consumption and indexed to tissue wet weight.

$\beta = 0.57$, $p < 0.01$

ADP – adenosine diphosphate, MCAD – medium chain acyl-CoA dehydrogenase

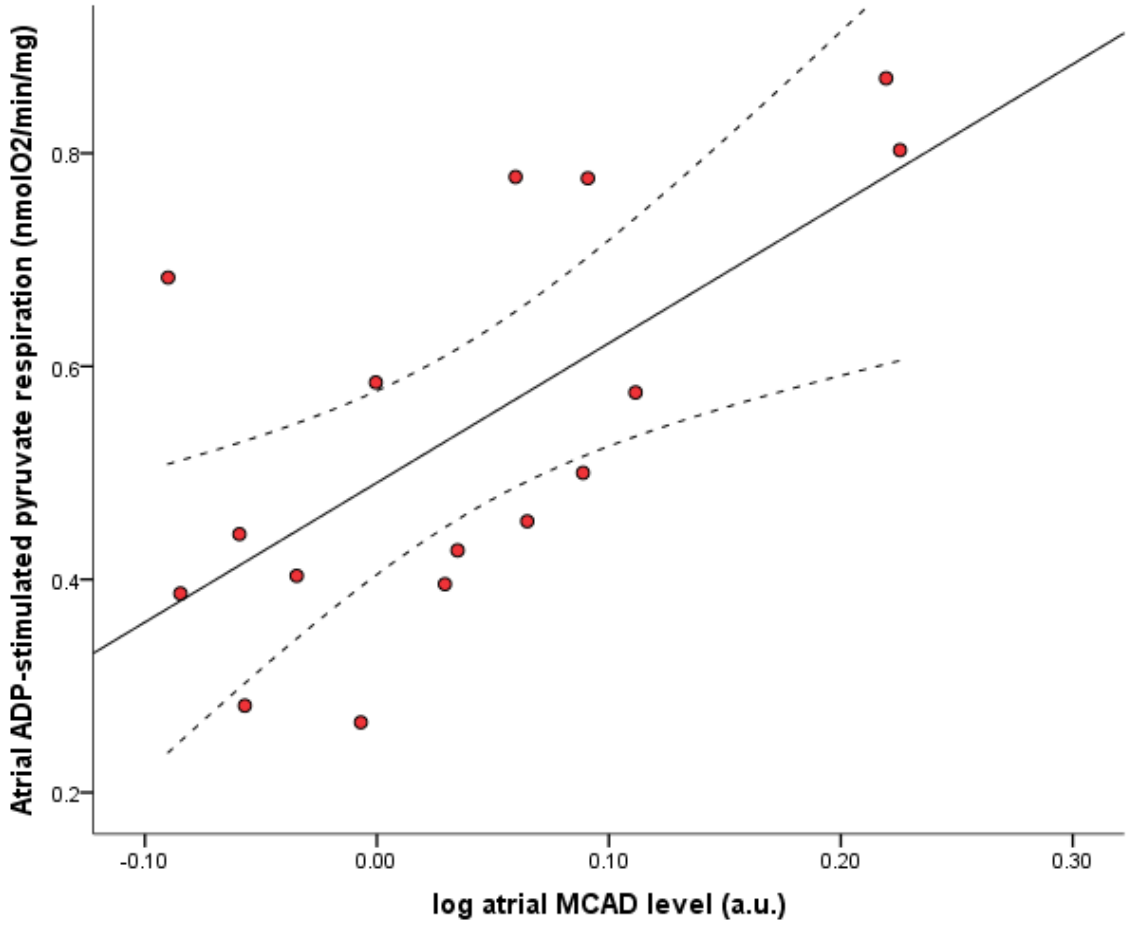

Figure 6.12. Scatter-plot showing atrial ADP-stimulated pyruvate respiration plotted against atrial MCAD levels.

The solid line is the regression line and the dashed lines are the 95% confidence intervals of the regression line. Values of atrial MCAD level had a positively skewed distribution. These were successfully transformed to statistical normality by taking logarithms (base 10). Permeabilised tissue was incubated with pyruvate as substrate and respiration was stimulated by the addition of ADP. Respiration was measured as oxygen consumption and indexed to tissue wet weight.

$\beta = 0.66$, $p < 0.01$

ADP – adenosine diphosphate, MCAD – medium chain acyl-CoA dehydrogenase

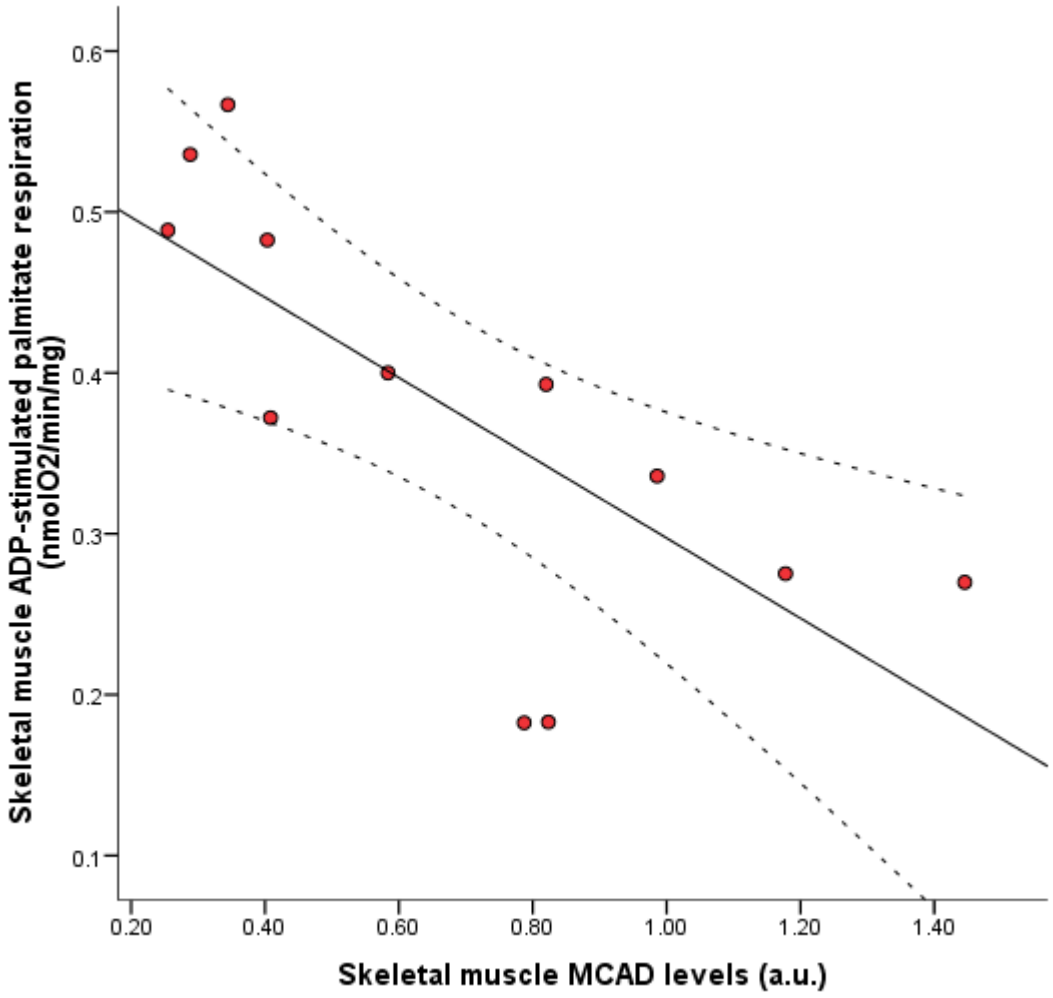

Figure 6.13. Scatter-plot showing skeletal muscle ADP-stimulated palmitate oxygen consumption plotted against skeletal muscle MCAD levels.

The solid line is the regression line and the dashed lines are the 95% confidence intervals of the regression line. Permeabilised tissue was incubated with palmitate as substrate and respiration was stimulated by the addition of ADP. Respiration was measured as oxygen consumption and indexed to tissue wet weight.

$\beta = -0.73$, $p < 0.01$

ADP – adenosine diphosphate, MCAD – medium chain acyl-CoA dehydrogenase

Atrial and skeletal muscle levels of UCP3 were not predictive of pyruvate, glutamate or palmitate (Figures 6.14 and 6.15) respiration rates from respective tissues, or oligomycin-inhibition. UCP3 levels did not negatively predict respiratory control ratios (an index of mitochondrial coupling, calculated as state 3 respiration/state 4 respiration - or in these experiments taken as ADP-stimulated respiration/substrate only respiration) (Table 6.11).

Table 6.11 Table showing correlations between atrial and skeletal muscle UCP3 levels and mitochondrial respiration rates and respiratory control ratios

	Atrial UCP3 level			**Skeletal muscle UCP3 level**		
	Standardised β	p	n	Standardised β	p	n
Glu	-0.25	0.19	17	-0.02	0.48	12
Pyr	-0.02	0.48	17	-0.32	0.13	15
Palm	0.07	0.47	17	-0.48	0.08	12
Glu + Oligo	0.22	0.23	17	-0.04	0.46	12
Pyr + Oligo	-0.14	0.31	17	-0.44	0.06	15
Palm + Oligo	0.14	0.29	17	-0.55	0.05	12
Glu RCR	0.73	0.002	17	0.09	0.41	12
Pyr RCR	0.03	0.47	17	-0.11	0.35	15
Palm RCR	-0.13	0.32	17	0.35	0.16	12

Glu – glutamate, Pyr – pyruvate, Palm – palmitate, Oligo – oligomycin, RCR – respiratory control ratio (state 3 respiration/state 4 respiration – in these experiments taken as (ADP stimulated respiration/substrate only respiration), UCP3 – uncoupling protein-3.

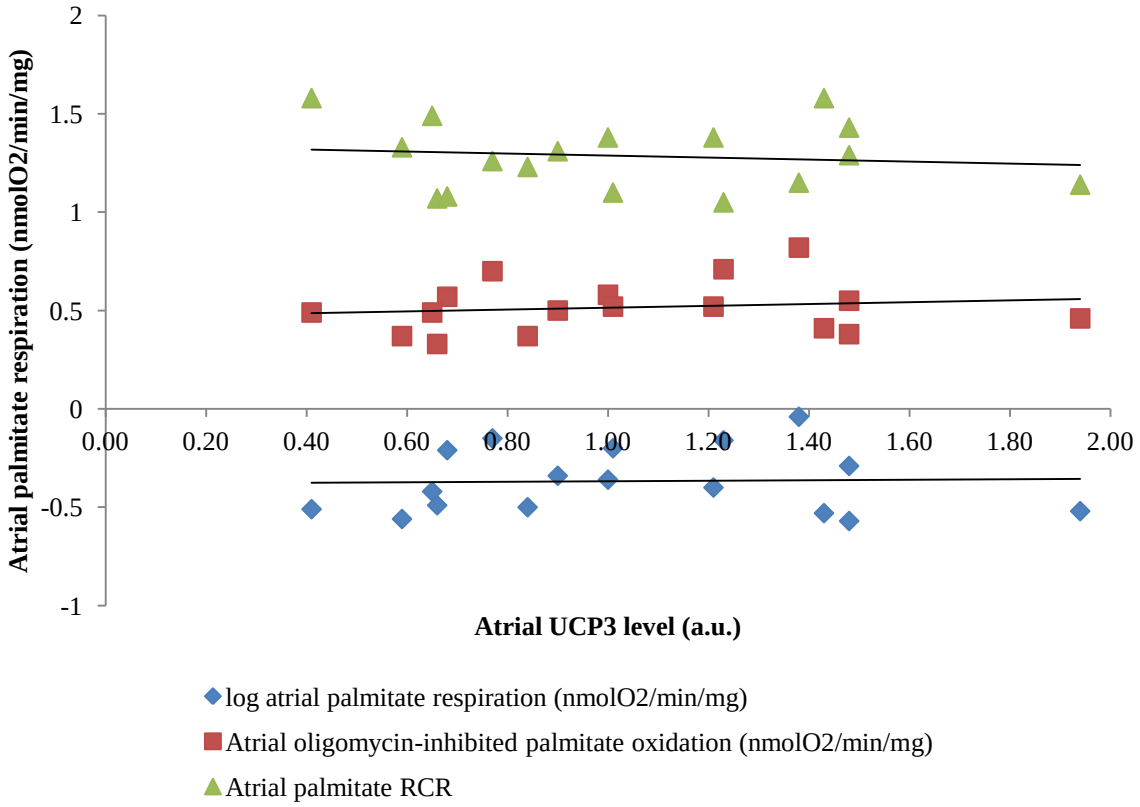

Figure 6.14. Scatter plots showing atrial palmitate, oligomycin-inhibited palmitate and palmitate RCR respiration plotted against atrial UCP3 levels.

The lines are the regression lines for each variable. Values of atrial palmitate respiration had a positively skewed distribution. These were successfully transformed to statistical normality by taking logarithms (base 10). Permeabilised tissue was incubated with palmitate as substrate. Respiration was measured as oxygen consumption and indexed to tissue wet weight.

Atrial palmitate $\beta = 0.07$, $p = 0.47$

Atrial oligomycin-inhibited palmitate $\beta = 0.14$, $p = 0.29$

Atrial palmitate RCR $\beta = -0.13$, $p = 0.32$

RCR - respiratory control ratio, UCP3 - mitochondrial uncoupling protein-3

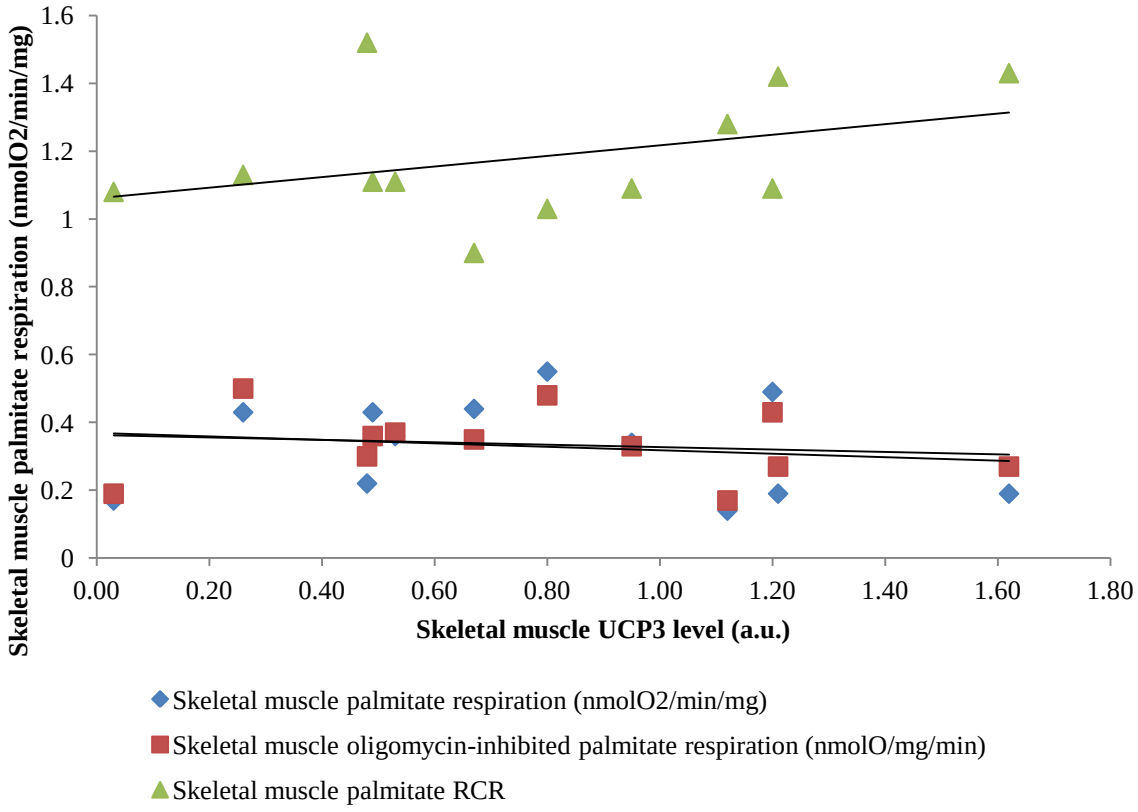

Figure 6.15. Scatter plots showing skeletal muscle palmitate, oligomycin-inhibited palmitate and palmitate RCR respiration plotted against skeletal muscle UCP3 levels.

The lines are the regression lines for each variable. Permeabilised tissue was incubated with palmitate as substrate. Respiration was measured as oxygen consumption and indexed to tissue wet weight.

Skeletal muscle palmitate $\beta = -0.48$, $p = 0.08$

Skeletal muscle oligomycin-inhibited palmitate $\beta = -0.55$, $p = 0.05$

Skeletal muscle palmitate RCR $\beta = 0.35$, $p = 0.16$

RCR - respiratory control ratio, UCP3 - mitochondrial uncoupling protein-3

6.5. Discussion

This study did not show a relationship between heart failure severity and mitochondrial respiration or indices of mitochondrial coupling; furthermore, tissue levels of UCP3 were not related to the indices of mitochondrial coupling measured here. The atrial expression of a number of mitochondrial proteins (ANT, α-KGD, CS and ETC complexes-1, -2 and -3) increased with increasing LV-EDV, perhaps a response to increased atrial work in the face of elevated ventricular end-diastolic pressure.

The increased expression of ANT in the atrium was associated with an increase in mitochondrial oxygen consumption using pyruvate (Figure 6.8) and palmitate (Figure 6.9) as substrates but not with glutamate. Increased respiration is an expected finding with increased ANT levels (Kholodenko, Zilinskiee *et al* 1987). As ADP import and ATP export from the mitochondrial matrix is facilitated, ADP concentration is maintained at the ATP synthase (ETC complex-5), driving respiration. The controlling influence of ANT is lost when the membrane potential is dissipated by FCCP which explains the absence of an association between ANT levels and FCCP-stimulated respiration. It is not clear why atrial glutamate respiration rates were not related to atrial ANT levels but this may be secondary to an unmeasured variable, for example changes in glutamate dehydrogenase levels or activity. Skeletal muscle ANT levels, however, were unrelated to mitochondrial respiration rates, perhaps suggesting that changes in ANT expression in skeletal muscle *in vivo* have little overall influence on oxidative capacity.

The subjects defined as having ventricular dysfunction, whilst not having decreased skeletal muscle mitochondrial respiration rates overall, demonstrated a decrease in the skeletal muscle levels of αKGD, MCAD and ANT compared to subjects with normal ventricular

function. There were no differences, however, if subjects were divided into NYHA classes 1 + 2 and class 3, and none of the skeletal muscle mitochondrial proteins were predicted by 6MWT distance, left ventricular end-diastolic volume, ejection fraction or E/E' ratio, suggesting no clear relationship between skeletal muscle mitochondrial proteins and heart failure of the severity studied here.

Work performed previously has not demonstrated gross changes in mitochondrial protein levels occurring in early heart failure. In pigs, ANT levels are normal in the compensated remodelled ventricle following left anterior descending coronary artery ligation, but decrease in decompensated cardiac failure (Ning, Zhang *et al* 2000). A recent proteomic study of rats that underwent aortic constriction showed no change in myocardial citrate synthase levels compared with controls (Bugger, Schwarzer *et al* 2009). Atrial and skeletal muscle MCAD levels were found to be unrelated to heart failure severity in infarcted rat hearts (Morgan, Chandler *et al* 2006), indicating that gross changes in the fatty acid oxidation enzymes occur relatively late in heart failure.

In this study, atrial ETC complexes-1, -2 and -3 were increased as LV-EDV increased, perhaps secondary to an increase in atrial work, as mentioned previously, although this interpretation is forwarded cautiously, as the the atrial proteins were measured in right atrial appendage tissue and end-diastolic volume was measured in the left ventricle. Otherwise no associations were found between heart failure severity and ETC complex levels in atria or skeletal muscle. Studies have previously shown no changes in ETC complex activity in heart failure induced by coronary artery microembolisation, but with an apparent defect in the electron transport chain found in isolated mitochondrial respiration experiments (Rosca, Vazquez *et al* 2008). The suggestion has therefore been advanced that there may be an

abnormality in the supra-molecular architecture of the inner mitochondrial membrane, which would not be detected by experiments examining the level or activity of individual ETC complex proteins (Rosca, Vazquez *et al* 2008).

Together with ANT, discussed earlier, MCAD levels appeared to relate to mitochondrial respiration rate. Atrial MCAD levels were predictive of palmitate respiration rate. In skeletal muscle, however, MCAD levels were negatively predictive of palmitate respiration, which was not expected, and implies the presence of a greater and unmeasured controlling influence on skeletal muscle palmitate oxidation rate in these patients.

Citrate synthase levels were found to be related to pyruvate oxidation rates in skeletal muscle. However, palmitate and glutamate respiration rates were unrelated to citrate synthase levels, perhaps implying greater defects upstream in the palmitate and glutamate metabolic pathways, rendering the influence of citrate synthase levels redundant.

Limitations

There are a number of limitations to the work described in this chapter. Firstly, the respiration rates were measured on different tissue to that measured by the MRS studies: for example atrial respiration was compared to ventricular PCr/ATP ratio, and pectoralis major respiration was compared to gastrocnemius high energy phosphous metabolite concentrations and kinetics. Ventricular biopsies were too small in this study to measure mitochondrial respiration and also perform Western blot analysis, so consequently the atrial biopsies alone were used to measure respiration rates from the heart. The different tissues used may explain the lack of relationship between atrial mitochondrial respiration rates and cardiac PCr/ATP ratios, and between skeletal muscle respiration and PCr recovery rate or Q_{max}. It may be, however, that the relationship between mitochondrial respiration and

cardiac PCr/ATP ratio is more complicated than a simple linear function, moreover, the cardiac PCr/ATP ratio is a global average of all sub-cellular compartments, and is perhaps not reflective of the ATP/ADP ratio in the mitochondrial matrix where oxidative phosphorylation takes place. It would have been preferable to have acquired gastrocnemius biopsies with which to compare the MRS data. This would have been possible from the patients having saphenous vein harvested as a coronary artery bypass graft, but more problematic from those not having coronary artery bypass grafting.

The number of skeletal muscle respiration measurements was lower than for the atrium, which was a more consistent surgical biopsy. It is possible that numbers were too low, resulting in type 2 statistical errors, however visual inspection of the scatter-plots showed no apparent linear relationship where none was reported. Further work will be necessary to examine these relationships in greater detail.

It would be useful to compare mitochondrial respiration and protein expression from patients with overt heart failure with normal control tissue to look for differences between the two, or as an adjunct to using regression with measurements of cardiac function as was performed here. Due to the invasive nature of biopsies for skeletal muscle and heart in particular, it was not feasible to collect control tissue; and the numbers of patients undergoing heart surgery with overt heart failure is not substantial, even in centres offering cardiac transplantation. For these reasons it was decided to perform an observational-type study aiming to include a full range of cardiac function, and to look for relationships between variables. Data were also analysed in this way to avoid having to use arbitrary points to delineate between normal/abnormal cardiac function, although for completeness of analysis, patients were divided into groups according to the presence/absence of objective evidence of cardiac

dysfunction. However, the degree of heart failure in the cohort studied was mild-moderate and well compensated, and therefore perhaps not severe enough for overt changes in mitochondrial respiration or protein levels to be apparent.

It was decided to define systolic dysfunction as a left ventricular ejection fraction of less than 55%, and this is somewhat arbitrary. This value was chosen because the normal range for ejection fraction, measured by MRI, used locally (OCMR, John Radcliffe Hospital, Oxford), is 57-81%. It could be argued that ejection fraction is not a completely representative measure of systolic function, and is not reflective of subtle systolic dysfunction which might involve changes in torsion, longitudinal shortening and strain rates, for example, but it is widely clinically used and has been shown to be prognostically important (Dickstein, Cohen-Solal *et al* 2008).

This study also used the NYHA classification of functional capacity as one way of classifying the severity of heart failure. This is a subjective method of classifying the degree of functional capacity and severity of heart failure, relying on patients' reporting of symptoms. The use of the NYHA classification, however, is also a widely clinically accepted means to classify heart failure severity (Dickstein, Cohen-Solal *et al* 2008), and is consistent with previous work examining the relationship between heart failure severity and cardiac PCr/ATP ratio (Neubauer, Krahe *et al* 1992; Neubauer, Horn *et al* 1997). The 6MWT was used as a more objective method to assess functional capacity, albeit in the context of subjects with angina, but the most objective method of assessing heart failure, cardiopulmonary exercise testing, was not performed for reasons previously discussed in Chapters 4 and 5.

Lastly, no evidence for mitochondrial uncoupling was observed, but the *in-situ* tissue permeabilisation technique does not allow for the measurement of ADP/O ratios because of the presence of functioning ATPases within the tissue. This would have been the preferred method of quantifying mitochondrial coupling. Instead, uncoupling was inferred by either increased oxygen consumption in the presence of oligomycin (an ATP synthase inhibitor), substrate alone, or by a decrease in respiratory control ratio. The respiratory control ratios were all quite low in these experiments and this may have been because of the use of a submaximal ADP stimulus. In the present experiments 0.1 mM ADP was used, whereas Kuznetsov and colleagues suggest 1 mM (Kuznetsov, Veksler *et al* 2008). This may result in low apparent "state 3" respiration and low RCR, however RCR should still be proportional to the degree of coupling. Tissue levels of UCP3 were not predictive of any of these measures of mitochondrial coupling which is an interesting finding. This could be because the presence/absence of activators of UCP3 are more important than the quantity of protein itself, although in the presence of fatty acid, a known activator of UCP3 (Echtay, Winkler *et al* 2001), as was the case in the palmitate respiration experiments, there were still no relationships between UCP3 levels and mitochondrial coupling. The possibility cannot be excluded that, despite every effort to keep the tissue samples on ice and to carry out the experiments as quickly as possible following biopsy collection, either the mitochondria became partly disrupted, resulting in uncoupling to an extent rendering an effect through UCP3 insignificant, or that the UCP3 protein itself was damaged/denatured in some way during the experimental protocol.

Further research

It would be interesting to investigate the relationship between ventricular function, ANT levels and myocardial PCr/ATP ratio, as ANT levels appear to predict mitochondrial respiration rate (at least for pyruvate and palmitate in atrial tissue). There is evidence in animal studies for improvements in cardiac energetics with increased ANT levels: ANT overexpressing mice showed improved cardiac function six weeks following the induction of type 1 diabetes mellitus by streptozotocin compared with controls (Wang, Ebermann *et al* 2009).

To further investigate the role that UCP3 might play in altering mitochondrial function, further experiments could use a wider range of the known activators and inhibitors of UCP3 to delineate the precise effect of UCP3 on mitochondrial respiration rate. The results could be related to measurements of the membrane potential ($\Delta\Psi$) itself.

6.6. Conclusions

In heart failure of mild-moderate severity there were no significant changes in atrial or skeletal muscle mitochondrial respiration rates, and no associations were found between atrial and skeletal muscle UCP3 levels and indices of mitochondrial coupling; however, given the low numbers studied, this will require confirmation. These findings suggest that mitochondrial uncoupling is not a major influence on mitochondrial function in heart failure of the severity studied presently; and moreover, that UCP3 levels are not related to the degree of mitochondrial uncoupling.

CHAPTER 7

GENERAL SUMMARY AND CONCLUSIONS

7.1. Summary of findings

The aim of the work in this thesis was to investigate the hypothesis that heart failure is accompanied by increased plasma non-esterified fatty acid (NEFA) concentration, which in turn increases mitochondrial uncoupling protein-3 (UCP3) expression via peroxisome proliferator-activated receptor α (PPARα) activation in the heart and skeletal muscle. The increased UCP3 impairs the ability of mitochondria to synthesise adenosine triphosphate (ATP) by oxidative phosphorylation, and perhaps underlies the decreased cardiac phosphocreatine (PCr)/ATP ratio previously demonstrated in heart failure patients. In skeletal muscle, the increased expression of UCP3 provides a possible explanation for the decreased exercise capacity in heart failure patients and the apparent mitochondrial dysfunction observed.

The main findings of this work were that fasting plasma NEFA concentrations increased with increasing heart failure severity (Chapter 4), showing a negative relationship with left ventricular ejection fraction (LVEF), a positive relationship to New York Heart Association (NYHA) class, and were increased in patients with objective ventricular dysfunction (defined as LVEF <55% and/or diastolic dysfunction). Cardiac PCr/ATP ratio was also related to NYHA class and the presence of objective ventricular dysfunction, but not six-minute walk test distance (6MWT) (Chapter 4). Skeletal muscle energetic abnormalities were related to the severity of heart failure, with initial skeletal muscle PCr consumption at exercise onset and PCr consumption during exercise relating negatively to LVEF, and PCr consumption was increased in patients with ventricular dysfunction compared to those with normal ventricular function (Chapter 5). The maximal rate of skeletal muscle ATP synthesis (Q_{max}) was found to be related to NYHA functional class and 6MWT test distance, as was

the dissociation between PCr recovery and muscle reoxygenation following exercise, but was unrelated to objective measures of ventricular dysfunction, suggesting a peripheral cause for exercise limitation in heart failure (Chapter 5).

Fasting plasma NEFA concentrations were also found to relate to resting skeletal muscle PCr/ATP ratio, ADP concentration and skeletal muscle Q_{max} (Chapter 5), but were unrelated to the cardiac PCr/ATP ratio (Chapter 4). Fasting plasma NEFA concentrations did not predict ventricular (Chapter 4) or skeletal muscle (Chapter 5) UCP3 levels, but were moderately predictive of atrial UCP3 levels (Chapter 4). No associations were found between ventricular UCP3 levels and cardiac PCr/ATP ratio (Chapter 4), or with skeletal muscle UCP3 levels and skeletal muscle high energy phosphate concentrations or PCr kinetics during exercise (Chapter 5). Moreover, no associations were found between atrial and skeletal muscle UCP3 levels and indices of mitochondrial coupling measured directly in mitochondrial respiration experiments (Chapter 6).

Ventricular UCP3 levels were related to NYHA class (Chapter 4), as were skeletal muscle UCP3 levels (Chapter 5), but only skeletal muscle UCP3 levels were related to objective measurements of ventricular dysfunction, being weakly predicted by LVEF (Chapter 5).

Notwithstanding the small sample size, no relationship was found between heart failure severity and mitochondrial respiration rates (Chapter 6). The skeletal muscle expression of adenine nucleotide transporter, α-ketoglutarate dehydrogenase and medium chain acyl-CoA dehydrogenase was decreased in patients with objective ventricular dysfunction, but this did not result in apparent mitochondrial dysfunction (Chapter 6).

7.2. Limitations

There are a number of limitations to the work presented in this thesis. Firstly, the study was designed as an observational study and had no control group. This was because it was considered impractical to obtain reliable myocardial control tissue. The only option for obtaining normal control myocardial biopsies comes from unused normal donor hearts. These are kept on ice for a number of hours whilst delivered to the transplant centre before the decision not to transplant is made. The effect of this cold ischaemic time on UCP3 protein levels is unknown, but the half life of UCP3 is known to be relatively short for a mitochondrial protein (Azzu, Jastroch *et al* 2010). The control hearts are also very unlikely to be age matched – the majority coming from young trauma victims as opposed to the older patients presenting for cardiac surgery. However, within the cohort studied it was possible to divide patients into those with ventricular dysfunction and those without ventricular dysfunction, based upon LVEF and E/E'.

Systolic dysfunction was defined as a left ventricular ejection fraction of less than 55%, and this was somewhat arbitrary. This value was chosen because the normal range for ejection fraction, measured by MRI, used locally (OCMR, John Radcliffe Hospital, Oxford), is 57-81%. It could be argued that ejection fraction is not a completely representative measure of systolic function, and is not reflective of subtle systolic dysfunction, but it is widely clinically used and has been shown to be of prognostic importance in heart failure (Dickstein, Cohen-Solal *et al* 2008).

One of the ways in which this study classified heart failure severity was using the NYHA classification of functional capacity. This is a subjective method of classifying the severity of heart failure, relying on patients' reporting of symptoms. The use of the NYHA

classification, however, is also a widely clinically accepted means to classify the severity of heart failure (Dickstein, Cohen-Solal *et al* 2008), and is consistent with previous work examining the relationship between heart failure severity and cardiac PCr/ATP ratio (Neubauer, Krahe *et al* 1992; Neubauer, Horn *et al* 1997). The 6MWT was used in the studies presented here, as a more objective method to assess functional capacity, albeit in the context of subjects with angina, but the most objective method of assessing heart failure, cardiopulmonary exercise testing, was not performed, partly because of concerns over exercising patients with left main coronary artery disease or critical aortic stenosis, and also because of the lack of local expertise in performing this test. There was also concern over recruiting sufficient numbers to adequately power the principle findings, so the protocol was prevented from becoming too arduous for patients.

Furthermore, in order to obtain myocardial tissue biopsies, the cohort studied comprised patients undergoing cardiac surgery. Particularly in the case of valvular pathology, one of the aims of surgery is to prevent heart failure from occurring, so there were few patients with severely impaired ventricular function, as could have been the case if patients with dilated cardiomyopathy, for example, were studied. This is perhaps why no associations were found between ventricular function and mitochondrial respiration rates. On the other hand, the advantage of not only selecting patients with impaired ventricular function, was that there was a wide range of ventricular function in the cohort, making regression analyses more likely to be successful.

The ventricular biopsies were taken from the epicardial layer which may have a different metabolic profile to the endocardium. It would have been preferable for full thickness biopsies to be taken from the ventricle, but the provision of ventricular biopsies was left to

the judgement of the operating surgeon and the techniques with which they were familiar, in order to avoid exposing patients to undue risk. The skeletal muscle biopsies were also taken from a different muscle than the muscle on which NIRS and ^{31}P MRS were performed. It would have been preferable to have acquired gastrocnemius biopsies with which to compare with MRS/NIRS data. This may have been possible from those patients having saphenous vein harvested as a coronary artery bypass graft, but more difficult from those not having coronary artery bypass grafting. It was felt that, as the proposed mechanism was not specific to a particular muscle group, and as a general mechanism would be expected to occur throughout all skeletal muscle, it was preferable to avoid the inclusion of a separate invasive muscle biopsy, and instead use the readily accessible pectoralis major muscle as a metabolic surrogate for gastrocnemius.

The skeletal muscle expression of UCP3, however, is fibre-type dependant (Hesselink, Keizer *et al* 2001), and the fibre-type composition of the two muscles could have been different. The patient population is that of relatively elderly, sedentary people with cardiac disease, who are not athletically trained. It was therefore felt unlikely that the fibre-type expression between gastrocnemius/soleus (NIRS/MRS) and pectoralis major (UCP3 levels) would be dissimilar, secondary to a specific training effect on one or other muscle group. The human skeletal muscle fibre-type composition of gastrocnemius and parasternal intercostal muscle has been shown to be similar (Gollnick, Sjödin *et al* 1974; Mizuno and Secher 1989).

The patients studied in the cohort had differing pathology. The cardiac energetic abnormalities in heart failure, measured using ^{31}P MRS, appear to be similar regardless of the aetiology of the failure (Shivu, Abozguia *et al* 2010; Conway, Allis *et al* 1991; de Roos,

Doornbos *et al* 1992; Neubauer, Krahe *et al* 1992; Conway, Bottomley *et al* 1998; Beyerbacht, Lamb *et al* 2001), therefore a study such as this, testing a unifying hypothesis, would need to include different aetiologies. It is not as clear whether the skeletal muscle energetic abnormalities in heart failure are independant of the aetiology, so it may have been preferable to enrol equal numbers of patients into different groups: comprising aortic stenosis, coronary artery disease and mitral regurgitation, each with sufficient numbers to be powered to detect effect sizes of a moderate magnitude. The paucity of local patients undergoing valve surgery meant that this approach was not feasible, and it was decided that, in order to enrol sufficient numbers within a reasonable time frame, all surgical pathology would be recruited and treated as a single group.

It was only possible to measure relative concentrations of high energy phosphorus metabolites using ^{31}P MRS. A "normal" ratio of PCr/ATP therefore may be misleading if ATP concentration is decreased as well as PCr. This does occur in heart failure, but is thought to be a relatively late phenomenon (Shen, Asai *et al* 1999; Beer, Seyfarth *et al* 2002), and therefore the patients in this cohort were assumed to have normal ATP concentrations.

The hypothesised sequence of events, following ventricular dysfunction, begins with an increase in sympathetic tone, but this was not directly measured in this study. There is an established relationship between ventricular function and plasma noradrenaline concentration, so it was felt unnecessary to repeat this (Thomas and Marks 1978; Francis, Goldsmith *et al* 1982; Levine, Francis *et al* 1983).

The measurement of plasma NEFA concentration is known to vary considerably, depending on the dietary state and prevailing sympathetic tone (Frayn 1998). In the present studies,

plasma NEFA concentrations were always measured in the fasting state, and at the same point within the protocol, therefore trying to minimise diurnal or contextual variation. Plasma NEFA concentrations measured on the day of surgery were again taken in the fasting state, although from arterial blood on this occasion. These measurements were only related to Western blot results from the biopsies taken on the same day, and not to the pre-operative investigations carried out previously, which were compared with the venous NEFA concentration taken contemporaneously.

The pre-operative investigations were necessarily carried out on a separate day to the biopsy collection. This resulted in cardiac PCr/ATP being related to ventricular UCP3 levels, for example, measured on a different occasion. This was unavoidable due to protocol length and the consequent time required for collection of all the necessary pre-operative data. It was felt that disease progression would be minimal in the interval between the pre-operative tests and the biopsies being taken. It is possible however, that patients' anxiety levels concerning impending major surgery were different on the day of surgery, resulting in differing degrees of sympathetic stimulation and hence UCP3 expression. All patients received sedative premedication in order to limit pre-operative anxiety; however, as demonstrated in Chapter 4, plasma NEFA concentrations were higher in those samples taken immediately pre-anaesthetic induction, compared with those samples taken at the pre-operative tests. This finding does suggest increased sympathetic tone was present immediately pre-operatively, as the samples were again taken in the fasting state. Any effect this may have had on changes in cardiac UCP3 levels is not known.

The studies presented in this thesis measured only absolute protein levels and not activity. Particularly in the case of UCP3 this could be of relevance, as UCP3 has been shown to

modulate an inducible proton leak rather than a basal leak (Brand, Pakay *et al* 2005), and its magnitude is related to the presence/absence of specific activators (Boudina, Sena *et al* 2007). Known activators of UCP3 (superoxide, hydroxynonenol and fatty acids) were not measured in this study. The plasma concentration of non-esterified fatty acids was measured, but it is the concentration of fatty acids within the mitochondria which would be relevant in this context. There may also be other activators of UCP3, of importance in heart failure, yet to be discovered.

The number of subjects in Chapter 6, particularly for skeletal muscle respiration experiments, was relatively low, and consequently may have resulted in type 2 statistical errors i.e. falsely accepting the null hypothesis. All scatterplots were inspected visually for emerging linear relationships, and none were present in these data, suggesting that the inclusion of greater numbers would probably have made no difference to the interpretation.

7.3. Clinical relevance

The results of this thesis have suggested abnormalities in cardiac and skeletal muscle high energy phosphate metabolism associated with ventricular dysfunction and heart failure. Therapeutic attempts to support mitochondrial function and enhance ATP synthesis may, particularly in the case of skeletal muscle, be beneficial in terms of symptoms, and may even improve cardiac function. Carnitine palmitoyl transferase-1 inhibitors such as etomoxir and perhexiline have been studied in humans with heart failure (Lee, Campbell *et al* 2005; Holubarsch, Rohrbach *et al* 2007), with the aim of preventing fatty acid entry into the mitochondrion, thereby increasing glucose oxidation and consequently optimising the oxygen efficiency of ATP synthesis. Results have demonstrated improvements in left

ventricular systolic function, symptoms, maximal oxygen uptake and gastrocnemius PCr recovery times following exercise (Lee, Campbell *et al* 2005), but safety concerns remain over the potential side-effects of CPT1 inhibition (Holubarsch, Rohrbach *et al* 2007). Similarly, trimetazidine, purported to be a ketoacyl-CoA thiolase antagonist (and hence a partial inhibitor of β-oxidation), has been studied in heart failure patients, where it increased left ventricular ejection fraction (LVEF) and cardiac PCr/ATP ratio (Fragasso, Perseghin *et al* 2006).

Exercise training has been found to improve functional capacity in heart failure patients (Belardinelli, Georgiou *et al* 1999). Whilst a complete understanding of the mechanisms underlying this result is not known, exercise improves skeletal muscle oxidative capacity (Forbes, Slade *et al* 2008), which may well account for some of the functional improvements seen in heart failure patients.

7.5. Future directions

The cohort studied in this thesis comprised of patients with only mild-to-moderate ventricular dysfunction and consequently may be one reason why no associations were found between UCP3 levels and cardiac and skeletal muscle energetics. At the level of dysfunction studied, mild mitochondrial uncoupling may make mitochondria less efficient, but perhaps not to the extent where ATP synthesis is grossly impaired. Provided substrate (including oxygen) supply is not limited, then inefficient mitochondria will use more substrate, but still be able to maintain stable ATP supply. It would be of interest to perform similar experiments on patients with end-stage or severe heart failure, when mitochondrial substrate supply is perhaps limited. It may be possible to obtain myocardial biopsies of

sufficient size from patients undergoing cardiac catheterisation. If no asssociation between ventricular UCP3 levels and cardiac PCr/ATP ratio and skeletal muscle UCP3 levels and PCr recovery rates following exercise were found with the inclusion of patients with severe heart failure, then it could be concluded that UCP3 is not adversely affecting mitochondrial function in heart failure. Indeed, recent studies suggest that despite increased mitochondrial uncoupling, UCP3 may preserve mitochondrial function, through protection against free-radical induced mitochondrial damage (Bugger, Guzman *et al* 2011).

It is starting to become clear that metabolic interventions may be beneficial in a multitude of clinical settings, from acute myocardial infarction to the peri-operative cardiac surgical setting, and also perhaps in chronic cardiac failure. Further studies will be required to ascertain optimal dosing, timing of intervention, and side-effect profiles of these emerging therapeutic strategies.

7.4. Conclusions

This work has shown that in patients presenting for cardiac surgery, fasting plasma non-esterified fatty acids are increased in those with poorer ventricular function, and are associated with impaired skeletal muscle high energy phosphate metabolism, but not to cardiac PCr/ATP ratios. The cardiac PCr/ATP ratio was decreased in patients reporting worse heart failure symtoms, but was unrelated to objective measurements of ventricular function. Skeletal muscle PCr kinetics were impaired in those with ventricular dysfunction and related to functional capacity. No evidence was found to support mitochondrial uncoupling, mediated through UCP3, as a cause of the abnormalities in cardiac and skeletal muscle high energy phosphate metabolism.

REFERENCES

Aguirre E, Cadenas S. GDP and carboxyatractylate inhibit 4-hydroxynonenal-activated proton conductance to differing degrees in mitochondria from skeletal muscle and heart. *Biochimica et Biophysica Acta.* 2010;1797(10):1716-1726.

Almsherqi ZA, McLachlan CS, Slocinska MB, Sluse FE, Navet R, Kocherginsky N, Kostetski I, Shi DY, Liu SL, Mossop P, Deng Y. Reduced cardiac output is associated with decreased mitochondrial efficiency in the non-ischemic ventricular wall of the acute myocardial-infarcted dog. *Cell Research.* 2006;16(3):297-305.

Ashrafian H, Frenneaux MP, Opie LH. Metabolic mechanisms in heart failure. *Circulation.* 2007;116(4):434-448.

Azzu V, Jastroch M, Divakaruni AS, Brand MD. The regulation and turnover of mitochondrial uncoupling proteins. *Biochimica et Biophysica Acta - Bioenergetics.* 2010;1797(6-7):785-791.

Balady GJ, Arena R, Sietsema K, Myers J, Coke L, Fletcher GF, Forman D, Franklin B,Guazzi M, Gulati M, Keteyian SJ, Lavie S, Macko R, Mancini D, Milani RV. Clinician's guide to cardiopulmonary exercise testing in adults: A scientific statement from the American heart association. *Circulation.* 2010;122(2):191-225.

Beer M. Cardiac spectroscopy: techniques, indications and clinical results. *European Radiology.* 2004;14(6):1034-1047.

Beer M, Machann W, Sandstede J, Buchner S, Lipke C, Kostler H, Lorenz R, Harre K, Spindler M, Hahn D. Energetic differences between viable and non-viable myocardium in patients with recent myocardial infarction are not an effect of differences in wall thinning- a multivoxel (31)P-MR-spectroscopy and MRI study. *European Radiology.* 2007;17(5):1275-1283.

Beer M, Sandstede J, Landschutz W, Viehrig M, Harre K, Horn M, Meininger M, Pabst T, Kenn W, Haase A, von Kienlin M, Neubauer S, Hahn D. Altered energy metabolism after myocardial infarction assessed by 31P-MR-spectroscopy in humans. *European Radiology.* 2000;10(8):1323-1328.

Beer M, Seyfarth T, Sandstede J, Landschutz W, Lipke C, Kostler H, von Kienlin M, Harre K, Hahn D, Neubauer S. Absolute concentrations of high-energy phosphate metabolites in normal, hypertrophied, and failing human myocardium measured noninvasively with (31)P-SLOOP magnetic resonance spectroscopy. *Journal of the American College of Cardiology.* 2002;40(7):1267-1274.

Belardinelli R, Capestro F, Misiani A, Scipione P, Georgiou D. Randomized, controlled trial of long-term moderate exercise training in chronic heart failure: effects on functional capacity, quality of life, and clinical outcome. *Circulation.* 99(9):1173-1182.

Beyerbacht HP, Lamb HJ, Van Der Laarse A, Vliegen HW, Leujes F, Hazekamp MC, De Roos A, Van Der Wall EE. Aortic valve replacement in patients with aortic valve stenosis improves myocardial metabolism and diastolic function. *Radiology.* 2001;219(3):637-643.

Bezaire V, Seifert EL, Harper ME. Uncoupling protein-3: clues in an ongoing mitochondrial mystery. *FASEB.* 2007;21(2):312-324.

Bezaire V, Spriet LL, Campbell S, Sabet N, Gerrits M, Bonen A, Harper ME. Constitutive UCP3 overexpression at physiological levels increases mouse skeletal muscle capacity for fatty acid transport and oxidation. *FASEB.* 2005;19(8):977-979.

Boehm EA, Jones BE, Radda GK, Veech RL, Clarke K. Increased uncoupling proteins and decreased efficiency in palmitate-perfused hyperthyroid rat heart. *American Journal of Physiology.*2001;280(3):H977-983.

Bottomley PA. "NMR Spectroscopy of the Human Heart" in Encyclopedia of Magnetic Resonance, Eds R. K. Harris and R. E. Wasylishen, John Wiley: Chichester. 2009.

Boudina S, Sena S, Theobald H, Sheng X, Wright JJ, Hu XX, Aziz S, Johnson JI, Bugger H, Zaha VG, Abel ED. Mitochondrial energetics in the heart in obesity-related diabetes: direct evidence for increased uncoupled respiration and activation of uncoupling proteins. *Diabetes.* 2007;56(10):2457-2466.

Brand MD. The sites and topology of mitochondrial superoxide production. *Experimental Gerontology.* 2010;45(7-8):466-472.

Brand MD, Pakay JL, Ocloo A, Kokoszka J, Wallace DC, Brookes PS, Cornwall EJ. The basal proton conductance of mitochondria depends on adenine nucleotide translocase content. *Biochemical Journal.* 2005;392(2):353-362.

Brand MD, Pamplona R, Portero-Otin M, Requena JR, Roebuck SJ, Buckingham JA, Clapham JC, Cadenas S. Oxidative damage and phospholipid fatty acyl composition in skeletal muscle mitochondria from mice underexpressing or overexpressing uncoupling protein 3. *Biochemical Journal.* 2002;368(2):597-603.

British Heart Foundation. Economic costs of heart failure. 2010. Available at: www.heartstats.org

Brown GC. Control of respiration and ATP synthesis in mammalian mitochondria and cells. *Biochemical Journal.* 1992;284(1):1-13.

Buchwald A, Till H, Unterberg C, Oberschmidt R, Figulla HR, Wiegand V. Alterations of the mitochondrial respiratory chain in human dilated cardiomyopathy. *European Heart Journal.* 1990;11(6):509-516.

Bugger H, Guzman C, Zechner C, Palmeri M, Russell KS, Russell III, RR. Uncoupling protein downregulation in doxorubicin-induced heart failure improves mitochondrial coupling but increases reactive oxygen species generation. *Cancer Chemotherapy and Pharmacology.* 2011;67(6):1381-1388.

Bugger H, Schwarzer M, Chen D, Schrepper A, Amorim PA, Schoepe M, Nguyen TD, Mohr FW, Khalimonchuk O, Weimer BC, Doenst T. Proteomic remodelling of mitochondrial oxidative pathways in pressure overload-induced heart failure. *Cardiovascular Research.* 2009;85(2):376-384.

Cadenas S, Buckingham JA, Samec S, Seydoux J, Din N, Dulloo AG, Brand MD. UCP2 and UCP3 rise in starved rat skeletal muscle but mitochondrial proton conductance is unchanged. *FEBS Letters.* 1999;462(3):257-260.

Chandler MP, Kerner J, Huang H, Vazquez E, Reszko A, Martini WZ, Hoppel CL, Imai M, Rastogi S, Sabbah HN, Stanley WC. Moderate severity heart failure does not involve a downregulation of myocardial fatty acid oxidation. *American Journal of Physiology - Heart and Circulatory Physiology.* 2004;287(4 56-4): H1538-H1543.

Clapham JC, Arch JRS, Chapman H, Haynes A, Lister C, Moore GBT, Piercy V, Carter SA, Lehner I, Smith SA, Beeley LJ, Godden RJ, Henity N, Skehel M, Changani KK, Hockings PD, Reid DG, Squires SM, Hatcher J, Trall B, Latcham J, Rastan S, Harper AJ, Cadenas S, Buckingham JA, Brand MD, Abuin A. Mice overexpressing human uncoupling protein-3 in skeletal muscle are hyperphagic and lean. *Nature.* 2000;406(6794):415-418.

Cohen J. A power primer. *Psychological Bulletin* 1992;112(1):155-159.

Cohn JN, Johnson GR, Shabatei R, Loeb H, Tristani F, Rector T, Smith R, Fletcher R. Ejection fraction, peak exercise oxygen consumption, cardiothoracic ratio, ventricular arrhythmias, and plasma norepinephrine as determinants of prognosis in heart failure. The V-HeFT VA Cooperative Studies Group. *Circulation.* 1993;87(6 Suppl):VI5-16.

Conway MA, Allis J, Ouwerkerk R, Niioka T, Rajagopalan B, Radda GK. Detection of low phosphocreatine to ATP ratio in failing hypertrophied human myocardium by ^{31}P magnetic resonance spectroscopy. *Lancet.* 1991;338(8773):973-976.

Conway MA, Bottomley PA, Ouwerkerk R, Radda GK, Rajagopalan B. Mitral regurgitation: impaired systolic function, eccentric hypertrophy, and increased severity are linked to lower phosphocreatine/ATP ratios in humans. *Circulation.* 1998;97(17):1716-1723.

Cowie MR, Wood DA, Coats AJS, Thompson SG, Suresh V, Poole-Wilson PA, Sutton GC. Survival of patients with a new diagnosis of heart failure: A population based study. *Heart.* 2000;83(5):505-510.

Crapo RO, Casaburi R, Coates AL, Enright PL, MacIntyre NR, McKay RT, Johnson D, Wanger JS, Zeballos RJ, Bittner V, Mottram C. ATS statement: Guidelines for the six-minute walk test. *American Journal of Respiratory and Critical Care Medicine*. 2002;166(1):111-117.

Crow MT, Kushmerick MJ. Chemical energetics of slow- and fast-twitch muscles of the mouse. *Journal of General Physiology.* 1982;79(1):147-166.

Davila-Roman VG, Vedala G, Herrero P, De Las Fuentes L, Rogers JG, Kelly DP, Gropler RJ. Altered myocardial fatty acid and glucose metabolism in idiopathic dilated cardiomyopathy. *Journal of the American College of Cardiology.* 2002;40(2):271-277.

de Roos A, Doornbos J, Luyten PR, Oosterwaal LJ, van der Wall EE, den Hollander JA. Cardiac metabolism in patients with dilated and hypertrophic cardiomyopathy: assessment with proton-decoupled P-31 MR spectroscopy. *Journal of Magnetic Resonance Imaging.* 1992;2(6):711-719.

Desvergne B, Wahli W. Peroxisome proliferator-activated receptors: nuclear control of metabolism. *Endocrine Reviews.* 1999;20(5):649-688.

Dickstein K, Cohen-Solal A, Filippatos G, McMurray JJV, Ponikowski P, Poole-Wilson PA, Stromberg A, van Veldhuisen DJ, Atar D, Hoes AW, Keren A, Mebazaa A, Nieminen M, Priori SG, Swedberg K. ESC guidelines for the diagnosis and treatment of acute and chronic heart failure. *European Heart Journal.* 2008;29(19):2388-2442.

Echtay KS, Roussel D, St-Plerre J, Jekabsons MB, Cadenas S, Stuart JA, Harper JA, Roebuck SJ, Morrison A, Pickering S, Clapham JC, Brand MD. Superoxide activates mitochondrial uncoupling proteins. *Nature.* 2002;415(6867):96-99.

Echtay KS, Winkler E, Frischmuth K, Klingenberg M. Uncoupling proteins 2 and 3 are highly active H+ transporters and highly nucleotide sensitive when activated by coenzyme Q (ubiquinone). *Proceedings of the National Academy of Sciences of the United States of America.* 2001;98(4):1416-1421.

Field A. Discovering Statistics Using SPSS. 3rd Edition. SAGE Publications Inc. London. 2009.

Forbes SC, Slade JM, Meyer RA. Short-term high-intensity interval training improves phosphocreatine recovery kinetics following moderate-intensity exercise in humans. *Applied Physiology, Nutrition and Metabolism*. 2008;33(6): 1124-1131.

Fragasso G, Perseghin G, De Cobelli F, Esposito A, Palloshi A, Lattuada G, Scifo P, Calori G, Del Maschio A, Margonato A. Effects of metabolic modulation by trimetazidine on left ventricular function and phosphocreatine/adenosine triphosphate ratio in patients with heart failure. *European Heart Journal.* 2006;27(8):942-948.

Franciosa JA, Park M, Levine TB. Lack of correlation between exercise capacity and indexes of resting left ventricular performance in heart failure. *American Journal of Cardiology.* 1981;47(1):33-39.

Francis GS, Goldsmith SR, Ziesche SM, Cohn JN. Response of plasma norepinephrine and epinephrine to dynamic exercise in patients with congestive heart failure. *American Journal of Cardiology.* 1982;49(5):1152-1156.

Frayn KN. Regulation of fatty acid delivery in vivo. *Advances in Experimental Medicine and Biology.* 1998;441:171-179.

Gajarsa JJ, Kloner RA. Left ventricular remodeling in the post-infarction heart: a review of cellular, molecular mechanisms, and therapeutic modalities. *Heart Failure Reviews.* 2011;16(1):13-21.

Gollnick PD, Sjödin B, Karlsson J, Jansson E, Saltin B. Human soleus muscle: A comparison of fiber composition and enzyme activities with other leg muscles. *Pflügers Archiv European Journal of Physiology.* 1974;348(3):247-255.

Hamaoka T, McCully KK, Quaresima V, Yamamoto K, Chance B. Near-infrared spectroscopy/imaging for monitoring muscle oxygenation and oxidative metabolism in healthy and diseased humans. *Journal of Biomedical Optics.* 2007;12(6):062105.

Hanada A, Okita K, Yonezawa K, Ohtsubo M, Kohya T, Murakami T, Nishijima H, Tamura M, Kitabatake A. Dissociation between muscle metabolism and oxygen kinetics during recovery from exercise in patients with chronic heart failure. *Heart.* 2000;83(2):161-166.

Hardy CJ, Weiss RG, Bottomley PA, Gerstenblith G. Altered myocardial high-energy phosphate metabolites in patients with dilated cardiomyopathy. *American Heart Journal.* 1991;122(3, Part 1):795-801.

Hesselink MKC, Greenhaff PL, Constantin-Teodosiu D, Hultman E, Saris WHM, Nieuwlaat R, Schaart G, Kornips E, Schrauwen P. Increased uncoupling protein 3 content does not affect mitochondrial function in human skeletal muscle in vivo. *Journal of Clinical Investigation.* 2003;111(4):479-486.

Holubarsch CJF, Rohrbach M, Karrasch M, Boehm E, Polonski L, Ponikowski P, Rhein S. A double-blind randomized multicentre clinical trial to evaluate the efficacy and safety of two doses of etomoxir in comparison with placebo in patients with moderate congestive heart failure: The ERGO (etomoxir for the recovery of glucose oxidation) study. *Clinical Science.* 2007;113(3-4):205-212.

Hoppel CL, Tandler B, Parland W. Hamster cardiomyopathy. A defect in oxidative phosphorylation in the cardiac interfibrillar mitochondria. *Journal of Biological Chemistry.* 1982;257(3):1540-1548.

Hudsmith LE, Neubauer S. Detection of myocardial disorders by magnetic resonance spectroscopy. *Nature Clinical Practice.* 2008;5 Suppl 2:S49-56.

Ingle L, Goode K, Rigby ASR, Cleland JGF, Clark AL. Predicting peak oxygen uptake from 6-min walk test performance in male patients with left ventricular systolic dysfunction. *European Journal of Heart Failure.* 2006;**8**(2):198-202.

Ingwall JS, Shen W. The Chemistry of ATP in the Failing Heart-The Fundamentals. *Heart Failure Reviews.* 1999;4:221-228.

Jiang N, Zhang G, Bo H, Qu J, Ma G, Cao D, Wen L, Liu S, Ji LL, Zhang Y. Upregulation of uncoupling protein-3 in skeletal muscle during exercise: a potential antioxidant function. *Free Radical Biology and Medicine.* 2009;46(2):138-145.

Jubrias SA, Crowther GJ, Shankland EG, Gronka RK, Conley KE. Acidosis inhibits oxidative phosphorylation in contracting human skeletal muscle in vivo. *Journal of Physiology.* 2003;553(Pt 2):589-599.

Kammermeier H, Schmidt P, Jungling E. Free energy change of ATP-hydrolysis: a causal factor of early hypoxic failure of the myocardium? *Journal of Molecular and Cellular Cardiology.* 1982;14(5):267-277.

Karamitsos TD, Hudsmith LE, Selvenayagam JB, Neubauer S, Francis JM. Operator induced variability in left ventricular measurements with cardiovascular magnetic resonance is improved after training. *Journal of Cardiovascular Magnetic Resonance* 2007;9(5): 777-783.

Kemp GJ, Radda GK. Quantitative interpretation of bioenergetic data from ^{31}P and ^{1}H magnetic resonance spectroscopic studies of skeletal muscle: an analytical review. *Magnetic Resonance Quarterly.* 1994;10(1):43-63.

Kemp GJ, Thompson CH, Stratton JR, Brunotte F, Conway M, Adamopoulos S, Arnolda L, Radda GK, Rajagopalan B. Abnormalities in exercising skeletal muscle in congestive heart failure can be explained in terms of decreased mitochondrial ATP synthesis, reduced metabolic efficiency, and increased glycogenolysis. *Heart.* 1996;76(1):35-41.

Kemps HM, Prompers JJ, Wessels B, De Vries WR, Zonderland ML, Thijssen EJ, Nicolay K, Schep G, Doevendans PA. Skeletal muscle metabolic recovery following submaximal exercise in chronic heart failure is limited more by O_2 delivery than O_2 utilization. *Clinical Science (London).* 2010;118(3):203-210.

Kersten S, Desvergne B, Wahli W. Roles of PPARs in health and disease. *Nature.* 2000;405(6785):421-424.

Kholodenko B, Zilinskiee V, Borutaite V, Ivanoviene L, Toleikis A, Praskevicius A. The role of adenine nucleotide translocators in regulation of oxidative phosphorylation in heart mitochondria. *FEBS Letters.* 1987;223(2):247-250.

Klingenberg M. The ADP,ATP shuttle of the mitochondrion. *Trends in Biochemical Sciences.* 1979;4(11):249-252.

Korshunov SS, Skulachev VP, Starkov AA. High protonic potential actuates a mechanism of production of reactive oxygen species in mitochondria. *FEBS Letters.* 1997;416(1):15-18.

Kruger C, Durr S, Gerber SH, Haunstetter A, Hornig K, Kubler W, Haass M. Is the 6-minute walk test a reliable substitute for peak oxygen uptake in patients with dilated cardiomyopathy? *European Heart Journal.* 2000;21(7):540-549.

Kuznetsov AV, Veksler V, Gellerich FN, Saks V, Margreiter R, Kunz WS. Analysis of mitochondrial function in situ in permeabilized muscle fibers, tissues and cells. *Nature Protocols.* 2008;3(6):965-976.

Lee L, Campbell R, Scheuermann-Freestone M, Taylor R, Gunaruwan P, Williams L, Ashrafian H, Horowitz J, Fraser AG, Clarke K, Frenneaux M. Metabolic modulation with perhexiline in chronic heart failure: a randomized, controlled trial of short-term use of a novel treatment. *Circulation.* 2005;112(21):3280-3288.

Lei B, Lionetti V, Young ME, Chandler MP, D'Agostino C, Kang E, Altarejos M, Matsuo K, Hintze TH, Stanley WC, Recchia FA. Paradoxical downregulation of the glucose oxidation pathway despite enhanced flux in severe heart failure. *Journal of Molecular and Cellular Cardiology.* 2004;36(4):567-576.

Levine TB, Francis GS, Goldsmith SR, Cohn JN. The neurohumoral and hemodynamic response to orthostatic tilt in patients with congestive heart failure. *Circulation.* 1983;67(5): 1070-1075.

Lommi J, Kupari M, Yki-Jarvinen H. Free fatty acid kinetics and oxidation in congestive heart failure. *American Journal of Cardiology.* 1998;81(1):45-50.

Longmore DB, Underwood SR, Hounsfield GN. Dimensional accuracy of magnetic resonance in studies of the heart. *Lancet* 1985;1(8442):1360-1362.

Madsen PL, Secher NH. Near-infrared oximetry of the brain. *Progress in Neurobiology.* 1999;58(6):541-560.

Mancini DM, Coyle E, Coggan A, Beltz J, Ferraro N, Montain S, Wilson J.R. Contribution of intrinsic skeletal muscle changes to ^{31}P NMR skeletal muscle metabolic abnormalities in patients with chronic heart failure. *Circulation.* 1989;80(5):1338-1346.

Mancini DM, Bolinger L, Li H, Kendrick K, Chance B, Wilson JR. Validation of near-infrared spectroscopy in humans. *Journal of Applied Physiology.* 1994;77(6):2740-2747.

Mann DL, Bogaev R, Buckberg GD. Cardiac remodelling and myocardial recovery: Lost in translation? *European Journal of Heart Failure*. 2010;12(8):789-796.

Marin-Garcia J, Goldenthal MJ, Moe GW. Mitochondrial pathology in cardiac failure. *Cardiovascular Research.* 2001;49(1):17-26.

Maslov MY, Chacko VP, Hirsch GA, Akki A, Leppo MK, Steenbergen C, Weiss RG. Reduced in vivo high-energy phosphates precede adriamycin-induced cardiac dysfunction. *American Journal of Physiology.* 2010;299(2):H332-337.

Massie B, Conway M, Yonge R, Frostick S, Ledingham J, Sleight P, Radda G, Rajagopalan B. Skeletal muscle metabolism in patients with congestive heart failure: Relation to clinical severity and blood flow. *Circulation.* 1987;76(5):1009-1019.

Massie BM, Conway M, Rajagopalan B, Yonge R, Frostick S, Ledingham J, Sleight P, Radda G. Skeletal muscle metabolism during exercise under ischemic conditions in congestive heart failure. Evidence for abnormalities unrelated to blood flow. *Circulation.* 1988;78(2):320-326.

Massie BM, Conway M, Yonge R. ^{31}P nuclear magnetic resonance evidence of abnormal skeletal muscle metabolism in patients with congestive heart failure. *American Journal of Cardiology.* 1987;60(4):309-315.

Mettauer B, Zoll J, Sanchez H, Lampert E, Ribera F, Veksler V, Bigard X, Mateo P, Epailly E, Lonsdorfer J, Ventura-Clapier R. Oxidative capacity of skeletal muscle in heart failure patients versus sedentary or active control subjects. *Journal of the American College of Cardiology.* 2001;38(4):947-954.

Middlekauff HR. Making the case for skeletal myopathy as the major limitation of exercise capacity in heart failure. *Circulation. Heart failure.* 2010;3(4):537-546.

Mills EM, Banks ML, Sprague JE, Finkel T. Uncoupling the agony from ecstasy: A mitochondrial protein may mediate a dangerous side-effect of some recreational drugs. *Nature.* 2003;426(6965):403-404.

Mizuno M, Secher NH. Histochemical characteristics of human expiratory and inspiratory intercostal muscles. *Journal of Applied Physiology.* 1989;67(2):592-598.

Morgan EE, Chandler MP, Young ME, McElfresh TA, Kung TA, Rennison JH, Tserng KY, Hoit BD, Stanley WC. Dissociation between gene and protein expression of metabolic enzymes in a rodent model of heart failure. *European Journal of Heart Failure.* 2006;8(7):687-693.

Murray AJ, Anderson RE, Watson GC, Radda GK, Clarke K. Uncoupling proteins in human heart. *Lancet.* 2004;364(9447):1786-1788.

Murray AJ, Cole MA, Lygate CA, Carr CA, Stuckey DJ, Little SE, Neubauer S, Clarke K. Increased mitochondrial uncoupling proteins, respiratory uncoupling and decreased efficiency in the chronically infarcted rat heart. *Journal of Molecular and Cellular Cardiology.* 2008;44(4):694-700.

Murray AJ, Panagia M, Hauton D, Gibbons GF, Clarke K. Plasma free fatty acids and peroxisome proliferator-activated receptor alpha in the control of myocardial uncoupling protein levels. *Diabetes.* 2005;54(12):3496-3502.

Nakamura Y, Nagase I, Asano A, Sasaki N, Yoshida T, Umekawa T, Sakane N, Saito M. Beta 3-adrenergic agonist up-regulates uncoupling proteins 2 and 3 in skeletal muscle of the mouse. *The Journal of Veterinary Medical Science / The Japanese Society of Veterinary Science.* 2001;63(3):309-314.

Naressi A, Couturier C, Castang I, de Beer R, Graveron-Demilly D. Java-based graphical user interface for MRUI, a software package for quantitation of in vivo/medical magnetic resonance spectroscopy signals. *Computers in Biology and Medicine.* 2001;31(4):269-286.

Neubauer S. The failing heart - an engine out of fuel. *New England Journal of Medicine.* 2007;356(11):1140-1151.

Neubauer S, Horn M, Cramer M, Harre K, Newell JB, Peters W, Pabst T, Ertl G, Hahn D, Ingwall JS, Kochsiek K. Myocardial phosphocreatine-to-ATP ratio is a predictor of mortality in patients with dilated cardiomyopathy. *Circulation.* 1997;96(7):2190-2196.

Neubauer S, Horn M, Pabst T, Harre K, Stromer H, Bertsch G, Sandstede J, Ertl G, Hahn D, Kochsiek K. Cardiac high-energy phosphate metabolism in patients with aortic valve disease assessed by 31P-magnetic resonance spectroscopy. *Journal of Investigative Medicine.* 1997;45(8):453-462.

Neubauer S, Krahe T, Schindler R, Horn M, Hillenbrand H, Entzeroth C, Mader H, Kromer EP, Riegger GAJ, Lackner K, Ertl G. 31P magnetic resonance spectroscopy in dilated cardiomyopathy and coronary artery disease: Altered cardiac high-energy phosphate metabolism in heart failure. *Circulation.* 1992;86(6):1810-1818.

The Criteria Committee of the New York Heart Association. *Nomenclature and Criteria for Diagnosis of Diseases of the Heart and Great Vessels*. 1st ed. Boston, Mass: Little, Brown & Co; 1928.

Nicholls DG. Mitochondrial membrane potential and aging. *Aging Cell.* 2004;3(1):35-40.

Nicholls DG, Bernson VS, Heaton GM. The identification of the component in the inner membrane of brown adipose tissue mitochondria responsible for regulating energy dissipation. *Experientia. Supplementum.* 1978;32:89-93.

Ning XH, Zhang J, Liu J, Ye Y, Chen SH, From AHL, Bache RJ, Portman MA. Signaling and expression for mitochondrial membrane proteins during left ventricular remodeling and contractile failure after myocardial infarction. *Journal of the American College of Cardiology.* 2000;36(1):282-287.

Osorio JC, Stanley WC, Linke A, Castellari M, Diep QN, Panchal AR, Hintze TH, Lopaschuk GD, Recchia FA. Impaired myocardial fatty acid oxidation and reduced protein expression of retinoid X receptor-α in pacing-induced heart failure. *Circulation.* 2002;106(5):606-612.

Owen-Reece H, Smith M, Elwell CE, Goldstone JC. Near infrared spectroscopy. *British Journal of Anaesthesia.* 1999;82(3):418-426.

Paolisso G, Gambardella A, Galzerano D, D'Amore A, Rubino P, Verza M, Teasuro P, Varrichio M, D'Onofrio F. Total-body and myocardial substrate oxidation in congestive heart failure. *Metabolism: Clinical and Experimental.* 1994;43(2):174-179.

Paulus WJ, Tschope C, Sanderson JE, Rusconi C, Flachskampf FA, Rademakers FE, Marino P, Smiseth OA, De Keulenaer G, Leite-Moreira AF, Borbely A, Edes I, Handoko ML, Heymans S, Pezzali N, Pieske B, Dickstein K, Fraser AG, Brutsaert DL. How to diagnose diastolic heart failure: a consensus statement on the diagnosis of heart failure with normal left ventricular ejection fraction by the Heart Failure and Echocardiography Associations of the European Society of Cardiology. *European Heart Journal.* 2007;28(20):2539-2550.

Pennell DJ. Cardiovascular magnetic resonance: Twenty-first century solutions in cardiology. *Clinical Medicine.* 2003;3(3):273-278.

Pfaff E, Klingenberg M. Adenine nucleotide translocation of mitochondria. 1. Specificity and control. *European Journal of Biochemistry / FEBS.* 1968;6(1):66-79.

Phan TT, Abozguia K, Nallur Shivu G, Mahadevan G, Ahmed I, Williams L, Dwivedi G, Patel K, Steendijk P, Ashrafian H, Henning A, Frenneaux M. Heart failure with preserved ejection fraction is characterized by dynamic impairment of active relaxation and contraction of the left ventricle on exercise and associated with myocardial energy deficiency. *Journal of the American College of Cardiology.* 2009;54(5):402-409.

Poole-Wilson PA, Buller NP. Causes of symptoms in chronic congestive heart failure and implications for treatment. *American Journal of Cardiology.* 1988;62(2):31A-34A.

Poole-Wilson PA, Ferrari R. Role of skeletal muscle in the syndrome of chronic heart failure. *Journal of Molecular and Cellular Cardiology.* 1996;28(11):2275-2285.

Rosca MG, Vazquez EJ, Kerner J, Parland W, Chandler MP, Stanley W, Sabbah HN, Hoppel CL. Cardiac mitochondria in heart failure: Decrease in respirasomes and oxidative phosphorylation. *Cardiovascular Research.* 2008;80(1):30-39.

Sanbe A, Tanonaka K, Hanaoka Y, Katoh T, Takeo S. Regional energy metabolism of failing hearts following myocardial infarction. *Journal of Molecular and Cellular Cardiology.* 1993;25(9):995-1013.

Scheubel RJ, Tostlebe M, Simm A, Rohrbach S, Prondzinsky R, Gellerich FN, Silber RE, Holtz J. Dysfunction of mitochondrial respiratory chain complex I in human failing myocardium is not due to disturbed mitochondrial gene expression. *Journal of the American College of Cardiology.* 2002;40(12):2174-2181.

Scheuermann-Freestone M, Madsen PL, Manners D, Blamire AM, Buckingham RE, Styles P, Radda GK, Neubauer S, Clarke K. Abnormal cardiac and skeletal muscle energy metabolism in patients with type 2 diabetes. *Circulation.* 2003;107(24):3040-3046.

Schrauwen P, Hinderling V, Hesselink MK, Schaart G, Kornips E, Saris WH, Westerterp-Plantenga M, Langhans W. Etomoxir-induced increase in UCP3 supports a role of uncoupling protein 3 as a mitochondrial fatty acid anion exporter. *FASEB.* 2002;16(12):1688-1690.

Schrauwen P, Saris WHM, Hesselink MKC. An alternative function for human uncoupling protein 3: Protection of mitochondria against accumulation of nonesterified fatty acids inside the mitochondrial matrix. *FASEB Journal.* 2001;15(13):2497-2502.

Sharov VG, Goussev A, Lesch M, Goldstein S, Sabbah HN. Abnormal mitochondrial function in myocardium of dogs with chronic heart failure. *Journal of Molecular and Cellular Cardiology.* 1998;30(9):1757-1762.

Sharov VG, Todor AV, Silverman N, Goldstein S, Sabbah HN. Abnormal mitochondrial respiration in failed human myocardium. *Journal of Molecular and Cellular Cardiology.* 2000;32(12):2361-2367.

Shen W, Vatner DE, Vatner SF, Ingwall JS. Progressive loss of creatine maintains a near normal Δ_GATP in transgenic mouse hearts with cardiomyopathy caused by overexpressing Gsα. *Journal of Molecular and Cellular Cardiology.* 2010;48(4):591-599.

Shivu GN, Abozguia K, Phan TT, Ahmed I, Henning A, Frenneaux M. ^{31}P magnetic resonance spectroscopy to measure in vivo cardiac energetics in normal myocardium and hypertrophic cardiomyopathy: Experiences at 3T. *European Journal of Radiology.* 2010;73(2):255-259.

Shivu GN, Phan TT, Abozguia K, Ahmed I, Wagenmakers A, Henning A, Narendran P, Stevens M, Frenneaux M. Relationship between coronary microvascular dysfunction and cardiac energetics impairment in type 1 diabetes mellitus. *Circulation.* 2010;121(10):1209-1215.

Smith CS, Bottomley PA, Schulman SP, Gerstenblith G, Weiss RG. Altered creatine kinase adenosine triphosphate kinetics in failing hypertrophied human myocardium. *Circulation.* 2006;114(11):1151-1158.

Solanes G, Pedraza N, Calvo V, Vidal-Puig A, Lowell BB, Villarroya F. Thyroid hormones directly activate the expression of the human and mouse uncoupling protein-3 genes through a thyroid response element in the proximal promoter region. *Biochemical Journal.* 2005;386(3):505-513.

Solanes G, Pedraza N, Iglesias R, Giralt M, Villarroya F. Functional Relationship between MyoD and Peroxisome Proliferator-Activated Receptor-Dependent Regulatory Pathways in the Control of the Human Uncoupling Protein-3 Gene Transcription. *Molecular Endocrinology.* 2003;17(10):1944-1958.

Stanley WC, Recchia FA, Lopaschuk GD. Myocardial substrate metabolism in the normal and failing heart. *Physiological Reviews.* 2005;85(3):1093-1129.

Taylor DJ, Bore PJ, Styles P, Gadian DG, Radda GK. Bioenergetics of intact human muscle. A ^{31}P nuclear magnetic resonance study. *Molecular Biology & Medicine.* 1983;1(1):77-94.

Taylor M, Wallhaus TR, Degrado TR, Russell DC, Stanko P, Nickles RJ, Stone CK. An evaluation of myocardial fatty acid and glucose uptake using PET with [^{18}F]fluoro-6-thia-heptadecanoic acid and [^{18}F]FDG in patients with congestive heart failure. *Journal of Nuclear Medicine.* 2001;42(1):55-62.

Thomas JA, Marks BH. Plasma norepinephrine in congestive heart failure. *American Journal of Cardiology.* 1978;41(2):233-243.

Tian R. Thermodynamic limitation for the sarcoplasmic reticulum Ca(2+)-ATPase contributes to impaired contractile reserve in hearts. *Annals of the New York Academy of Sciences.* 1998;853:322-324.

Tian R, Christe ME, Spindler M, Hopkins JC, Halow JM, Camacho SA, Ingwall JS. Role of MgADP in the development of diastolic dysfunction in the intact beating rat heart. *Journal of Clinical Investigation.* 1997;99(4):745-751.

Trenell MI, Sue CM, Kemp GJ, Sachinwalla T, Thompson CH. Aerobic exercise and muscle metabolism in patients with mitochondrial myopathy. *Muscle and Nerve.* 2006;33(4):524-531.

Tyler DJ, Emmanuel Y, Cochlin LE, Hudsmith LE, Holloway CJ, Neubauer S, Clarke K, Robson MD. Reproducibility of ^{31}P cardiac magnetic resonance spectroscopy at 3T. *NMR in Biomedicine.* 2009;22(4):405-413.

Vasan RS, Larson MG, Benjamin EJ, Evans JC, Levy D. Left ventricular dilatation and the risk of congestive heart failure in people without myocardial infarction. *New England Journal of Medicine.* 1997;336(19):1350-1355.

Vidal-Puig AJ, Grujic D, Zhang CY, Hagen T, Boss O, Ido Y, Szczepanik A, Wade J, Mootha V, Cortright R, Muoio DM, Lowell BB. Energy metabolism in uncoupling protein-3 gene knockout mice. *The Journal of Biological Chemistry.* 2000;275(21):16258-16266.

Vogt AM, Kubler W. Heart failure: is there an energy deficit contributing to contractile dysfunction? *Basic Research in Cardiology.* 1998;93(1):1-10.

Wallimann T, Wyss M, Brdiczka D, Nicolay K, Eppenberger HM. Intracellular compartmentation, structure and function of creatine kinase isoenzymes in tissues with high and fluctuating energy demands: the 'phosphocreatine circuit' for cellular energy homeostasis. *Biochemical Journal.* 1992;281(1):21-40.

Wallis J, Lygate CA, Fischer A, ten Hove M, Schneider JE, Sebag-Montefiore L, Dawson D, Hulbert K, Zhang W, Zhang MH, Watkins H, Clarke K, Neubauer S. Supranormal myocardial creatine and phosphocreatine concentrations lead to cardiac hypertrophy and heart failure: insights from creatine transporter-overexpressing transgenic mice. *Circulation.* 2005;112(20):3131-3139.

Wang Y, Ebermann L, Sterner-Kock A, Wika S, Schultheiss HP, Dorner A, Walther T. Myocardial overexpression of adenine nucleotide translocase-1 ameliorates diabetic cardiomyopathy in mice. *Experimental Physiology.* 2009;94(2):220-227.

Weiss RG, Bottomley PA, Hardy CJ, Gerstenblith G. Regional myocardial metabolism of high-energy phosphates during isometric exercise in patients with coronary artery disease. *New England Journal of Medicine.* 1990;323(23):1593-1600.

Wolcott RG, Boyer PD. The reversal of the myosin and actomyosin ATPase reactions and the free energy of ATP binding to myosin. *Biochemical and Biophysical Research Communications.* 1974;57(3):709-716.

Yabe T, Mitsunami K, Inubushi T, Kinoshita M. Quantitative measurements of cardiac phosphorus metabolites in coronary artery disease by ^{31}P magnetic resonance spectroscopy. *Circulation.* 1995;92(1):15-23.

Yabe T, Mitsunami K, Okada M, Morikawa S, Inubushi T, Kinoshita M. Detection of myocardial ischemia by 31P magnetic resonance spectroscopy during handgrip exercise. *Circulation.* 1994;89(4):1709-1716.

Yusuf S, Pitt B, Davis CE, Hood WB, Cohn JN. Effect of enalapril on mortality and the development of heart failure in asymptomatic patients with reduced left ventricular ejection fractions. *New England Journal of Medicine.* 1992;327(10):685-691.

Zungu M, Young M, Stanley W, Essop M. Chronic treatment with the peroxisome proliferator-activated receptor α agonist Wy-14,643 attenuates myocardial respiratory capacity and contractile function. *Molecular and Cellular Biochemistry.* 2009;330(1):55-62.

Appendix 1: New York Heart Association Classification

Table A1.1. The New York Heart Association classification of Functional Capacity.

Class	Patient Symptoms
Class I (Mild)	No limitation of physical activity. Ordinary physical activity does not cause undue fatigue, palpitation, or dyspnoea (shortness of breath).
Class II (Mild)	Slight limitation of physical activity. Comfortable at rest, but ordinary physical activity results in fatigue, palpitation, or dyspnoea.
Class III (Moderate)	Marked limitation of physical activity. Comfortable at rest, but less than ordinary activity causes fatigue, palpitation, or dyspnoea.
Class IV (Severe)	Unable to carry out any physical activity without discomfort. Symptoms of cardiac insufficiency at rest. If any physical activity is undertaken, discomfort is increased.

Appendix 2: Cardiac ^{31}P MRS acquisition

The 3D-CSI acquisition is run with the following parameters:

Field of view 240x240x200 mm, acquisition matrix 16x16x8, output matrix 16x16x8, Free Induction Decay (FID) size 1024 pts, bandwidth 4000 Hz.

The sequence is acquisition weighted with 10 averages in the centre of k-space. TR = 1 ECG R-R interval with a 400 ms acquisition delay from trigger. The pulse programme incorporates an ultra-short echo time to minimize baseline roll. The centre frequency is positioned between the gamma and alpha ATP peaks to ensure that all resonances of interest are equally excited to allow use of all three ATP peaks in calculation of the PCr/ATP ratio. To achieve the desired flip angle and bandwidth the pulse is 2.4 ms long and is set to coil voltage of 262 V.

Nuclear Overhauser effect (NOE) is employed by the use of 5 NOE pulses (length 2.5 ms, inter-pulse delay 80.5 ms, flip angle 500˚). Two saturation bands are used to eliminate as much of the skeletal muscle signal as possible from the anterior chest wall (width 25 mm, scaling factor 2.4 x excitation pulse).

Appendix 3: Skeletal muscle ^{31}P MRS acquisition

A series of gradient-echo images were acquired in the transverse, sagittal and coronal planes to ensure correct positioning of the subject's leg, and to allow for localized shimming of the region of interest (ROI). This increased the local magnetic field homogeneity and reduced the line-widths in the acquired spectra.

Prior to the acquisition of the ^{31}P spectra during the leg exercise protocol, a series of three baseline scans were acquired to allow calculation of correction factors for partial saturation, caused by the short repetition time (TR) used in the spectral acquisition, and nuclear Overhauser effect (NOE). The first baseline scan was acquired with a long TR to ensure complete relaxation of all resonances between subsequent excitations. The scan parameters were as follows; TR: 30 s, TE: 0.35 ms, bandwidth: 2000 Hz, 8 averages, acquired data points: 512, excitation flip angle: 90° and no NOE pulses. The second baseline scan was run with scan parameters of TR: 500 ms, TE: 0.35 ms, bandwidth: 2000 Hz, 60 averages, acquired data points: 512, excitation flip angle 25° and 10 rectangular NOE pulses, with a pulse duration of 10 ms, an inter-pulse delay of 10 ms and an excitation flip angle of 180°. The third baseline scan was run with identical parameters to the second with the exception of no excitation flip angle on the NOE pulses. The ratio of the resonance areas in the first and third scans were used to calculate a correction factor for the effects of partial saturation and, in the same way, the second and third baseline scans were used to calculate a NOE correction factor.

The data acquisition protocol consisted of the acquisition of a series of individual ^{31}P spectra acquired throughout the exercise protocol with a temporal resolution of 5 s. The acquisition parameters were as follows; TR: 500 ms, TE: 0.35 ms, bandwidth: 2000 Hz, 10 averages,

excitation flip angle 25° and 10 rectangular NOE pulses, with a pulse duration of 10 ms, an inter-pulse delay of 10 ms and an excitation flip angle of 180°.

Appendix 4: Western blotting solutions

Table A4.1. Resolving gel buffer

Solute	Concentration (mmol.L^{-1})
Tris base	1500
SDS	14

Tris base – 2-amino-2-(hydroxymethyl)propane-1,3-diol, SDS – Sodium dodecyl sulphate

pH 8.8

Table A4.2. Stacking gel buffer

Solute	Concentration (mmol.L^{-1})
Tris HCl	500
SDS	14

Tris HCl – 2-amino-2-(hydroxymethyl)propane-1,3-diol hydrochloride, SDS – Sodium dodecyl sulphate

pH 6.8

Table A4.3. Sample buffer

Solute	Concentration (mmol.L^{-1})
Tris HCl	187.5
SDS	209
Glycerol	4

Tris HCl – 2-amino-2-(hydroxymethyl)propane-1,3-diol hydrochloride, SDS – Sodium dodecyl sulphate

pH 6.8

Table A4.4. Lysis buffer

Solute	Concentration (mmol.L^{-1})
Tris HCl	75
SDS	125
Urea	4000
Glycerol	2.7

Tris HCl – 2-amino-2-(hydroxymethyl)propane-1,3-diol hydrochloride, SDS – Sodium dodecyl sulphate

pH 6.8

Table A4.5. SDS transfer buffer

Solute	Concentration (mmol.L^{-1})
Tris base	48
SDS	1
Glycine	39
Methanol	4938

Tris base – 2-amino-2-(hydroxymethyl)propane-1,3-diol, SDS – Sodium dodecyl sulphate

pH 8.5

Table A4.6. TBS-Tween

Solute	Concentration (mmol.L^{-1})
Tris base	10
NaCl	154
Tween	0.45

Tris base – 2-amino-2-(hydroxymethyl)propane-1,3-diol, NaCl – sodium chloride, Tween – polyethylene glycol sorbitan monolaurate

pH 7.4

Table A4.7. Composition of resolving gel

	Volume per gel (ml)
30% acrylamide bis-acrylamide	3.75
Resolving gel buffer	3.13
Water	2.5
10% ammonium peroxodisulphate	0.13
Tetramethylethylenediamine	0.01

Table A4.8. Composition of stacking gel

	Volume per gel (ml)
30% acrylamide bis-acrylamide	0.85
Stacking gel buffer	1.25
Water	1.88
10% ammonium peroxodisulphate	0.02
Tetramethylethylenediamine	0.01

Appendix 5

Table A5.1. Antibody concentrations used for Western blotting.

Protein	Primary antibody			Secondary antibody
	Concentration	Dilution (v/v)	Manufacturer	Dilution (v/v)
UCP3	1 $mg.ml^{-1}$	1:2500	Abcam	1:2500
CS	1 $mg.ml^{-1}$	1:2000	Alpha Diagnostic	1:5000
ANT	200 $\mu g.ml^{-1}$	1:1000	Santa Cruz	1:2000
MCAD	200 $\mu g.ml^{-1}$	1:500	Santa Cruz	1:2000
αKGD	200 $\mu g.ml^{-1}$	1:1000	Santa Cruz	1:2000
GLUT4	Gift from G Holman, University of Bath, UK			1:2500
ETC	1.5 $mg.ml^{-1}$	1:200	Mitosciences	1:2500

UCP3 – mitochondrial uncoupling protein-3, CS – citrate synthase, ANT – adenine nucleotide transporter, MCAD – medium chain acyl-CoA dehydrogenase, αKGD – alpha-ketoglutarate dehydrogenase, GLUT4 – glucose transporter-4, ETC – electron transport chain.

Secondary antibodies were from Santa Cruz Biotechnology, supplied at a concentration of 200 $\mu g.ml^{-1}$.

Abcam (Cambridge, UK)

Alpha Diagnostic (San Antonio, Texas, USA)

Santa Cruz Biotechnology (Santa Cruz, California, USA)

Mitosciences (Eugene, Oregon, USA)

Appendix 6: The Borg Scale

0 - Nothing at all

0.5 - Very, very slight (just noticeable)

1 - Very slight

2 - Slight (light)

3 - Moderate

4 - Somewhat severe

5 - Severe (heavy)

6

7 - Very severe

8

9

10 - Very, very severe (maximal)